UNIVERSITY OF CALIFORNIA

Los Angeles

Estimating Volatilization Rates and Gas/Liquid Mass Transfer Coefficients in Aeration Systems

A dissertation submitted in partial satisfaction of the requirements for the degree of Doctor of Philosophy in Civil Engineering

by

Chu-Chin Hsieh

1991

DEDICATION

To God

To my wife, Grace (Jen-Heui)

To my parents and parents-in-law

TABLE OF CONTENTS

Page

LIST OF TABLES

LIST OF FIGURES

ACKNOWLEDGEMENTS

I thank Professor H. David Stensel for introducing me to my advisor, Professor Michael K. Stenstrom. I would like to express my great appreciation to Dr. Stenstrom for his guidance, support and encouragement throughout my graduate studies. It has been an honor to work with him and to be his friend. I would like to thank the other members of my committee: Professor Elimelech, Professor Vilker, Professor Winer, and Professor Yeh.

I would like to thank Dr. Jack Lee for his help with the use of the Statistical Analysis System (SAS) to analyze my data. Thanks to Dr. Lynne Cardinal, Dr. K.S. Ro, and Dr. Judy Libra for their encouragement and guidance. Special thanks to Eddie Tzeng for his assistance in sample-taking, GC analysis and modeling work. Thanks also to Roger W. Babcock for being there and helping me with my grammar. Debby, thanks for getting me in to see MKS and for editing my dissertation.

I would like to give thanks to Home No. 2 Fellowships of Christian Assembly Church at Culver City, and to the following colleagues for their advice and companionship throughout this project: Robert Cheng, Naci Ozgur, Daylin Liu, Rich Yates, Simlin Lau, Jiachi Teng, Weibo Yuan, Brian Alvis, Ken Wong, and Jonathan Chen. Finally, exceptional thanks to my wife and our family for full support and never giving up on me.

This research was supported in part by the Engineering Research Center for Hazardous Substances Control, a National Science Foundation industry-university cooperative center for hazardous waste research at the University of California, Los Angeles, and an environmental engineering fellowship from BP America.

VITA

October 28, 1956	Born, Kaoshiung, Taiwan, R.O.C.
1979	B.S. Civil Engineering National Chung-Hsing University Taichung, Taiwan
1979-1981	Second Lieutenant Army Corps of Engineers, R.O.C.
1981-1986	Associate Engineer & Project Engineer Sewerage Engineering Department Kaoshiung, Taiwan
1987	Research Assistant Department of Civil Engineering University of Washington Seattle, Washington
1988	M.S. Civil Engineering University of Washington
1988-1991	Graduate Student Researcher Civil Engineering Department University of California, Los Angeles

PUBLICATIONS AND PRESENTATIONS

Babcock, R.W., Jr., K.R. Ro, C.-C. Hsieh, and M.K. Stenstrom, "Development of an Off-Line Enricher-Reactor Process for Activated Sludge Degradation of Hazardous Wastes," Submitted to Research Journal of the Water Pollution Control Federation.

Babcock, R.W., Jr., C.-C. Hsieh, C.-J. Tzeng, K.S. Ro, and M.K. Stenstrom, Degradation of 1-Naphthylamine by Activated Sludge using Bioaugmentation," ASCE, Environmental Engineering, Annual Conference, Reno, Nevada, June, 1991.

Hsieh, C.-C., K.S. Ro, and M.K. Stenstrom, "Estimating Stripping Rate and Gas/Liquid Mass-Transfer Coefficients in Surface Aeration," Water Pollution Control Federation, 6th Annual Conference, Toronto, Ontario, October, 1991.

ABSTRACT OF THE DISSERTATION

Estimating Volatilization Rates and Gas/Liquid
Mass Transfer Coefficient in Aeration Systems

by

Chu-Chin Hsieh

Doctor of Philosophy in Civil Engineering
University of California, Los Angeles, 1991
Professor Michael K. Stenstrom, Chair

The mass-transfer coefficients (K_La's) for oxygen and twenty volatile organic compounds (VOCs) were simultaneously measured in bench-scale surface and bubble column aeration systems under a range of hydrodynamic conditions. Henry's coefficients for selected compounds were measured using the Equilibrium Partitioning in Closed System (EPICS) procedure, and compared to previously reported values. Using these measurements, the ratio of gas-phase to liquid-phase mass transfer coefficients and liquid-phase resistance were estimated using nonlinear regression.

A corrected Ψ-value, called Ψ_m, was proposed as a method for improving the estimation of stripping rates for low volatility compounds. Good correlations between predicted (using Ψ_m) and measured (in experiments) values of K_La of twenty VOCs proves the validity of the Ψ_m concept.

In these experiments the ratio of gas-phase to liquid-phase mass transfer coefficients was found to vary with the hydrodynamic conditions of the gas-phase and liquid-phase, instead of being a fixed value as suggested by previous studies. Surface

aeration experiments performed with constant air velocity resulted in a relatively constant gas transfer coefficient. However, the air phase hydrodynamic condition in the bubble column varied with the air flow rate. The ratios of gas-phase to liquid-phase mass transfer coefficients in the bubble column (2.2 - 4.6) were much smaller than those in the surface aeration experiments (38 - 110), indicating that gas-phase resistance in the bubble column is much more significant than in surface aeration.

The use of a transfer parameter to predict volatilization rates of VOCs from bubble aeration has been confirmed by analysis of dimensionless parameters. Dimensionless parameters incorporating the Henry's coefficient (Hc) and the air flow-to-liquid volume ratio were developed to predict the volatilization rate of VOCs.

Finally, the application of the Ψ_m-concept was demonstrated by means of an example for surface aeration and bubble column. The calculated results indicated that the oxygen transfer rate of the bubble column is higher than that of surface aeration. However, the volatilization rates of VOCs are greater with surface aeration than with bubble column. These results can be attributed to the higher gas-phase resistance which occurs in the bubble column.

1. INTRODUCTION

Volatile organic compounds (VOCs) frequently contaminate waters and wastewaters and can be stripped during treatment, particularly aeration, to generate air contaminants (Chang et al. 1987, Boyle et al. 1989). Many VOCs are non-biodegradable in conventional wastewater treatment plants, and volatilization can become a significant removal mechanism in the activated sludge process (Namkung and Rittmann, 1987). Moreover, many of these substances are thought to be toxic, and may pose health risks. Controlling VOC emissions from treatment plants therefore has become an important environmental issues.

Many VOCs have been listed as priority pollutants (1979 Amendments to the Clean Water Act) or toxicants (1980 Resources Conservation and Recovery Act, the 1986 Superfund Amendments and Reauthorization Act, and the 1986 Soft Drinking Water Act Amendments). Additional regulation is pending in the amendments to the Clean Air Act (S-1630), and emissions from Publicly Owned Treatment Works (POTWs) have been specifically implicated (Baillod et al. 1990).

Among wastewater treatment facilities, aeration tanks are a significant source of VOC emissions. Two types of aeration systems, surface aeration and diffused or bubble aeration, are widely used to achieve oxygen transfer. The volatilization/stripping rates of VOCs can be estimated by the two resistance model which is broadly used to estimate oxygen transfer rate in the aeration systems. Previous research (Smith et al. 1980, 1981; Matter-Muller et al. 1981; Rathbun and Tai 1982, 1984; Mumford and Schnoor 1982; Roberts et al. 1983, 1984a; Truong and Blackburn 1984; and Cadena et al. 1984) defined a proportional relationship of mass

transfer coefficients between VOCs and oxygen as Ψ, which can be used to estimate VOCs stripping rate from the oxygen transfer rate. This application, however, is only valid for highly volatile compounds and may not be applied to less volatile compounds. Thus, theoretical analyses of emissions of low volatility compounds needs further investigation.

In order to use the Ψ-value concept, Mackay et al. (1979) suggested that stripping of volatile organic compounds with Henry's law coefficients higher than 5.00 x 10^{-3} atm m^3 mol^{-1}, or dimensionless Henry's law coefficients of 0.20. at 20 °C is controlled by liquid film resistance. Several researchers (Smith et al. 1980, 1981; Matter-Muller et al. 1981; Rathbun and Tai 1982, 1984; and Truong and Blackburn 1984) adopted that criterion with minor modification. For these conditions, the gas film resistance is negligible and the liquid film mass transfer coefficient is assumed to be approximately equal to the overall mass transfer coefficient.

The relative importance of gas and liquid resistance is estimated by a ratio of gas-film to liquid-film transfer coefficients (k_G/k_L) with a reported average value of 150. The average ratio of 150 (range from 50 to 300) was introduced by Mackay and Leionoen (1975) and Mackay et al. (1979). They estimated this value using k_G for water (1000-3000 cm hr^{-1}) and k_L for O_2 (20 cm hr^{-1}) at the air and ocean surface interface data provided by Liss and Slater (1974). This assumption has been widely applied to aeration systems (Smith et al. 1980; Roberts et al. 1983).

This high ratio might be valid for natural bodies of water, but for more turbulent aeration systems such as surface and bubble aeration systems, Munz and Roberts (1984) demonstrated k_G/k_L to be closer to 20. They developed an indirect

approach of fitting overall mass transfer rate constants to the two-resistance model with appropriate corrections for molecular diffusivities from Goodgame and Sherwood (1954). In such systems, the compounds must be quite volatile (Hc > 1.27 or 3.05×10^{-2} atm m^3 mol^{-1}) to ensure that at least 95% of mass transfer resistance is in liquid film in order to justify ignoring the gas film resistance.

In this study, a modification of Ψ-value, corrected for liquid resistance and referred to as Ψ_m, was proposed as a method for predicting stripping rates of VOCs with widely varying properties. Such a methodology improves the estimation of stripping rates for intermediate and low-volatility compounds by eliminating the error introduced by ignoring liquid resistance.

In a bench-scale surface aeration, mass transfer rates of twenty VOCs and oxygen transfer rates were simultaneously measured. From these measurements, Ψ_M was determined over a range of hydrodynamic conditions to verify this methodology. Finally, the relationship between stripping rates of VOCs and power input per unit volume were conducted to develop a protocol for scale-up application.

In a bubble column, mass transfer rate, the degree of equilibrium or Henry's coefficient (Hc), were investigated. The value of Henry's coefficient (Hc) is an important factor for determining the degree of transfer rate, and literature values for VOCs can differ by more than 50%. Therefore, Henry's coefficient of twenty VOCs were measured by Equilibrium Partitioning in Closed System (EPICS), and was compared to the results of bubble column. The relationship between the degree of transfer during bubble aeration and Henry's coefficient for 20 VOCs were studied.

1.1 Choice of Organic Compounds

Table 1 shows the properties of organic compounds chosen for this study. Figure 1 plots log solubility versus log vapor pressure illustrating the properties of twenty VOCs used. These 20 organic compounds span the range of volatility to simulate systems with liquid side resistance controlling to systems with both gas and liquid side resistance. The values for S (solubility), P (vapor pressure), B.P. (boiling point) and Hc (dimensionless Henry's coefficients) in Table 1 were obtained form published data (Mackay et al. 1979; Roberts et al. 1984, and Verschueren, 1977). The agreement in values of P and S among various workers is quite good, but there are wide discrepancies in values of Hc for some of the compounds. Values of Hc were chosen either on the basis of agreement among various workers or the data judged to be most accurate. Additionally, Henry's law coefficients for selected compounds were measured.

1.2 Objectives

The objectives of this study were:

- To estimate the stripping rate of 20 organic compounds spanning a wide range of Henry's coefficients;
- To estimate the ratio of gas-phase and liquid-phase mass transfer coefficients;
- To determine the fraction of liquid resistance to overall resistance for 20 VOCs under different hydrodynamic conditions;
- To verify the modified approach (Ψ_m) for correcting liquid resistance and for predicting the stripping rate of wide range of compounds;
- To determine the degree of equilibrium of 20 VOCs in a bubble column;
- To measure Henry's coefficient in equilibrium experiments and in a

Table 1. Properties of twenty VOCs studied

Compounds	Formula	ABB	M.W.	S	P	B.P.	Hc	R.T.
(760 mmHg, 20oC)			grams	(mg/L)	(mmHg)	(C)	(-)	(min)
1,2-Dichloroethene (cis)	CHCl=CHCl	12DCE	96.9	3500.0	206.02	60.3	0.170	4.6
Chloroform	CHCl3	CLF	119.4	8000.0	160.00	61.7	0.160	5.2
1,1,1-Trichloroethane	CCl3CH3	111TCA	133.4	720.0	100.00	74.1	0.530	5.5
Carbon Tetrachloride	CCl4	CT	153.8	800.0	90.00	76.5	1.316	5.8
Benzene	C6H6	BZ	78.1	1780.0	76.00	80.0	0.230	6.2
Trichloroethylene	CCl2=CHCl	TCE	131.4	1100.0	58.00	87.0	0.250	7.6
Toluene	C6H5-CH3	TLN	92.1	515.0	22.00	110.0	0.230	10.6
Perchlorothylene	CCl2=CCl2	PCE	165.8	140.0	18.00	121.0	0.570	11.9
Ethylenebromide	CH2BrCH2Br	EDB	187.9	4310.0	11.00	131.6	0.041	12.8
Chlorobenzene	C6H5-Cl	CBZ	112.6	500.0	8.80	132.0	0.150	14.1
Ethylbenzene	C6H5-CH2CH3	EBZ	106.2	152.0	7.00	136.0	0.260	14.6
1,3-Xylene (m)	C6H4-(CH3)2	MXY	106.2	146.0	6.00	139.0	0.240	14.9
1,2-Xylene (O)	C6H4-(CH3)2	OXY	106.2	213.0	5.00	144.4	0.180	15.9
Bromoform	CHBr3	BF	252.8	3033.0	5.60	149.5	0.041	16.4
Bromobenzene	C6H5Br	BBZ	157.0	500.0	3.30	156.0	0.100	17.7
1,1,2,2-Tetrachloroethan	CHCl2CHCl2	1122TCA	167.9	3100.0	6.50	146.2	0.042	18
1,3-Dichlorobenzene	C6H4Cl2	13DCB	147.0	111.0	1.49	173.0	0.120	20.5
1,4-Dichlorobenzene	C6H4Cl2	14DCB	147.0	79.0	0.60	174.0	0.110	20.8
1,2-Dichlorobenzene	C6H4Cl2	12DCB	147.0	100.0	1.00	179.0	0.087	21.8
Naphthalene	C10H8	NAPH	128.2	30.0	0.0109	217.9	0.038	27.3

ABB: Abbreviation M.W.: Molecular Weight B.P.: Boiling Point

S: Solubility Hc: Henry's Coefficient

P: Partial Pressure R.T.: Retention Time in GC

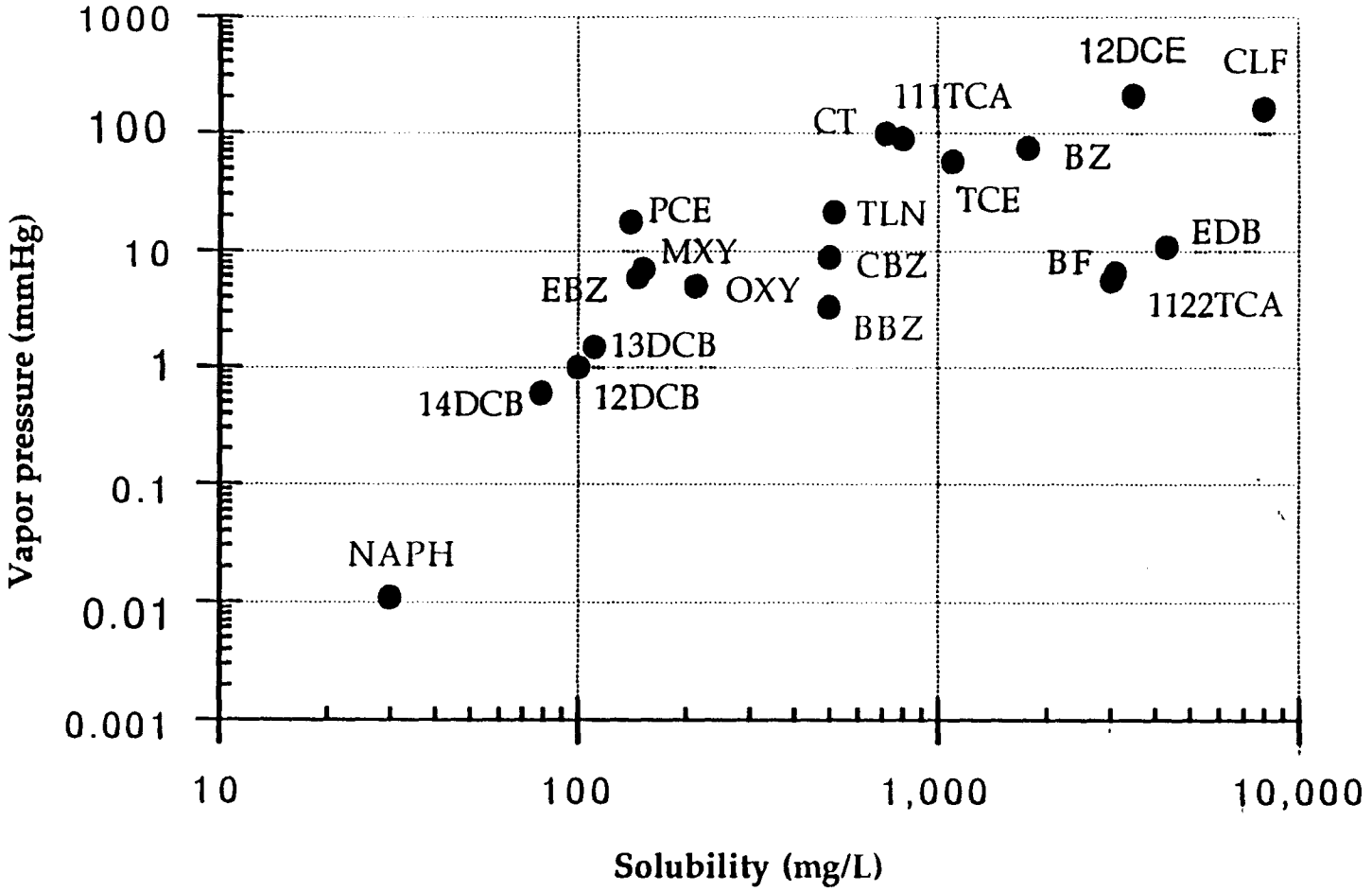

Figure 1. Plot of log solubility vs log vapor pressure illustrating the properties of twenty VOCs used

bubble column for 20 VOCs, and

- To develop a simple mathematical model with these data to describe VOCs removal in aeration systems typically found in water and wastewater treatment plants.

2. LITERATURE REVIEW AND THEORETICAL DEVELOPMENT

2.1 Phase Equilibrium - Henry's Coefficients

Henry's Law has been widely used to express the equilibrium between air and water phases in the dilute concentration range as shown in the following equation.

$$H = \frac{C_G}{C_L} \tag{1}$$

where C_G is the air phase concentration in equilibrium with the liquid phase concentration, C_L. The Henry's coefficient is represented by H. In the literature, Henry's coefficient has been expressed in a variety of units. The three most common units to express Henry's coefficient are: (1) atm, (2) atm-m^3/mole and (3) no unit (dimensionless).

If the units of Henry's coefficients are given in atmospheres (atm), then the following equation is used:

$$Hi = \frac{Pi}{X_i} \tag{2}$$

where Pi is vapor pressure of the solute i in equilibrium with mole fraction of the solute i in water X_i (mole/mole).

For units of atm-m^3/mole, Henry's coefficients are often defined as

$$H = \frac{Pi\ [atm]}{C_L^S\ [mole\ m^{-3}]} \tag{3}$$

where Pi is the vapor pressure of the solute i in equilibrium with the liquid phase concentration C_L^S.

The dimensionless Henry's coefficients can be estimated from the pure solute vapor pressure and its solubility, and are defined as:

$$Hc = \frac{C_G^*[mg/L]}{C_L[mg/L]} = \frac{16.04PM}{TS} \tag{4}$$

where

C_G^* = the equilibrium concentration in the gas phase for the liquid concentration, C_L

P = vapor pressure of the pure solute in mm of Hg

M = gram molecular weight of the solute

T = temperature in °K

S = solubility of the solute in water in mg/L.

The relation between the two forms of Henry's coefficient, Hc (dimensionless) and H (atm-m^3/mole), is given by

$$Hc = \frac{H}{RT} \tag{5}$$

where

R = universal gas constant = 8.2×10^{-5} [atm m^3 mol^{-1} K^{-1}]

T = temperature [°K]

The larger the Henry's coefficient, the greater the equilibrium concentration of solute in the air. Thus, contaminants with large Henry's coefficients are more easily removed by aeration. However, it is experimentally difficult to determine Henry's coefficients, and the differences in published values are large. Mackay and Shiu (1981) reviewed Henry's coefficients for environmentally relevant chemicals and

found that considerable discrepancies exist in the literature, even for common chemicals.

Platford (1977) and Nicholson et al. (1984) stated that Henry's law coefficients estimated from vapor pressure and solubility data may not be valid for the low solute concentrations typically encountered in environmental engineering. Lalezary et al. (1984) and Gossett and Lincoff (1981) reported increasing Henry's coefficients with increasing concentration. However, Munz and Roberts (1986, 1987) presented a comprehensive study which contradicts previous reports. They made three conclusions in their studies:

1. No effect of solute concentration on solute's Henry's coefficients was observed up to solute-liquid mole fractions of $\approx 10^{-3}$;

2. Very high cosolvent concentrations, in excess of $\approx$ 10 g/L, are required to reduce the solute's Henry's coefficients;

3. No change in Henry's coefficient was observed in a multisolute system up to a total mixture concentration of 375 mg/L.

2.1.1 Determination of Henry's Coefficients

In order to accurately estimate the stripping rates and the degree of equilibrium of VOCs in our bubble column experiments, accurate Henry's coefficients of 20 compounds were required.

Mackay and Shiu (1981) presented a comprehensive review of the common methods for measuring Henry's coefficients along with their respective advantages

and disadvantages. They cited three basic methods:

1. Use of vapor pressure and solubility data;

2. Direct measurement of air and aqueous concentrations in a system at equilibrium, and

3. Measurement of relative changes in concentration within one phase, while effecting a near-equilibrium exchange with the other phase.

The first method suffers from the lack of reliable solubility data because the measurement of aqueous solubility of hydrophobic compounds is very difficult. The second method usually is applied only to fairly high concentrations because of the difficulty of sampling and analyzing the absolute values of the low concentrations typical of environmental levels in both phases. The third method, the batch air stripping procedure presented by Mackay et al. (1979), was evaluated in our bubble column test. This method occasionally suffers from experimental difficulty in achieving equilibrium (Lincoff and Gossett, 1984).

More recently, Gossett (1987) presented a novel approach involving measurement of liquid phase or gas headspace concentration ratios from pairs of sealed bottles possessing differing liquid volumes, termed EPICS (Equilibrium Partitioning in Closed Systems). The precision of this technique depends on the selected volume ratio and can be controlled by proper experimental design.

Method 1 and 2 are not suitable for the low concentrations typically found in environmental engineering. Method 3 requires equilibrium, which may be difficult to achieve and verify. Roberts et al. (1982) reported that the Henry's coefficients

measured with this technique depended upon turbulence, which may have been an artifact of not obtaining equilibrium. The EPICS method was found to be suitable for this study in terms of precision, simplicity, and the capability to handle large numbers of samples in a reasonably short time. Therefore, the EPICS method was used with analysis of the aqueous phase to measure Henry's coefficients.

2.1.2 Derivation of EPICS's Equations and Application

The EPICS procedure is based on closed-system mass balances developed by Lincoff and Gossett (1984). The procedure is derived in the following paragraphs and equations. The total mass of a volatile solute added to a serum bottle will be partitioned between gas and liquid phases at equilibrium according to

$$M = C_L V_L + C_G V_G = C_L V_L + (HcC_L)V_G = C_L(V_L + Hc\ V_G) \quad (6)$$

where

C_L = concentration of solute in the water (mg/L)

C_G = concentration of solute in the gas (mg/L)

Hc = Henry's coefficient (dimensionless),

M = total mass

V_G = volume of headspace in the bottle (L),

V_L = volume of liquid in the bottle (L).

If two bottles are prepared with differing liquid volumes, V_{L1} and V_{L2}, equation (6) can be written for each as follows:

$$M_1 = C_{L1}\ (V_{L1} + Hc\ V_{G1}) \quad (7)$$

$$M_2 = C_{L2}\,(V_{L2} + Hc\,V_{G2}) \tag{8}$$

If equation (7) is divided by M_1 and equation (8) divided by M_2, the left-hand sides of each equation will be unity, allowing them to be equated, as follows:

$$(C_{L1}/M_1)(V_{L1} + Hc\,V_{G1}) = (C_{L2}/M_2)(V_{L2} + Hc\,V_{G2}) \tag{9}$$

Solving for Hc yields

$$Hc = \frac{V_{L2} - rV_{L1}}{rV_{G1} - V_{G2}} \tag{10}$$

where $r = \left[\frac{C_{L1}}{C_{L2}}\right]\left[\frac{M_2}{M_1}\right]$. Evaluation of Hc using equation (10) does not actually require that M_1 and M_2 be known; only that their ratio be known. This is a critical point for reducing experimental error and laboratory time. It means that if a stock solution of a solute is used to prepare EPICS bottles, it is not necessary to know the actual concentration of the stock solution. A gravimetric measure of the relative quantity of the stock added to the two EPICS bottles suffices. Similarly, a relative measure of sample concentration, such as the ratios of peak heights or areas, can be used in place of the absolute concentrations, as long as the measurements are made in the linear detection ranges of analytical instruments. Gravimetric measures are far more precise than volumetric measures. Therefore, gravimetric analysis of the stock masses were used to measure the mass differences in the stock solution (i.e., weighing of a syringe or bottle just before and after rejection).

2.2 Mass Transfer Models

Mass transfer of stripping/absorption is a first-order process. The volatilization/stripping rate of volatile organic compounds in natural water or an engineered system can be estimated by the two-film model which is broadly used to estimate oxygen transfer rate in the aeration systems. This theory assumes the concentration gradient is linear (see Figure 2). Solute is transported from the bulk of liquid-film to film boundary, and then from the interface to the bulk of gas-film. The mass transport flux can be expressed, in the form of Fick's first law, as proportional to the concentration difference and the interfacial area:

$$\text{(amount of mass transferred)} = k\ \text{(area)}\ \text{(concentration difference)} \tag{11}$$

where the proportionality is summarized by k, called a mass transfer coefficient. This expression makes practical sense. It shows that if the concentration difference is doubled, the flux will double. It also suggests that if the area is doubled, the total rate of mass transferred will be also double, but the flux per area will not change. If we divide equation (11) by area, the mass transfer flux can be shown that

$$\text{mass transfer flux} = N = k_G(C_{Gi} - C_G) = k_L\ (C_L - C_{Li}) \tag{12}$$

By introducing the volume of the liquid, V, into equation (11), the specific mass transfer rate (mass/time/volume) can be stated as follows:

$$\text{specific mass transfer rate} = \frac{dm}{dt}\left(\frac{1}{V}\right) = \frac{dC_L}{dt} = k_L\ \frac{A}{V}\ (C_L - C_{Li}) \tag{13}$$

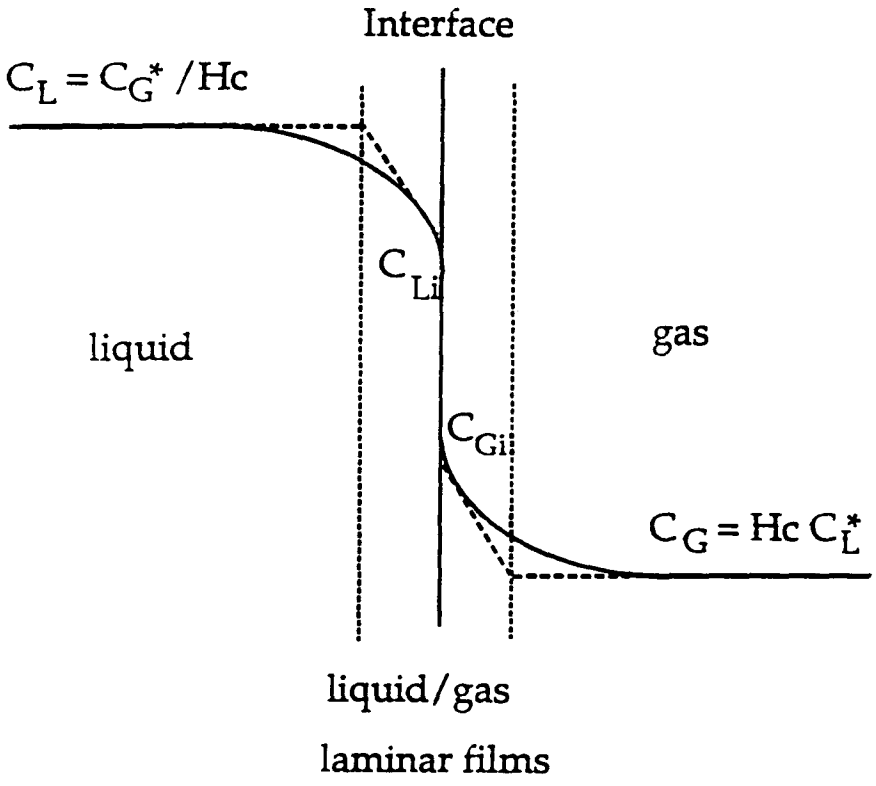

Figure 2. Two-Film Theory with linear concentration gradient

In most cases the interfacial area of contact, $a = \frac{A}{V}$, is difficult to determine, so that a constant, $K_L a$, is introduced. This constant has a value equal to the product of k_L and $\frac{A}{V}$ (transfer area/volume). Substituting this constant into equation (13) gives

$$\frac{dC_L}{dt} = - k_L a (C_L - C_{Li}) \tag{14}$$

In a laboratory experiment, C_L and C_G are determined easily, whereas the determination of C_{Li} and C_{Gi} is almost impossible. It is more convenient to define overall mass transfer coefficients based on overall concentration difference.

$$\frac{dC_L}{dt} = - K_L a (C_L - C_L^*) \tag{15}$$

where $\frac{dC_L}{dt}$ is the rate of volatilization (mass/volume-time). K_L, the overall mass transfer coefficient based on the aqueous-film driving force. a is the area available for mass transfer per volume. C_L is liquid-film concentration and C_L^* (= C_G/Hc) is the concentration in water that would be in equilibrium with the air-film concentration.

2.2.1 Two-Film Theory

A major assumption in the Two-Film Theory (Lewis and Whitman, 1924) is the additivity of resistances; the total resistance to mass transfer across the interface is the sum of gas-film resistance plus liquid-film resistance. The general mathematical expression for this process is as follows:

$$\frac{1}{K_L} = \frac{1}{k_L} + \frac{1}{Hc(k_G)} \tag{16}$$

where

K_L = overall liquid-film mass transfer coefficient, [time^{-1}]

k_L, k_G = local liquid-film and gas-film mass transfer coefficient, respectively, [time^{-1}]

Hc = Henry's law coefficient [dimensionless]

The ratio of liquid to gas resistance can be rearranged as

$$\frac{R_L}{R_G} = Hc\left(\frac{k_G}{k_L}\right) \tag{17}$$

where

R_L, R_G = liquid, gas resistances, respectively [dimensionless]

Therefore, the percentage resistance in the liquid-film is given by

$$\frac{R_L}{R_T} = \frac{R_L}{R_L + R_G} = \frac{1}{1 + \frac{R_G}{R_L}} = \frac{1}{1 + \frac{1}{Hc\,\frac{k_G}{k_L}}} \tag{18}$$

Equation (17) shows that the relative importance of liquid and gas resistance can be estimated by the ratio of $\frac{k_G}{k_L}$ and Hc (Henry's coefficient). The ratio of $\frac{k_G}{k_L}$ is a function of hydrodynamic conditions, and Hc is a property of the compound. In order to show the interaction of the three parameters, a graph of the percentage resistance in the liquid-film as a function of Hc and k_G/k_L is calculated from equation (13) as shown in Figure 3. Compounds and conditions exhibiting both high Hc and k_G/k_L, in which liquid film control dominates, such as oxygen or 1,1,1 -TCA are in the upper

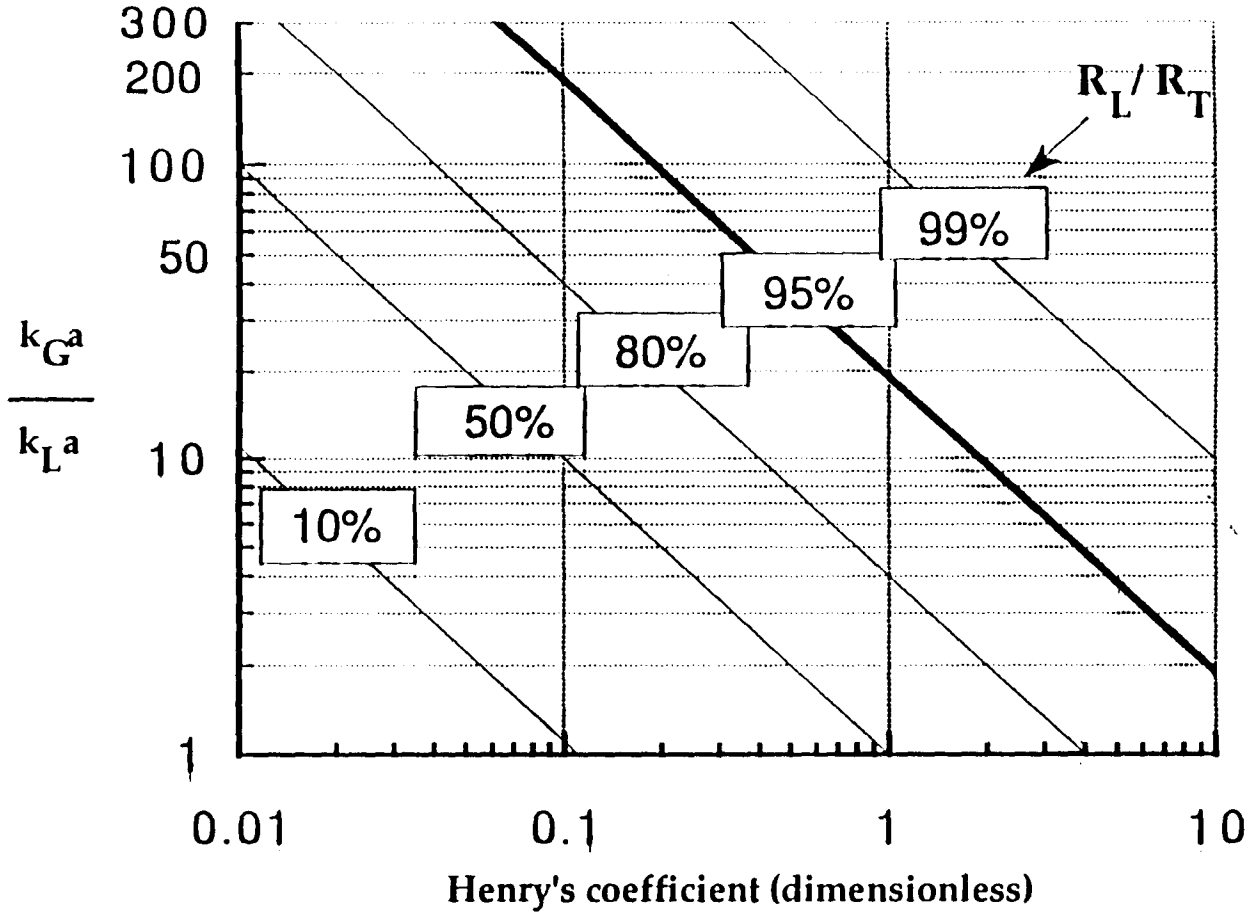

Figure 3. The fraction of liquid-phase resistance to total resistance as a function of ratios of gas-phase to liquid-phase mass transfer coefficient and Henry's coefficient

right hand corner of the graph. Compounds and conditions characterized by low values of Hc and $\frac{k_G}{k_L}$, in which gas film control is more important, such as naphthalene, or 1,1,2,2- tetrachloroethane, bromoform, are shown in the lower left hand corner of this graph.

Figure 4 shows fraction of liquid-phase resistance to total resistance as a function of ratios of gas-phase to liquid-phase mass transfer coefficients and Henry's coefficient and is useful for showing some interesting trends. The X-axis shows the ratio of gas to liquid coefficients, $\frac{k_G}{k_L}$, with lower values of $\frac{k_G}{k_L}$ denoting high turbulence and higher values for $\frac{k_G}{k_L}$ denoting low turbulence. For compounds with higher Henry's coefficient, Hc, such as oxygen, more resistance may be attributed to liquid-film and the degree of turbulence does not affect the values of R_L/R_T. The degree of turbulence affects liquid-film resistance dramatically for compounds with lower values of Hc such as naphthalene. For high turbulence conditions, i.e. $\frac{k_G}{k_L}$ of 20, the value is 23% for naphthalene and the liquid-film resistance increases to 69% in lower turbulence conditions. The other two compounds shown in this graph also exhibit the same tendencies.

This example shows the importance of the ratio of $\frac{k_G}{k_L}$. The principle of resistance additivity cannot be used accurately unless the relative importance of two resistances are properly estimated.

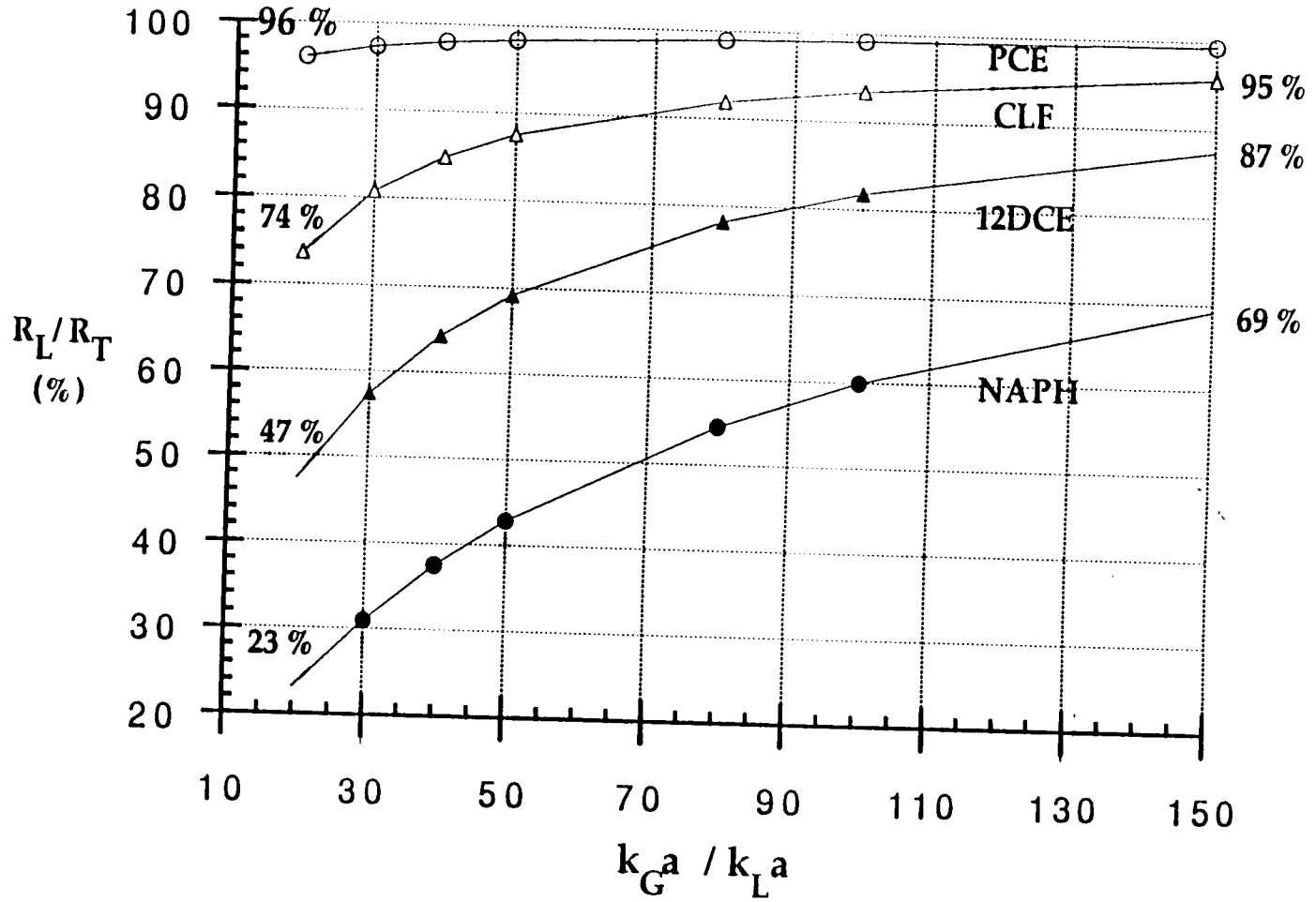

Figure 4. Fraction of liquid-phase resistance to total resistance as a function of ratios of gas-phase to liquid-phase mass transfer coefficients and Henry's coefficient

The two-film theory predicts that the transfer coefficients are proportional to the first power of the diffusivity. Later theories, proposed by Higbie (1935) and Danckwerts (1951) conclude that the transfer coefficients are proportional to the square root of diffusivity. Section 2.4.2 discusses this difference in greater detail. For the purposes of this dissertation the term two resistance theory will be used, which assumes that the resistances of the two phases are additive, as in the two-film theory, but that the transfer coefficients are proportional to the diffusivity to the n power, and n is not equal to 1.0.

2.2.2 Surface Aeration

In surface aeration, liquid is brought into contact with large volumes of air (i.e., Q_G is large) and saturation condition of headspace may never be reached (Metcalf and Eddy, 1979). Then we can assume $C_G = 0$ (i.e. $C_L^* = \frac{C_G}{Hc}$). Therefore, equation (18) can be integrated as follows:

$$\ln\left(\frac{C_L}{C_{Lo}}\right) = -K_L a(t - t_o) \tag{19}$$

where $t_o = 0$, C_{Lo} = initial concentration. Thereafter, we can estimate $K_L a$ from a log-linear regression of concentration ratio versus time.

2.2.3 Bubble Aeration

Mass transfer in a bubble column is a dynamic process in which the local equilibrium concentration (to be considered in the driving force) changes as the bubble rise though the liquid column. To model this process we can begin with the two-film theory applied to gas-film concentration of a rising gas bubble and assume that:

1. The overall mass transfer coefficient, K_L, is constant during an experiment;

2. Equilibrium holds at the interface and is described by Henry's Law;

3. Gas flow rate and temperature are constant;

4. The rising bubbles are distributed uniformly across the column;

5. Change of pressure and volume of the air bubbles are neglected;

6. The liquid-film is well mixed (homogeneous);

7. The liquid-film concentration is time-dependent but remains constant during the residence time of a single bubble; and

8. The gas-film concentration is dependent on bubble residence time and vertical position.

The mass balance for a single rising bubble can be expressed as:

$$V_b \frac{dC_G}{dt} = K_L(A_b)(C_L - C_L^*) \tag{20}$$

V_b, A_b = volume[L^3] and surface area [L^2] of a single bubble, respectively. Substituting the Henry's law coefficient [$C_G = C_L^*$ (Hc)] and rearranging equation (20) yields:

$$\frac{dC_L^*}{(C_L - C_L^*)} = \frac{K_L}{Hc} \frac{A_b}{V_b} dt \tag{21}$$

$$\frac{dC_L^*}{(C_L - C_L^*)} = \frac{K_L a(V_L)}{Q_G\, Hc}\,\frac{t}{t_r} \tag{25}$$

Integrating equation (25) yields:

$$\ln (C_L - C_L^*) = -\left(\frac{K_L a(V_L)}{Q_G\, Hc}\right)\frac{t}{t_r} + C \tag{26}$$

where C is the integration constant. With the initial condition that the bubbles contain no VOCs at formation, then $C_L^* = C_{GI} = 0$, and assuming that C_L remains constant during the residence time of a single bubble, the constant of the integration, C, becomes ln (C_L). Equation (26) can be rewritten to obtain:

$$\ln\left(1 - \frac{C_L^*}{C_L}\right) = -\left(\frac{K_L a(V_L)}{Q_G\, Hc}\,\frac{t}{t_r}\right) \tag{27}$$

This equation can be used to predict the degree of bubble saturation as follows:

$$Sd = \frac{C_L^*}{C_L} = \frac{C_G}{C_G^*} = 1 - \exp\left[-\frac{K_L a(V_L)}{Q_G\, Hc}\left(\frac{t}{tr}\right)\right] \tag{28}$$

where

Sd = degree of saturation of VOCs in the bubble [dimensionless]

At the free water surface, $t = t_r$, then

$$Sd = \frac{C_L^*}{C_L} = \frac{C_G}{C_L\, Hc} = 1 - \exp\left[-\frac{K_L a(V_L)}{Q_G\, Hc}\right] \tag{29}$$

Roberts et al. (1982) defined the term in the square brackets of equation (29) as saturation parameter ϕ:

The relationship between a single bubble and a series of bubbles can be developed as follows:

$$t_r = \frac{V_G}{Q_G} \tag{22}$$

$$Vs = \frac{Zs-Z}{t} = \frac{Zs}{t_r} \tag{23}$$

$$\frac{A_b}{V_b} = [\frac{nA_b}{V_L}] [\frac{V_L}{nV_b}] = \frac{A_B}{V_L} [\frac{V_L}{V_G}] = a \frac{V_L}{V_G} \tag{24}$$

where

Vs	=	velocity of rising bubble [L/time],
n	=	number of bubbles,
A_B	=	nA_b total surface area of all bubbles at any given time [L^2],
a	=	$\frac{A_B}{V_L}$, specific interfacial surface area [L^{-1}],
Q_G	=	gas flow rate [L^3/time],
V_L	=	liquid volume [L^3],
V_G	=	total volume of gas bubbles in the system [L^3],
t	=	retention time of the gas bubble rising through the liquid [time],
t_r	=	total retention time of the gas bubble rising from diffuser to free water surface [time],
Zs	=	submergence of the diffuser, relative to the liquid surface [L],
Z	=	submergence of the bubble, relative to the liquid surface [L].

Substituting equation (22) and (24) into equation (21) yields:

$$\phi\, Zs = \frac{K_L a(V_L)}{Hc(Q_G)} \tag{30}$$

This parameter is constant for any particular experiment since $K_L a$, Hc, Q_G and V_L are all constant. For very large values of ϕ the exit bubbles approach saturation.

Rearranging equation (23) one obtains:

$$\frac{t}{tr} = \frac{Zs-Z}{Zs} \tag{31}$$

Substituting equation (31) into equation (29), one obtains:

$$C_G = C_L Hc\{1 - \exp[-\phi Zs(\frac{Zs-Z}{Zs})]\} \tag{32}$$

or

$$C_G = C_L Hc\{1 - \exp[-\phi Zs(1 - \frac{Z}{Zs})]\} \tag{33}$$

Which describes the change in gas-film concentration of the organic compounds with submergence Z.

Figure 5 indicates the degree of saturation $(\frac{C_G}{C_G^*})$ of a volatile compound from a batch reactor as a function of fraction of retention time or submergence and saturation parameter $\frac{K_L a(V_L)}{Hc(Q_G)}$.

Finally, we can use a liquid phase mass balance to describe the transfer of organic compounds from liquid-film into the gas-film:

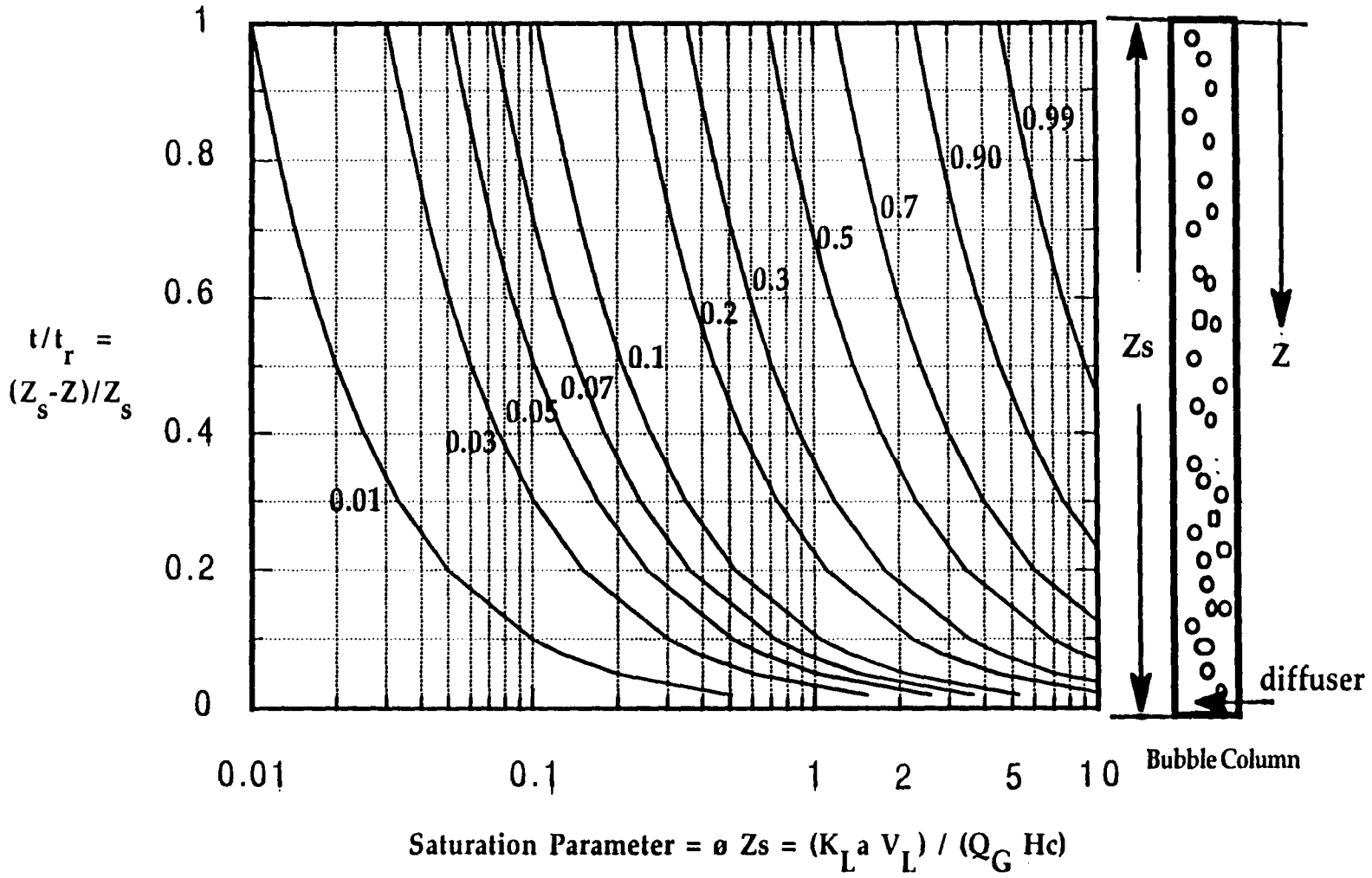

Figure 5. Degree of equilibrium of rising bubbles as a function of two dimensionless parameters

$$\text{in} - \text{out} = \text{accumulation}$$

and after appropriate substitution

$$V_L \frac{dC_L}{dt} = Q_G C_{GI} - Q_G C_{GE} \tag{34}$$

For the initial condition, we assume $C_{GI} = 0$; then the exit gas-film concentration, C_{GE}, is obtained by evaluating equation (30) at free water surface Z = 0. Substituting the expression for C_{GE} from equation (33) into equation (34)

$$V_L \frac{dC_L}{dt} = - Q_G C_L Hc\{1 - \exp[-\phi Zs]\} \tag{35}$$

After integrating from t_o to t and liquid-film concentration from C_{Lo} to C_L we obtain

$$\ln\left(\frac{C_L}{C_{Lo}}\right) = - \frac{Q_G Hc}{V_L} Sd(t - t_o) \tag{36}$$

where

Q_G = air flow rate [L^3 $time^{-1}$]

V_L = reactor volume [L^3]

A plot of the negative log-linear regression of the concentration ratio versus time gives the following slope:

$$\text{slope} = - \frac{Q_G Hc}{V_L} Sd \tag{37}$$

Consequently,

$$Sd = \frac{\text{slope}}{-\frac{Q_G Hc}{V_L}} \tag{38}$$

or

$$\frac{Q_G Hc}{V_L} = - \frac{slope}{Sd} \tag{39}$$

The mass transfer coefficient for volatile compounds can be estimated from experimental results by transforming equation (36) to the following:

$$K_L a = \frac{Q_G Hc}{V_L} \ln [\, 1 - (slope) \frac{V_L}{HcQ_G}] \tag{40}$$

Substituting equation (39) into equation (40) we obtain

$$K_L a = - slope \, [\frac{-\ln(1-Sd)}{Sd}] \tag{41}$$

We can define the term in the square brackets of equation (41) as transfer parameter, $f_{K_L a}$, which can be used to convert the slope of a log-linear regression of concentration ratio versus time into the stripping rate. Thus, equation (41) can be rearranged as:

$$K_L a = - slope \, f_{K_L a} \tag{42}$$

where

$f_{K_L a}$ = transfer parameter, $\frac{-\ln(1-Sd)}{SD}$.

Figure 6 shows the relationship predicted from equation (42) between the degree of saturation of VOCs in the rising bubble and transfer parameter. It is useful to define three cases depending upon the magnitude of Sd.

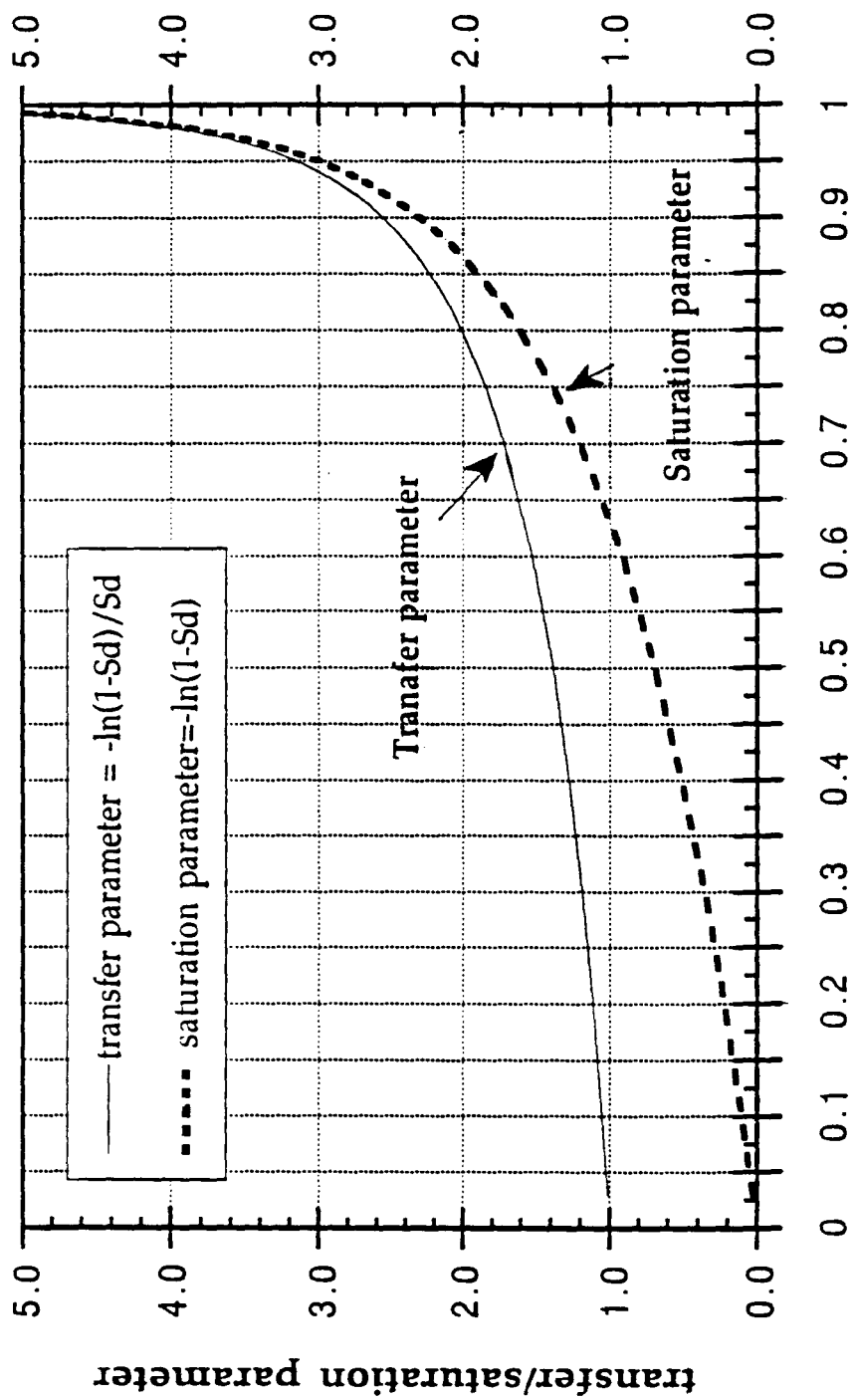

Figure 6. Transfer and saturation parameters as a function of degree of saturation of VOCs in rising bubbles

2.2.3.1 Case 1: For Sd ≤ 0.1

The transfer parameter equals 1.05 and for Sd = 0.1 and approaches 1 as Sd approaches zero. Therefore, slope is approximately equal to $K_L a$. Equation (36) can be reduced to obtain:

$$\ln\left(\frac{C_L}{C_{Lo}}\right) = -K_L a(t - t_o) \tag{43}$$

Equation (43) is the same as equation (19) which has been used to estimate $K_L a$ for surface aeration. This represents the situation where the exit air is far from saturation (less than 10%). This may be the case for large Hc (i.e. O_2) or for large Q_G. In surface aeration the continuous and rapid renewal of fresh air above water surface is provided, and the saturation of bubbles is insignificant. Under these circumstances the stripping rate may be predicted from equation (43) directly.

2.2.3.2 Case 2: For Sd ≥ 0.99

Equation (36) can be simplified to become:

$$\ln\left(\frac{C_L}{C_{Lo}}\right) = -\frac{Q_G Hc}{V_L}(t - t_o) \tag{44}$$

This represents the case where the exit gas is saturated (> 99%) with the volatile compound being stripped. This may occur because of low values of Hc or long bubble retention time. According to Matter-Muller et al. (1981), compounds that have high Henry's coefficient such as oxygen (Hc = 30.02) may require at least 30 meters of tank depth to attain saturation (or equilibrium). Conversely, compounds with small

Henry's coefficients, such as toluene (0.24) achieve saturation after rising less than 0.8 meter. Under these latter conditions equation (44) may be used as a procedure for determining the Henry's coefficient (Hc) as proposed by Mackay et al. (1979) and described previously in Section 2.1.1 as Method 3. Under these conditions the mass transfer coefficient for $K_L a$ cannot be determined accurately.

2.2.3.3 Case 3: 0.1 < Sd < 0.99

Most of the volatile compounds are in this case. The exit gas is partially saturated with the volatile compound (between 10% to 99% saturation). Equations (36) and (42) must be used to describe this situation. In this case mass transfer rate for volatile compounds depends on mass transfer rate coefficients as well as the degree of saturation of the exit gas.

2.2.3.4 Summary of Degree of Saturation

There are two common ways to present the degree of saturation of rising bubbles with VOCs in the bubble column:

$$1. \quad Sd = 1 - \exp\left[- \frac{K_L a V_L}{Q_G \, Hc} \right] \tag{45}$$

$$2. \quad Sd = \frac{slope}{-\frac{Q_G \cdot Hc}{V_L}} = \frac{slope\left(\frac{V_L}{Q_G}\right)}{Hc} \tag{46}$$

According to equation (45), the degree of saturation (Sd) should never exceed 1.0. As shown in Figure 5, if ϕZs or $\frac{K_L a(V_L)}{Q_G Hc}$ is higher than 5.0, saturation of the exit gas bubble (Sd) would be greater than 99.33% but always less than 1.0. Conversely, if ϕ Zs is lower than 0.1, saturation of the exit gas bubble should be less than 10%. If Sd is greater than 1.0, it indicates experimental error in measuring one or more parameters, or an underestimate for Hc.

2.3 Diffusion Coefficients

2.3.1 Liquid Diffusion Coefficient

Theoretical and experimental investigations of molecular diffusion in binary systems have been studied for almost a century. The Stokes-Einstein equation (as cited by Sherwood, Pigford, and Wilke, 1975), based on a spherical solute molecular moving through a column of solvent, is

$$D_{AB} = \frac{kT}{6\pi r\mu} \tag{47}$$

where r is the radius of the "spherical" solute, k is Boltzmann's constant, and μ is viscosity of the solvent. Although this fixed relation was derived for a very special situation, many authors have used the form as a starting point in developing correlations for molecular diffusivity (Reid et al. 1987). Two widely used correlations are described in the next sections.

2.3.1.1 Othmer and Thakar Method

For dilute aqueous solutions Othmer and Thakar (1953) developed a correlation as follows:

$$D_{AB} = 5.57 \times 10^{-4} \mu V_A^{-0.6} \tag{48}$$

where

V_A = molal volume of solute A [cm^3/mole]

μ = viscosity of water [kg/m-sec]

The average error in using equation (48) for the estimation of D_{AB} in aqueous systems is 10 to 15 percent (Sherwood, Pigford, and Wilke, 1975).

2.3.1.2 Wilke-Chang Estimation Method

Wilke and Chang (1955) modified Stokes-Einstein equation to provide a procedure for estimating molecular diffusivity as follows:

$$D_{AB} = 7.4 \times 10^{-8}[(Y M_B)^{0.5} \frac{T}{\mu_B V_A^{0.6}}] \tag{49}$$

where

D_{AB} = mutual diffusion coefficient of solute A at very low concentration in solvent B [cm^2/sec],

Y = association parameter of B usually taken as 2.6 for water [dimensionless],

M_B = molecular weight of the solvent [g/mole],

μ_B = viscosity of the solvent [cp],

V_A = molal volume of the solute at its normal boiling point [cm^3/mole], and

T = temperature [K].

The association parameter Y is introduced to define the effective molecular weight of the solvent with respect to the diffusion process. For nonassociated solvents Y = 1 and for the water (associated solvent) Y = 2.6. The correlation represented by equation (49) is satisfactory for estimation of diffusion coefficients in dilute solutions with sufficient precision for most engineering purposes, i.e., about 10% average error (Wilke and Chang, 1955).

2.3.2 Gas Diffusion Coefficient

The kinetic theory of gases, in which molecules are regarded as rigid spheres performing elastic collisions, is well developed. For binary gas systems at low pressures in the ideal-gas law a widely used expression (Reid et al. 1987) is:

$$D_{AB} = \frac{0.00266\, T^{3/2}}{P M_{AB}^{0.5}\, \sigma_{AB}^{2}\, \Omega d} \qquad (50)$$

where

D = diffusion coefficient [cm^2/sec],

T = absolute temperature [K],

M_{AB} = $2\,(\frac{1}{M_A} + \frac{1}{M_B})^{-1}$,

M_A = molecular weight of solute [g/mole],

M_B = molecular weight of gas [g/mole],

P = pressure [bar],

σ = length [A °], and

M_A = molecular weight of air [g/mole), and

P = pressure [bar].

2.4 Relation of Mass-Transfer Coefficient to Diffusivity

2.4.1 Dimensionless Analysis

The dimensionless analysis presented by Roberts et al. (1982) suggests that the functional equation for forced-convection mass transfer is

$$Sh = c1\ Re^{c2}\ Sc^{c3} \tag{52}$$

where

Sh = $\frac{kd}{D}$, Sherwood number [dimensionless],

Re = $\frac{ud}{\nu}$, Reynolds number [dimensionless], and

Sc = $\frac{\nu}{D}$, Schmidt number [dimensionless].

solving for k yields

$$k = c_1 u^{c2}\ d^{(c2-1)}\ \nu^{(c3-c2)}\ D^{(1-c3)} \tag{53}$$

where

d = characteristic length [L],

u = characteristic velocity [L/time],

ν = kinematic viscosity of water [L^2/time], and

D = diffusivity of the solute [L_2/time].

Ωd = diffusion collision integral [dimensionless].

Ωd is a function of temperature; it depends upon the choice of the intermolecular force between colliding molecules. σ also depends upon the intermolecular force selected. To use equation (50), an intermolecular force law must be chosen and the constants σ_{AB} and Ωd must be evaluated. Usually the Lennard-Jones potential (Reid et al. 1987, pp. 582) is used to estimate these quantities. It is very important to employ values of σ_{AB} and Ωd obtained from the same source. Published values of these parameters differ considerably, but using σ_{AB} and Ωd estimates from the same source often provide satisfactory results (Reid et al., 1987).

Several proposed semi-empirical corrections for estimating D_{AB} in low pressure binary systems have the general form of equation (50), with empirical constants based on experimental data. Lugg (1968), in an extensive study of 147 vapors diffusing in air, found that the Wilke and Lee (1955) and Chen and Othmer (Reid et al., 1987) correlations fit best. However, the latter employs critical constants not available for all compounds.

The Wilke and Lee correction (1955) is used in this study, as follows:

$$D_{AB} = \{0.00303 - 0.00098\, M_{AB}^{-0.5}\} \frac{T^{3/2}}{P M_{AB}^{0.5} \sigma_{AB}^{2} \Omega d} \qquad (51)$$

D = diffusion coefficient [cm^2/sec],

T = absolute temperature [K],

M_{AB} = $2\,(\frac{1}{M_A} + \frac{1}{M_B})^{-1}$,

M_A = molecular weight of solute [g/mole),

Equation (53) shows that the mass-transfer coefficient is a function of turbulence, the kinematic viscosity, and the diffusion coefficient. Under known experiment conditions (same temperature and hydrodynamic), the characteristic length, turbulence, and kinematic viscosity of water will not vary with different organic compounds. Therefore, we can assume that k_L is only proportional to D^n, where n = 1-c3. The exponent n of diffusivity coefficient will depend on which model is used and will be discussed in the following section.

2.4.2 Comparison of exponent value of diffusivity with three mass transfer models

The two-film model predicts the mass transfer coefficient's dependence on the first-power of molecular diffusion coefficient (Lewis and Whitman, 1924), that is $K_L \propto D^n$ where n = 1. Moreover, it usually neglects the effective film thickness which may depend on the hydrodynamic conditions and surfactant effects. Other aeration models, such as penetration theory (Higbie, 1935) and surface renewal (Danckwerts, 1951), predict that mass transfer across an air-water interface is proportional to the square root of the molecular diffusion coefficient (n = 0.5). Therefore, the mass transfer coefficient is related to the molecular diffusivity, D, by the expression

$$k_L \propto D^n \tag{54}$$

where D = molecular diffusion coefficient and $0.5 \leq n \leq 1.0$.

Under very turbulent conditions, n approaches 0.5 (surface-renewal model or penetration theory), while under less turbulent conditions n approaches 1.0 (two-film model). Thus, the choice of a particular model to predict mass-transfer rates should depend on

0.47 which is very close to value 0.50 commonly found in the literature. The data support the concept of adding individual phase resistance, and suggest that overall coefficients may be reliably calculated from the individual coefficients.

2.4.3.1 Gas-film side exponent: m

Several researchers have proposed values of gas-film exponent m from 0.61 to 1.0 (Mackay and Leinon, 1975; Mackay and Yeun, 1983) and suggested that m = 0.67 is the best estimate. Tamir and Merchuk (1978) have reported that the gas-film mass transfer coefficient, k_G, varies as the diffusivity, D_G, raised to the power of 0.684 (≈ 2/3). Yadav and Sharma (1979) showed that k_G varies as $D_G^{0.5}$. Because gas phase diffusivities are proportional to $M^{-0.5}$ according to the simple kinetic theory of gases (Reid et al., 1987), one can use the following correlation in the absence of data on diffusivity.

$$k_{G,i} = k_{G,j}(M_j/M_i)^{1/3} \tag{58}$$

where

M_i, M_j = molecular weights of the solute i and j [g/mole]

2.4.3.2 Liquid-film side exponent: n

There is less data on the dependency of k_L on M (molecular weight). Matter-Muller et al. (1981) reported $k_L \propto M^{-0.5}$ for hydrocarbons and chlorohydrocarbons. Some experimenters have suggested exponent values for n. Rathbun and Tai (1981) analyzed volatilization data for a number of chlorinated hydrocarbons presented by Dilling (1977) to obtain a value of n = 1.19; however, the 95% confidence limits were

the degree of turbulence in the system (Atlas et al. 1982).

2.4.3 The additivity of two-film resistance

The result of dimensional analysis and comparison of the three mass-transfer models suggests that the mass transfer coefficients for VOCs as compared to the mass transfer coefficient for oxygen, depend only on the diffusion coefficient of the compounds. Therefore, we can propose that k_L is proportional to D_L^n and k_G is proportional to D_G^m, where D_L and D_G are the molecular diffusivities in water and air, respectively.

Liquid-film side:

$$k_{L\,VOC} = k_{L,O2}\,(D_{L,VOC}/D_{L,O2})^n \tag{55}$$

Gas-film side:

$$k_{G\,VOC} = k_{G,O2}\,(D_{G,VOC}/D_{G,O2})^m \tag{56}$$

If we substitute equations (55) and (56) into the two resistance equations (equation 16), we obtain:

$$\frac{1}{K_{LVOC}} = \frac{1}{k_{LO2}(D_{LVOC}/D_{LO2})^n} + \frac{1}{(Hc)k_{GO2}(D_{GVOC}/D_{GO2})^m} \tag{57}$$

The concept and validity of equation (57) has been confirmed by Goodgame and Sherwood (1954) who measured transfer coefficients for vaporization of water into air, and the absorption of carbon dioxide, ammonia, and acetone from air into water. They assumed both exponent m and n to be equal to 0.5 and found that the observed and calculated values of K_L agreed well, if these exponents were taken as

$\pm$ 0.64. Tamir and Merchuk (1978 and 1979) found n = 0.632 based on data from evaporating several pure liquids into pure gases. Roberts and Daendliker (1983) measured $k_L \propto D_L^{0.66}$ for six chlorinated and fluorinated hydrocarbons. Smith et al. (1980) found $k_L \propto D_L^{0.61}$. Mackay and Yeun (1983) report values of n to be 0.5 and 0.67 and suggest that $k_L \propto D_L^{0.50}$ is the most reliable.

2.5 Modified Ψ-value for application of semivolatile and volatile compounds

According to the relation of mass-transfer coefficient to diffusivity, previous studies (Smith et al. 1980, 1981; Matter-Muller et al. 1981; Rathbun and Tai 1982, 1984; Mumford and Schnoor 1982; Roberts et al. 1983, 1984a; Truong and Blackburn 1984; and Cadena et al. 1984) have defined the proportional relationship of mass transfer coefficients between VOCs and oxygen as Ψ:

$$\Psi = \frac{k_{LVOC}}{k_{LO2}} = \left(\frac{D_{LVOC}}{D_{LO2}}\right)^n \simeq \frac{K_{LVOC}}{K_{LO2}} \qquad (59)$$

where

Ψ	=	transfer constant proportionality coefficient, dimensionless,
k_{LVOC}, k_{LO2}	=	local mass transfer coefficient for VOC and O_2 [1/time],
D_{LVOC}, D_{LO2}	=	liquid diffusivities for VOC and O_2 [L^2/time], and
K_{LVOC}, K_{LO2}	=	overall mass transfer coefficient for VOC and O_2 [1/time].

Rathbun and Tai (1980, 1981) found that this approach was useful for stream flow. Studies in engineering systems have also shown to produce very good results (Smith 1981; Roberts 1982, 1983, 1984a). This method is potentially very valuable for engineering applications, since the oxygen transfer coefficients are often known.

The VOCs mass transfer coefficients can be estimated using the Ψ value which is estimated from known diffusivities.

The technique is only valid for highly volatile compounds in which liquid phase resistance is almost equal to the total resistance. However, gas-film transport becomes more important as turbulence increases and the Henry's coefficient decreases. In this study we are proposing the modified Ψ-value (Ψ_M), corrected by accounting for liquid-film resistance, as a method of predicting stripping rates for semi-volatile and volatile organic compounds (VOCs). The Ψ-values corrected for fraction of liquid resistance can be derived (the derivation is shown in Appendix A) from the two-resistance model as follows:

$$\Psi_M = \frac{K_{LVOC}}{K_{LO2}} = \left(\frac{D_{LVOC}}{D_{LO2}}\right)^n \frac{R_L}{R_T} = \Psi \frac{R_L}{R_T} \tag{60}$$

where

Ψ_M = modified Ψ-value [dimensionless],

Ψ = $\frac{k_L a_{VOC}}{k_L a O_2} = \left(\frac{D_{LVOC}}{D_{LO2}}\right)^n$ [dimensionless], and

R_L, R_T = liquid and gas resistance, respectively [dimensionless].

Consequently,

$$\Psi = \Psi_M \frac{R_T}{R_L} \tag{61}$$

We can apply equation (61) to estimate volatilization rate for compounds of intermediate and low volatility as long as the mass transfer coefficient of oxygen and fraction of liquid-film resistance are known. Such a methodology improves

estimation of stripping rate for intermediate and low-volatility compounds by incorporating liquid resistance. In order to estimate volatilization rate of particular compound conveniently, equation (60) can be rearranged as:

$$K_{LVOC} = K_{LO2} \left(\frac{D_{LVOC}}{D_{LO2}}\right)^n \frac{R_L}{R_T} = K_{LO2} (\Psi) \frac{R_L}{R_T} \tag{62}$$

Therefore,

$$K_{LVOC} = \Psi_M K_{LO2} \tag{63}$$

2.6 Mixing and Scale-up of Surface Aeration

2.6.1 Characterization of Hydrodynamic Conditions

A surface aerator is characterized by the mechanical creation of large liquid/gas interfaces by the impeller action in the creation of a hydraulic jump. The associated oxygen transfer from the atmosphere is assumed to be a function of three possible mechanisms (Schmidtke et al. 1977):

1. Entrainment of oxygen in the hydraulic jump,
2. Oxygen absorption from air bubbles, and
3. Oxygen absorption due to surface turbulence.

Eckenfelder et al. (1967) attempted to determine the amount of oxygen transferred by the three mechanisms. He concluded that approximately 60% of the oxygen transfer resulted from the liquid spray generated in the hydraulic jump and 40% from bubble entrainment and surface turbulence. Kishinevsky (1956) concluded

that the amount of oxygen transfer from the free surface into the liquid by molecular diffusion is negligible during conditions of high turbulence.

The hydrodynamic conditions of surface aeration can be characterized by interpreting power consumption. By means of dimensional analysis, the power consumption of impellers (power number) can be correlated with the Reynolds number. These numbers are described in the following sections.

2.6.2 Impeller Reynolds Number

The Reynolds number (Re), the ratio of inertia force in the impellers to viscous forces in the fluid, can be used to represent the presence or absence of turbulence in an impeller-stirred tank as follows:

$$Re = \frac{Da^2 N \rho}{\mu} \tag{64}$$

where

N = rotational speed [r/s],

Da = impeller diameter, [m] or [ft],

ρ = fluid density, [kg/m^3] or [lb/ft^3], and

μ = viscosity, [Pa-s] or [lb/ft^3].

Flow in the tank is turbulent when Re > 10,000. Thus, viscosity alone is not a valid indication of the type of flow to be expected. Schmidtke et al. (1977) divided turbulence into two fluid regime regions: (1) high turbulence - where eddy diffusion is the predominant mass transfer mechanism; (2) low turbulence - where molecular diffusion is predominant. Between Re of 10,000 and approximately 10 is a transition

range in which flow is turbulent at the impeller surface and laminar in remaining parts of the tank; when Re < 10, flow is laminar only.

2.6.3 Power Number

Power number, relating to fluid density, fluid viscosity, rotational speed, power input, and impeller diameter, is defined as:

$$Po = \frac{g_c P}{\rho N^3 Da^5} \tag{65}$$

where

Po = power number [dimensionless],

P = power input [N-m/s] or [ft-lbf/s],

g_c = dimensional constant [32.2 (ft-lb)/(lbf-s2)] [g_c = 1 when using SI units], and

ρ = density of liquid [mass/volume].

2.6.4 Power Measurement

In order to draw power curves for a reactor, it is necessary to measure power input at various impeller speeds. A convenient and accurate procedure to determine power is to measure the torque generated by the rotating agitator. The power can be estimated from the torque as follows:

$$P = \tau\omega = \tau(2\pi N) \tag{66}$$

where

P = power input [lbs-in/s],

τ = torque imposed on impeller [lbs-in],

ω = rotational velocity [radius/s], and

N = rotational speed [rpm].

In order to convert P to units of horsepower, when the units of τ are [lb-ft], equation (66) can be transformed to

$$P = \tau(2\pi N)(\frac{1}{12})(\frac{1}{60})(\frac{1}{550})\ (746) = (1.183 \times 10^{-2})\ (\tau N) \tag{67}$$

where

P = impeller horsepower [watt],

N = rotational speed [rpm], and

τ = torque imposed on impeller [lbs-in].

2.6.5 Power Consumption of Impellers

The power drawn by an impeller in a liquid mixing system is determined by its rotational speed and geometry, as well as by the environment in which is operates. Using dimensional analysis Holland and Chapman (1966) obtained

$$Po = c1(Re)^{c2}(Fr)^{c3} \tag{68}$$

Equation (68) relates the power number Po to the Reynolds number, Re; the Froude number, Fr, and a dimensionless shape factor, c1. The Reynolds and Froude numbers represent ratio of inertial to viscous and gravitational forces. For nonvortexing systems, gravitational forces have a negligible effect, and the exponent c3 of the Froude number is zero. Therefore, $(Fr)^{c3} = 1$ and equation (68) becomes

$$Po = c1(Re)^{c2} \tag{69}$$

A plot of power number (Po) versus Reynolds number (N_{Re}) on log-log coordinates is usually named a power curve.. An individual power curve is valid only for a particular geometrical configuration, but is independent of reactor size. Figure 7 illustrates the typical power curve for impeller operating in baffled and unbaffled cylindrical vessels. The power curve for baffled vessels explains some general principles. At Reynolds numbers less than 10 (segment A-B), which is typical for laminar flow, the power number is highly dependent of Reynolds number. As the Reynolds number increases, the flow changes from laminar to turbulent (segment B-D). When the flow becomes fully turbulent (segment D-E), the power curve becomes horizontal which indicates the flow is independent of the Reynolds number and the power number is essentially constant. Under constant power number, scale-up of mixing can be achieved (Nagata, 1975).

2.6.6 Scale-up of Mixing

The scale-up equations for surface aeration are generally in terms of performance indices such as power per unit volume (P/V), torque per unit volume (τ/V), or speed ratio (N2/N1). These are termed "translation equations" (Uhl and Essen, 1987). Translation equations, also called scale-up rules, have become popular in recent years. Uhl and Essen (1987) suggested that the most frequently used relationships for scale-up rule was constant power input per unit volume. It is often expressed as Hp/1000 gal.

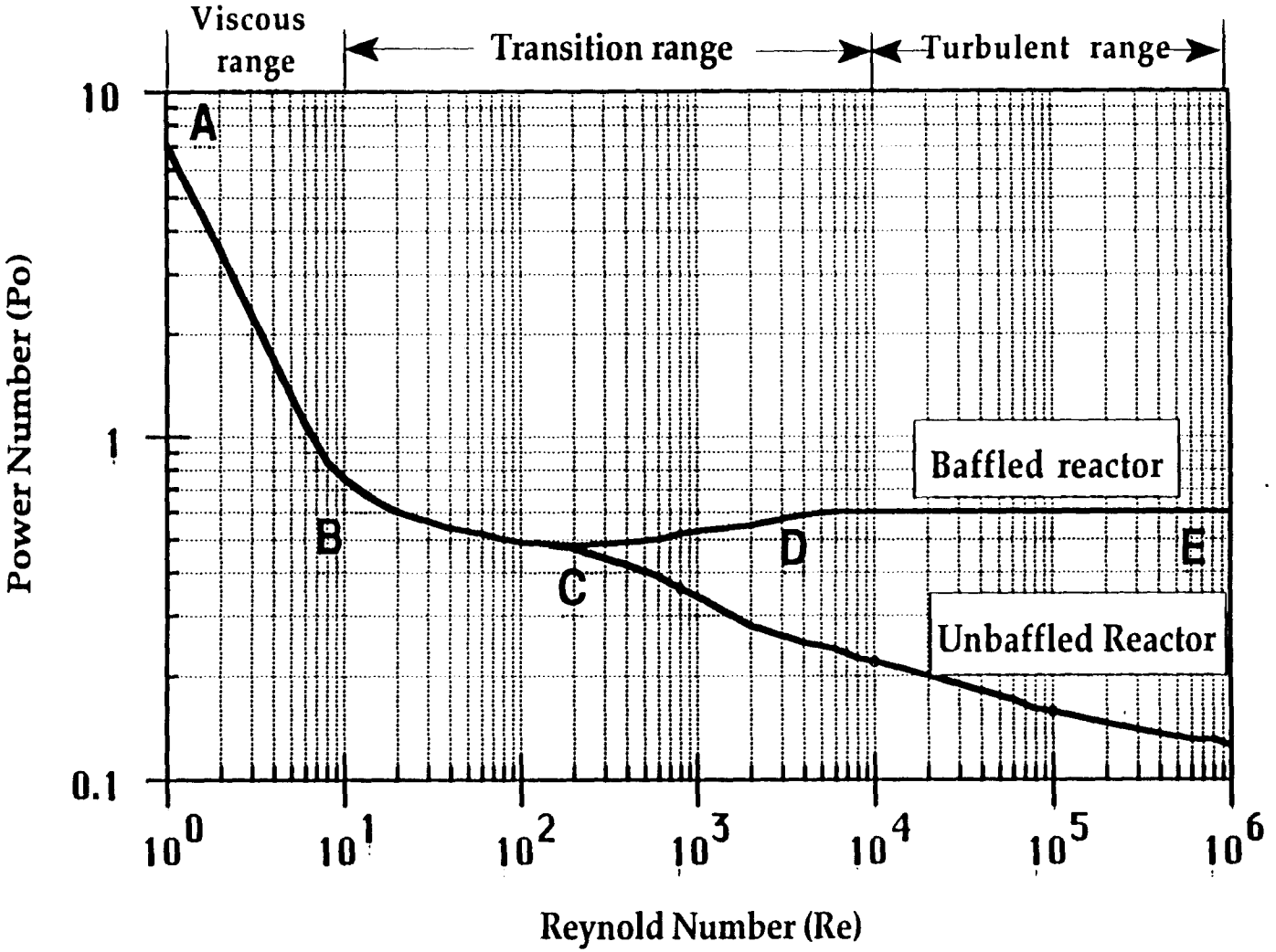

Figure 7. Power consumption curve of a mixing impeller (after Uhl & Essen, 1987)

Hwang and Stenstrom (1983) conducted experiments in three geometrically similar baffled cylindrical aeration tanks of 30 gal, 55 gal, and 200 gal liquid volumes to develop scale-up equation which indicates that volumetric mass transfer coefficient can be related to power input per unit volume as:

$$K_L a_{O2} = 0.032 \left(\frac{P}{V}\right)^{0.97} \tag{70}$$

where

$K_L a_{O2}$ = oxygen transfer coefficient [1/hr]

$\frac{P}{V}$ = power input per unit volume [watt/m^3]

Another relation, which is termed the "speed correlation," appears to have been first introduced by Rushton (1951). More recently Schmidtke et al. (1977) have popularized this approach. They developed a scale-up equation for unbaffled, square, surface turbine agitated, geometrically similar tanks. This relationship requires that geometric similitude be strictly maintained. For constant impeller immersion simplex ($\frac{HI}{DI}$), HI = impeller immersion depth, DI = impeller diameter) in both model and prototype, the scale-up is achieved when the overall oxygen transfer coefficient ($K_L a$) in a model and prototype are equal. The scale-up transform becomes:

$$\frac{N2}{N1} = \left(\frac{D2}{D1}\right)^{0.65} \tag{71}$$

where

N1, N2 = turbine impeller speed in model and prototype [$time^{-1}$], and

D1, D2 = turbine impeller diameter in model and prototype [L].

2.7 Flow Behavior of Air Bubbles in Bubble Column

Several workers (Hammerton and Garner, 1954; Haberman and Morton, 1956; Fair et al., 1962; Barnhart, 1969; Akita and Yoshida, 1974; Grace et al., 1976) have tried to correlate the mass-transfer coefficient, K_L, by the following parameters: equivalent bubble diameter, $d_{b,e}$; volumetric gas holdup ratio, ε; bubble rising velocity, u_s; fluid properties; geometry, etc. However, it is practically impossible to make a single general correlation due to the multiplicity of factors and interactions (Roberts et al. 1982). The major parameters of flow behavior are discussed in Section 2.7.1.

2.7.1 Shape and Motion of Bubbles

Haberman and Morton (1956) investigated the shape and motion of air bubbles in various liquids and observed that as bubble size increased, a change of bubble shape from spherical to ellipsoidal and from ellipsoidal to spherical cap occurred in all liquids. Barnhart (1969) correlated bubble shape and motion with Reynold's number as:

$Re < 300$	spherical bubbles act as rigid spheres
	the rise is characterized as rectilinear motion,
$300 < Re < 4000$	bubble has ellipsoidal shape
	the rise is characterized as helical motion, and
$Re > 4000$	bubbles formed spherical caps
	the rise is like rectilinear with rocking motion.

Garner and Hammerton (1954) observed phenomena of bubble shape and motion from straight to helical at bubble diameter of 1 mm in water. In the helical or zig-zag motion, the pitch and amplitude were both approximately two bubble diameters. The size of the helix increased with bubble diameter up to 5 mm, when the straight vertical rise interrupted the helical path. When bubble diameter was greater than 8 mm, bubbles nearly always rose in straight lines.

2.7.2 Bubble Rise Velocity

Bubble rise velocity, i.e. the speed of movement of bubbles with respect to the water, is a function of water quality, the size of the bubbles, and the hydrostatic pressure. Haberman et al. (1954) derived bubble size velocity in tap water from Stoke's law as a function of the equivalent bubble diameter. For a bubble rising at its terminal velocity, they defined the drag coefficient to be:

$$C_D = \frac{8}{3} \frac{g\, r_e}{3\,(u_s)^2} \tag{72}$$

where

C_D = drag coefficient,

g = gravitational constant,

r_e = equivalent radius of bubble, and

u_s = terminal velocity of bubble.

Haberman and Morton (1954) obtained a constant drag coefficient of 2.6 for spherical bubbles which could be rearranged to give an expression for terminal velocity of bubbles:

$$u_s = 1.02\,(g\,r_e)^{0.5} \tag{73}$$

Their results are shown in Figure 8. According to Figure 8, u_s is increasing up to 0.23 m/s with increasing equivalent diameter, until $d_{b,e}$ = 3.0 mm is reached. For $d_{b,e}$-values from 3 to 8 mm the rising velocity remains constant at u_s = 0.23 m/s. Thereafter, the rise velocity is increasing steadily again to achieve a maximum value of 0.35 m/s.

2.7.3 Gas Holdup

Gas holdup, the relative content of air dispersed in the water (ε), is determined by the ratio of air volume (Va) to the volume of water (V). For vertical walled vessels this corresponds to the relative increase of the water depth without aeration (h) compared to the total depth during aeration (ha):

$$\varepsilon = \frac{Va}{V} = \frac{(ha-h)}{h} \tag{74}$$

2.7.4 Specific Interfacial Area

The specific interfacial area a is defined as the ratio of the total interfacial area A divided by the volume of water under aeration V: $a = \frac{A}{V}\ [m^{-1}]$. A is defined as the surface area of all bubbles present in the water plus the area of the free surface. The latter can generally be neglected compared to the bubble surface area. When the number of air bubbles present in water (n) having a diameter ($d_{b,e}$) and also the gas holdup (ε) are known, then the specific interfacial area (a) can be calculated:

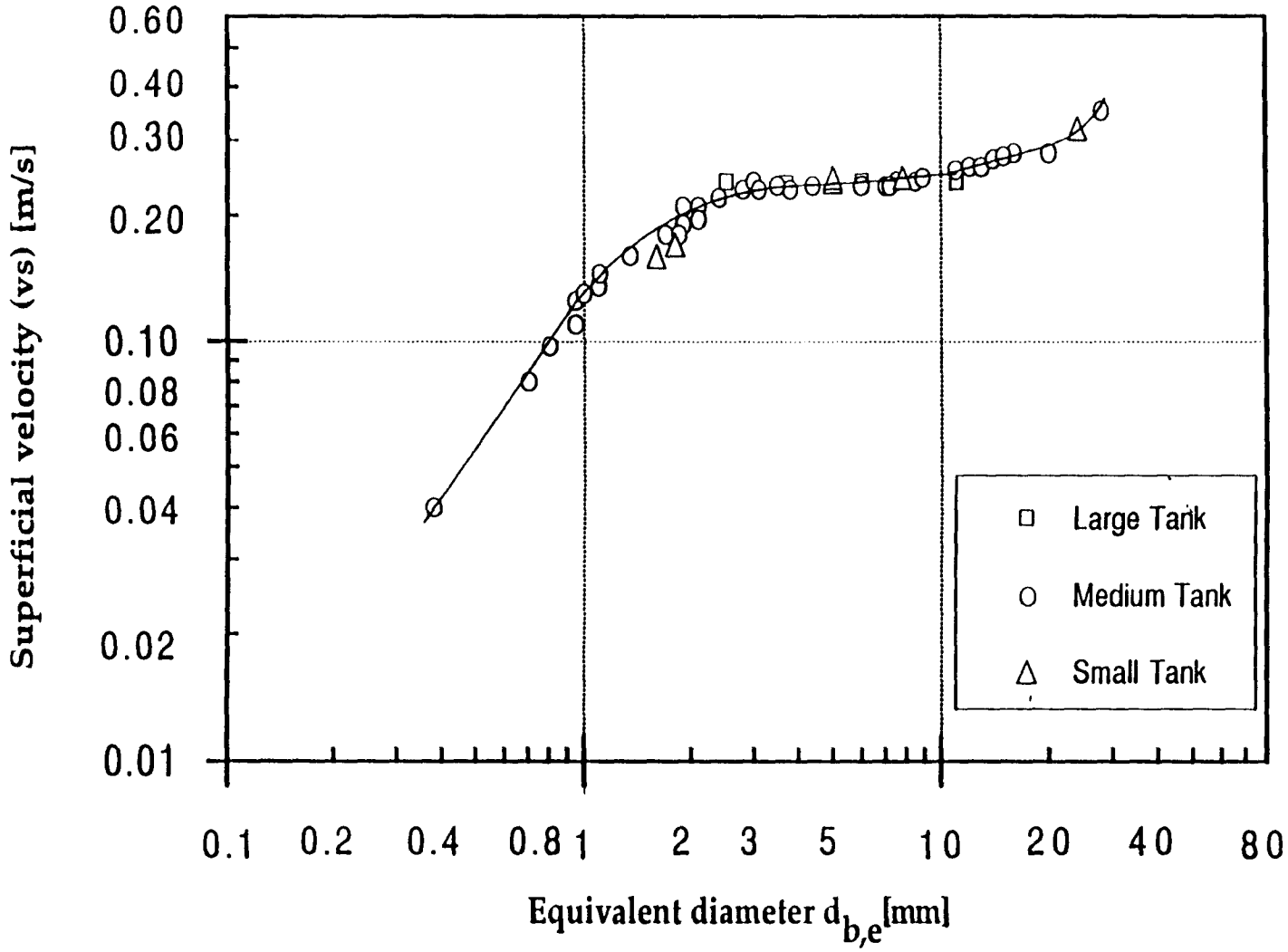

Figure 8. Superficial velocity (vs) of air bubbles in tap water as a function of the equivalent diameter

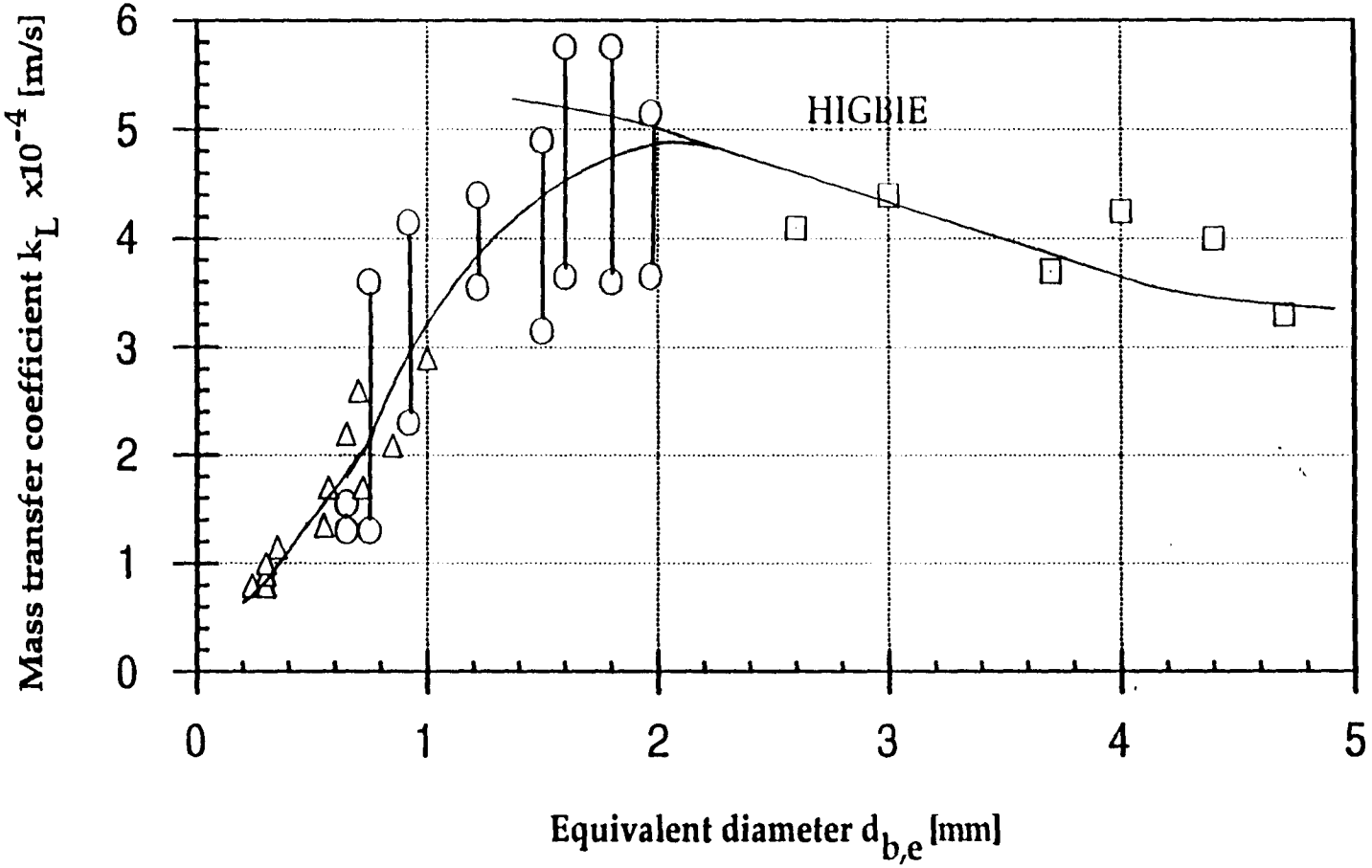

Figure 9. Mass transfer coefficient k_L as a function of the equivalent bubble diameter (Motarjemi et al., 1978)

$$a = \frac{6\varepsilon}{d_b} \tag{75}$$

2.7.5 Mass-Transfer Coefficient and Air Flow Rate

The overall mass-transfer coefficient of oxygen, K_L, in pure or tap water is related to the diameter of the air bubble by several workers (Coppock and Meiklejohn, 1951; Garner and Hammerton, 1954; Calderbank and Moo-Young, 1961; Barnhart, 1969; Akita and Yoshida, 1974). Figure 9 shows the corresponding coefficient as a function of the equivalent bubble diameter $d_{b,e}$ (Motarjemi et al. 1978). The mass-transfer coefficient increases exponentially over bubble sizes from 0.2 to 2.0 mm and gradually decreases thereafter to 5.0 mm diameter. Model equations for describing the first part of this range (0.2 to 2.0 mm) have not yet been proposed. The size range from 2.0 to 5.0 mm can be represented by the penetration theory (Higbie, 1935):

$$K_L = 2\left[\frac{D}{\pi t_r}\right]^{0.5} = 2\left[\frac{D\, u_s}{\pi (d_{b,e})}\right]^{0.5} \tag{76}$$

where

D = molecular diffusivity [m^2/s],

t_r = contact time of bubble during rise in water [s],

u_s = rise velocity of bubble in water [m/s], and

$d_{b,e}$ = equivalent bubble diameter [m].

Jackson and Shen (1978) and Jackson and Hoech (1977) related $K_L a$ value to the power of superficial air velocity, and found that the exponent varied from 1.08 and 1.13. Smith (cited by Schmidtke and Smith, 1983) developed a general dimensional relationship relating key parameters directly to oxygen transfer coefficient ($K_L a_{O2}$), as

follows:

$$K_L a_{O2} = 28.6\, Q_G^{0.86} V^{-1.06} Zs^{0.724} \tag{77}$$

where

Q_G = air flow rate [volume/time],

V = liquid volume [volume], and

Zs = diffuser depth [L].

Equation (77) predicted his data with a mean error of less than 8 percent. Eckenfelder (1959) also derived a nondimensional expression for $K_L a_{O2}$ as follows:

$$K_L a_{O2} = \frac{6\, Cc\, Q_G (Zs)^{2/3}}{d_e V} \tag{78}$$

where

Q_G = air flow rate [volume/time],

Cc = constant,

V = liquid volume [volume],

Zs = diffuser depth [L], and

d_e = equilibrium bubble diameter [L].

Since bubble diameter varies with gas flow rate over the range used in practice for the same reactor liquid volume and diffuser depth, equations (77) and (78) can be simplified as:

$$K_L a \propto Q_G^k \tag{79}$$

Eckenfelder (1959) found that the value of k depended on diffuser type as follows:

k = 0.71 - 0.77 for plate diffusers with full floor coverage,

0.78 for 4 nozzle spargers with centerline header,

0.45 for tube diffusers with one side header, and

0.8 - 1.0 for small orifice diffuser.

King (1955) independently derived equations based upon his experimental observation using bench scale experimental facilities, which showed the rate of oxygen transfer varied with (0.825 - 0.86) power of air flow rate, depending on liquid depth and geometry.

3. MATERIALS AND METHODS

3.1 Oxygen Transfer Measurement

A standard method for the measurement of oxygen transfer in clean water developed by ASCE (1984) was used to measure the rate of oxygen transfer from diffused and surface aerator to water. The test method was based upon removal of dissolved oxygen (DO) from the water volume by sodium sulfite followed by reoxygenation to near the saturation level. These DO concentrations may be either sensed in situ using membrane probes or measured by the Winkler or probe method applied to pumped samples. The procedure is frequently called the nonsteady-state reaeration method.

The data are then analyzed by a simplified mass transfer model to estimate the apparent volumetric mass transfer coefficient, $K_L a$, and the equilibrium concentration, C^*_∞. The basic model described in equation (18) can be integrated to obtain:

$$C_L = C^*_\infty - (C^*_\infty - C_{Lo})\exp[-K_L a(t)] \tag{80}$$

where

C_L = DO concentration [mgL^{-3}],

C^*_∞ = equilibrium DO concentrations, the concentration attained as time approaches infinity [mgL^{-3}],

C_{Lo} = DO concentration at time zero [mgL^{-3}], and

$K_L a$ = apparent volumetric mass transfer coefficient, [$time^{-1}$].

The recommended method to estimate the parameters $K_L a$, C^*_∞ and Co is the nonlinear regression (Stenstrom et al. 1988) based on the exponential form using

unsteady-state test data. Libra (1991) has reviewed this technique with other techniques and defined regions of power derivatives where different estimation methods are applicable. At high power density in subsurface aeration systems the nonsteady-state technique can introduce large errors due to gas side oxygen depletion. The range of experimental conditions used in this study avoids this problem.

The empirical parameters α, β and θ can be used to relate the oxygen transfer rate (OTR) in the field to the standard oxygen transfer rate. Standard oxygen transfer rate (SOTR) is defined as the amount of oxygen transferred to tap water at 20°C with zero initial dissolved oxygen concentration under 760 mm Hg barometric pressure and at 36% relative humidity. OTR is related to SOTR by:

$$OTR = \alpha\left\{\frac{\beta C^*_\infty - C_L}{C^*_\infty}\right\}\theta^{(T-20)}SOTR \tag{81}$$

$$\alpha = \frac{K_L a_{ww}}{K_L a_{cw}} \tag{82}$$

$$\beta = \frac{C^*_{\infty\,ww}}{C^*_{\infty cw}} \tag{83}$$

$$\theta^{(T-20)} = \frac{K_L a_{(T°C)}}{K_L a_{(20°C)}} \tag{84}$$

where

$K_L a$ = volumetric mass transfer coefficient [time^{-1}],

C^*_∞ = saturated DO concentrations [mgL^{-3}],

C_L = desired DO concentration at time zero [mgL^{-3}],

ww = subscript indicating wastewater,

cw = subscript indicating clean water (or tap water), and

$K_L a(T)$ = $K_L a$ at temperature T [$time^{-1}$].

Stenstrom and Gilbert (1981) provide a comprehensive review for α, β, and θ factors. The value of 1.024 for θ for test conditions close to 20°C has reached acceptability and has been incorporated into the ASCE Standard (ASCE, 1984). The β factor, normally close to unity, can be determined by the Winkler test (*Standard Methods*, 16th edition, 1985) if there are no test interferences, or can be correlated to total dissolved solids concentration. The α factor is dependent on the aeration system, geometry, power density as well as the wastewater characteristics.

3.2 Concerns Relating to the Use of Organics Mixtures

The use of solute mixtures and the presence of methanol may change experimental conditions, such as Henry's coefficients or α factors (see Section 2). Previous research (Roberts, 1986, 1987) indicated no mutual effects of organic mixtures on the Henry's coefficients for PCE, TCE, 111-TCA, chloroform, and dichloromethane in an aqueous mixture of the five compounds up to a total mixture concentration of 375 mg/L. Gossett (1987) verified that measurements of Henry's coefficient using the EPICS procedure on dilute, aqueous mixtures of solutes agree well with values obtained for single solutes. In this study, the maximum total organic mixture concentration was between 20 to 40 mg/L (in bubble column) and 10 to 140 mg/L (in EPICS) which was below Robert's experimental conditions. In order to meet the objectives of this research, it was necessary to conduct experiments with aqueous-phase mixtures containing 20 volatile compounds. Methanol was present in the systems, since it was used as a solvent in preparation of the stock mixtures that were injected into the

reactor or EPICS bottles.

3.3 Chemicals and Water

All volatile compounds were obtained from Aldrich Chemical Co. (St. Louis, MO) and Fisher Scientific Co. (Pittsburgh, PA). Methanol was high performance liquid chromatography grade from Fisher Scientific Co.

Truong and Blackburn (1984) have shown that the mass transfer coefficient of tap water and de-ionized water (DI) were similar. For convenience, tap was was used for all experiments, and was referred to as pure water. The conductivity of tap water was about 450 to 500 μmhos/cm. After adding sodium sulfide, the conductivity increased to about 650 to 700 μmhos/cm which was equal to 0.005 N KCl. Fresh tap water was used for each experiment. Conductivity measurements were made with a YSI glass probe, Model 3403 with cell constant 1.0 cm^{-1}.

3.4 Surface Aeration Experimental Description

3.4.1 Reactor for Preliminary Experiments

The cylindrical plexiglass reactor shown on Figure 10 was used in the surface aeration tests. The jacketed reactor was constructed of 40.00 cm long sections of concentric 23.50 cm diameter and 30.48 cm diameter plexiglass tubing. The reactor had a total volume of 17.4 liters. A working volume of 14.0 liters with water depth 32.3 cm was used in all preliminary experiments. A Haake KT 33 Circulating Water Bath circulated through the water jacket at a rate of up to 77.5 liters per hour to maintain the temperature in the reactor to within ± 0.3°C of the set point. The experimental conditions were modified slightly during the project and the differences and reasons for the

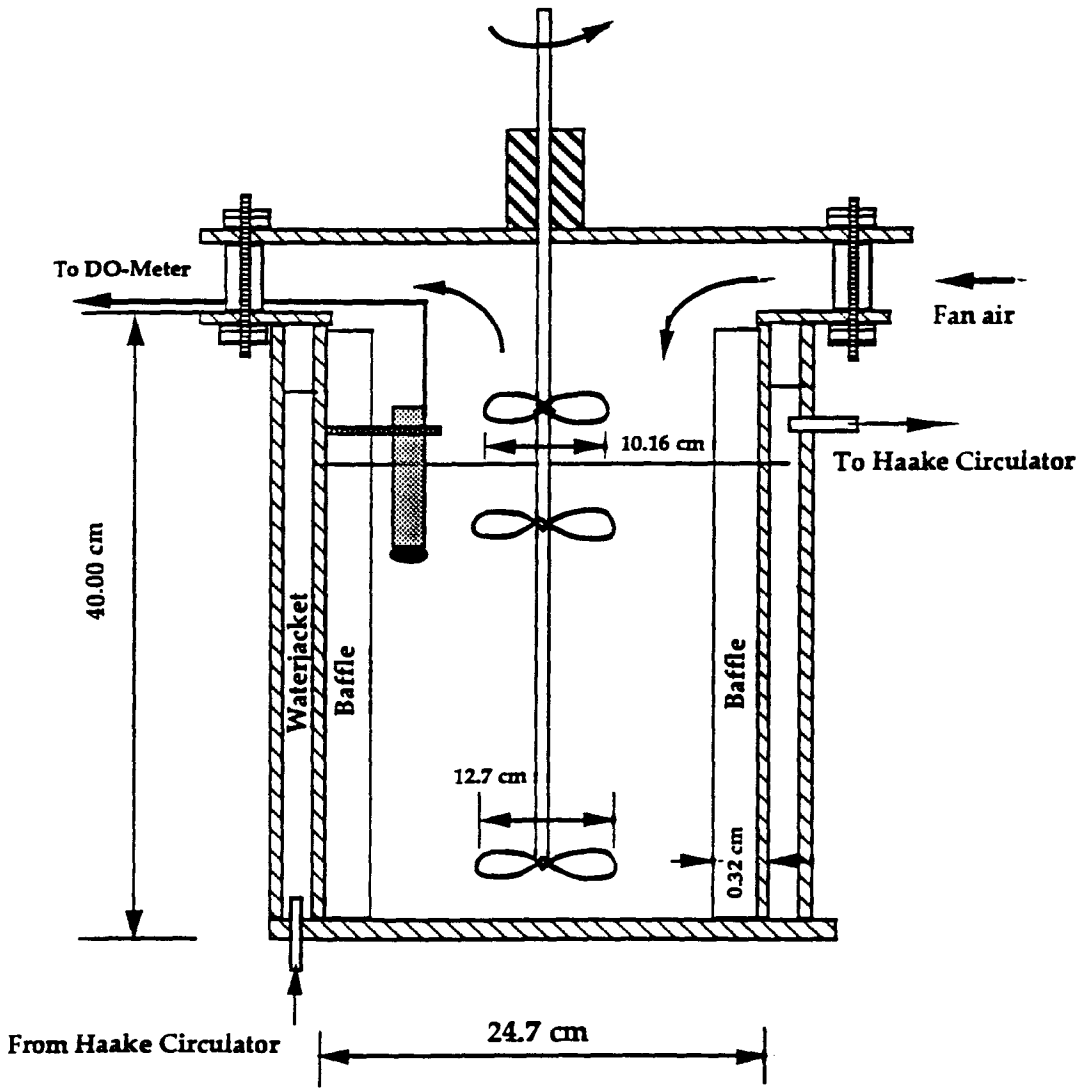

Figure 10. Configuration of surface aeration reactor

modifications are described in subsequent sections.

Agitation was provided by three axial flow impellers. The impellers were mounted on a common shaft and located at 6.35 cm, 28.49 cm, and 36.07 cm from the bottom of the reactor. The middle impeller, located about 3.81 cm below the surface of the liquid, assured adequate mixing of the bulk liquid at low speeds. The upper impeller, located 3.81 cm above the water surface, served as a gas agitator to maintain complete mixing in the headspace. The impellers were marine-type impellers provided by Michigan Industrial propellers (Grand Rapids, Michigan). The impellers mounted below the water surface had a diameter of 12.7 cm and a width of 3.18 cm, and the headspace impeller had diameter of 10.16 cm and a width of 2.54 cm. The reactor's cover contained a bearing to support the stirrer shaft to maintain consistent shaft and impeller position throughout the tests.

The driven system consisted of two parts, a permanent magnetic DC motor-generator (Motomatic by Electro-Craft Co.) and a solid state electronic controller (Master Servodyne by Cole Palmer, Chicago, IL). The motor and controller provide a signal which is related to the torque. The manufacturer's calibration charts were used to obtain torques. The impeller rotational speed was monitored by a General Radio Company stroboscope, type 1531-A. The speed can be varied from zero to 1725 rpm and the direction of flow is reversible. To assure adequate mixing and avoid vortex motion, four 7/8 in. (9.0% of the tank diameter) stainless steel baffles were inserted into the tank 90° apart. The use of baffles results in large top-to-bottom circulation without vortexing or severely unbalanced fluid forces on the impeller shaft.

3.4.2 Modified Surface Aeration Reactor I

The experiments performed in the modified reactor I were similar to those in the preliminary experiments. However, the cover was elevated 5.08 cm above the top of the reactor in order to allow access of large volumes of air to avoid the VOC headspace saturation problem. A 10.16 cm diameter personal fan (Krups, Model 952) was used to increase air circulation in the reactor's headspace. The air velocity above water surface was measured by an Air Velocity Meter (Kurz Instrument Inc., Series 440). The air velocity above the water surface ranged between 0.3 and 0.6 m/s (meter per second).

3.4.3 Modified Surface Aeration Reactor II

The difference between modified reactors I and II were water volume, location of impellers, and the size of fan (velocity of wind speed). The working volume of water was increased to 16.0 liters with a water depth of 36.83 cm. The location of impellers were changed to 6.35 cm, 30.48 cm, and 40.00 cm from the bottom of the reactor. The middle impeller was located 7.62 cm below the surface of the liquid. The upper impeller was located 3.18 cm above the water surface. A 40.64 cm fan (Dayton, Model 14C508D) was used to increase air circulation in the reactor's headspace. The wind velocity above the water surface ranged between 1.5 and 2.4 m/s.

3.4.4 Experimental Procedures of Surface Aeration

The impeller speed was first adjusted to the desired value by means of a stroboscope. After the water had been equilibrated to a constant temperature of 20°C, the oxygen was removed using sodium sulfide with a cobalt chloride catalyst. The cobalt

chloride dose was less than 0.5 mg/L. Theoretically, 7.9 mg/L of sodium sulfide is required for each mg/L of oxygen present. Since it was common practice to add 1.5 to 2.0 times of this amount to ensure complete deoxygenation, about 14 mg/L per mg of DO was used.

The target compounds were dissolved in methanol and approximately 5 ml was introduced with a pipette which provided approximately 1.0 - 2.0 mg/L initial concentration of each VOC in the surface aeration. The initial sample was taken after 1 minute of mixing. Next, 15 to 20 additional samples were taken. The sampling intervals were shorter at the beginning of a test due to the larger driving force. The samples were taken from the reactor with a 25 ml pipette and then transferred into two 9 ml hypovials and sealed with teflon-faced rubber septa. The vials were chilled to 4 °C on the day of collection and maintained at that temperature until analysis. Samples were allowed be allowed to warm to ambient temperature before analysis. Analysis was usually completed within one day after sampling.

The oxygen concentration in the reactor was measured continuously with a dissolved oxygen (DO) probe (Yellow Springs Instruments, Model 58) with a standard membrane and plotted on a strip chart recorder. At the end of each test three water samples were taken and analyzed for DO by the Winkler method. For data analysis mean values of initial and final temperature and liquid volume were used.

3.5 Bubble Column Experimental Description

3.5.1 Bubble Column

Figure 11 shows the bubble column which consisted of a 91.44 cm high, 20.32 cm plexiglass cylindrical column equipped with a bubble diffuser to introduce the air. Air diffuser stones supplied by Fisher Scientific Co. were used and were composed of fused crystalline alimina grains with an average pore size of 60 μm. The liquid volume was kept at a constant volume of 20.1 liters and air flow rates varied from 0.8 scfh (standard cubic feet per hour) to 5.4 scfh (2.52 L/min). The air flow was measured and controlled by Cole Parmer Model 3216-45G aluminum flowmeter with FM 102-05 flow tube (1/8" flow tube with glass float).

The dissolved oxygen concentration was measured with a YSI Model 58 dissolved oxygen meter with probe hanging upside down at 1/3 of submergence. In order to avoid excessive evaporation, the air was passed through a humidifier and then directed to the diffuser at the bottom of the column. The humidifier was made of 7.62 cm diameter and 91.44 cm height of clear PVC pipe filled with approximately 76.2 cm height of water equipped with air diffuser stones (same as used in the bubble column).

Both bubble column and humidifier were immersed in a water bath to maintain a constant water temperature of 20 ± 0.3 °C. A Haake KT 33 Circulating System which circulated the water bath was used to maintain the desired temperature.

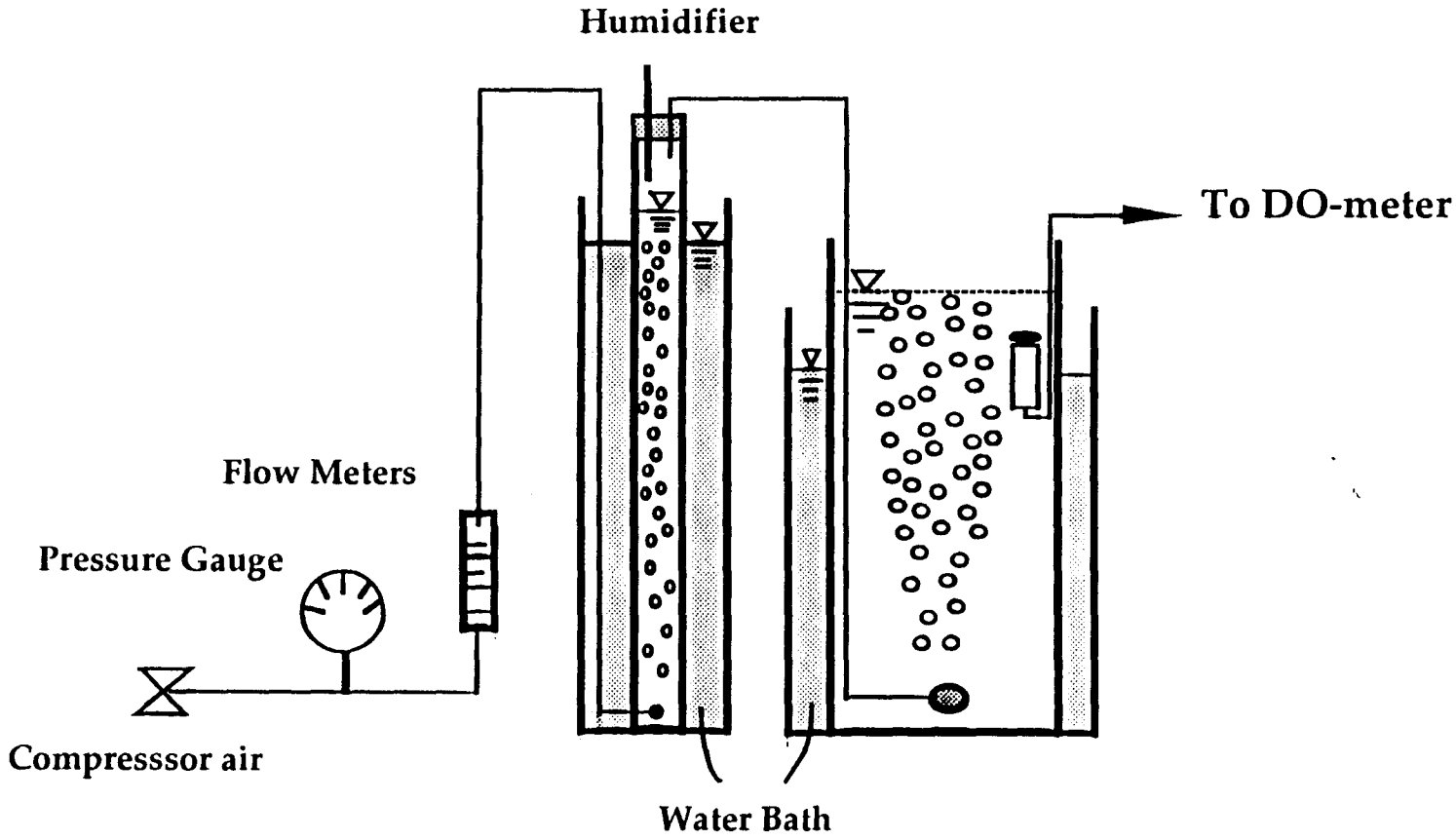

Figure 11. Schematic diagram of bubble column and appurtenances

3.5.2 Experimental Procedures for the Bubble Column

Before the test, the bubble column was washed with tap water thoroughly and dried overnight with a fan. Tap water was transferred into the column to the desired volume on the day before the experiment. During filling, a small air flow (approximately 0.27 scfh) was used to provide mixing and to avoid water entering the diffuser stone and air line.

After the water temperature reached 20°C the air flow was adjusted to the desired rate. Next, sodium sulfide and cobalt chloride were added to deoxygenate the water. The column was then spiked with the stock solution of twenty volatile compounds after the oxygen was reduced to almost zero. The target compounds were dissolved in methanol and approximately 5 ml was introduced with a pipette, which provided approximately 1.0 - 2.0 mg/L initial concentration of each VOC in the bubble column. The sampling procedure was the same as in the surface aeration tests and the sampling point was within 2 cm of the oxygen probe tip. The initial sample was taken after 3 minutes of bubbling. Next, 15 to 20 additional samples were taken as before. The sampling intervals were shorter at the beginning of a test due to a larger driving force.

3.5.3 Measurement of Bubble Diameter

Bubble diameter was measured using photography and is similar to the procedure described by Masutani (1988). A clear acrylic 1 ft x 1 ft x 3 ft box was used as an aeration vessel to determine bubble sizes. Bubbles were formed in an aeration vessel under conditions identical to the bubble column and were photographed using a

35 mm SLR camera fitted with a 55 mm macro lens. A ruler with 0.4 mm graduations was included in each photograph and served as a reference measurement. Bubbles were successfully captured at a shutter speed of 1/125 second with an automatic electronic flash for each flow rate. Bubble diameters were measured from projected slide images with suitable correction factors for enlargement. All bubbles in a 2.54 cm square template were measured.

3.6 Determination of Hc by EPICS Method

Four methods for determination of Henry's coefficients were compared in Section 2.1.2. The Equilibrium Partitioning in Closed System (EPICS) method (Gossett, 1987) was selected for its superior precision and simplicity, and its analytical requirements, which allowed the analysis of large numbers of samples in a reasonably short time.

3.6.1 Sensitivity Analysis of the Volume Ratio in the EPICS Procedure

In order to maximize the precision of the EPICS procedure, it was necessary to analyze the effects of the volume ratio of the bottles pairs. A sensitivity analysis was made to determine the minimum error in analysis $\frac{\Delta H}{H}$. Figures 12, 13, and 14 show the sensitivity of the volume ratio for different Henry's coefficient values (1.2, 0.2, 0.01). Thus, for a Henry's coefficient of 1.2, a volume ratio of 5 is required, whereas a volume ratio of 200 is requisite for Hc = 0.01. For a compound of intermediate volatility (Hc = 0.2), it is necessary to have a volume ratio of 10. The volume ratio of 10 was used to measure Hc in this study, since the largest serum bottle available had the volume of 120 ± 0.5 ml and the analytical balance had a capacity of 160 g with preci-

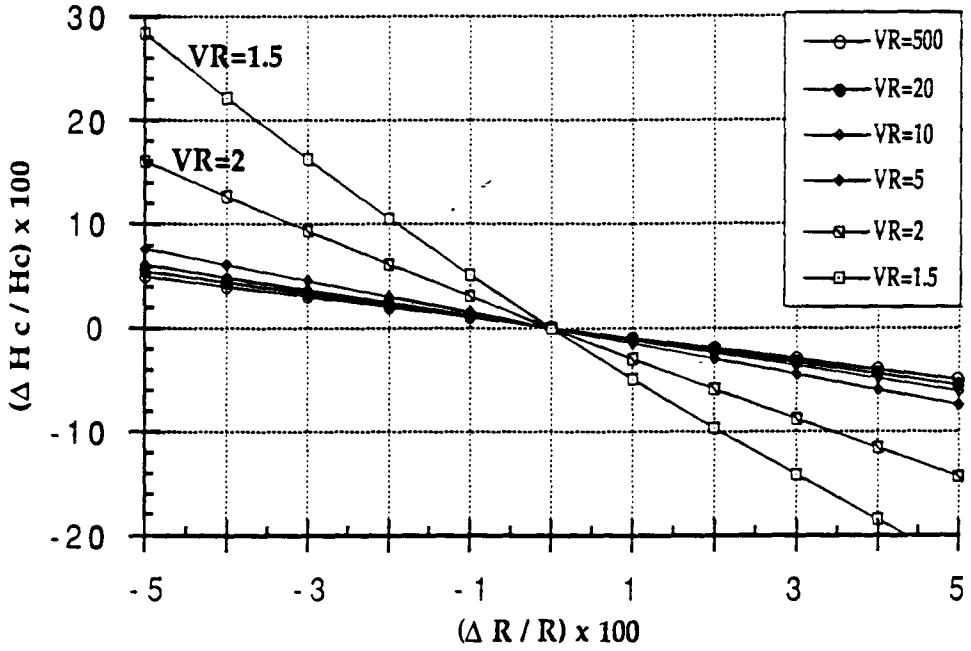

Figure 12. Senstivity analysis for the volume ratio within EPICS bottles pair to the change of Henry's coefficient for VOCs with Hc =1.2

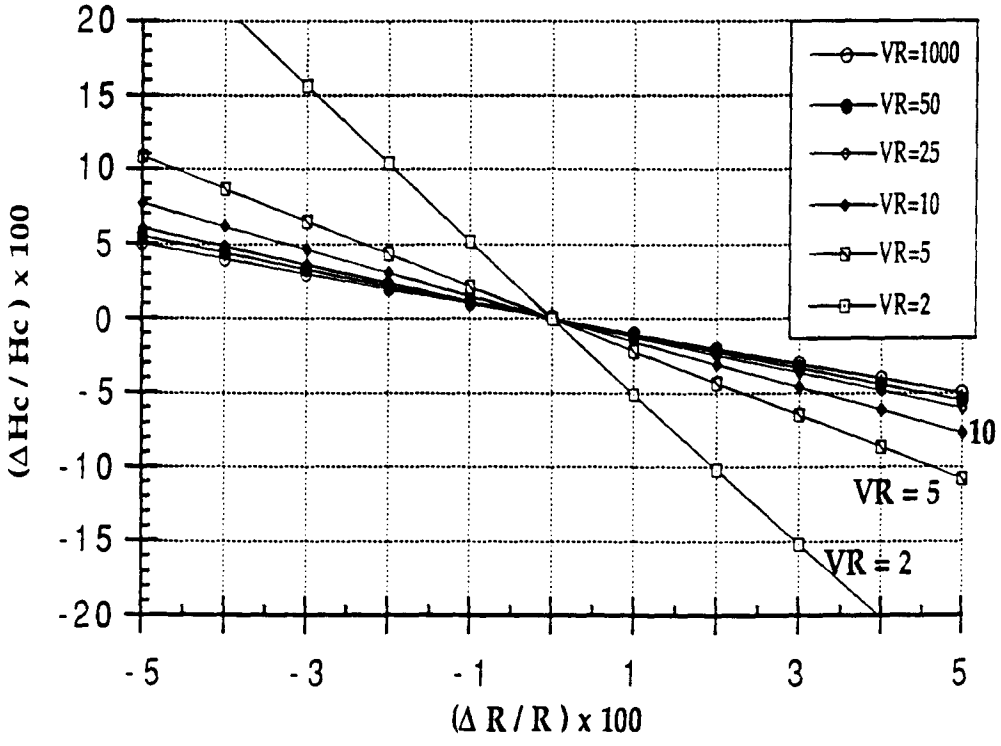

Figure 13. Senstivity analysis for the volume ratio within EPICS bottles pair to the change of Henry's coefficient for VOCs with Hc =0.2

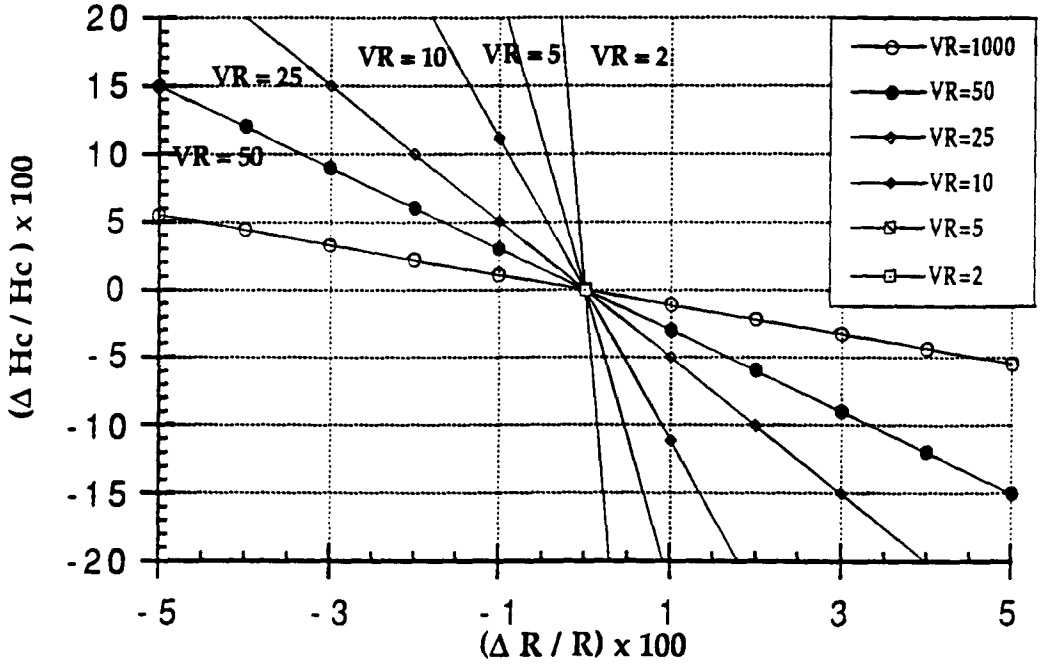

Figure 14. Senstivity analysis for the volume ratio with bottle pair to the change of Henry's coefficient for VOCs with Hc = 0.01

sion of 0.0001 g. The results for low volatility compounds with Henry's coefficient less than 0.04, such as naphthalene, EDB, bromoform, 1,1,2,2-TCA could have higher coefficient of variation (CV) than 7.5%.

3.6.2 Procedures of Measurement of Henry's Coefficient

For each Hc determination, 3 sets of 2 serum bottles, with 120 ± 0.5 ml of internal volume, were used. In order to maintain a volume ratio of 10, three of these bottles had liquid volumes about 10 ml; liquid contents of the remaining three bottles were about 100 ml. Deionized water was used as dilution water. After placing a known volume of water in a bottle, it was sealed with teflon-faced seals and aluminum crimp caps. The mixtures of compounds were injected under the water surface using a precision syringe. The serum bottles were weighed just before and after injection. The volume of liquid was determined gravimetrically because of its superior accuracy and precision. Next, the bottles were then shaken (at 2500 rpm) for 4 hours. At the end of shaking, serum bottles were placed in constant temperature water bath for 2 hours and then analyzed by purge-and-trap/GC.

Equilibrium was experimentally verified by analysis of a special series of bottles. Equilibrium in low liquid volume systems is very rapid, but high liquid volume systems take longer (Lincoff et al., 1984). Therefore, the experiment was performed using a high liquid volume with 20 VOCs to ensure that equilibrium would be attained for all compounds used. Fifty μL of stock solution containing 20 VOCs was injected into seven serum bottles containing 100 ml of distilled water. The bottles were then sealed and placed in a shaker table at 2500 RPM. At the end of each period of shaking, each serum bottle was placed in a 20°C water bath for 2 hours and then analyzed

by GC. The following liquid concentrations were measured at times ranging from 2 min. to 1378 min. The results of this experiment, shown in Figures 15 and 16, indicate that complete equilibrium was approached within about 30 min. The high fluctuation for naphthalene indicates a carry-over problem in the purge-and-trap sampler. The area corresponding to concentration in some compounds decreased slightly with elapsed time which implies the solute leaked from the bottles or adsorbed onto the glass or Teflon.

3.7 Organic Analysis - Analysis Procedure

The volatile compounds were analyzed by gas chromatograph having a purge-and-trap and flame-ionization detector (FID), which was used to provide both qualitative and quantitative information. The flame-ionization detector was chosen over an electron capture detector (ECD) since FID has a greater dynamic range.

The purge-and-trap device was a Tekmar Model 00-996367-00 set with the following program: 11 minutes purge, 4 minutes desorb, and 12 minutes bake time. The purge-and-trap device was attached to a Hewlett-Packard Model 5890 GC equipped with a flame-ionization detector (FID). Before initial use, the trap was conditioned overnight at 180°C by backflushing with an inert gas flow of at least 20 ml/min. During purging the trap was vented to the room, and not to the analytical column. Prior to beginning analysis each day, the trap was conditioned for 10 minutes at 180°C with backflushing.

The GC capillary column was a J&W (Folsom, CA) DB-624 with a 1.8 μm film thickness and the dimensions of 30 m by 0.32 mm diameter. GC time and tem-

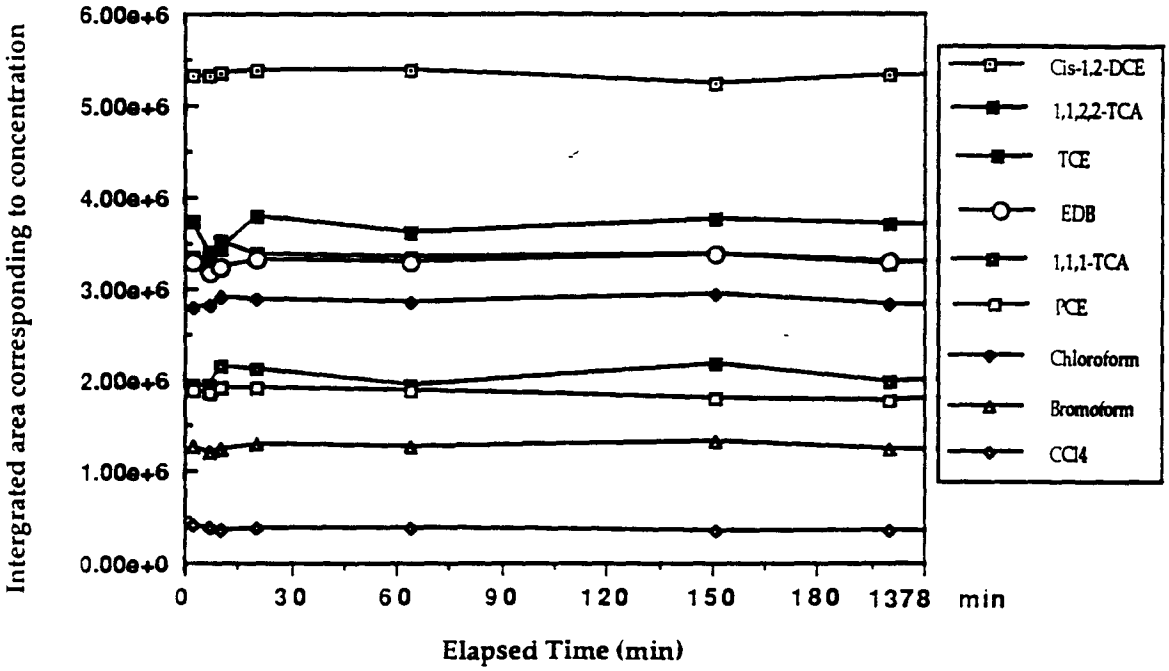

Figure 15. Equilibrium time required in EPICS serum bottle (a)

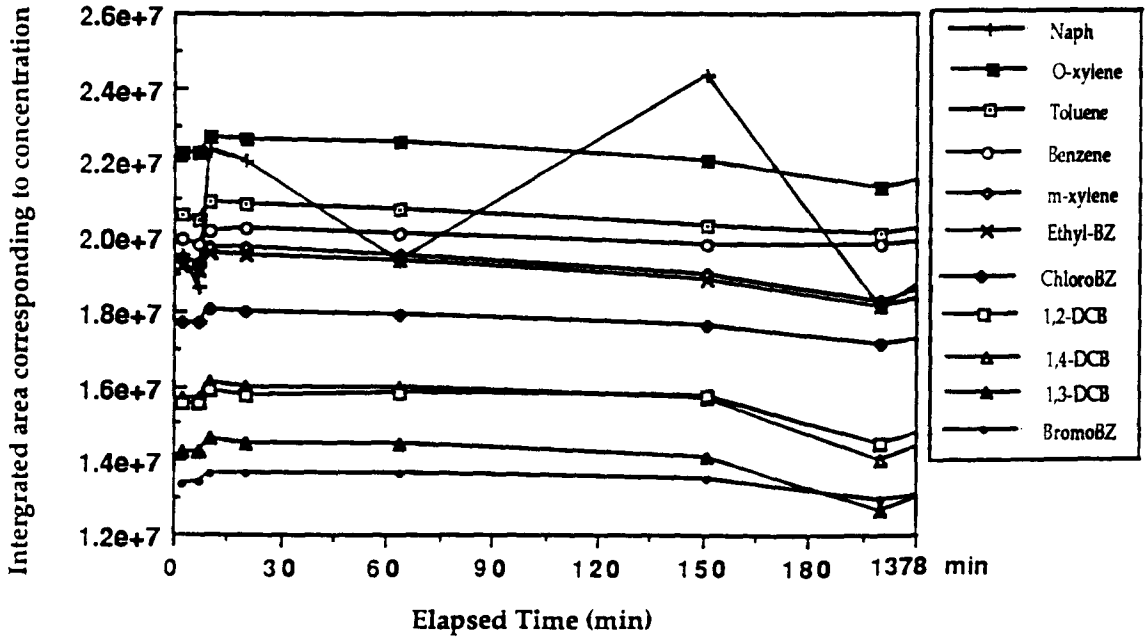

Figure 16. Equilibrium time required in EPICS serum bottle (b)

perature program were as follows: 35°C initial temperature, 150 °C final temperature, 5 minutes initial hold, 1 minute final hold time, and a 5°C/min temperature program. GC and purge-and-trap gases flow rate were controlled as follows: helium carrier gas at 20.0 ml/min, hydrogen combustion gas at 47.2 ml/min, and dry air purge gas at 314.8 ml/min. The Hewlett-Packard Model 3396A integrator used to record GC output had the following settings: attenuation of 4, chart speed of 0.5 cm/min, peak width of 0.04, area rejection of 3,000 and threshold of -1. Retention times of the twenty volatile compounds used in this research for these GC conditions are listed in Table 1. The typical plot of 20 VOCs analyzed by an HP 5890 GC and integrated by an HP 3396 integrator is shown in Figure 17. Figure 18 shows the concentrations of 20 VOCs versus elapsed time during surface aeration.

Prior to the analysis of samples, three compounds were used as external standards. Carbon tetrachloride (CCl_4), benzene, and bromoform were injected into the purge-and-trap at a concentration of 0.5 mg/L each. A maximum acceptable error (MAE) for these compounds should be less than 10%. The MAE was defined as:

$$\text{MAE}\,(\%) = \frac{(A - Ai)}{Ai} \times 100 \tag{85}$$

where

A = current integrated area from integrator corresponding to concentration, and

Ai = initial integrated area from integrator corresponding to concentration.

This criterion must be demonstrated before analyzing every set of test (about 20 samples). If the maximum acceptable error for any external standards was higher than

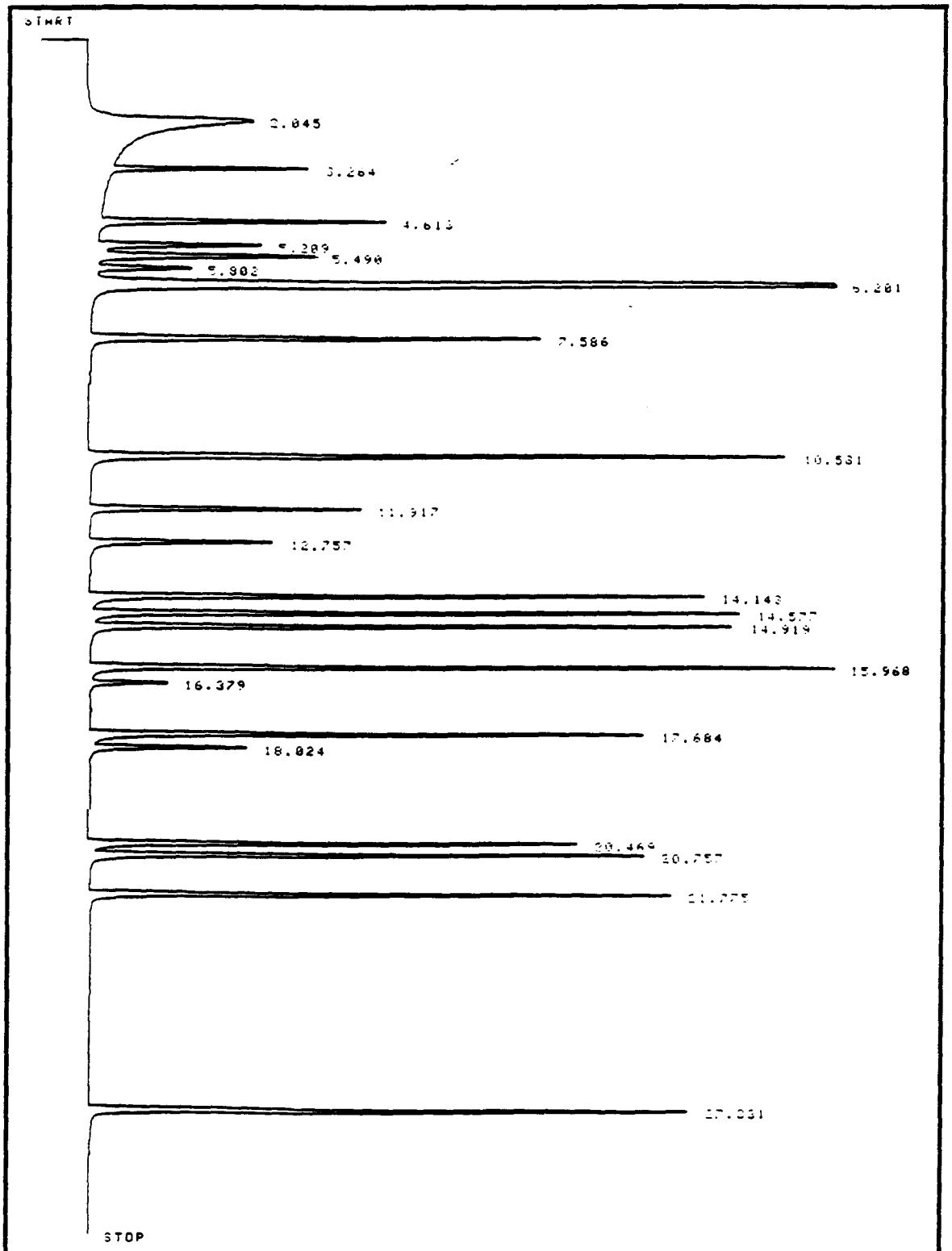

Figure 17. Typical chromatogram of twenty VOCs from Gas Chromatogaph

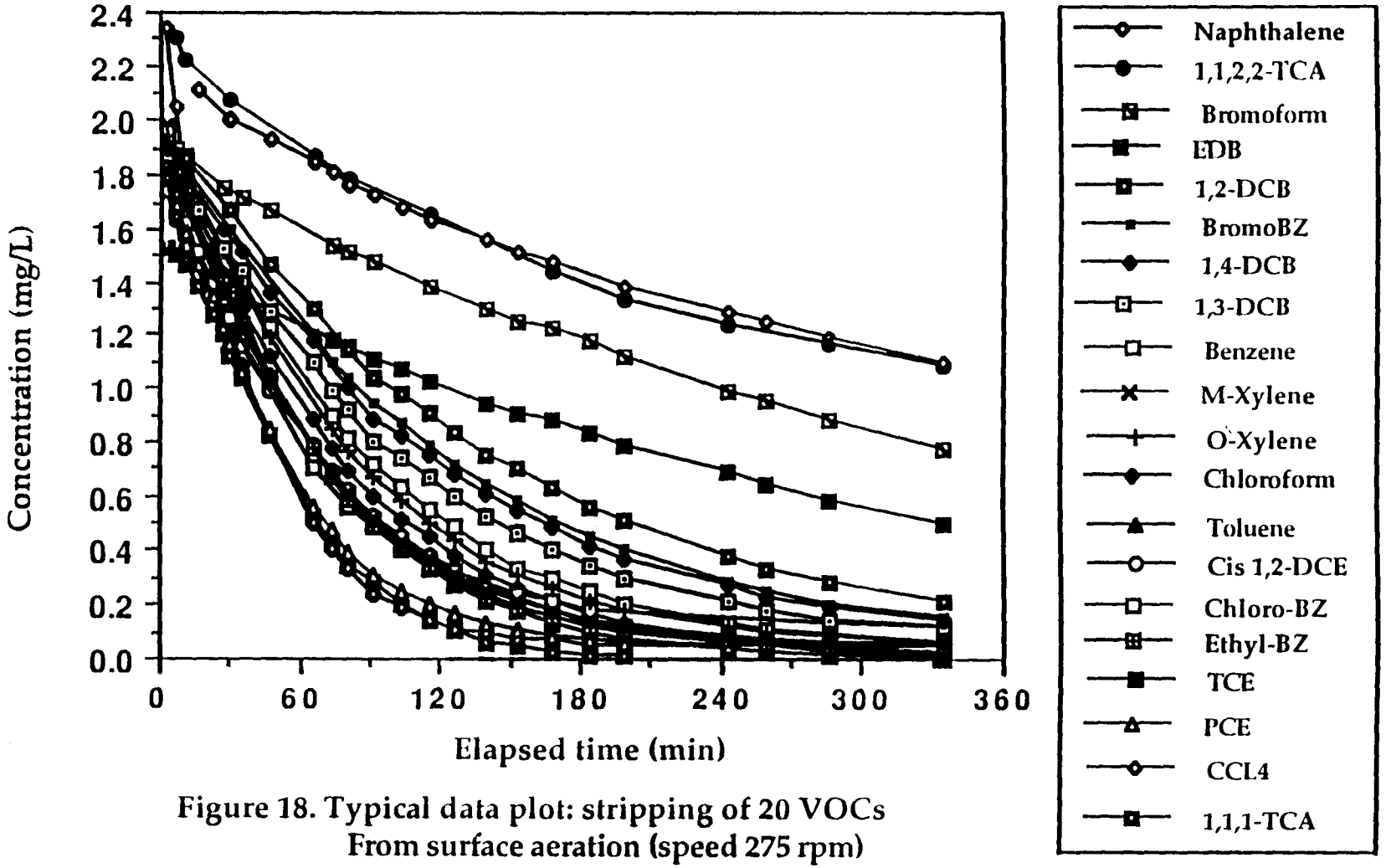

Figure 18. Typical data plot: stripping of 20 VOCs
From surface aeration (speed 275 rpm)

10%, the system (including purge-and-trap device, GC, helium, hydrogen, and air) were checked. The demonstration was performed again until the criterion was met.

3.7.1 Carry-Over Problem in Analysis Procedure

During analysis, the carry-over problem in the purge-and-trap sampler was found for naphthalene was, stated in Section 3.6.2. Several purge sample cleaning methods were developed in order to reduce this problem. The results are given in Table 2. The best results with carry-over of 3% were obtained by putting the purge sampler in the oven at 150°C for 15 min., followed by flushing with air for 10 min. This procedure was carried out through all the experiments.

3.8 Statistical Analysis

The mathematical expression of the two-resistance model with appropriate correction of diffusivity (equation 57) can be rearranged as follows:

$$X = A\,Y^n + W\,B\,Z^m \tag{86}$$

where

$$X = (K_{LVOC})^{-1},$$

$$Y = (D_{LVOC}/D_{LO2})^{-1},$$

$$Z = (D_{GVOC}/D_{GO2})^{-1},$$

$$W = \frac{1}{Hc},$$

$$A = \frac{1}{k_{LO2}},$$

$$B = \frac{1}{k_{GO2}},$$

Table 2 Comparison of cleaning method for purge sampler

Test No.	Clean Method	Original Intergrated area	Carry-Over Intergrated area	C-O* (%)
A-1	Pentane	2173842	419055	19.3
A-4	Methanol	1541070	515530	33.5
A-9	Air**	1351006	197779	14.6
B-2	Oven#+air	2780901	120408	4.3
B-7	Oven#+air	1604603	48721	3.0
B-8	Oven 30min	1789305	365866	20.4
B-9	AIr	1377819	236870	17.2
B-11	Air	1245888	127859	10.3

* Percentage of carry-over

** flush with air for 10 min

put in the oven (temperature 150 degree C) for 10 min

n = power of liquid diffusivity,

m = power of gas diffusivity, and

$$\frac{A}{B} = \frac{k_{GO2}}{k_{LO2}}$$

From equation (86), there were four knowns: X, Y, Z, W, and four unknowns: A, B, m, n. In the analysis, oxygen was used as the reference compound since it was the most volatile of the chosen compounds, and because oxygen transfer rates are generally known at wastewater treatment plants. We can assume that the overall oxygen of overall transfer coefficient was equal to the liquid film transfer coefficient. Therefore, A is known and there are three unknowns: B (the inverse of the gas film transfer coefficient of oxygen), m, and n to be estimated using three-parameter nonlinear regression.

The nonlinear regression (NLIN) procedure from SAS (Statistical Analysis System, 1982 edition) was used to fit the parameters of a nonlinear model by least-squares best fit. A typical program is shown in Appendix B.

The procedure was evaluated using Roberts' (1983) data. The additional degree of freedom (20 compounds used in this study, as compared to 6 compounds used by Roberts) provided better estimates of the parameters.

After a grid of values was specified, NLIN evaluates the residual sum of squares at each combination of values to determine the best set of values to start the iterative algorithm. The iterative algorithm regresses the residuals of the partial derivatives of the model with respect to the parameters until convergence is obtained.

4. RESULTS AND DISCUSSION

4.1 Results of Determination of Henry's Coefficient

4.1.1 Result of Measurement of Henry's Coefficient

Measured mean values of Henry's coefficient are shown in Table 3, along with observed coefficients of variation (CVs). The value shown in each test (Q12, Q14, and Q15) is the average value of nine sets of data. The results reported here are based upon studies in which mixtures of 20 compounds in methanol were used. In this investigation, tests Q12, Q14, and Q15 were carried out with the volume ratio of 10; this ratio was the largest our equipment allowed. The CVs values for test Q12, Q14, and Q15 were between 1.1% and 10.0%. Table 3 shows that the precision of EPICS procedure decreases as Hc decreases, except for CCl_4. The high CVs of CCl_4 is due to its lower GC response which produces higher deviation. The reduced precision and disagreement for these semi-volatile compounds was explained in Section 3.6.1. The volume ratio of 10 is satisfactory for Hc of 0.2 or greater. For low volatility compounds, greater precision in the EPICS procedure can be reached as the volume ratio is increased.

Present and previously reported Hc values for 20 VOCs are summarized in Table 4. The consistency of the data from this study is generally good. Mackay and Shiu (1991) have compiled estimates of Hc from a number of sources and found wide variations. In this study, among the low volatility compounds, the values of bromoform and EDB are a little bit lower than previous studies and literature data, whereas 1,1,2,2-TCA and naphthalene are very close to previous data. Mackay and

Table 3. Results of measurement of Henry's coefficients by EPICS

Compounds	Test-Q12#	Test-Q14#	Test-Q15#	Mean	STDEV*	% CV≠
12DCE	0.140	0.136	0.136	0.138	0.0025	1.8
CLF	0.133	0.136	0.132	0.134	0.0019	1.4
111TCA	0.526	0.508	0.523	0.519	0.0097	1.9
CCl4	1.261	1.400	1.287	1.316	0.0739	5.6
Benzene	0.198	0.195	0.194	0.196	0.0021	1.1
TCE	0.276	0.247	0.266	0.263	0.0147	5.6
Toluene	0.215	0.209	0.208	0.211	0.0036	1.7
PCE	0.573	0.562	0.560	0.565	0.0071	1.3
EDB	0.022	0.020	0.021	0.021	0.0011	5.1
CBZ	0.124	0.121	0.118	0.121	0.0032	2.6
EBZ	0.256	0.251	0.245	0.251	0.0055	2.2
m-xylene	0.230	0.224	0.219	0.224	0.0056	2.5
O-xylene	0.159	0.153	0.150	0.154	0.0045	2.9
Bromoform	0.022	0.019	0.020	0.020	0.0018	8.8
BBZ	0.076	0.082	0.075	0.078	0.0037	4.7
1122TCA	0.021	0.025	0.023	0.023	0.0022	9.7
13DCB	0.100	0.118	0.108	0.109	0.0091	8.3
14DCB	0.086	0.098	0.090	0.091	0.0061	6.7
12DCB	0.067	0.073	0.070	0.070	0.0028	3.9
Naphthalene	0.016	0.020	0.018	0.018	0.0018	10.0

Average of nine sets of data

* STDEV = standard deviation

≠ % CV = Percentage of coefficient of variation

Table 4. Summary of present Henry's coefficients with previously reeported data (760 mm Hg, 20 degree C)

Methods	EPICS	EPICS	EPICS	Batch-air stripping	Batch-air stripping	UNIFAC	Noll & Depaul	Mackay (25C)	Calculation	Calculation	EPICS	EPICS	Used in this study
Researchers	Gossett	Gossett	Ashworth	Mackay	Roberts	Arbuckle		recom	Low-value	High-value	Yurteri	Hsieh	
Year (19XX)	83 & 85	87	86	79	82	83	87	81	81	81	87	91	
12DCE	0.182	0.123	0.186						0.312	0.312	0.181	0.138	0.170
PCE	0.540	0.549	0.699	0.665	0.627		1.176	0.819	0.817	1.076	0.535	0.565	0.570
CT	1.264	0.971	1.206	1.139	1.007	0.992	1.236	0.928	0.965	0.965	0.936	1.316	1.122
111TCA	0.715	0.552	0.712	0.831	0.621	0.249	0.202	1.130	0.989	1.461	0.645	0.519	0.530
TCE	0.398	0.299	0.417	0.404	0.410		0.479	0.365	0.385	0.534	0.430	0.263	0.250
BZ			0.216	0.227		0.226	0.227	0.222	0.227	0.234	0.306	0.196	0.230
EBZ								0.323	0.266	0.423		0.251	0.260
TLN			0.262	0.266		0.339	0.242	0.270	0.229	0.287	0.244	0.211	0.230
MXY								0.283	0.245	0.358		0.224	0.240
OXY			0.199					0.202	0.181	0.230	0.175	0.154	0.180
CBZ			0.147	0.135		0.224	0.160	0.141	0.145	0.155	0.131	0.121	0.150
CLF		0.118	0.172		0.224		0.139	0.153	0.120	0.204		0.134	0.160
13DCB								0.145	0.150	0.150		0.109	0.120
12DCB								0.077	0.078	0.081		0.070	0.087
14DCB								0.065	0.060	0.071	0.078	0.091	0.110
BBZ								0.085	0.087	0.099		0.078	0.100
BF								0.025	0.026	0.026		0.020	0.041
1122TCA			0.010				0.018	0.019	0.020	0.020		0.023	0.042
NAPH						0.012		0.017	0.017	0.026	0.015	0.018	0.038
EDB									0.026	0.026		0.021	0.041

Shiu (1981) pointed out that the vapor pressure of naphthalene (a polynuclear aromatic) is very small and less accurately known, thus Hc values have wide error limits. They suggested the preferred method of obtaining reliable data for polynuclear aromatic compounds is to measure solubility, vapor pressure, and Hc and to check the internal consistency of the values. The vapor pressure of naphthalene is between 0.0109 and 0.0311 (kPa) and the solubility is between 22.0 and 34.4 (mg/L) (Mackay and Shiu, 1981). Usually, values of 0.0109 (kPa) and 34.4 (mg/L) predict an Hc value of 0.018. If we use the vapor pressure as 0.0311 (kPa) and a solubility of 22.0 (mg/L), the Hc value is four times higher. Henry's coefficient of low volatility compounds are rarely reported in the literature and the published values have wide variations. The higher estimates of Hc for low volatility compounds were used to provide a better fit the mass-transfer model for the bubble column.

4.1.2 Experimental Error of Determination of Henry's Coefficient

Random errors include analytical error and the precision of the volume measurements, V_L and V_G. Potential systematic errors include (a) incomplete equilibrium between the gas and liquid phase, (b) leaks from the bottles, (c) absorption (diffusion) of the solutes into the Teflon polymer matrix, and (d) adsorption of the solute onto glass or Teflon.

Findings from adsorption experiments by Munz and Roberts (1986) indicate that 1-2% of the C_2Cl_6 mass might have adsorbed onto the walls of the experimental vessels over the duration of an experiment (4-5 hour). Similarly, absorption/desorption experiments with CCl_4 suggest that most solutes will absorb or diffuse into Teflon in substantial amounts if given enough time. However, they are

confident that none of these potential systematic errors (a-d) had a significant influence on their experimental data. This suggests that the largest sources of error are the GC procedure and the analysis of volume ratios.

4.2 Results of Surface Aeration Experiments

4.2.1 Hydrodynamic Condition of Surface Aeration

The mixing conditions in the baffled surface aeration reactor were measured to facilitate scale-up. Figure 19 shows the power number as a function of the Reynolds number for the surface aerator reactor. Figure 19 can be separated into a turbulent and a transitional region, which is similar to the typical trend shown in Figure 7. In the range of Reynolds number between 60,000 and 130,000, the power number remains almost constant as 0.4; complete mixing can be assumed. The power number decreases slightly with the decrease of turbulence as a Reynolds number below 60,000; suggesting that the reactor is in a transition range. In the transition range, the molecular diffusion may have influence over certain degree of mass-transfer rate; thus, mass-transfer rate is expected to be much lower than that of complete mixing.

4.2.2 The Dependence of Oxygen $K_L a$ on Power Input

The $K_L a$-value of oxygen for the modified surface reactor II increased from 0.23 to 7.2 (1/hr) as the impeller speed was performed from 150 to 500 rpm. Figure 20 shows the dependence of log $(\frac{P}{V})$ on the impeller speed (N). The correlation is given by

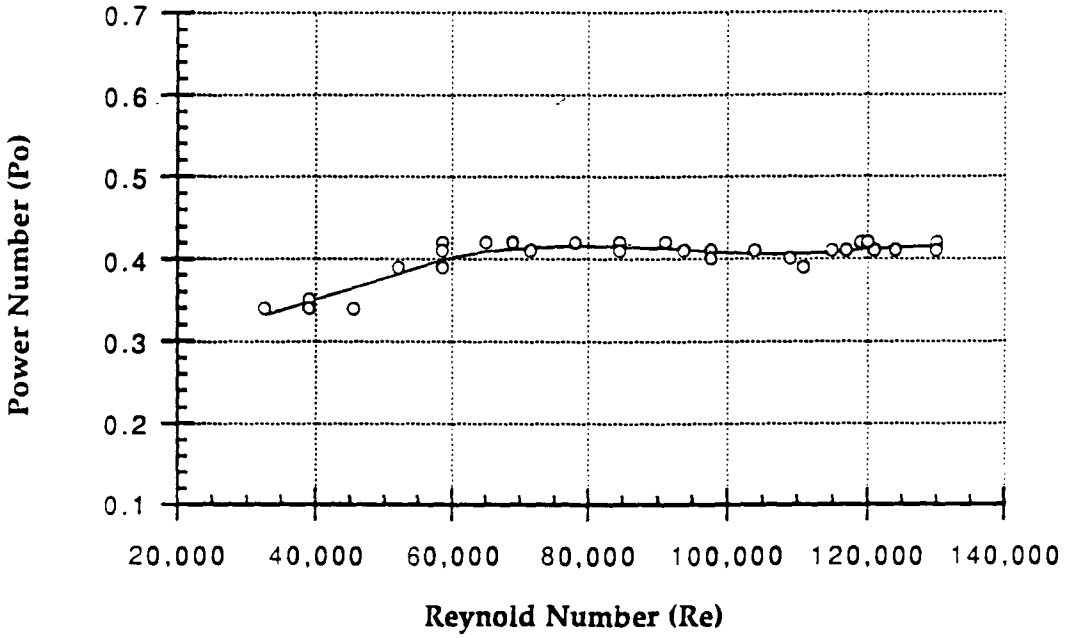

Figure 19. Power curve for impeller used in surface aeration experiments

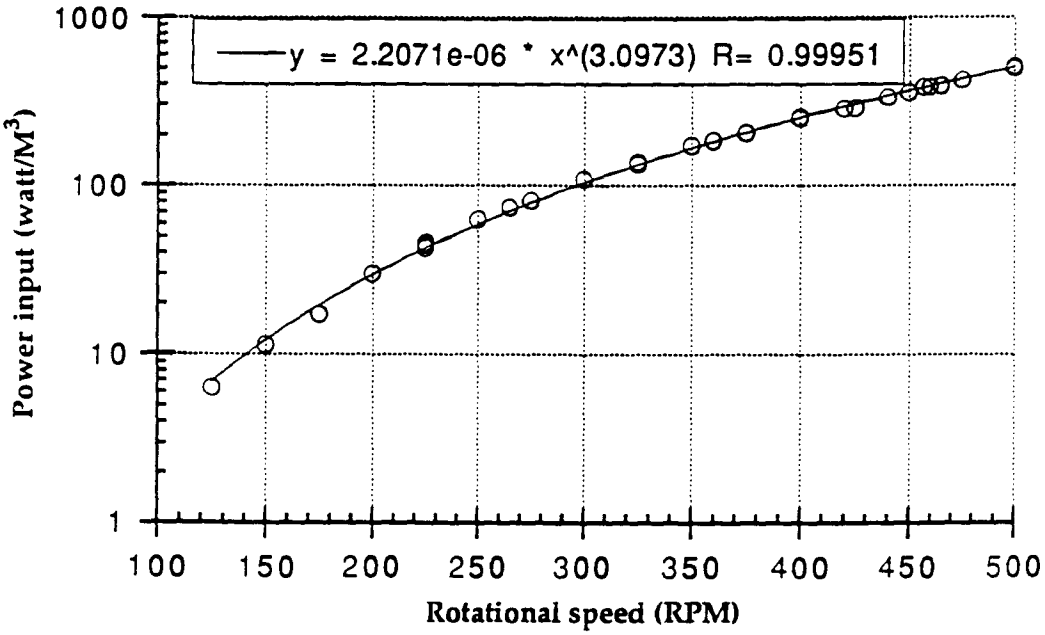

Figure 20. Correlation between power input and rotational speed in surface aeration

$$\frac{P}{V} = 2.0475 \times 10^{-6} (N)^{3.11} \tag{87}$$

where

$\frac{P}{V}$ = specific power input [watt/m^3], and

N = rotational speed [rpm].

This agrees well with equation (65) that the specific power input is proportional to third power of the impeller speed. The power input is between 0.13 and 8.0 watts which is equivalent to a range of specific power input from 8 to 500 watt/m^3. Paulson (1979) reported that the specific power input ranges from 8 to 60 watt/m^3 (0.04 to 0.3 hp/1000 gal) in the municipal activated sludge systems. Industrial activated sludge system power input may be much higher, up to 800 watt/m^3 (Libra, 1991). The range of specific power input used in this study covers the typical range in practice.

Figure 21 shows the oxygen transfer rate as a function of power input. Below, a specific power input of 30 watt/m^3 (Reynolds number less than 60,000), the turbulence is in the transition range. With very high power input (250 watt/m^3 < P/V < 500 watt/m^3), the aerator created a continuous sheet of spray and entrained air bubbles which increased the rate of oxygen transfer dramatically. Eckenfelder et al. (1967) reported that 60% of oxygen transfer came from liquid spray and 40% from turbulence entrainment. With high air entrainment, the mass-transfer model changes from pure surface aeration to a combination of diffused and surface aeration. Currently, no relationship exists to quantitatively describe this phenomenon. Therefore, this high power density region was excluded from further analysis.

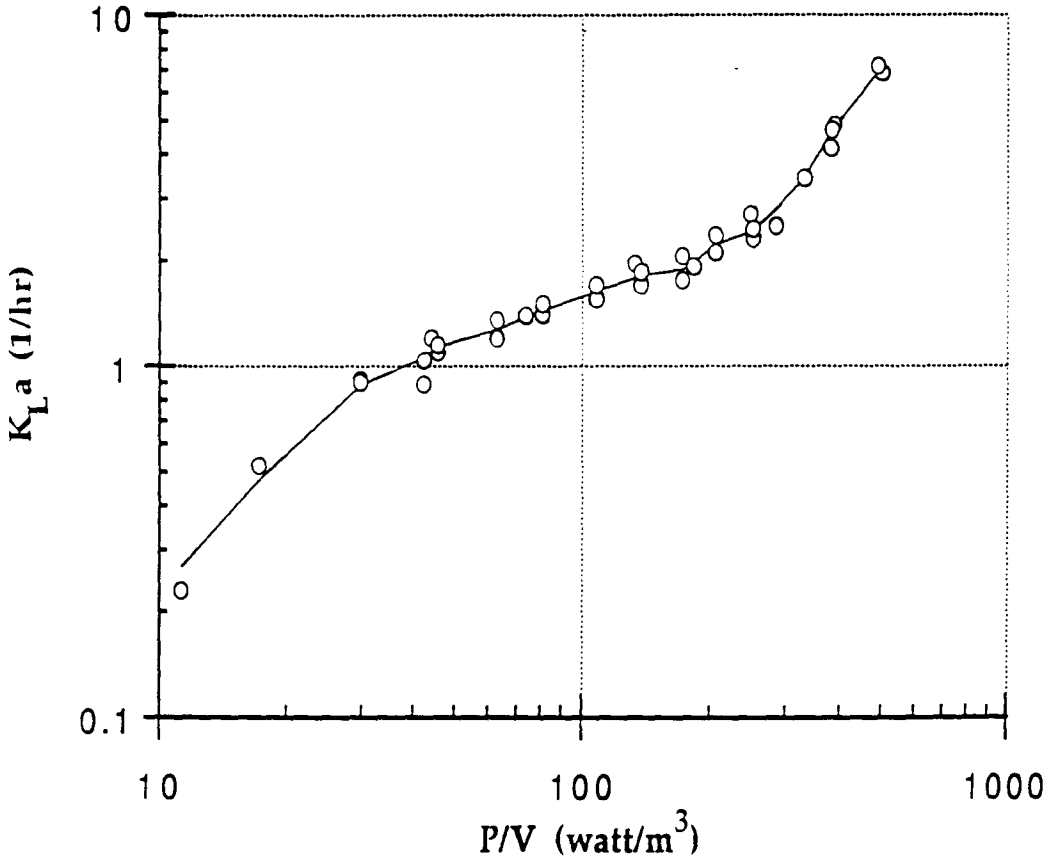

Figure 21. Oxygen transfer coefficient vs. specific power input in surface aeration

Using a power input range of 30 watt/m^3 < (P/V) < 250 watt/m^3, Kozinski and King (1966) predicted that the mass-transfer coefficient ($K_L a$) should be proportional to $(\frac{P}{V})^{1/3}$ for surface aeration at an unbroken liquid surface. Kozinski and King (1966) summarized twelve studies and reported $K_L a \approx (\frac{P}{V})^n$ with n ranging from 0.2 to 0.4 at an unbroken air-water interface. Figure 22 shows the correlation between the $K_L a$-value and unit volume of power input generates for the completely turbulent range (Nre > 60,000). The correlation is given by

$$K_L a = 0.167 \, (\frac{P}{V})^{0.483} \tag{88}$$

where

$K_L a$ = oxygen transfer coefficient [1/hr], and

$\frac{P}{V}$ = power input per unit volume [watt/m^3].

The n-value of this experiment is 0.48 as shown in equation (88) which is in approximate agreement with the observation reported by Kozinski and King (1966).

For impellers, the square root of power per unit volume divided by the viscosity is related to the mean velocity gradient, G. The equation is given by:

$$G = \left[\frac{P}{\mu V}\right]^{0.5} \tag{89}$$

where

G = mean velocity gradient [1/sec],

P = power requirement [watt] or [lb-ft/sec],

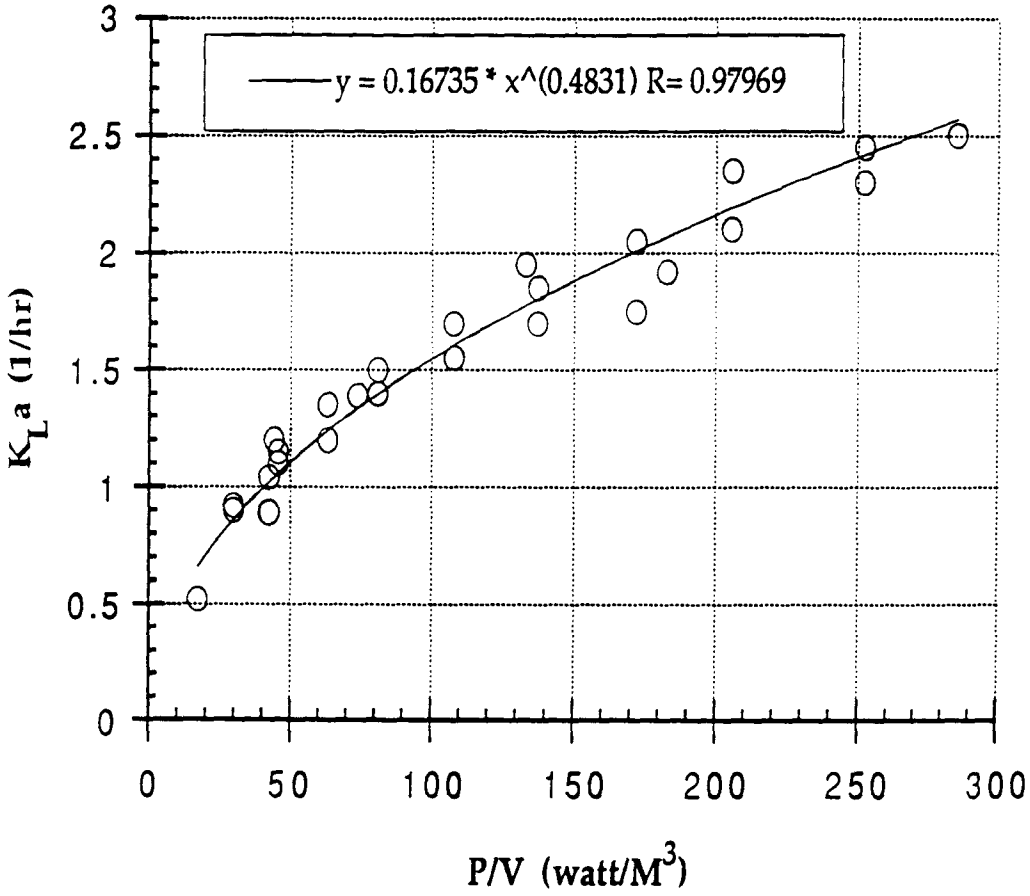

Figure 22. Correlation between oxygen transfer coefficient and specific power input in surface aeration

V = reactor volume [m^3] or [ft^3], and

μ = dynamic viscosity [N-sec/m^2] or [lb-sec/ft^2].

Figure 23 shows the dependence of log (G) on the impeller speed. For standard temperature (20°C), viscosity of water should be the same; hence, the square root of power per unit volume is proportional to G-value. Therefore, velocity gradient (G) can be used to correlate with $K_L a_{O2}$ as well. The correlation (Figure 24) is given by:

$$K_L a = 0.00843\ (G)^{0.91} \tag{90}$$

The velocity gradient in typical activated sludge plants ranges from 90 to 220 (1/sec) (Parker et al., 1970). The range of G-value used to correlate $K_L a$ in this study is between 180 to 500 (1/sec).

4.2.3 Determination of Volatilization Rate of VOCs

The mass-transfer rate equation (91) was employed to estimate volatilization rate of VOCs and expressed as follows:

$$\ln\left[\frac{C_L}{C_{Lo}}\right] = -K_L a\ (t - t_o) \tag{91}$$

Using equation (91), a semi-log plot of $\frac{C_L}{C_{Lo}}$ versus $(t - t_o)$ can obtain a slope of $K_L a$. A typical plot for the results of an experiment with toluene is shown in Figure 25. Using this technique, an estimate of the initial concentration is critical for the accuracy of the $K_L a$-value. Equation (91) can be transformed from logarithmic to exponential form as follows:

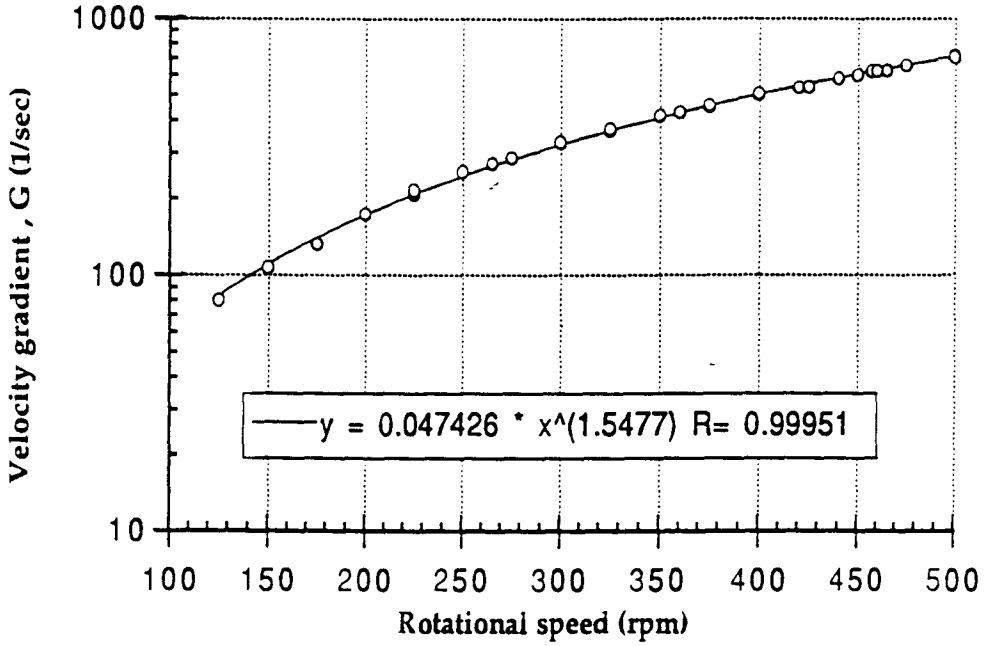

Figure 23. Correlation between velocty gradient and rotational speed in surface aeration

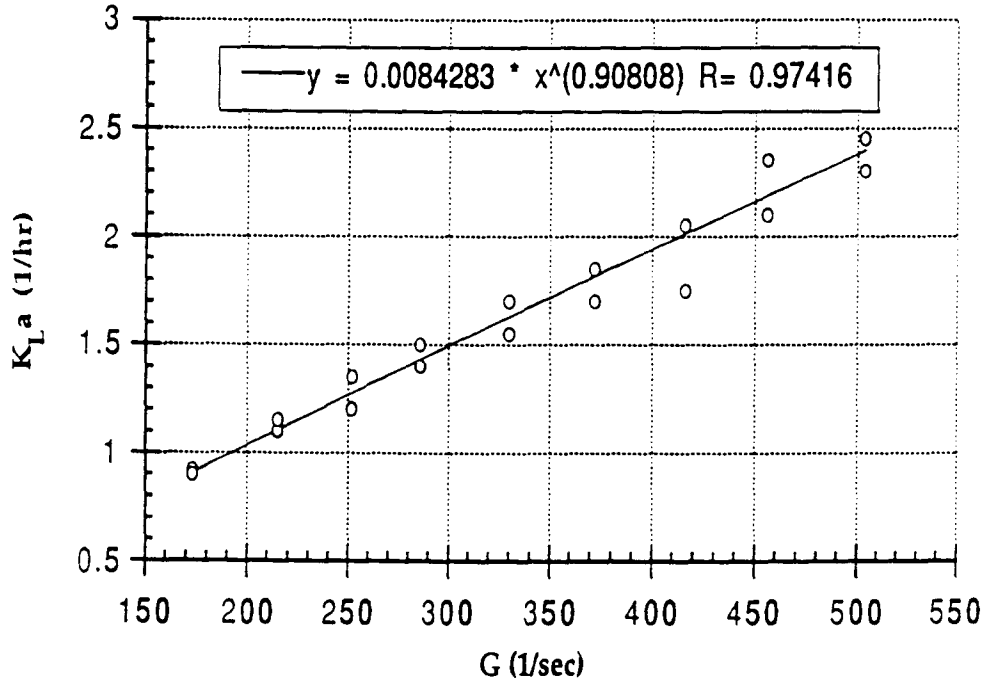

Figure 24. Correlation of oxygen transfer coefficient ($K_L a$) to velocity gradient (G) in surface aeration

$$C_L = C_{Lo} \exp(K_L a\,(t - t_o)) \tag{92}$$

Using the exponential form of the mass transfer rate equation and a two-parameter estimate nonlinear regression, the concentration change over time can be used to determine mass-transfer coefficient ($K_L a$) and initial concentration (C_{Lo}) directly. This technique provides greater precision since the entire data set is used to estimate C_{Lo}, as opposed to a single data point. A typical plot is shown in Figure 26.

Up to this point, the question is whether to run a two-parameter estimate regression (exponential equation) or a one-parameter estimate regression (logarithmic equation). Roberts et al. (1982) studied these two techniques and concluded that neither technique was superior. For convenience, two-parameter estimate technique was chosen for the data analysis using the Kaleidagraph graphics package (Abelbeck Software, Version 2.0.2, October 1989) using the Exponential Least Squares Fit.

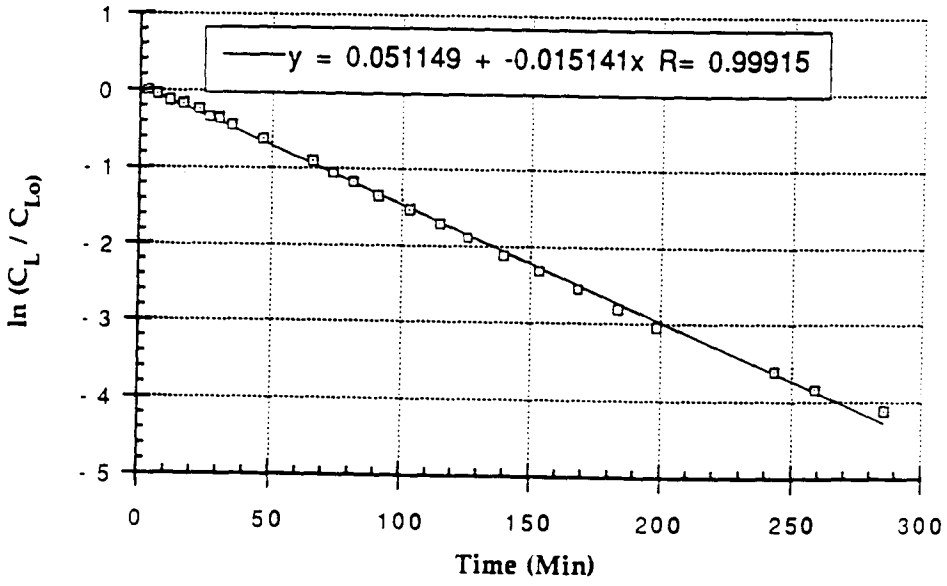

Figure 25. Typical plot of linear-regression (Toluene in surface aeration)

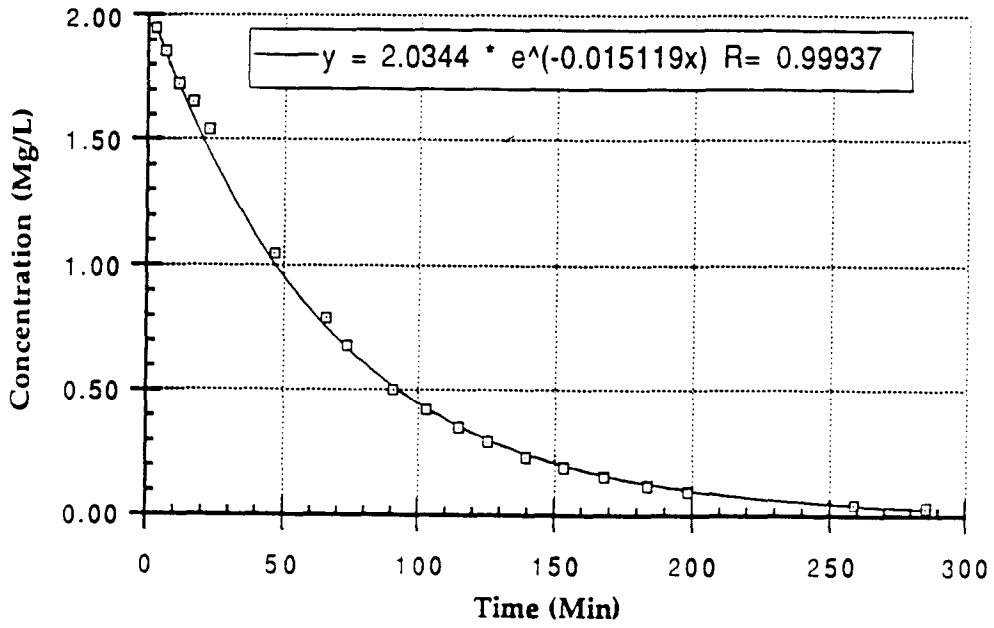

Figure 26. Typical plot of non-linear regression (Toluene at surface aeration)

4.2.3.1 Results of Modified Reactor I

The mass transfer coefficient data conducted in the modified reactor I are shown in Figure 27. The results show that 20 VOCs can be divided into two groups: less and highly volatile compounds. The turbulence created by the impeller speed (235 rpm to 505 rpm) effects the highly VOCs (Hc > 0.15) and oxygen. The impeller speed has little effect on the low volatility compounds, such as 1,2-DCB, 1,4-DCB, bromobenzene, EDB, 1,1,2,2,TCA, bromoform, and naphthalene. For the less volatile compounds, wind speed (1 to 2 fps) above the water surface was not sufficient to prevent headspace saturation. Saturation in the headspace above the water surface occurred for the less volatile compounds. In order to provide enough air flow for reac-

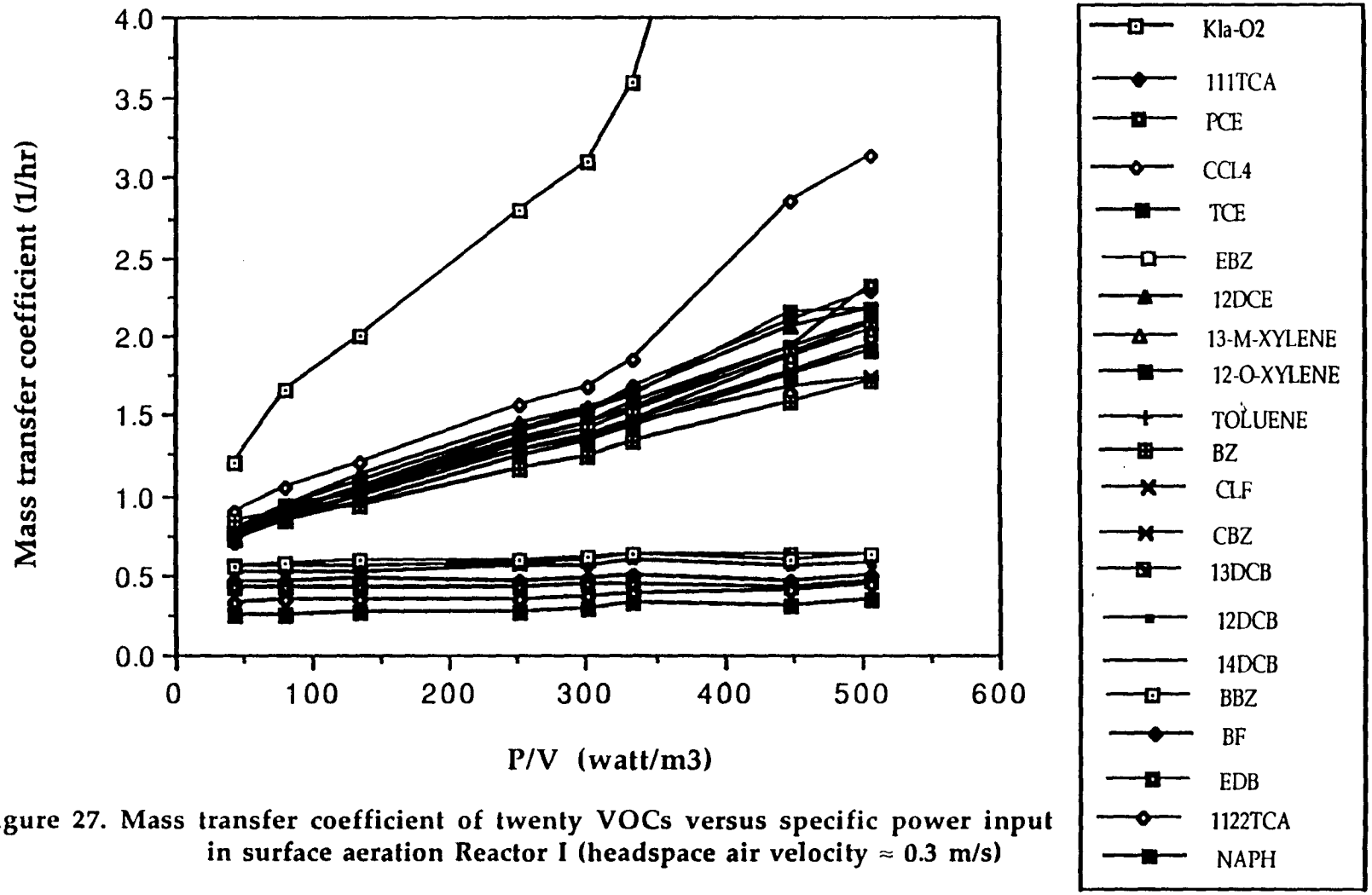

Figure 27. Mass transfer coefficient of twenty VOCs versus specific power input in surface aeration Reactor I (headspace air velocity ≈ 0.3 m/s)

tor and avoid headspace saturation problem, the reactor was modified to increase air velocity to 2.41 m/s. The location of impeller and liquid volume was also modified.

4.2.3.2 Results of Modified Reactor II

Table 5 shows the mass-transfer coefficient of twenty VOCs and oxygen performed at various impeller speeds (150 - 500 rpm). The specific power input (watt/m^3) is also shown. All of the experiments were carried out with baffles and surface air speed was above 1.5 ~ 2.4 m/s. Figures 28 and 29 show the dependence of the mass transfer coefficient ($K_L a$) on the specific power input. As can be seen from Figures 28 and 29, mass-transfer coefficient ($K_L a$) increases with power input. In general, as $\frac{P}{V}$ increases $K_L a$ increases for a given Hc, and as volatility (or Hc) increases, $K_L a$ increases for a given $\frac{P}{V}$.

Trends in the data of Table 5 can be seen in Figure 30 as well. For specific power input between 30 watt/m^3 and 350 watt/m^3, the correlation of mass-transfer coefficient ($K_L a$) of individual 20 VOCs to specific power input are shown in Figure 31 and Appendix D. The nonlinear regression is a simple power series of the form

$$K_L a = b\left[\frac{P}{V}\right]^m \tag{93}$$

Table 6 shows the parameters b and m for the 20 VOCs. Figure 32 shows b and m as a function of Henry's coefficient (Hc). The b-value is nearly inversely proportional to the Henry's coefficient. The power of m-value is between 0.26 and 0.43 which falls within the presented value of 0.20 - 0.40 by Kozinski and King (1966). The m-value curve appears to be a power function of Henry's coefficient. The most

Table 5. Summary of mass transfer coefficients of oxygen and twenty VOCs in surface aeration (Units: 1/hr)

Test No. =>	S20	S19	S26	S17	S22	S29	S27	S23	S28	S25	S29	S21	S24	S16
RPM =>	150	200	235	275	325	350	375	400	420	425	440	450	475	500
P/V(watt/m3)	11.3	30.9	50.2	80.7	133.7	167.3	206.0	250.4	290.1	300.7	331.6	353.9	420.3	491.5
G (1/sec)	106.8	176.5	225.1	285.4	367.3	410.8	455.9	502.6	541.0	550.7	578.3	597.4	651.0	704.0
O2	0.222	0.920	1.200	1.400	1.800	1.850	2.100	2.300	2.400	2.500	2.750	3.080	4.369	7.165
CT	0.169	0.636	0.780	0.935	1.195	1.280	1.408	1.540	1.630	1.668	1.810	1.866	2.022	2.345
PCE	0.120	0.563	0.750	0.829	1.028	1.125	1.210	1.306	1.368	1.446	1.520	1.568	1.719	1.896
111TCA	0.111	0.578	0.669	0.872	1.007	1.110	1.248	1.331	1.380	1.444	1.550	1.635	1.807	1.999
TCE	0.142	0.630	0.812	0.908	1.125	1.193	1.281	1.394	1.448	1.508	1.585	1.737	1.803	1.881
EBZ	0.131	0.575	0.745	0.825	1.000	1.065	1.162	1.290	1.360	1.407	1.493	1.575	1.661	1.744
12DCE	0.144	0.631	0.827	0.945	1.180	1.230	1.300	1.414	1.455	1.492	1.578	1.649	1.754	1.892
MXY	0.135	0.574	0.650	0.850	1.049	1.095	1.194	1.283	1.353	1.410	1.468	1.585	1.709	1.736
OXY	0.132	0.567	0.710	0.815	1.054	1.119	1.200	1.280	1.325	1.419	1.443	1.630	1.710	1.740
TLN	0.138	0.603	0.772	0.868	1.084	1.188	1.262	1.331	1.373	1.460	1.508	1.600	1.857	1.951
BZ	0.133	0.605	0.745	0.864	1.050	1.173	1.262	1.334	1.343	1.464	1.510	1.600	1.857	1.951
CLF	0.121	0.551	0.709	0.812	0.990	1.050	1.125	1.250	1.285	1.358	1.415	1.488	1.584	1.622
CBZ	0.134	0.594	0.764	0.860	1.052	1.170	1.245	1.300	1.361	1.423	1.470	1.580	1.670	1.740
132DCB	0.122	0.541	0.708	0.795	0.999	1.060	1.160	1.205	1.230	1.312	1.331	1.378	1.473	1.546
12DCB	0.124	0.534	0.689	0.777	0.944	1.033	1.094	1.153	1.178	1.256	1.273	1.342	1.403	1.460
14DCB	0.125	0.547	0.721	0.808	0.977	1.081	1.151	1.205	1.230	1.313	1.330	1.390	1.470	1.533
BBZ	0.134	0.582	0.733	0.824	1.007	1.120	1.170	1.241	1.270	1.337	1.390	1.463	1.530	1.602
BF	0.127	0.486	0.586	0.634	0.782	0.840	0.893	0.939	0.965	0.999	1.032	1.068	1.089	1.121
EDB	0.137	0.533	0.644	0.734	0.855	0.928	0.979	1.049	1.058	1.085	1.140	1.191	1.260	1.300
1122TCA	0.127	0.419	0.546	0.616	0.679	0.723	0.745	0.765	0.778	0.815	0.840	0.898	0.922	0.959
NAPH	0.123	0.428	0.518	0.600	0.714	0.771	0.798	0.848	0.867	0.899	0.923	0.972	1.000	1.039

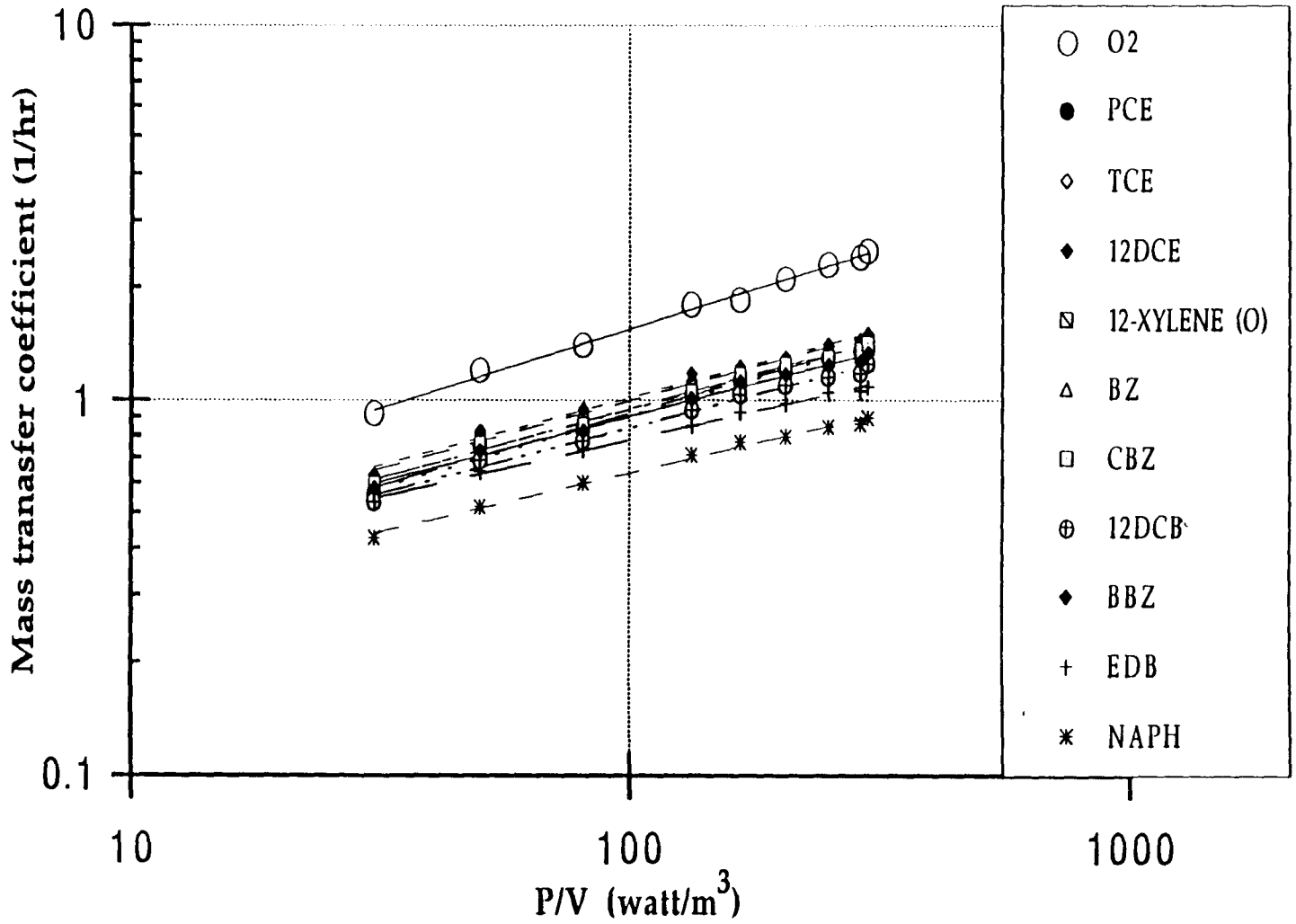

Figure 28. Dependence of mass transfer coefficient on specific power input in surface aeration (a)

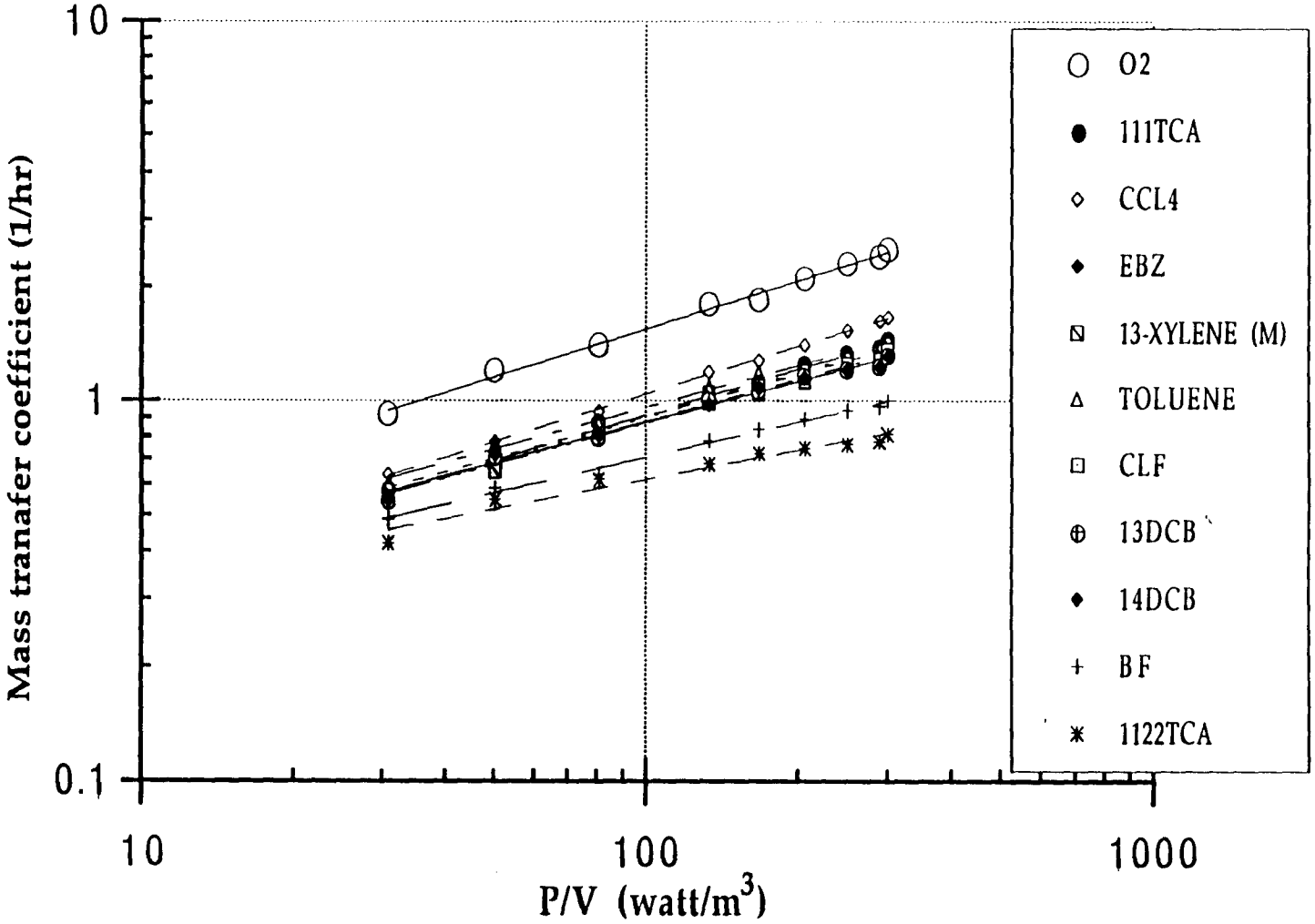

Figure 29. Dependence of mass transafer coefficient on specific power input in surface aeration (b)

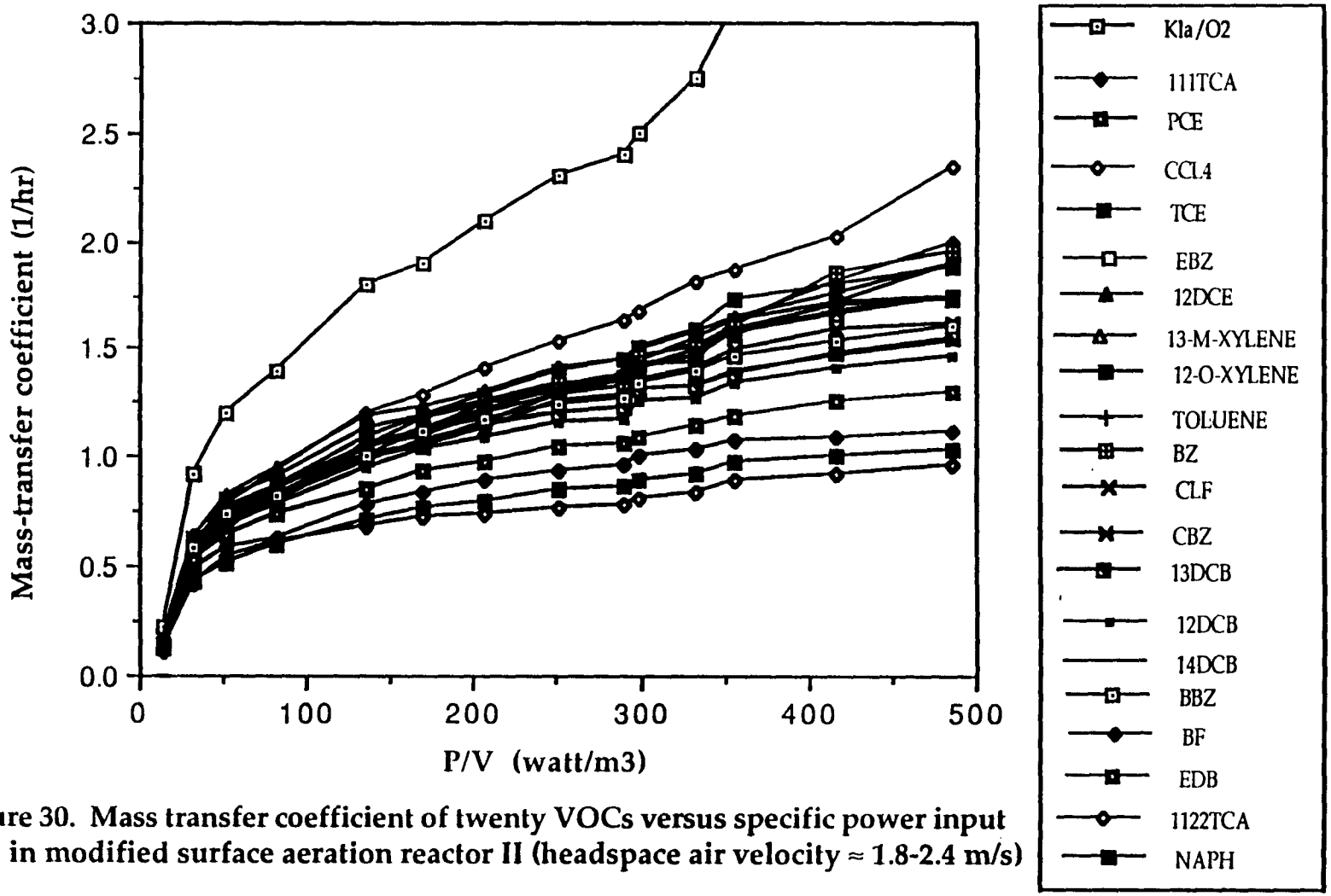

Figure 30. Mass transfer coefficient of twenty VOCs versus specific power input in modified surface aeration reactor II (headspace air velocity ≈ 1.8-2.4 m/s)

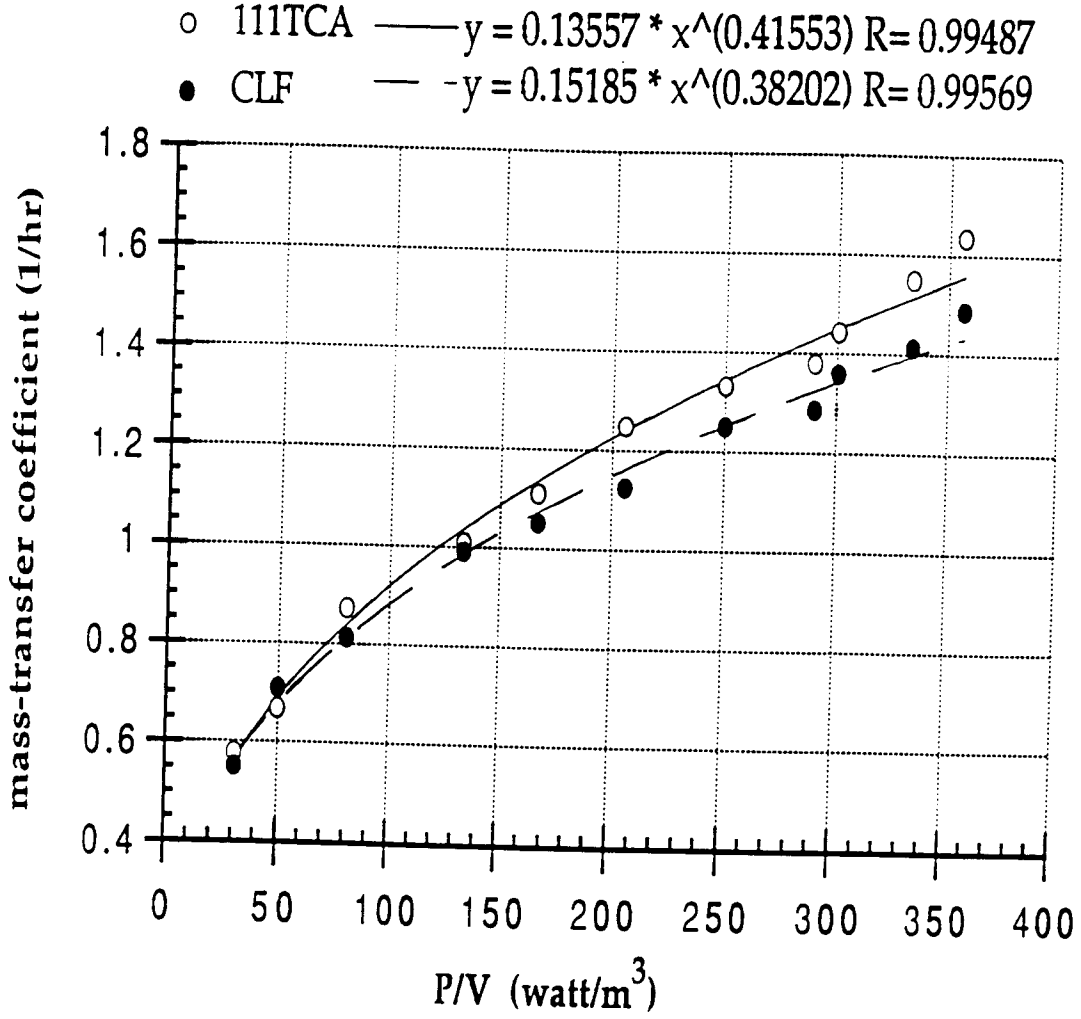

Figure 31. Correlation of mass transfer coefficient to specific power input (111TCA, CLF)

Table 6. Summary of parameters b and m for relating KLa = b (P/V)^m in surface aeration

Compounds	Hc	b	m
111TCA	0.530	0.1360	0.4155
PCE	0.570	0.1485	0.3967
CT	1.122	0.1419	0.4333
TCE	0.250	0.1752	0.3783
EBZ	0.260	0.1540	0.3864
12DCE	0.170	0.1901	0.3641
MXY	0.240	0.1396	0.4054
OXY	0.180	0.1458	0.3979
TLN	0.230	0.1703	0.3756
BZ	0.230	0.1647	0.3806
CLF	0.160	0.1519	0.3820
CBZ	0.150	0.1698	0.3728
13DCB	0.120	0.1627	0.3640
12DCB	0.087	0.1652	0.3536
14DCB	0.110	0.1683	0.3581
BBZ	0.100	0.1754	0.3563
BF	0.041	0.1665	0.3139
EDB	0.041	0.1864	0.3114
1122TCA	0.042	0.1844	0.2628
NAPH	0.038	0.1477	0.3175

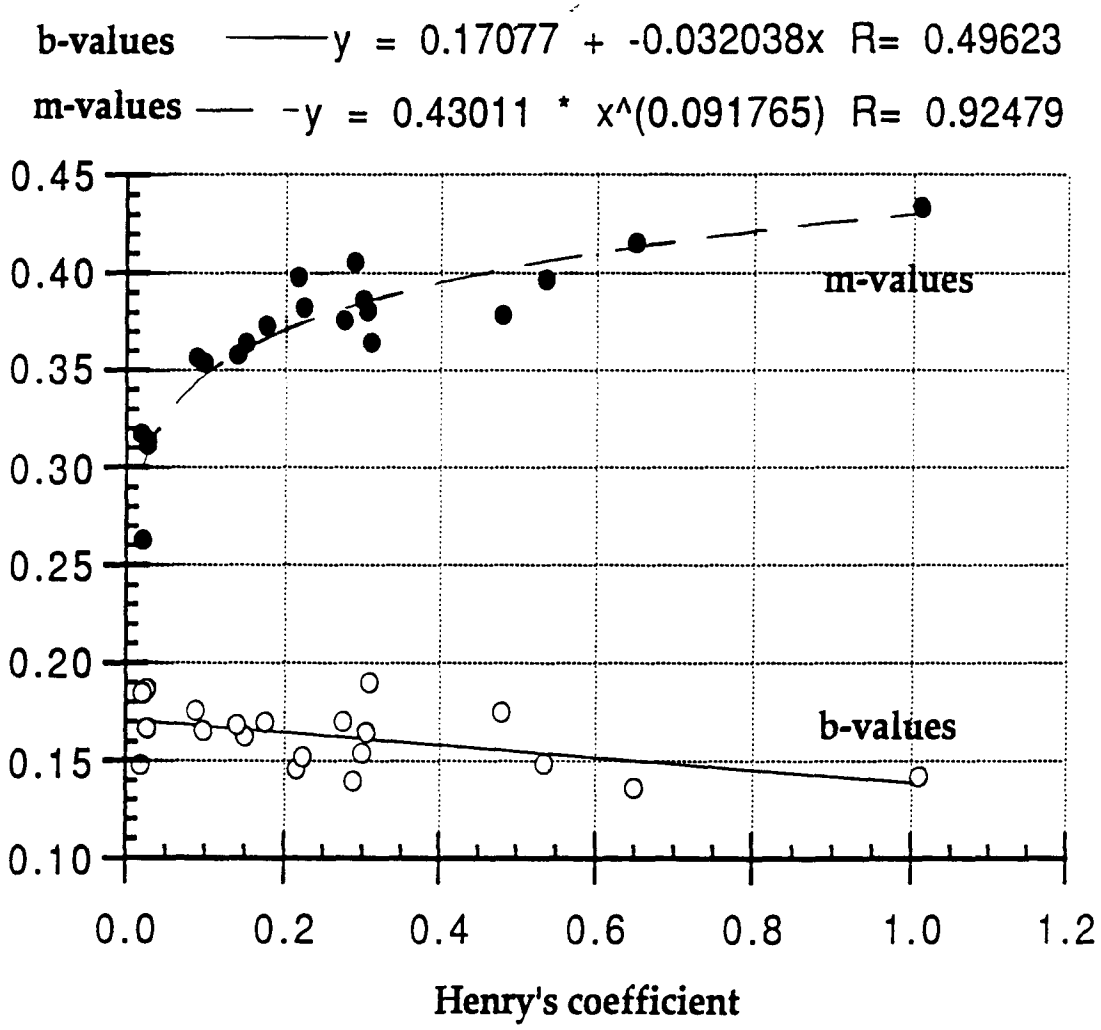

Figure 32. Parameters b and m for relating $K_L a = b\ (P/V)^m$ as a function of Henry's coefficient

dramatic effects are seen for Hc less than 0.2 which are near the steepest portion of the curve. It is suggested that gas phase mass transfer resistance becomes more important as Hc decreases, especially for Hc less than 0.2.

In Figure 33 and Appendix E, $K_L a_{VOC}$ versus G-value for 20 VOCs are developed for generalization, but the power of G-correlation (0.52 - 0.86) is about two times of specific power input (0.26 - 0.43) (Table 7). The curve of b and m versus Henry's coefficient (Hc) for G-value are plotted in Figure 34. The general tendency of b and m are similar in both diagrams (Figures 32 and 34).

4.2.4 Estimating the Ratio of Gas-Film to Liquid-Film Mass Transfer Coefficients

The ratios of gas to liquid mass-transfer coefficients ($\frac{k_G a}{k_L a}$) were estimated by fitting overall mass transfer coefficients of 20 VOCs to the two-film model with appropriate corrections for molecular diffusivities (equation 57). The data were analyzed by three-parameter nonlinear regression procedure described in Section 3.8.

A summary of ratios of gas to liquid mass-transfer coefficients ($\frac{k_G a}{k_L a}$) over the range of hydrodynamic conditions are listed in Table 8 and plotted in Figure 35. The ratio of $\frac{k_G a}{k_L a}$ was between 38 and 110 for experiments performed in the specific power input of 30 to 500 watt/m^3. The estimated value of $\frac{k_G a}{k_L a}$ in our experiments was smaller than the widely assumed range from 50 to 300 (average ratio of $\frac{k_G a}{k_L a}$ =

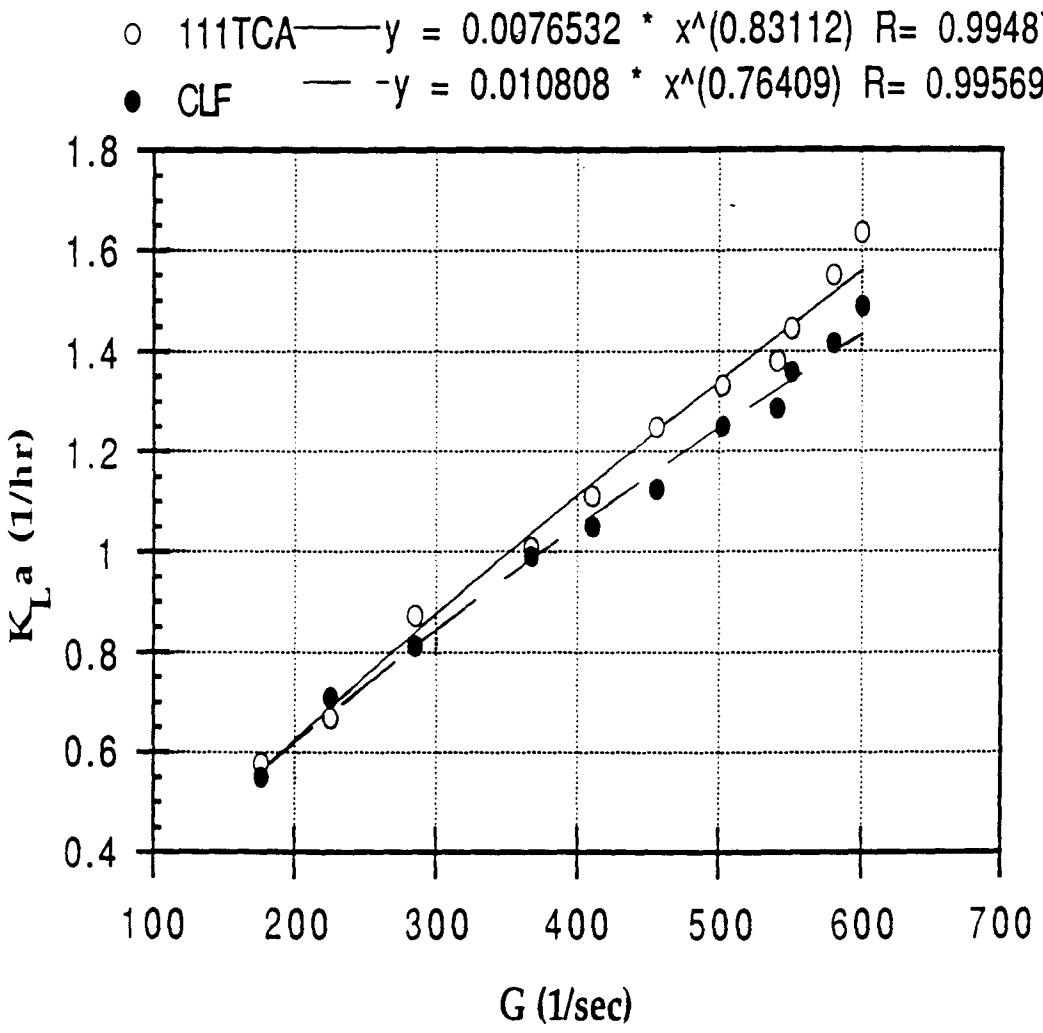

Figure 33. Correlation of mass transfer coefficient to velocity gradient in surface aeration (111TCA, CLF)

Table 7. Summary of parameters b and m for relating KLa = b (G)^m in surface aeration

Compounds	Hc	b	m
111TCA	0.53	0.0077	0.8311
PCE	0.57	0.0095	0.7935
CT	1.122	0.0071	0.8667
TCE	0.25	0.0128	0.7566
EBZ	0.26	0.0106	0.7729
12DCE	0.17	0.0153	0.7283
MXY	0.24	0.0085	0.8108
OXY	0.18	0.0093	0.7958
TLN	0.23	0.0127	0.7513
BZ	0.23	0.0118	0.7612
CLF	0.16	0.0108	0.7641
CBZ	0.15	0.0129	0.7457
13DCB	0.12	0.0131	0.7281
12DCB	0.087	0.0143	0.7073
14DCB	0.11	0.0141	0.7163
BBZ	0.1	0.0149	0.7127
BF	0.041	0.019	0.6278
EDB	0.041	0.0216	0.6229
1122TCA	0.042	0.0299	0.5256
NAPH	0.038	0.0164	0.635

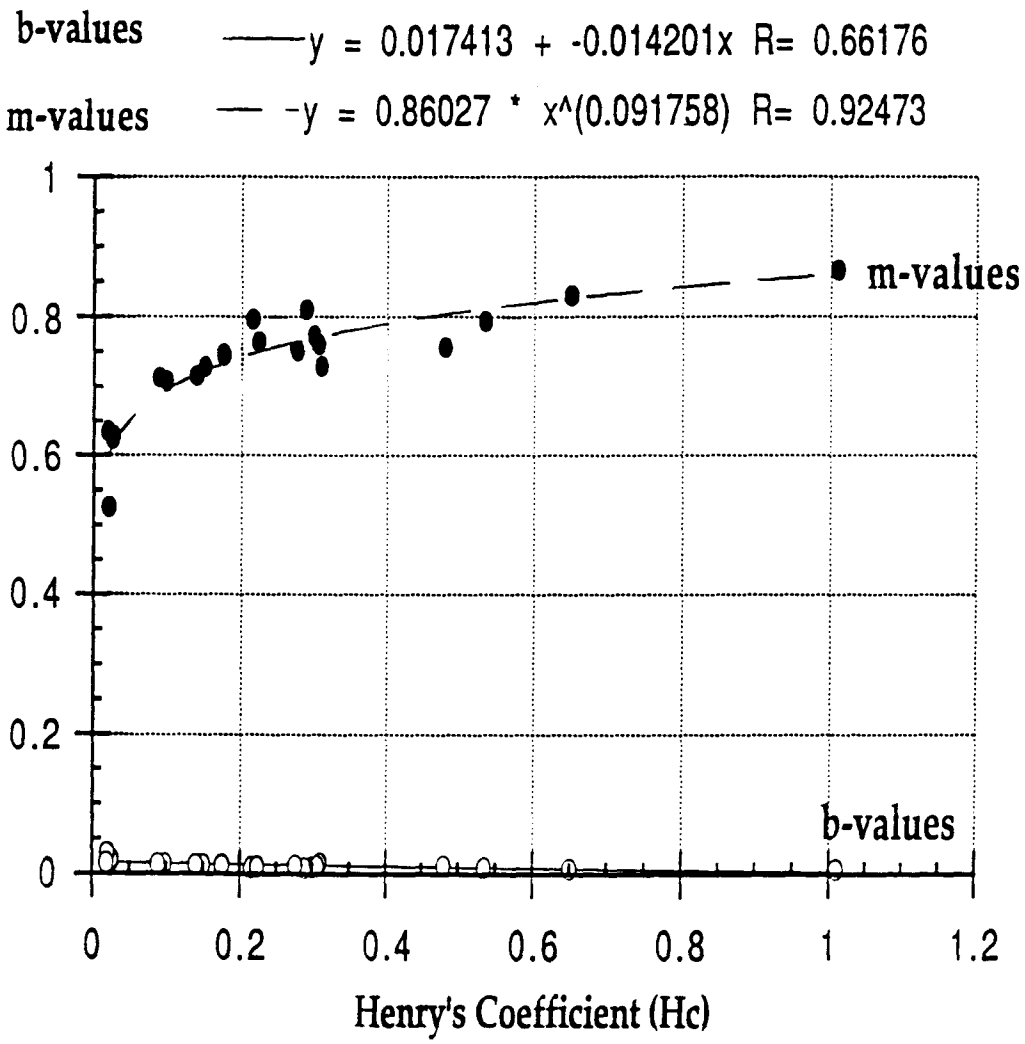

Figure 34. Parameters of b and m for relating $K_L a = b\,G^m$ as function of Henry's coefficient in surface aeration

Table 8. Ratios of gas-phase to liquid-phase mass transfer coefficients in surface.aeration

Speed# (RPM)	P/V (watt/m3)	Re* (–)	kGa/kLa (–)	kGa (m/hr)
200	30.8	5.16E+04	110.0	117.0
235	50.2	6.08E+04	101.6	121.9
275	80.7	7.14E+04	88.6	137.0
325	133.7	8.45E+04	70.8	126.4
350	137.6	9.11E+04	69.2	136.5
375	206.0	9.77E+04	62.3	135.2
400	250.4	1.04E+05	54.8	125.4
420	290.1	1.10E+05	50.8	116.8
450	357.3	1.17E+05	46.7	135.0
475	420.7	1.24E+05	39.2	119.0
500	492.0	1.31E+05	38.5	133.7

Speed = Rotational speed

* Re = Reynold Number

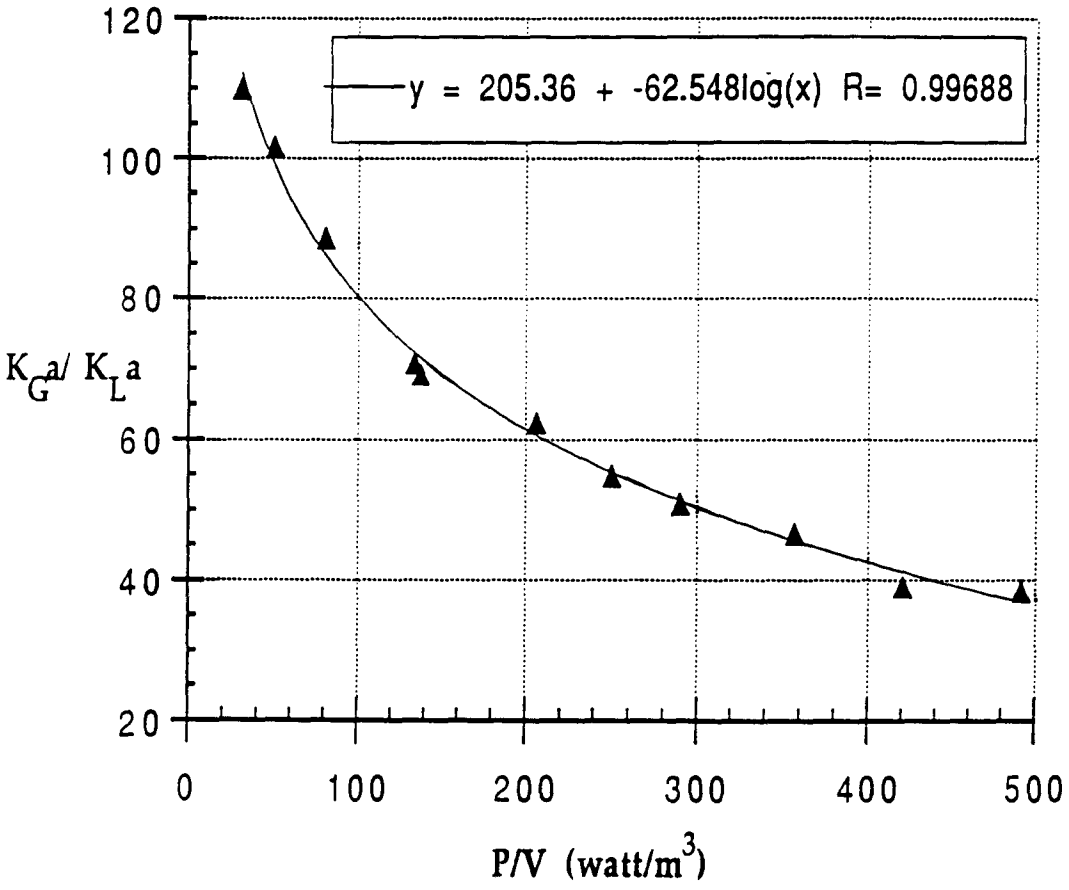

Figure 35. Correlation between $K_G a/K_L a$ and specific power input (W/m^3) in surface aeration

150) (Mackay and Leionoen, 1975; Mackay at al. 1979). However, this range was higher than the 20 to 60 range reported in Robert's work (1984). Concurrent work by Libra (1991) using stirred tank reactor with a turbine aerator (in a closed system) over a very wide range of power input (30 watt/m^3 ~ 3000 watt/m^3) found the $\frac{k_G a}{k_L a}$ ratio to be as low as 0.1. The finding suggests that the ratio will be highly dependent upon experimental conditions, such as reactor geometry and aerator type.

4.2.4.1 The Effect of Windspeed on $k_G a/k_L a$

Mackay and Yeun (1983) correlated gas and liquid mass-transfer coefficients with windspeed by measuring volatilization rates in a 6-m wind-wave tank for 11 VOCs of varying Henry's law constants. Their data also confirmed the validity of the two-resistance model and show that no interaction occurs when solutes are volatilized simultaneously. They showed that gas mass-transfer coefficients are proportional to friction velocity which relates to windspeed through the drag coefficient. Roberts' work (1984) demonstrated that the ratio of $\frac{k_G a}{k_L a}$ in the aeration systems was dependent on turbulence of liquid phase in terms of Reynold's number. Therefore, windspeed and turbulence in the air and water bulk phase can be used as the hydrodynamic parameter for gas and liquid mass-transfer coefficient, respectively. It may be concluded that the ratio of gas to liquid mass-transfer coefficient ($\frac{k_G a}{k_L a}$) should depend upon the hydrodynamic conditions produced by windspeed in the air phase as well as mixing of the water phase. The ratio is not fixed. Experiments performed with the windspeeds of 1.8 to 2.4 m/s and specific power input between 30 and 500 watt/m^3, gas mass-transfer coefficients ($k_G a$) in Table 8 are plotted in Figure 36. The

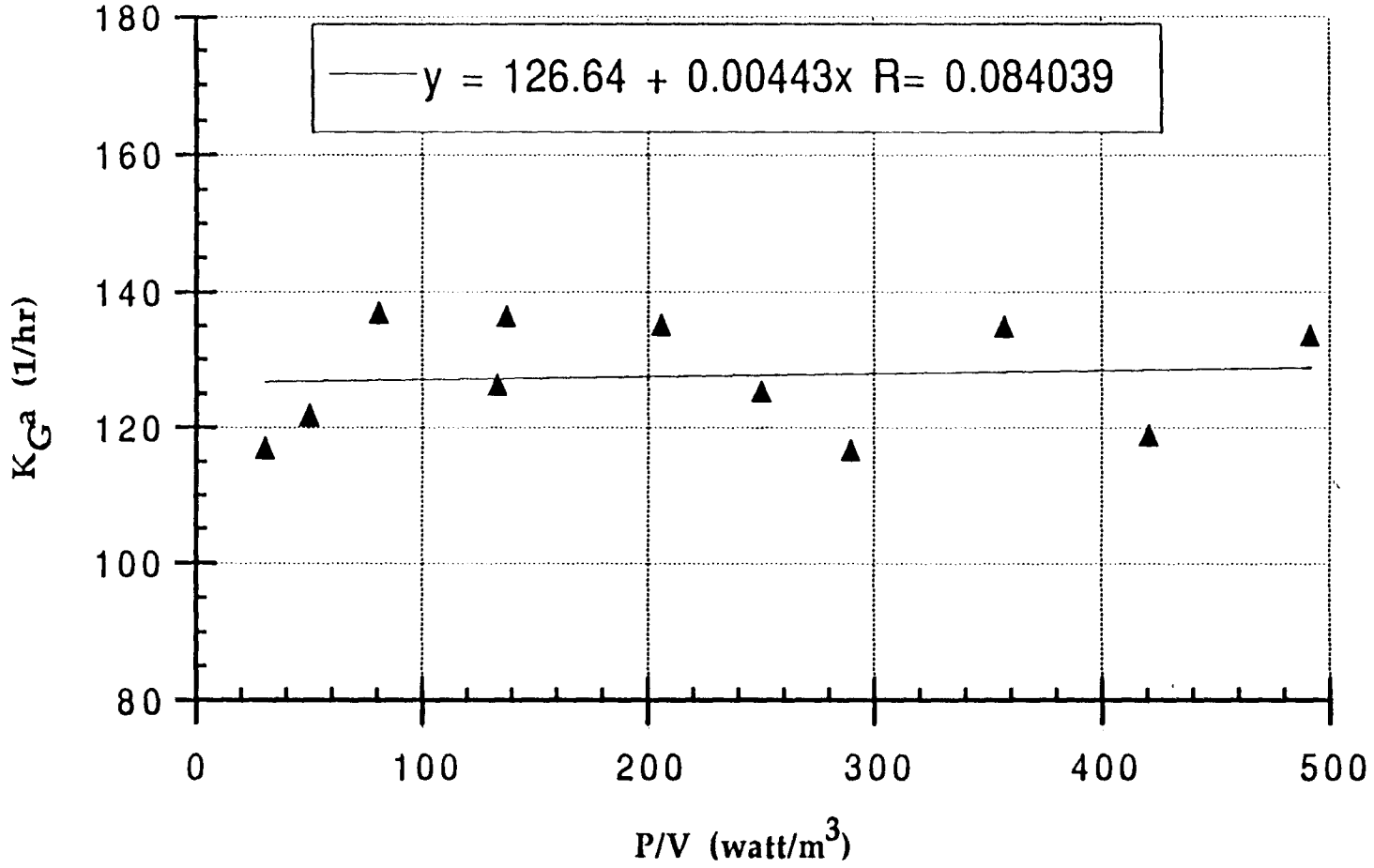

Figure 36. Correlation between gas-phase transfer coefficient and specific power input in surface aeration

mean value of gas mass-transfer coefficient ($k_G a$) in this work is 126 ± 7. This result agrees with the concept proposed by Mackay and Yeun (1983), in which the gas mass-transfer coefficient ($k_G a$) depends on windspeed above the water surface.

4.2.4.2 Correlation of $k_G a/k_L a$ to P/V

Roberts et al. (1984a) have correlated the ratio of $\frac{k_G a}{k_L a}$ to Reynolds number as follows:

$$\log\left(\frac{k_G a}{k_L a}\right) = -1.23 \log (Re) + 7.06 \tag{94}$$

The correlation for this study (Figure 37) is given as:

$$\log\left(\frac{k_G a}{k_L a}\right) = -1.18 \log (Re) + 7.66 \tag{95}$$

Comparing equations (94) and (95), the correlation performed in this study is very close to Roberts'. This is not surprising, since Roberts et al. (1984) conducted their experiments in a fume hood with linear air velocities on the order of 2 m/s (6.6 fps) in the vicinity of the surface aeration reactor which is similar to this experiment with windspeed of 1.8 - 2.4 (m/s). Therefore, the $k_G a$ should be relatively constant due to nearly constant windspeed above the water surface. Thus, the ratio of $\frac{k_G a}{k_L a}$ in this study depends on the hydrodynamic condition of the liquid phase in terms of Re or $\frac{P}{V}$. However, in the domain of high turbulence, Re is independent of oxygen transfer or power input; therefore, Re is not a good parameter to relate the ratio of $\frac{k_G a}{k_L a}$.

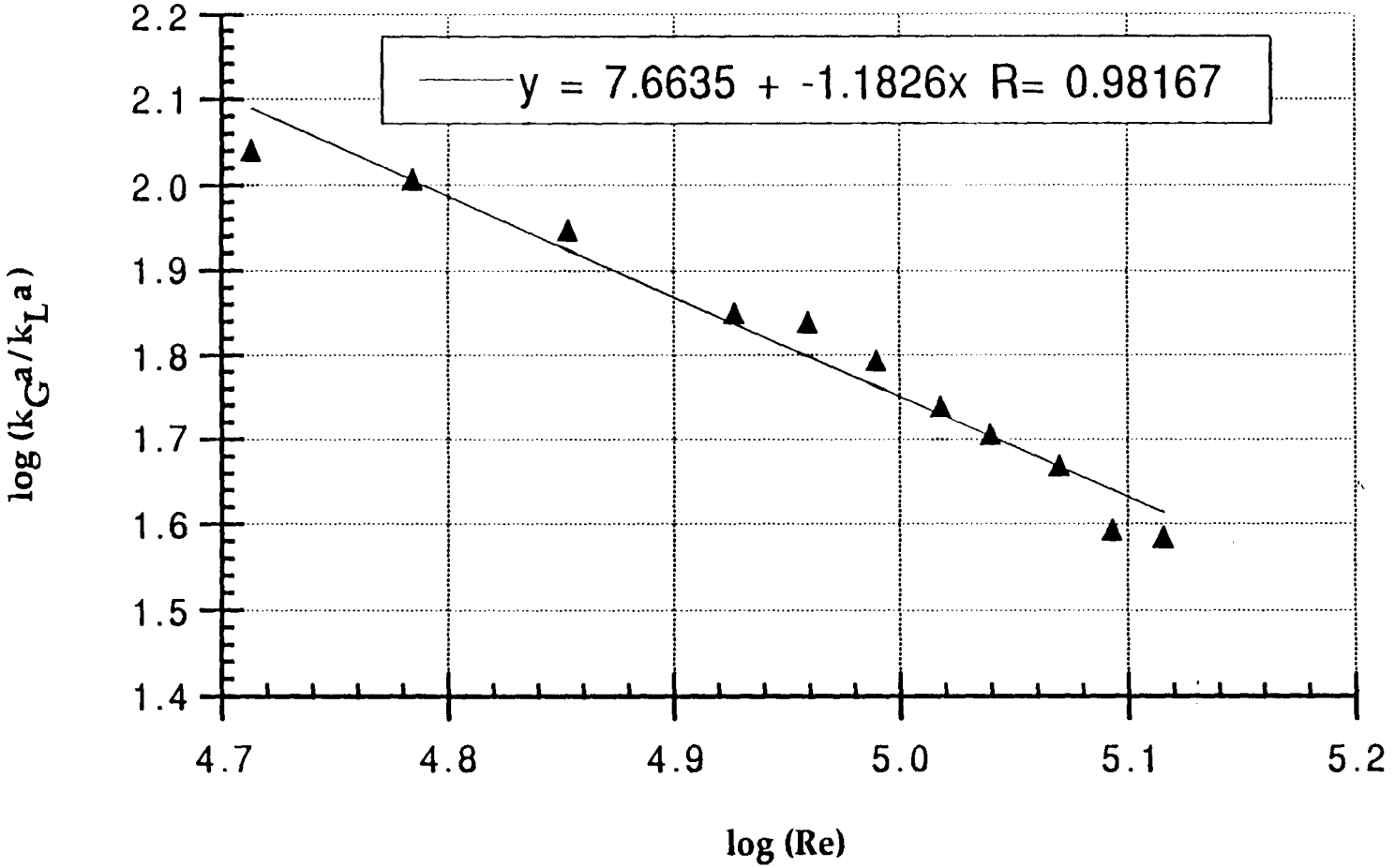

Figure 37. Correlation between log ratio of gas-phase to liquid-phase mass transfer coeffcient and log Reynolds number in surface aeration

Specific power input ($\frac{P}{V}$) would be a better parameter to correlate the ratio. The correlation of the ratio of $\frac{k_G a}{k_L a}$ to $\frac{P}{V}$ (watt/m^3) is shown in Figure 38. The equation takes the form

$$\log\left[\frac{k_G a}{k_L a}\right] = -0.397 \log\left(\frac{P}{V}\right) + 2.68 \tag{96}$$

4.2.5 Results of Modification of Ψ-value: Ψ_m-value

The ratios of $\frac{k_G a}{k_L a}$ can be used to determine the fraction of liquid to overall mass transfer resistance ($\frac{R_L}{R_T}$) for different hydrodynamic conditions using equation (18). The Ψ-value incorporating the fraction of liquid to overall mass-transfer resistance can be applied to estimate the stripping rate for a wide range of organic compounds using equations (60) and (62).

A summary of Ψ and Ψ_m-values at each impeller speed (235 rpm - 425 rpm) is shown in Table 9. Since $\Psi_m = \Psi \frac{R_L}{R_T}$, the difference between Ψ and Ψ_m is a comparison of the significance of $\frac{R_L}{R_T}$. The $\frac{R_L}{R_T}$ of twenty VOCs versus the specific power input are plotted in Figures 39a and 39b. For a given $\frac{P}{V}$, $\frac{R_L}{R_T}$ decreases with decreasing Hc. For a given Hc, $\frac{R_L}{R_T}$ is inversely proportional to $\frac{P}{V}$. The gas-phase resistance has very little effect on highly volatile compounds, such as oxygen, CCl_4, 111 TCA, and PCE. The gas-phase resistance has a significant effect on the com-

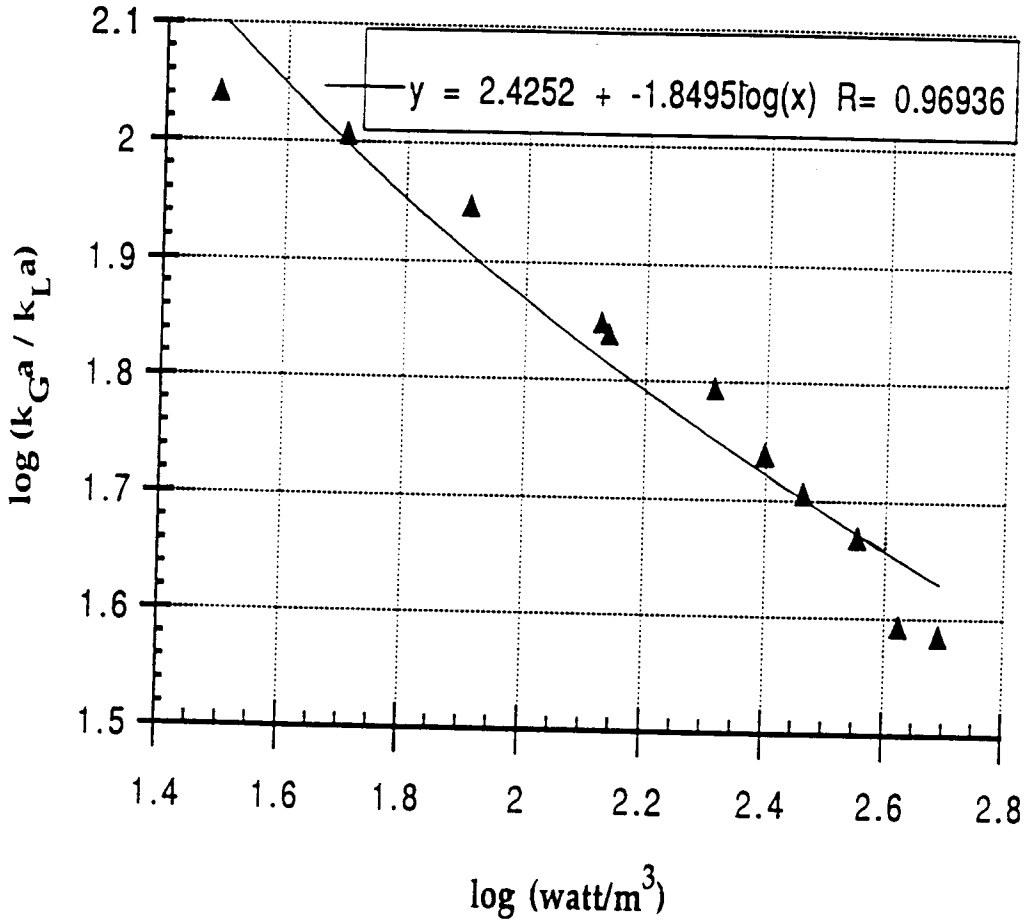

Figure 38. Correlation of log ($k_G a$ / $k_L a$) to log (P/V) in surface aeration

Table 9. Summary of values of Psi and Psi-m in surface aeration experiments

Run	Liquid		S19	S26	S17	S22	S29	S27	S23	S32	S25
rpm	Diffusion		200	235	275	325	350	375	400	420	425
kGa/kLa	Coeff.		110.0	101.0	88.6	70.8	69.2	62.4	54.8	50.8	48.0
	DL	Ψ	ΨM	ΨM	ΨM	ΨM	ΨM	ΨM	ΨM	ΨM	ΨM
O2	1.971										
111TCA	0.844	0.654	0.643	0.642	0.640	0.637	0.636	0.634	0.632	0.630	0.629
PCE	0.834	0.650	0.640	0.639	0.637	0.634	0.634	0.632	0.629	0.628	0.627
CT	0.862	0.661	0.656	0.656	0.655	0.653	0.653	0.652	0.651	0.650	0.649
TCE	0.899	0.675	0.652	0.650	0.646	0.640	0.639	0.635	0.630	0.626	0.624
EBZ	0.708	0.599	0.578	0.576	0.573	0.566	0.565	0.562	0.557	0.554	0.552
12DCE	0.977	0.704	0.660	0.657	0.650	0.638	0.637	0.630	0.621	0.616	0.611
MXY	0.706	0.598	0.574	0.572	0.569	0.562	0.561	0.557	0.552	0.549	0.546
OXY	0.706	0.598	0.565	0.562	0.557	0.548	0.547	0.541	0.534	0.530	0.526
TLN	0.787	0.632	0.605	0.603	0.599	0.591	0.590	0.586	0.580	0.576	0.573
BZ	0.892	0.673	0.643	0.640	0.636	0.627	0.626	0.622	0.615	0.611	0.608
CLF	0.938	0.690	0.646	0.643	0.637	0.625	0.623	0.617	0.608	0.602	0.598
CBZ	0.800	0.637	0.593	0.590	0.584	0.571	0.570	0.564	0.555	0.549	0.545
13DCB	0.727	0.607	0.561	0.557	0.551	0.538	0.537	0.530	0.521	0.515	0.511
12DCB	0.725	0.606	0.538	0.532	0.523	0.506	0.504	0.495	0.482	0.475	0.469
14DCB	0.710	0.600	0.547	0.542	0.535	0.521	0.519	0.512	0.502	0.495	0.490
BBZ	0.775	0.627	0.563	0.558	0.550	0.533	0.531	0.522	0.511	0.503	0.498
BF	0.865	0.662	0.455	0.443	0.423	0.388	0.385	0.368	0.346	0.334	0.324
EDB	0.908	0.679	0.545	0.535	0.520	0.491	0.488	0.474	0.455	0.443	0.434
1122TCA	0.763	0.622	0.446	0.435	0.417	0.385	0.382	0.367	0.347	0.335	0.326
NAPH	0.668	0.582	0.453	0.445	0.430	0.404	0.401	0.388	0.371	0.360	0.353

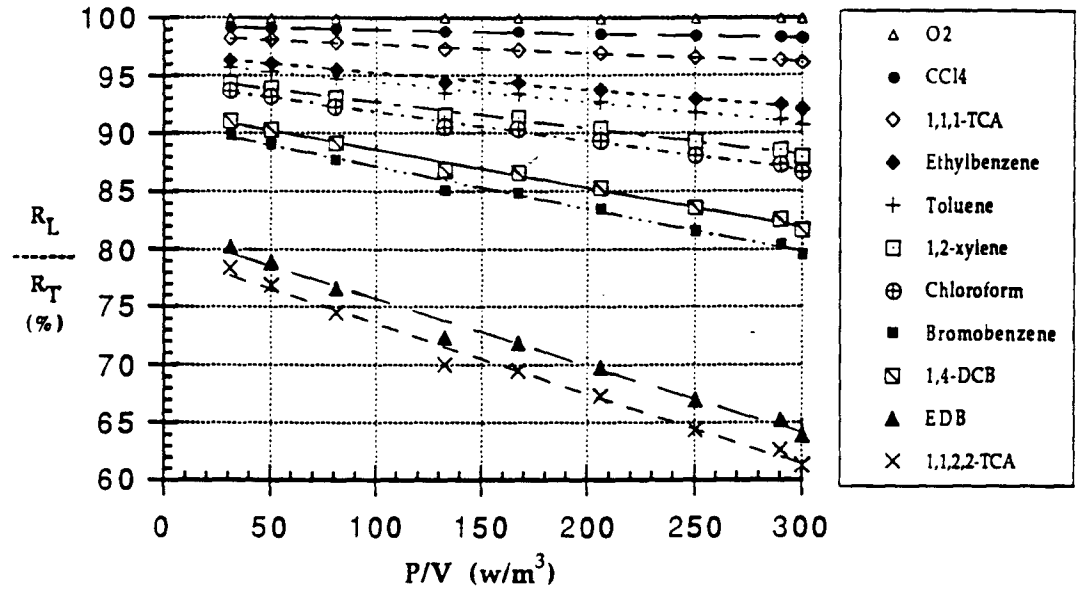

Figure 39A. Effect of specific power input on liquid-film resistance in surface aeration (a)

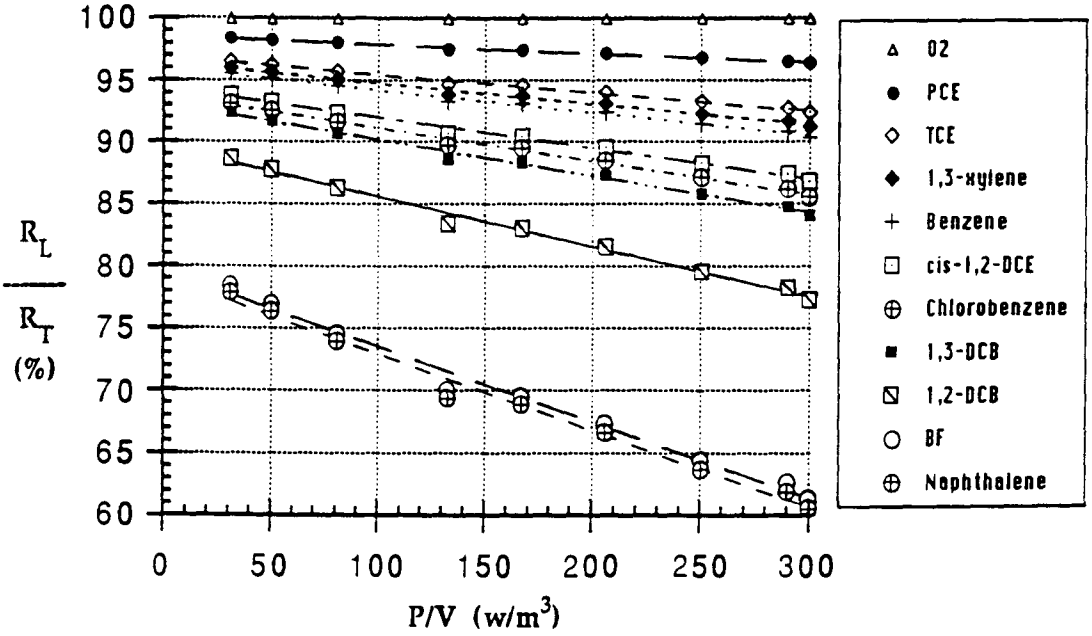

Figure 39b. Effect of specfic power input on liquid-film resistances in surface aeration (b)

pounds with Hc below 0.2, especially for low volatility compounds, such as 1,4-DCB, 1,2-DCB, EDB, bromoform, 1,1,2,2-TCA, and naphthalene. The impact of gas phase resistance increases in increasing P/V.

It is interesting to review predicted $K_L a$'s and measured $K_L a$'s. Equation (62) shows the predicted equation for $K_L a_{VOC}$

$$K_L a_{VOC} = \left[\frac{D_{LVOC}}{D_{LO2}}\right]^n \frac{R_L}{R_T} K_L a\, O_2 \tag{97}$$

The parameters n and $\frac{R_L}{R_T}$ were estimated using the nonlinear regression procedure from SAS (Statistical Analysis System, 1982 edition) to estimate the parameters by least squares best fit.

Figure 40 shows the results for measured and predicted $K_L a$ at 200 rpm (31 watt/m^3). Appendix F shows the result from 50 to 300 watt/m^3. Tables 10a and 10b show the predicted and measured $K_L a$'s for all impeller speed from 235 to 425 rpm (31 - 310 watt/m^3). Good correlations were observed. The regression line slopes are all very close to 1.0, but the intercepts decrease slightly with increasing power input, giving a consistent overestimation of $K_L a_{O2}$ at the higher power input used. The overestimation of $K_L a_{O2}$ may arise from entrainment of air bubbles which increases the oxygen transfer. However, the increase of $K_L a_{VOC}$ is not proportional to the increase of $K_L a_{O2}$ due to saturation of VOCs in the air phase.

The average discrepancy between measured and predicted values of $K_L a$ of twenty VOCs for nine sets of experiments was 5.8% (Table 10a). These errors may arise from the measurement of $K_L a_{O2}$ and $K_L a_{VOC}$ and the estimation of liquid

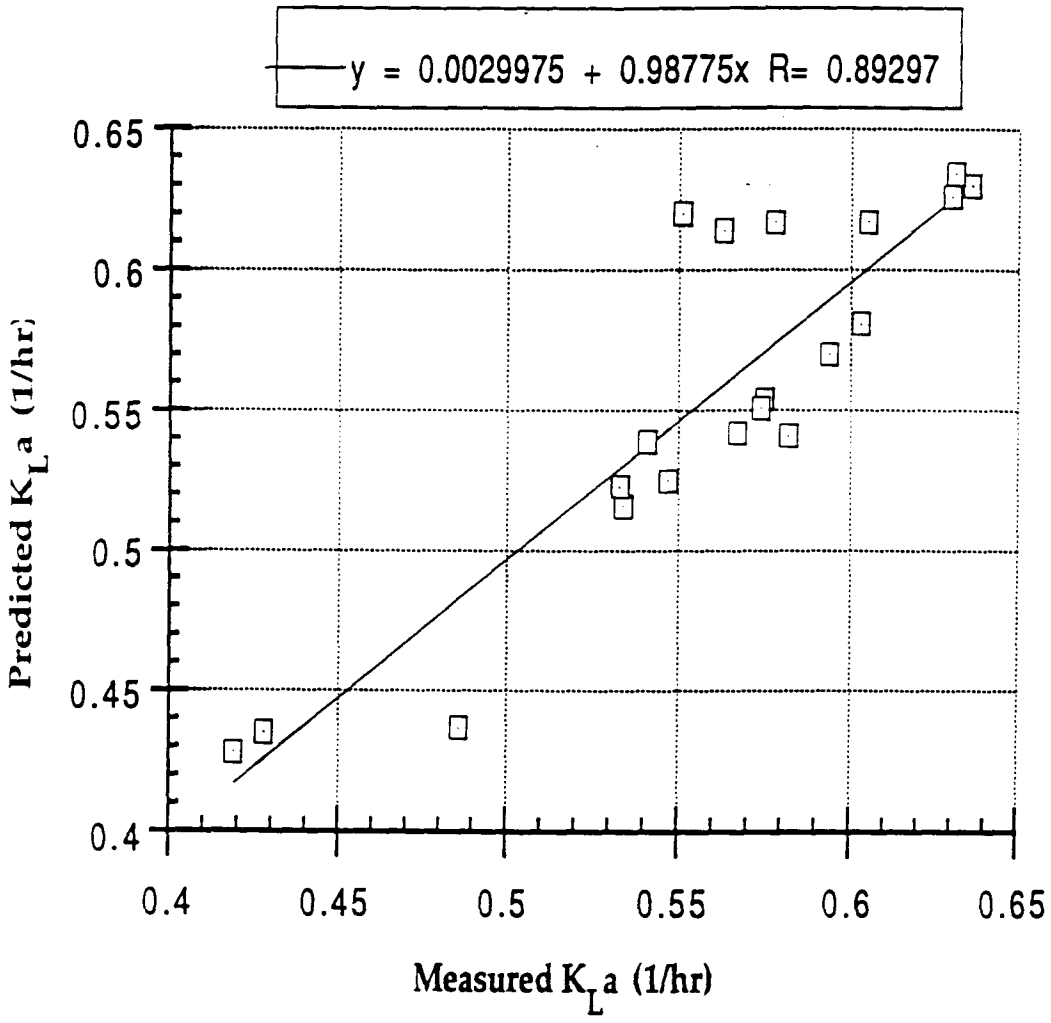

Figure 40. Comparison between predicted and measured mass transfer coefficients in surface aeration (200 rpm)

Table 10a. Summary of estimated and measured mass transfer coefficients of twenty VOCs in surface aeration

Run	Overall	S19			S26			S17			S22			S29		
RPM		200			235			275			325			350		
KLa (1/hr)	ARE#	EST*	PDT**	ARE#	EST*	PDT**	ARE#	EST*	PDT**	ARE#	EST*	PDT**	ARE#	EST*	PDT**	ARE#
kGa/kLa			110.0			101			88.6			70.8			69.2	
O2		0.96			1.25			1.35			1.75			1.9		
111TCA	5.4	0.58	0.62	-6.8	0.67	0.80	-19.9	0.87	0.86	0.9	1.11	1.11	-0.7	1.11	1.21	-8.9
PCE	4.8	0.56	0.61	-9.1	0.75	0.80	-6.5	0.83	0.86	-3.8	1.13	1.11	1.6	1.13	1.20	-7.0
CCl4	5.8	0.64	0.63	1.0	0.78	0.82	-5.1	0.94	0.88	5.5	1.20	1.14	4.4	1.28	1.24	3.1
TCE	1.5	0.63	0.63	0.7	0.81	0.81	0.0	0.91	0.87	3.9	1.13	1.12	0.5	1.19	1.21	-1.7
EBZ	4.4	0.58	0.55	3.6	0.75	0.72	3.4	0.83	0.77	6.3	1.00	0.99	0.9	1.07	1.07	-0.9
12DCE	3.4	0.63	0.63	-0.4	0.83	0.82	0.8	0.95	0.88	7.1	1.18	1.12	5.3	1.23	1.21	1.6
MXY	6.9	0.57	0.55	3.9	0.65	0.72	-10.1	0.85	0.77	9.6	1.05	0.98	6.3	1.10	1.07	2.6
OXY	7.8	0.57	0.54	4.4	0.71	0.70	1.1	0.82	0.75	7.7	1.05	0.96	9.1	1.12	1.04	7.2
TLN	5.3	0.60	0.58	3.7	0.77	0.75	2.4	0.87	0.81	6.9	1.08	1.03	4.6	1.19	1.12	5.6
BZ	2.8	0.61	0.62	-2.0	0.75	0.80	-7.4	0.86	0.86	0.6	1.05	1.10	-4.5	1.17	1.19	-1.4
CLF	8.9	0.55	0.62	-12.6	0.71	0.80	-13.3	0.81	0.86	-5.8	0.99	1.09	-10.4	1.05	1.18	-12.8
CBZ	6.4	0.59	0.57	4.1	0.76	0.74	3.5	0.76	0.79	-3.1	1.05	1.00	4.9	1.17	1.08	7.4
13DCB	5.0	0.54	0.54	0.5	0.71	0.70	1.6	0.71	0.74	-5.0	1.00	0.94	6.2	1.06	1.02	3.8
12DCB	6.9	0.53	0.52	3.3	0.69	0.67	3.4	0.69	0.71	-2.5	0.94	0.89	6.2	1.03	0.96	7.3
14DCB	6.9	0.55	0.52	4.0	0.72	0.68	6.0	0.72	0.72	-0.2	0.98	0.91	6.7	1.08	0.99	8.7
BBZ	8.2	0.58	0.54	7.1	0.73	0.70	4.8	0.73	0.74	-1.2	1.01	0.93	7.4	1.12	1.01	9.9
BF	14.1	0.49	0.44	10.0	0.59	0.55	5.5	0.59	0.57	2.4	0.78	0.68	13.1	0.84	0.73	13.0
EDB	3.9	0.53	0.52	1.9	0.64	0.67	-3.9	0.64	0.70	-9.0	0.86	0.86	-0.5	0.93	0.93	0.1
1122TCA	1.8	0.42	0.43	-2.2	0.55	0.54	0.4	0.55	0.56	-3.2	0.68	0.67	0.7	0.72	0.73	-0.4
NAPH	4.8	0.43	0.44	-1.7	0.518	0.556	-7.3	0.52	0.58	-12.2	0.71	0.71	1.0	0.77	0.76	1.2
Mean Error(%)	5.8			0.7			-2.0			0.2			3.1			1.9
ABS Mean (%)				4.2			5.3			4.9			4.8			5.2

EST* = Estimated KLa PDT** = Predicted KLa

ARE# = Absolute Relative Error (%) = (ESt* - PDT*)/EST*X100%

Table 10b. Summary of estimated and measured mass transfer coefficients of twenty VOCs in surface aeration

Test No	S27			S23			S32			S25		
RPM	375			400			420			425		
KLa (1/hr)	EST*	PDT**	ARE#	EST*	PDT**	ARE#	EST*	PDT**	ARE#	EST*	PDT**	ARE#
kGa/kLa		62.4			54.8			50.8			48	
O2	2			2.15			2.30			2.35		
111TCA	1.25	1.27	-1.7	1.33	1.36	-2.1	1.38	1.45	-5.0	1.44	1.48	-2.3
PCE	1.21	1.26	-4.4	1.31	1.35	-3.6	1.37	1.44	-5.6	1.45	1.47	-1.8
CCl4	1.41	1.30	7.4	1.54	1.40	9.2	1.63	1.49	8.3	1.67	1.53	8.5
TCE	1.28	1.27	0.9	1.39	1.35	2.9	1.45	1.44	0.5	1.51	1.47	2.8
EBZ	1.16	1.12	3.3	1.29	1.20	7.1	1.36	1.27	6.3	1.41	1.30	7.9
12DCE	1.30	1.26	3.0	1.41	1.34	5.5	1.46	1.42	2.7	1.49	1.44	3.7
MXY	1.19	1.11	6.6	1.28	1.19	7.5	1.35	1.26	6.7	1.41	1.28	9.0
OXY	1.20	1.08	9.8	1.28	1.15	10.2	1.33	1.22	8.0	1.42	1.24	12.8
TLN	1.26	1.17	7.2	1.33	1.25	6.3	1.37	1.33	3.5	1.46	1.35	7.7
BZ	1.26	1.24	1.5	1.33	1.32	0.9	1.34	1.41	-4.6	1.46	1.43	2.4
CLF	1.13	1.23	-9.6	1.25	1.31	-4.5	1.29	1.38	-7.8	1.36	1.40	-3.4
CBZ	1.25	1.13	9.5	1.30	1.19	8.2	1.36	1.26	7.2	1.42	1.28	10.0
13DCB	1.16	1.06	8.6	1.21	1.12	7.1	1.23	1.18	3.7	1.31	1.20	8.5
12DCB	1.09	0.99	9.5	1.15	1.04	10.0	1.18	1.09	7.3	1.26	1.10	12.3
14DCB	1.10	1.02	6.8	1.21	1.08	10.5	1.23	1.14	7.4	1.31	1.15	12.2
BBZ	1.17	1.04	10.7	1.24	1.10	11.5	1.27	1.16	8.9	1.34	1.17	12.6
BF	0.89	0.74	17.6	0.94	0.74	20.7	0.97	0.77	20.4	1.00	0.76	23.7
EDB	0.98	0.95	3.2	1.05	0.98	6.8	1.06	1.02	3.7	1.09	1.02	5.9
1122TCA	0.73	0.73	-0.3	0.77	0.75	2.5	0.78	0.77	0.9	0.82	0.77	5.9
NAPH	0.79	0.78	1.5	0.85	0.80	6.0	0.87	0.83	4.4	0.90	0.83	7.8
Mean Error(%)			4.6			6.1			3.8			7.3
ABS Mean (%)			6.2			7.2			6.1			8.1

EST* = Estimated KLa PDT** = Predicted KLa

ARE# = Absolute Relative Error (%) = (ESt* - PDT*)/EST*X100%

diffusivity. The estimation of liquid diffusivity has an error of 10-15% (Reid et al. 1986; Sherwood et al. 1977). The results (Tables 10a and 10b and Figure 40 and Appendix F) indicate that liquid diffusivity of chloroform and PCE are too great, whereas that of bromoform and bromobenzene are too small. The use of Ψ_m to estimate K_La depends on the accurate estimation of diffusivity. However, values of diffusivities of organic compounds are seldom reported in the literature, and the equations given by Stokes-Einstein (equation 47) or Wilke-Chang (equation 49) provide only approximations.

The original definition of Ψ is only useful for highly volatile compounds. The modification of Ψ (Ψ_m-value) corrected for liquid resistance can be used to improve the estimation of stripping rates for intermediate and low-volatility compounds as long as the oxygen transfer coefficient and liquid-phase resistance are known. It is concluded that the estimation method (Ψ_m) presented in this study works reasonably well.

4.2.6 Estimation of Liquid and Gas Diffusivities

Smith et al. (1980) suggested using the estimation method to calculate the diffusion coefficient for two principal reasons. First, in the case where some diffusion coefficients were known and the others had to be estimated, forming a mixed-ratio might bias the results. Second, in the case where all diffusivities were experimentally determined, there was still a large potential error. Rathbun (1978) assumed that film theory obtained (n=1) and calculated a (D_{LVOC}/D_{LO_2}) ratio for ethylene by using liquid diffusion coefficients for oxygen and ethylene which were measured by several investigators. When data for oxygen and ethylene measured by the same investigators

were used, the ratio was 0.77. If liquid diffusion coefficients measured by different investigators were used, the ratio varied from 0.57 to 0.96. This is a wider range than the range predicted by using the estimated values of the diffusion coefficients. Therefore, estimated diffusion coefficients were used for this study.

4.2.6.1 Liquid Diffusivity

Liquid diffusion coefficients were calculated with modified Wilke-Chang estimation method, equation (49), with associated parameter $\phi = 2.26$ for water. Equation (49) was selected because its form is closely related to the Stokes-Einstein equation (equation 47).

The solute molar volume at the normal boiling point, V_A, used in equation (49), was estimated with the Tyn and Calus correlation (T&C) increments (Reid et al. 1987). T&C increments were used because they provided molar volume for the compounds studied between the predictions of Le Bas additive method and the predictions of Schroeder increments. A table showing the estimated liquid molar volumes with the three methods and the corresponding diffusion coefficients, also using diverse methods, is given in Table C-1 of Appendix C. The values of the diffusion coefficients obtained using various alternative estimating approaches are summarized in Table C-2 of Appendix C.

4.2.6.2 Gas Diffusivity

The Wilke and Lee (Reid et al. 1987) correction was used in this study to estimate gas diffusivities. The solute molar volume at the normal boiling point (V_A) used in equation (51) was estimated with the Tyn and Calus correlation (T&C) increments

(Reid et al. 1987). The Lennard-Jones potential procedure (Reid et al. 1987, pp. 582) was used to estimate σ_{AB} and Ω_d (diffusion collision integral) which was described previously in Section 2.3. The values of the diffusion coefficients obtained using various alternative estimating approaches are summarized in Table C-3 of Appendix C.

4.2.7 The Effect of Liquid Volume and Water Temperature Change on $K_L a$

A potential error in the estimation of $K_L a$ is the change of volume in the reactor due to sampling and evaporation. The decrease in volume due to sampling was approximately 2.3%. The volume loss due to evaporation depended on the test time, air temperature, relative humidity, and wind velocity. The effect of evaporation on the volume loss was estimated by a commonly used empirical mass transfer equation developed by Meyer (Viessman et al. 1972). The equation is based primarily on the concept of the turbulent transfer of water vapor (by eddy motion) from an evaporating surface to the atmosphere. This equation takes the form

$$E = C\,(eo - ea)(1 + \frac{W}{10}) \tag{98}$$

where

E	=	the daily evaporation in inches depth,
eo and ea	=	the saturation vapor pressure at water surface temperature and the vapor pressure of air, respectively,
W	=	the wind velocity in mph measured about 25 ft above the water surface, and
C	=	an empirical coefficient.

For daily estimates of an ordinary lake, C is approximately 0.36. For wet soil surface, small puddles, and shallow pans, the value of C is approximately 0.50.

Water temperature of 20°C and air temperature of 25°C, wind speed of 5 mph (7.3 fps), relative humidity of 50%, and the C-value of 0.36 were used to estimate the evaporation rate of water. The estimated evaporation rate is about 0.17 mm/hr. For short runs (1 hr) the evaporation is 0.06% of total volume, whereas for long runs (12 hrs) the volume loss is 0.55%. The maximum volume loss due to sampling (2.3%) and evaporation (0.55%) is about 2.85%. It is believed that the effect of volume loss on K_La-value is insignificant.

Changes in water temperature also affect the K_La-value since the diffusion coefficient and viscosity change with temperature. Because the oxygen concentration C_L^* is temperature dependent, it is necessary to have the same initial and final temperature. It is crucial to keep the reactor at constant temperature during the test. For short tests (1 hr), fluctuations were less than 0.1 °C, whereas for a long run (12 hrs), the temperature varied ± 0.5 °C. Roberts et al. (1984) indicates that the higher temperature variation caused slightly greater scatter of the data, but the effect on the r^2-value of the regression may not be detectable.

4.3 Results of Bubble Aeration Experiments

4.3.1 Flow Behavior of Bubble Column

Table 11 shows that the average diameter of bubbles ranges from 1.67 to 3.65 mm and varies with the change of air flow rate (AFR) (1.09 scfh to 5.03 scfh). The corresponding standard deviations vary from 0.51 to 0.77 mm, the coefficients of variation are from 14.7 to 30.7%. Estimated Reynolds numbers fall in the range of $30 < Re < 84$, using the rise velocities given in Figure 8. Measurements were made at half

Table 11: Results of bubble size measurements

Test No.	air flow rate	bubble diameter	Standard Deviation	Coeff. of variation	Reynold Number
unit	scfh	mm	mm	%	(-)
1	1.09	1.67	0.51	30.5	30.1
2	1.64	1.93	0.54	28.0	38.6
3	2.29	2.28	0.68	29.8	48.0
4	2.99	3.21	0.59	18.4	73.8
5	3.67	2.94	0.63	21.4	67.6
6	4.37	3.15	0.67	21.3	72.5
7	5.03	3.65	0.54	14.8	84.0
8	4.37	3.22	0.77	23.9	74.0

of the diffuser depth of submergence. The correlation between bubble diameter and air flow rate is plotted in Figure 41. The relationship is as follows:

$$d_b = 1.5725\ (Q_G)^{0.50} \tag{99}$$

where

d_b = bubble diameter [mm], and

Q_G = air flow rate (scfh)

This correlation was employed to determine bubble diameter corresponding to experimental air flow rates.

The gas holdup ratio, ε, can be approximated with the Akita and Yoshida (1974) correlation using the relevant values of the gas flow rate (Q_G):

$$\varepsilon^{9/10} = \frac{1}{8.887}\left[\frac{(4Q_G)/(\pi\, d_c^2)}{g\, d_c^2}\right]\left[\frac{g\, d_c \rho}{\sigma}\right]^{1/8}\left[\frac{g\, d_c^3\, \rho^2}{\mu^2}\right]^{1/12} \tag{100}$$

where

ε = air holdup ratio [dimensionless],

Q_G = air flow rate [m^3/sec],

dc = column diameter [m],

g = gravity force [9.8 m/sec^2 at 20°C],

ρ = water density [980 kg/m^3 at 20°C],

σ = surface tension [0.0728 N/m at 20°C], and

μ = viscosity [0.001 N s /m^2 at 20°C].

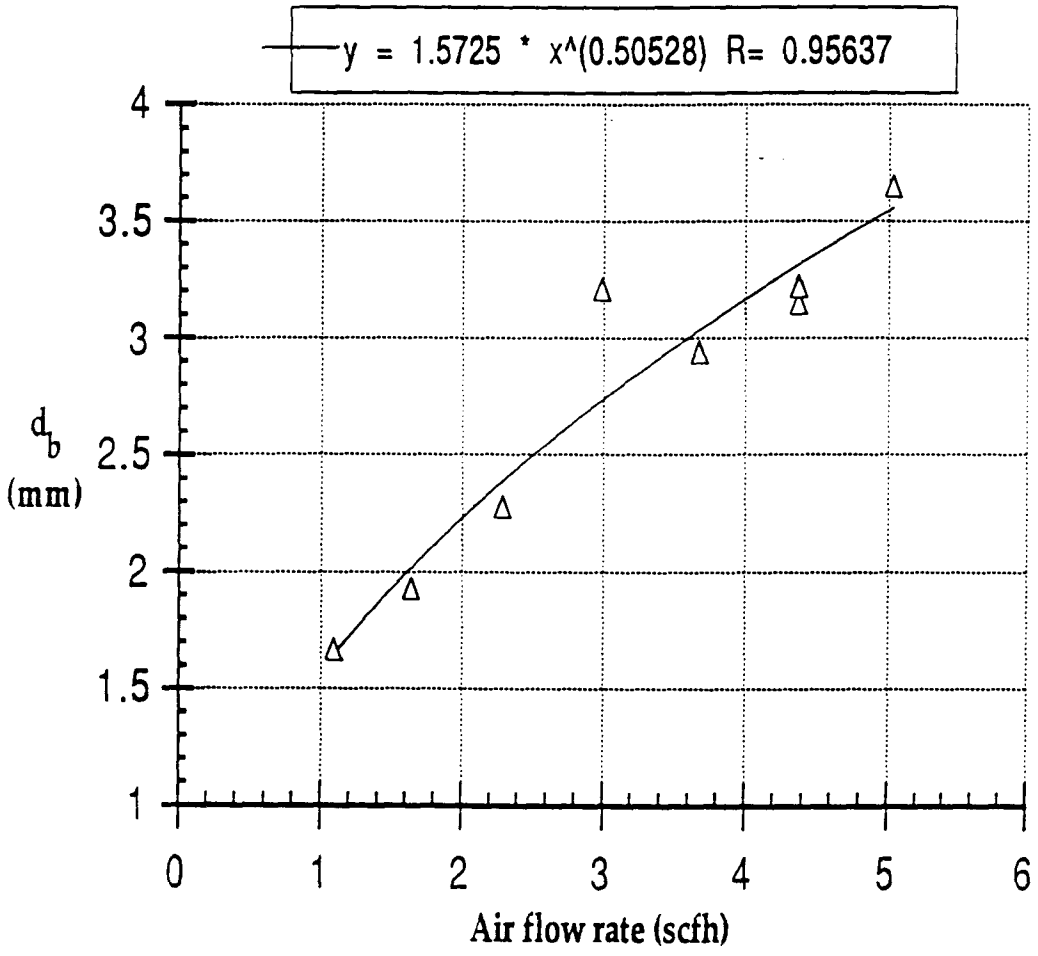

Figure 41. Correlation between bubble diameter and air flow rate in bubble column

The values of ε corresponding to the experimental air flow rates range from 0.09% to 0.34%. Equation (75) was used to estimate the specific interfacial area (a). The results of gas hold-up, wall-effect, superficial velocity, bubble diameter, and interfacial area in this study are listed in Table 12. Oxygen transfer coefficient (K_La), interfacial area (a), and mass-transfer coefficient (K_L) versus specific air flow rate (Q/V) are plotted in Figure 42. The correlation between a and specific air flow rate is as follows:

$$a = 2.65\left[\frac{Q_G}{V_L}\right]^{0.39} \tag{101}$$

where

a = interfacial area $= \frac{6\varepsilon}{d_b} = \frac{A_{total}}{V_L}$,

$\frac{Q_G}{V_L}$ = specific air flow rate [/hr],

A_{total} = total surface area [m^2],

d_b = diameter of air bubble [m], and

V_L = liquid volume [m^3].

It is interesting to note in Figure 42 and Table 12 that the order of interfacial area (3.2 - 5.76 1/m) is nearly two times that of K_L (1.67 - 2.67 m/hr) for a given K_La. Figure 42 indicates that the increase in the rate of mass transfer is mainly dependent on an increase in the interfacial area (a) and is only secondarily dependent on increases in K_L. Akita and Yoshida (1974) have related K_L to the square root of d_b for a constant temperature and surface tension. In this study, K_L is proportional to d_b raised to a power of 0.73 (Figure 43) which agrees reasonably well with the correla-

Table 12. Flow behavior and characteristic of bubble column

Items	Air flow rate	Specific air flow rate	Gas holdup	Bubble diameter	Wall effect	Superfacial velocity	Total bubble area	Interfacial area	Oxygen transfer coeff.	Mass-transfer coeff.
Abbreviation	AFR	Q/V	ε	db	η	vs	A	a=6e/db	KLa-O2	KL-O2
run\unit	(SCFH)	(1/hr)	(%)	(m)	(-)	(cm/sec)	(m2)	(1/m)	(1/hr)	(m/hr)
BC9	5.10	7.15	0.0034	0.00358	0.0179	0.128	0.1158	5.76	15.40	2.67
BC15	4.37	6.13	0.0030	0.00331	0.0166	0.109	0.1090	5.42	14.50	2.67
BC11	4.45	6.24	0.0030	0.00334	0.0167	0.111	0.1097	5.46	14.70	2.69
BC3	4.03	5.65	0.0028	0.00318	0.0159	0.101	0.1055	5.25	14.70	2.80
BC4	3.75	5.26	0.0026	0.00307	0.0153	0.094	0.1026	5.10	12.60	2.47
BC5	3.75	5.26	0.0026	0.00307	0.0153	0.094	0.1026	5.10	11.82	2.32
BC6	3.68	5.16	0.0026	0.00304	0.0152	0.092	0.1018	5.07	13.38	2.64
BC10	3.32	4.65	0.0023	0.00288	0.0144	0.083	0.0978	4.86	11.09	2.28
BC14	2.99	4.19	0.0021	0.00273	0.0137	0.075	0.0938	4.67	11.20	2.40
BC7	2.38	3.34	0.0017	0.00244	0.0122	0.060	0.0857	4.26	9.55	2.24
BC1	2.29	3.21	0.0017	0.00239	0.0120	0.057	0.0844	4.20	7.34	1.75
BC16	1.95	2.73	0.0014	0.00220	0.0110	0.049	0.0792	3.94	7.80	1.98
BC12	1.75	2.45	0.0013	0.00209	0.0104	0.044	0.0759	3.78	7.11	1.88
BC8	1.15	1.61	0.0009	0.00169	0.0084	0.029	0.0643	3.20	5.35	1.67

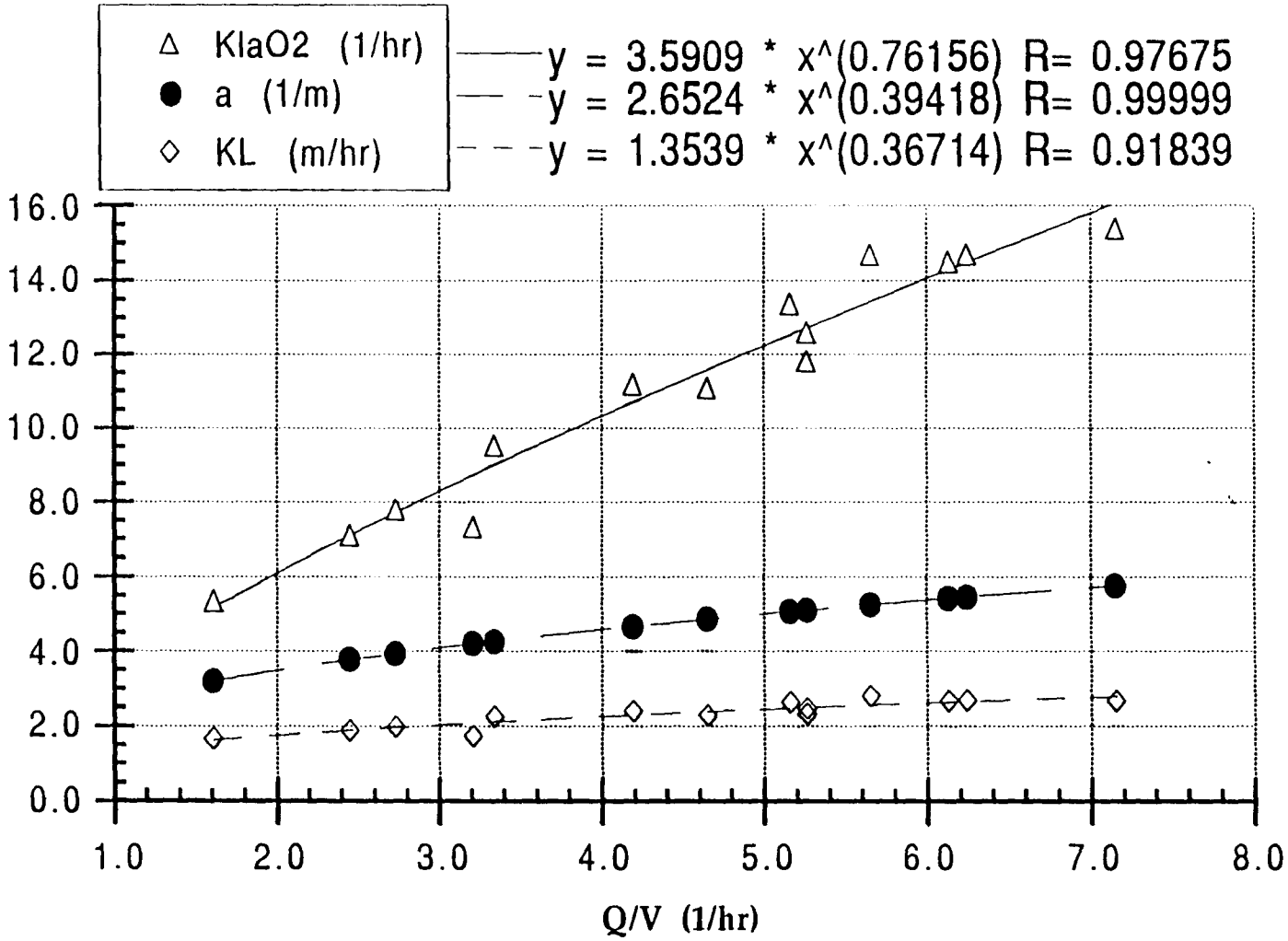

Figure 42. Correlation of oxygen transfer coefficient, interfacial area, and mass-transfer coefficient to specific air flow rates in buuble column

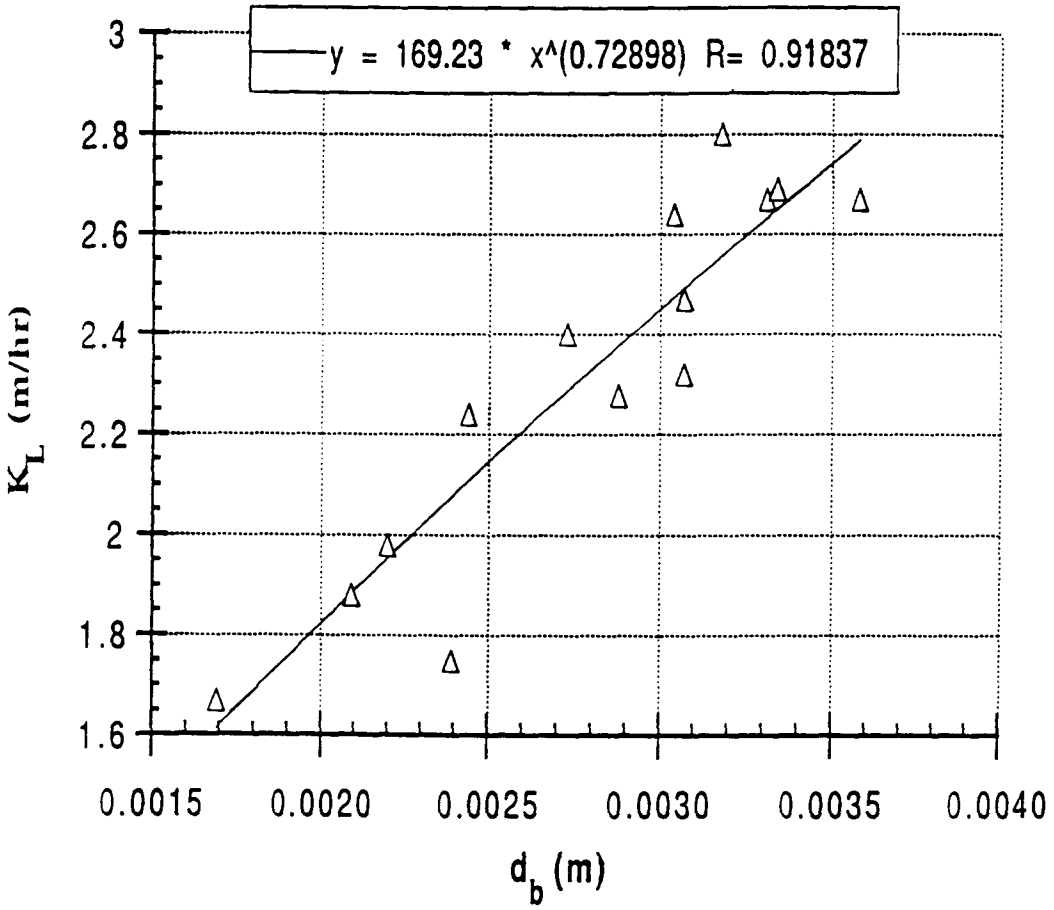

Figure 43. Correlation of mass-transfer coefficient (K_L) to bubble diameter

tion of Akita and Yoshida (1974).

Wall effects can bias results obtained in small scale reactors such as the ones used in this dissertation. According to Clift et al. (1978), the following conditions should apply to ensure that wall effects have negligible influence:

$$\eta < 0.08 + 0.02 \log (Re) \quad \text{for } 0.1 < Re < 100 \tag{102}$$

$$\eta < 0.12 \qquad \text{for } Re > 100 \tag{103}$$

where $\eta = d_b/d_c$, ratio of bubble diameter to column diameter. Using the bubble diameters and corresponding Reynolds numbers from this study, the range of $0.0084 < \eta < 0.0175$ is obtained, which is at least six times smaller than required ($\eta < 0.11$). Therefore, it is concluded that wall effects were negligible in these studies.

4.3.2 Determination of Volatilization Rate

The mass-transfer equation (36) describing the volatilization rate of VOCs in the bubble column was derived in Section 2 and is repreated here:

$$\ln\left[\frac{C_L}{C_{Lo}}\right] = -\frac{Q_G\, Hc}{V_L}\, Sd\, (t - t_o) \tag{36}$$

where

Q_G = air flow rate [L^3 $time^{-1}$],

V_L = reactor volume [L^3], and

Sd = degree of saturation [dimensionless].

The procedure to estimate the volatilization rate of VOCs in the bubble column is different from the surface aeration and is briefly described as follows:

1. According to equation (36), a plot of the negative log-linear regression of concentration ratio $\ln(\frac{C_L}{C_{Lo}})$ versus time $(t - t_o)$ gives the "slope" as follows:

$$\text{slope} = -\frac{Q_G Hc}{V_L} Sd \tag{37}$$

2. According to equation (36), Sd can be determined by

$$Sd = \frac{\text{slope}}{-\frac{Q_G Hc}{V_L}} = \frac{\text{slope}\frac{V_L}{Q_G}}{Hc} \tag{38}$$

3. Equation (42) can be used to convert the "slope" of a log-linear regression of concentration ratio versus time into the stripping rate via transfer parameter. The equation is as follows:

$$K_L a = -\text{slope } f_{K_L a} \,. \tag{42}$$

where

$f_{K_L a}$ = transfer parameter, $\frac{-\ln(1-Sd)}{Sd}$

Figure 44 shows the correlation between transfer parameter ($f_{K_L a}$) and degree of saturation (Sd). The stripping rate can be calculated using Figure 44 via transfer parameter, as long as the degree of saturation of VOCs is estimated by the "slope" and Hc.

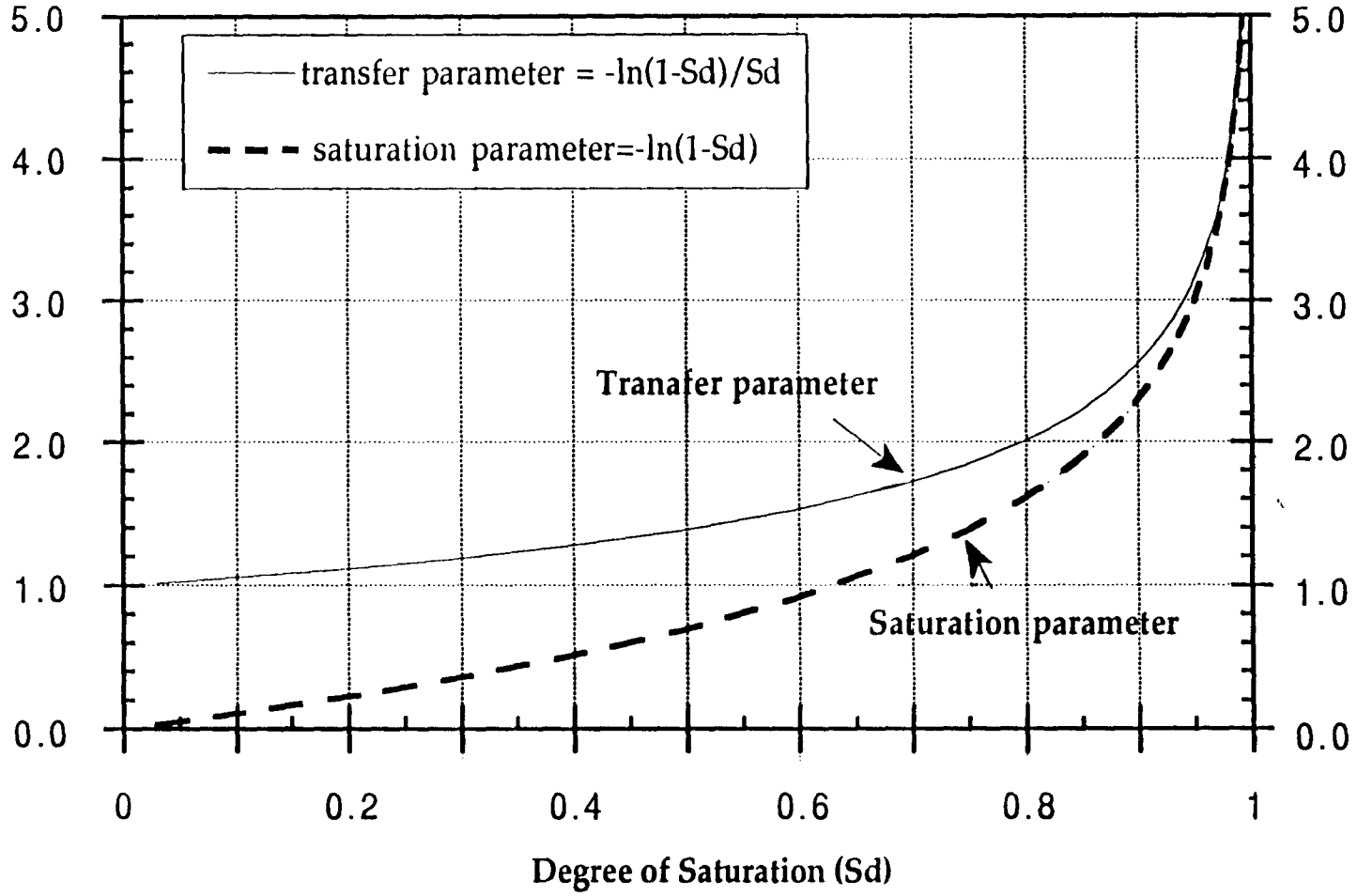

Figure 44. Correlation of tranafer parameter, saturation paramater to degree of saturation of VOCs in bubbles

The methodology developed in this study was used to estimate $K_L a$-values of twenty VOCs. Tables 13, 14, and 15 summarize slope, Sd, and $K_L a$-values of twenty VOCs and oxygen from experiments using different air flow rates from 1.15 scfh to 5.10 scfh. It was anticipated that higher Henry's coefficients correspond to higher mass-transfer coefficients. This trend can be seen in Figures 45a and 45b which show the dependence of $K_L a$ on the specific air flow rate ($\frac{Q_G}{V}$). In general, as $\frac{Q_G}{V}$ increases, $K_L a$ increases for a given Hc, and as volatility (or Hc) increases, $K_L a$ increases for a given $\frac{Q_G}{V}$.

The results from Tables 15 for $K_L a$ at different air flow rates can be correlated to produce a simple power function of the form, $Y = b\ X^m$. The individual plots of $K_L a$ versus $\frac{Q_G}{V}$ for twenty compounds are shown in Figure 46 and Appendix G. The values of b and m are listed in Table 16. The correlation of b and m with Hc are plotted in Figure 47. The m-values of the power function are all very close to 1.0 over a range of Hc from 0.04 to 30.2. The nearly constant m-values of 1.0 indicate that the relationship between $K_L a$ and $\frac{Q_G}{V}$ is linear. The increase of b-values with Hc for Hc < 1.2 imply that higher Henry's coefficients correspond to higher mass-transfer coefficients.

Figure 48 shows the percentages of the mean values of Sd for each compound versus the Hc. As can be seen in Figure 48, Sd increases with decreasing Hc. This implies that the gas-phase resistance becomes increasingly significant as Hc decreases for a given specific air flow rate. Table 14 shows that the coefficient of variation (CV)

Table 13. Summary of slope (log-linear regression of concentration ratio versus time) of twenty VOCs in bubble column (1/hr)

VOCs\run	Hc	BC9	BC15	BC11	BC3	BC4	BC5	BC6	BC10	BC14	BC7	BC1	BC16	BC12	BC8
Q (scfh)		5.10	4.37	4.45	4.03	3.75	3.75	3.68	3.32	2.99	2.38	2.29	1.95	1.75	1.15
O2	30.02	15.43	14.5	14.7	14.72	12.62	11.82	13.38	11.09	11.2	9.55	7.34	7.8	7.11	5.35
111TCA	0.525	3.208	2.626	3.101	2.593	2.525	2.389	2.344	2.010	1.948	1.591	1.378	1.228	1.211	0.764
PCE	0.565	3.490	2.843	3.312	2.577	2.524	2.461	2.402	2.103	1.991	1.498	1.331	1.293	1.207	0.787
CT	1.122	5.733	4.955	5.160	4.625	4.122	3.978	4.230	3.618	3.645	2.724	2.360	2.356	2.137	1.449
TCE	0.252	1.746	1.449	1.515	1.342	1.290	1.325	1.300	1.114	0.958	0.807	0.712	0.625	0.592	0.391
EBZ	0.260	1.752	1.480	1.605	1.372	1.288	1.262	1.247	1.117	1.010	0.799	0.675	0.656	0.606	0.382
12DCE	0.166	1.093	0.943	0.990	0.880	0.787	0.779	0.786	0.711	0.654	0.540	0.458	0.424	0.369	0.257
MXY	0.236	1.594	1.366	1.404	1.124	1.183	1.157	1.138	0.997	0.958	0.753	0.620	0.606	0.570	0.380
OXY	0.181	1.169	0.992	1.026	0.981	0.857	0.840	0.836	0.725	0.685	0.551	0.470	0.467	0.414	0.272
TLN	0.230	1.522	1.302	1.331	1.300	1.144	1.118	1.094	0.965	0.849	0.704	0.691	0.585	0.563	0.362
BZ	0.226	1.442	1.191	1.248	1.109	1.087	1.097	1.153	0.950	0.837	0.707	0.658	0.556	0.494	0.336
CLF	0.160	1.037	0.907	0.923	0.848	0.783	0.801	0.785	0.671	0.633	0.518	0.447	0.418	0.383	0.242
CBZ	0.146	0.976	0.840	0.846	0.797	0.731	0.722	0.704	0.636	0.559	0.468	0.429	0.354	0.342	0.231
BBZ	0.099	0.661	0.558	0.571	0.540	0.508	0.504	0.500	0.421	0.370	0.326	0.276	0.264	0.236	0.157
13DCB	0.124	0.841	0.704	0.728	0.691	0.616	0.616	0.601	0.537	0.496	0.396	0.346	0.328	0.289	0.192
12DCB	0.087	0.606	0.525	0.538	0.487	0.445	0.452	0.444	0.388	0.354	0.287	0.234	0.237	0.212	0.139
14DCB	0.108	0.744	0.642	0.652	0.603	0.546	0.546	0.533	0.469	0.441	0.348	0.315	0.289	0.258	0.172
BF	0.041	0.245	0.190	0.233	0.225	0.217	0.243	0.208	0.154	0.128	0.173	0.155	0.081	0.081	0.048
EDB	0.041	0.258	0.185	0.208	0.192	0.186	0.215	0.213	0.179	0.152	0.151	0.128	0.098	0.082	0.060
1122TCA	0.042	0.256	0.155	0.202	0.268	0.272	0.208	0.211	0.171	0.100	0.159	0.131	0.056	0.079	0.068
NAPH	0.038	0.237	0.168	0.218	0.161	0.231	0.195	0.212	0.171	0.108	0.108	0.123	0.060	0.072	0.055

Table 14. Summary of degree of saturation of twenty VOCs in bubble column

Run	Hc	BC9	BC15	BC11	BC3	BC4	BC5	BC6	BC10	BC14	BC7	BC1	BC16	BC12	BC8	Max	Mean	stdev	% CV
Q/V (1/hr)		7.19	6.16	6.27	5.68	5.28	5.28	5.18	4.68	4.21	3.35	3.23	2.75	2.47	1.62				
O2	30.02	0.07	0.08	0.08	0.09	0.08	0.07	0.09	0.08	0.09	0.09	0.08	0.09	0.10	0.11	0.11	0.09	0.01	12.5
111TCA	0.525	0.85	0.81	0.94	0.87	0.91	0.86	0.86	0.82	0.88	0.90	0.81	0.85	0.94	0.90	0.94	0.87	0.04	4.8
PCE	0.565	0.86	0.82	0.93	0.80	0.85	0.82	0.82	0.80	0.84	0.79	0.73	0.83	0.87	0.86	0.93	0.83	0.05	5.6
CT	1.122	0.71	0.72	0.73	0.73	0.70	0.67	0.73	0.69	0.77	0.72	0.65	0.76	0.77	0.80	0.80	0.73	0.04	5.7
TCE	0.252	0.96	0.93	0.96	0.94	0.97	–	0.99	0.95	0.90	0.95	0.88	0.90	0.95	0.96	0.99	0.94	0.03	3.4
EBZ	0.260	0.94	0.92	0.98	0.93	0.94	0.92	0.93	0.92	0.92	0.92	0.80	0.92	0.95	0.91	0.98	0.92	0.04	4.2
12DCE	0.166	0.92	0.92	0.95	0.93	0.90	0.89	0.91	0.92	0.94	0.97	0.86	0.93	0.90	0.96	0.97	0.92	0.03	3.2
MXY	0.236	0.94	0.94	0.95	0.84	0.95	0.93	0.93	0.90	0.96	0.95	0.81	0.93	0.98	0.99	0.99	0.93	0.05	5.3
OXY	0.181	0.90	0.89	0.90	0.95	0.90	0.88	0.89	0.86	0.90	0.91	0.80	0.94	0.93	0.93	0.95	0.90	0.04	4.1
TLN	0.230	0.92	0.92	0.92	–	0.94	0.92	0.92	0.90	0.88	0.91	0.93	0.93	0.99	0.97	0.99	0.93	0.03	3.2
BZ	0.226	0.89	0.86	0.88	0.86	0.91	0.92	0.98	0.90	0.88	0.93	0.90	0.90	0.89	0.92	0.98	0.90	0.03	3.5
CLF	0.160	0.90	0.92	0.92	0.93	0.93	0.95	0.95	0.90	0.94	0.97	0.87	0.95	0.97	0.93	0.97	0.93	0.03	3.0
CBZ	0.146	0.93	0.93	0.92	0.96	0.95	0.94	0.93	0.93	0.91	0.96	0.91	0.88	0.95	0.98	0.98	0.93	0.02	2.6
BBZ	0.099	0.93	0.92	0.92	0.96	0.97	0.96	0.97	0.91	0.89	0.98	0.86	0.97	0.97	0.98	0.98	0.94	0.04	4.0
13DCB	0.124	0.94	0.92	0.94	0.98	0.94	0.94	0.93	0.93	0.95	0.95	0.86	0.96	0.95	0.96	0.98	0.94	0.03	2.8
12DCB	0.087	0.97	0.98	0.99	0.99	0.97	0.98	0.98	0.95	0.97	0.98	0.83	0.99	0.99	0.99	0.99	0.97	0.04	4.2
14DCB	0.108	0.96	0.97	0.96	0.98	0.96	0.96	0.95	0.93	0.97	0.96	0.90	0.97	0.97	0.98	0.98	0.96	0.02	2.2
BF	0.041	0.83	0.75	0.91	0.97	–		0.98	0.80	0.74	–	–	0.72	0.80	0.72	0.98	0.82	0.10	11.8
EDB	0.041	0.88	0.73	0.81	0.82	0.86	0.99	–	0.93	0.88	–	0.97	0.87	0.81	0.90	0.99	0.87	0.07	8.3
1122TCA	0.042	0.85	0.60	0.77	–	–	0.94	0.97	0.87	0.57	–	0.97	0.49	0.76	–	0.97	0.78	0.17	22.5
NAPH	0.038	0.87	0.72	0.91	0.75	–	0.97	–	0.96	0.67	0.85	–	0.57	0.77	0.89	0.97	0.81	0.13	15.6

Note: max = maximum value; stdev = standard deviation; % CV = coefficient of variation = stdev/mean

Table 15. Summary of mass transfer coefficients of oxygen and VOCs in bubble column (unit: 1/hr)

Run	Hc	BC9	BC15	BC11	BC3	BC4	BC5	BC6	BC10	BC14	BC7	BC1	BC16	BC12	BC8	Max	Mean	stdev	% CV
Q/V (1/hr)		7.19	6.16	6.27	5.68	5.28	5.28	5.18	4.68	4.21	3.35	3.23	2.75	2.47	1.62				
O2	30.02	16.01	15.10	15.31	15.39	13.15	12.28	13.99	11.55	11.73	10.03	7.63	8.19	7.48	5.67	16.01	11.68	3.40	29.1
111TCA	0.525	7.17	5.41	9.38	6.08	6.69	5.48	5.37	4.19	4.70	4.12	2.84	2.75	3.55	1.94	9.38	4.98	1.98	39.8
PCE	0.565	7.97	5.91	9.68	5.22	5.58	5.19	5.02	4.20	4.31	2.96	2.39	2.78	2.80	1.80	9.68	4.70	2.20	46.8
CT	1.122	10.01	8.73	9.30	8.25	7.05	6.59	7.56	6.14	6.97	4.84	3.82	4.45	4.10	2.90	10.01	6.48	2.20	33.9
TCE	0.252	6.03	4.21	5.04	3.98	4.62	–	6.91	3.42	2.47	2.62	1.70	1.61	1.90	1.29	6.91	3.52	1.79	50.8
EBZ	0.260	5.19	4.14	6.80	3.91	3.81	3.45	3.49	3.05	2.80	2.16	1.37	1.79	1.86	1.00	6.80	3.20	1.57	49.0
12DCE	0.166	2.96	2.62	3.14	2.56	2.00	1.92	2.10	1.92	1.91	1.95	1.03	1.21	0.95	0.84	3.14	1.94	0.73	37.6
MXY	0.236	4.77	4.09	4.40	2.45	3.70	3.28	3.25	2.58	3.29	2.39	1.28	1.77	2.26	1.94	4.77	2.96	1.04	35.0
OXY	0.181	2.98	2.46	2.66	3.18	2.17	2.01	2.08	1.64	1.74	1.45	0.95	1.39	1.17	0.77	3.18	1.90	0.74	38.7
TLN	0.230	4.19	3.57	3.70	–	3.45	3.07	2.97	2.44	2.02	1.88	1.99	1.64	2.79	1.32	4.19	2.70	0.89	32.9
BZ	0.226	3.55	2.70	3.01	2.56	2.88	3.00	4.84	2.42	2.01	2.05	1.70	1.40	1.21	0.91	4.84	2.45	1.03	42.0
CLF	0.160	2.67	2.50	2.53	2.46	2.20	2.49	2.43	1.70	1.89	1.81	1.04	1.32	1.39	0.70	2.67	1.94	0.63	32.6
CBZ	0.146	2.79	2.45	2.36	2.70	2.28	2.12	2.01	1.83	1.47	1.53	1.14	0.86	1.08	0.89	2.79	1.82	0.67	36.5
BBZ	0.099	1.88	1.51	1.57	1.82	1.86	1.73	1.87	1.11	0.91	1.33	0.64	0.96	0.83	0.62	1.88	1.33	0.48	35.9
13DCB	0.124	2.57	1.95	2.14	2.81	1.85	1.85	1.76	1.51	1.56	1.27	0.80	1.12	0.89	0.63	2.81	1.62	0.64	39.7
12DCB	0.087	2.18	2.10	2.34	2.10	1.58	1.88	1.87	1.25	1.24	1.20	0.50	1.14	0.95	0.60	2.34	1.50	0.60	39.9
14DCB	0.108	2.47	2.24	2.23	2.51	1.79	1.79	1.70	1.33	1.58	1.17	0.82	1.08	0.92	0.71	2.51	1.60	0.61	38.3
BF	0.041	0.52	0.35	0.61	0.79	–	–	0.82	0.31	0.23	–	–	0.14	0.16	0.09	0.82	0.34	0.29	85.9
EDB	0.041	0.61	0.33	0.43	0.41	0.42	1.06	–	0.52	0.37	–	0.45	0.23	0.17	0.16	1.06	0.40	0.26	65.4
1122TCA	0.042	0.57	0.24	0.38	–	–	0.61	0.76	0.40	0.15	–	0.46	0.08	0.15	–	0.76	0.35	0.24	70.4
NAPH	0.038	0.55	0.30	0.59	0.30	–	0.71	–	0.58	0.18	0.24	–	0.09	0.14	0.14	0.71	0.35	0.22	63.8

Notes: Max = maximum; stdev = standard deviation; % CV = percentage of coefficient of variation

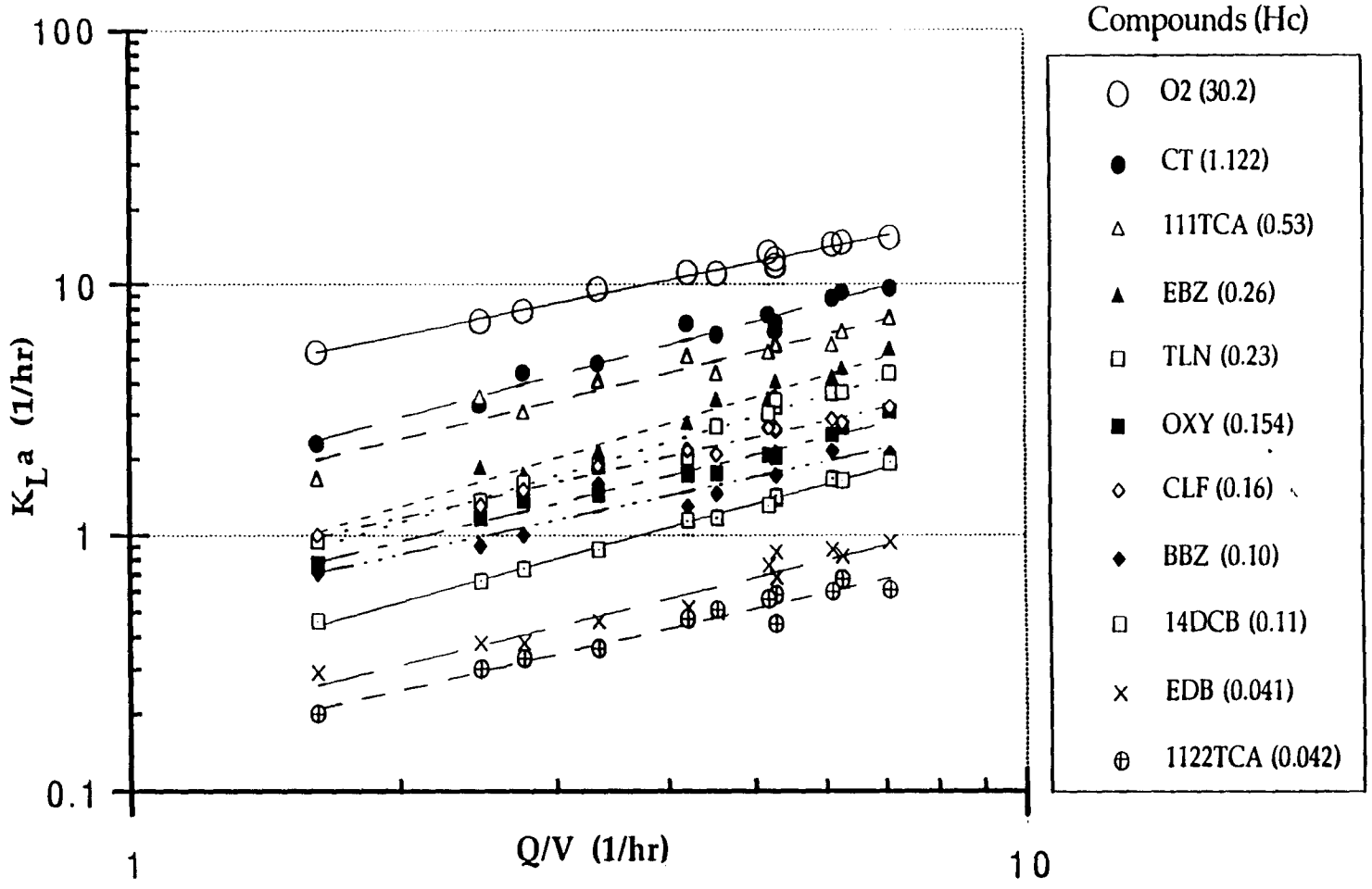

Figure 45a. Mass transfer coefficients as a function of specific air flow rate and Henry's coefficient in bubble column

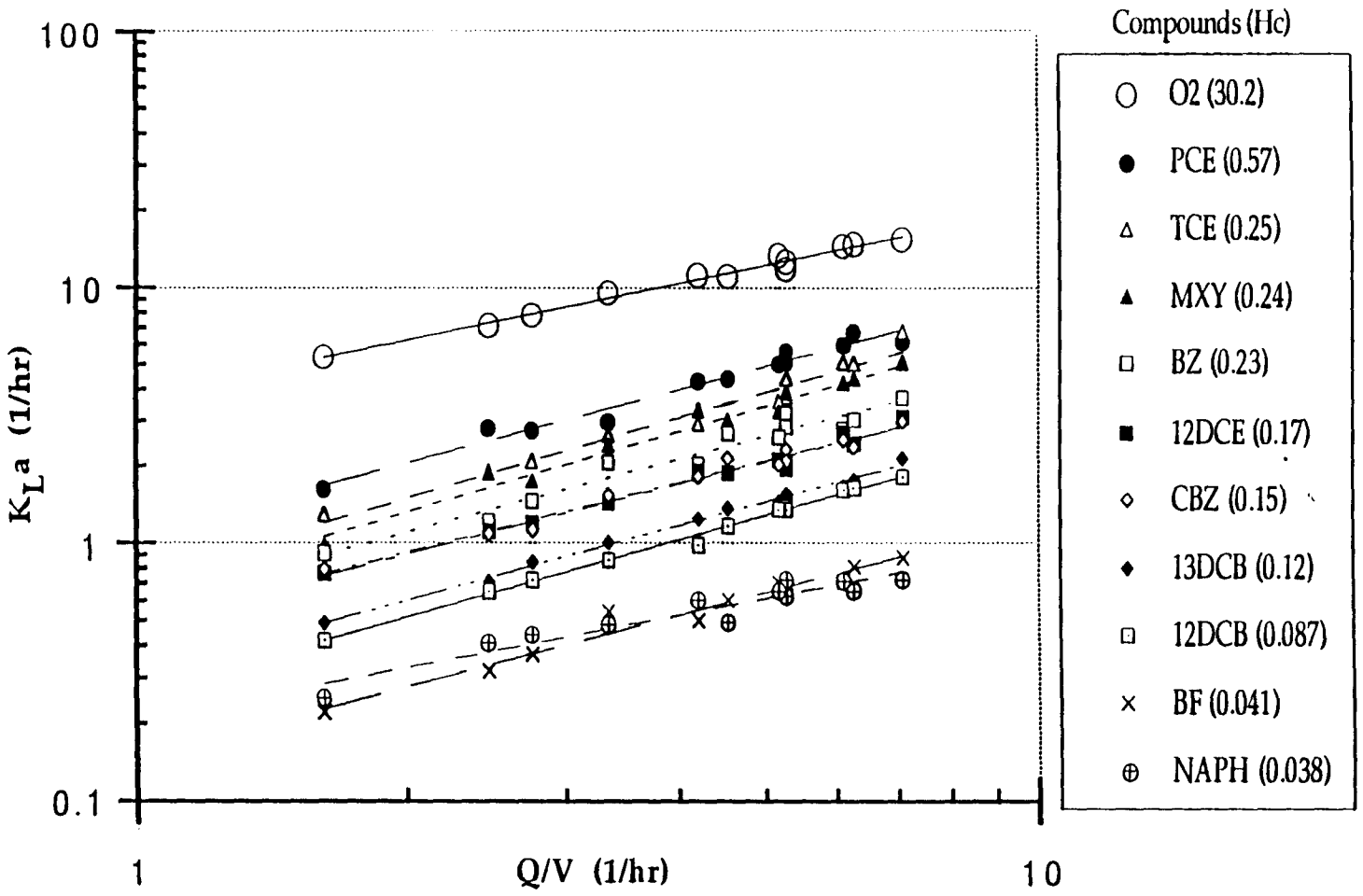

Figure 45b. Mass transfer coefficients as a function of specific air flow rate and Henry's constant in bubble column

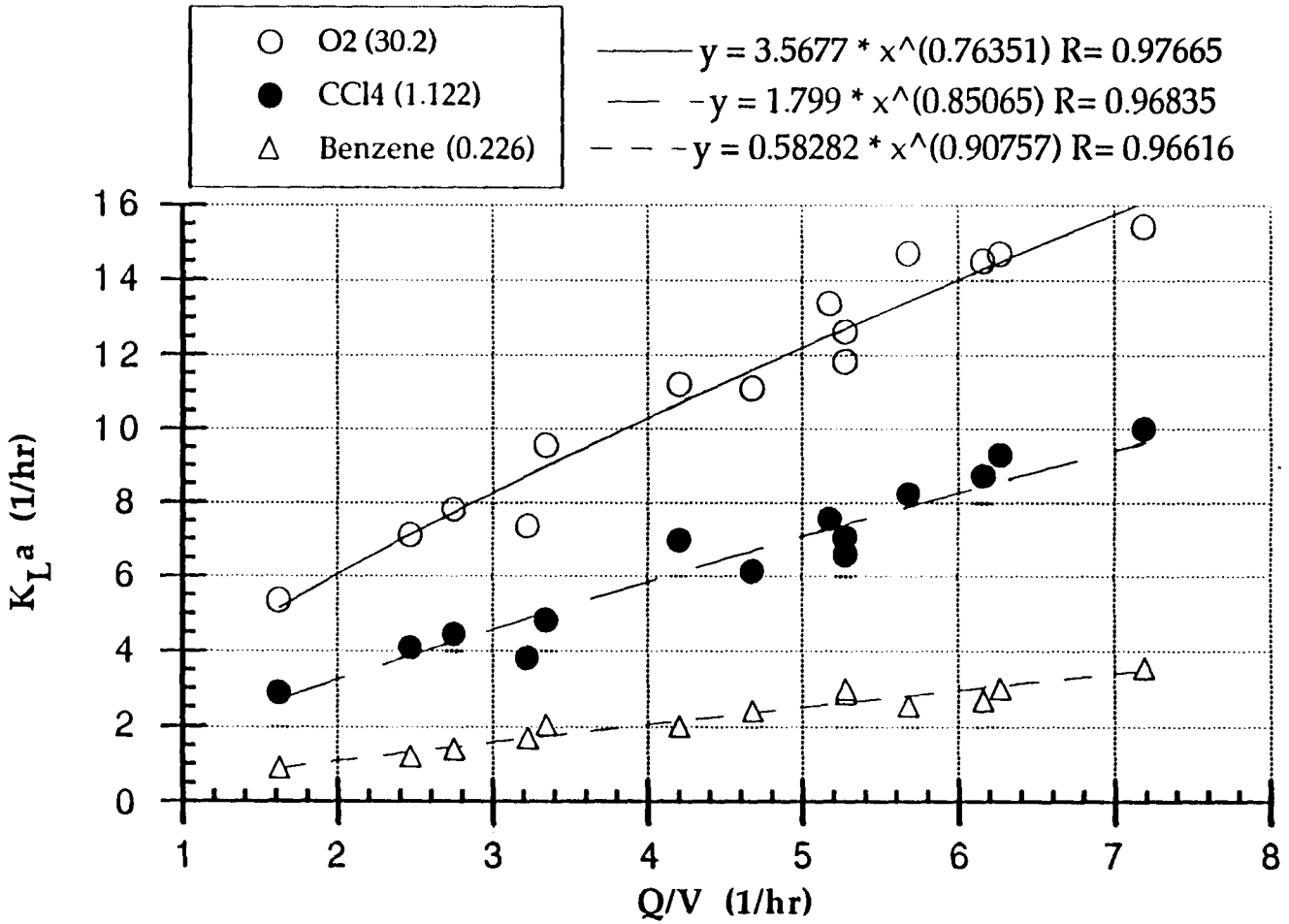

Figure 46. Correlation of mass transfer coefficient to specific air flow rate (O_2, CCl_4, Benzene)

Table 16. Summary of parameters b and m-value for relating KLa = b (Q/V)^m in bubble column

Compounds	Hc	b	m
O2	30.200	3.568	0.764
CT	1.122	1.799	0.851
PCE	0.570	1.025	0.967
111TCA	0.530	1.229	0.919
TCE	0.250	0.647	1.072
EBZ	0.260	0.572	1.093
MCY	0.240	1.171	0.658
TLN	0.230	0.753	0.833
BZ	0.226	0.562	0.963
OXY	0.181	0.465	0.927
12DCE	0.166	0.470	0.933
CLF	0.156	0.514	0.881
CBZ	0.146	0.463	0.904
BBZ	0.098	0.388	0.810
13DCB	0.120	0.384	0.926
14DCB	0.110	0.393	0.922
12DCB	0.087	0.338	0.972
E DB	0.041	0.107	0.810
BF	0.041	0.046	1.245
1122TCA	0.042	0.121	0.663
NAPH	0.038	0.053	1.110

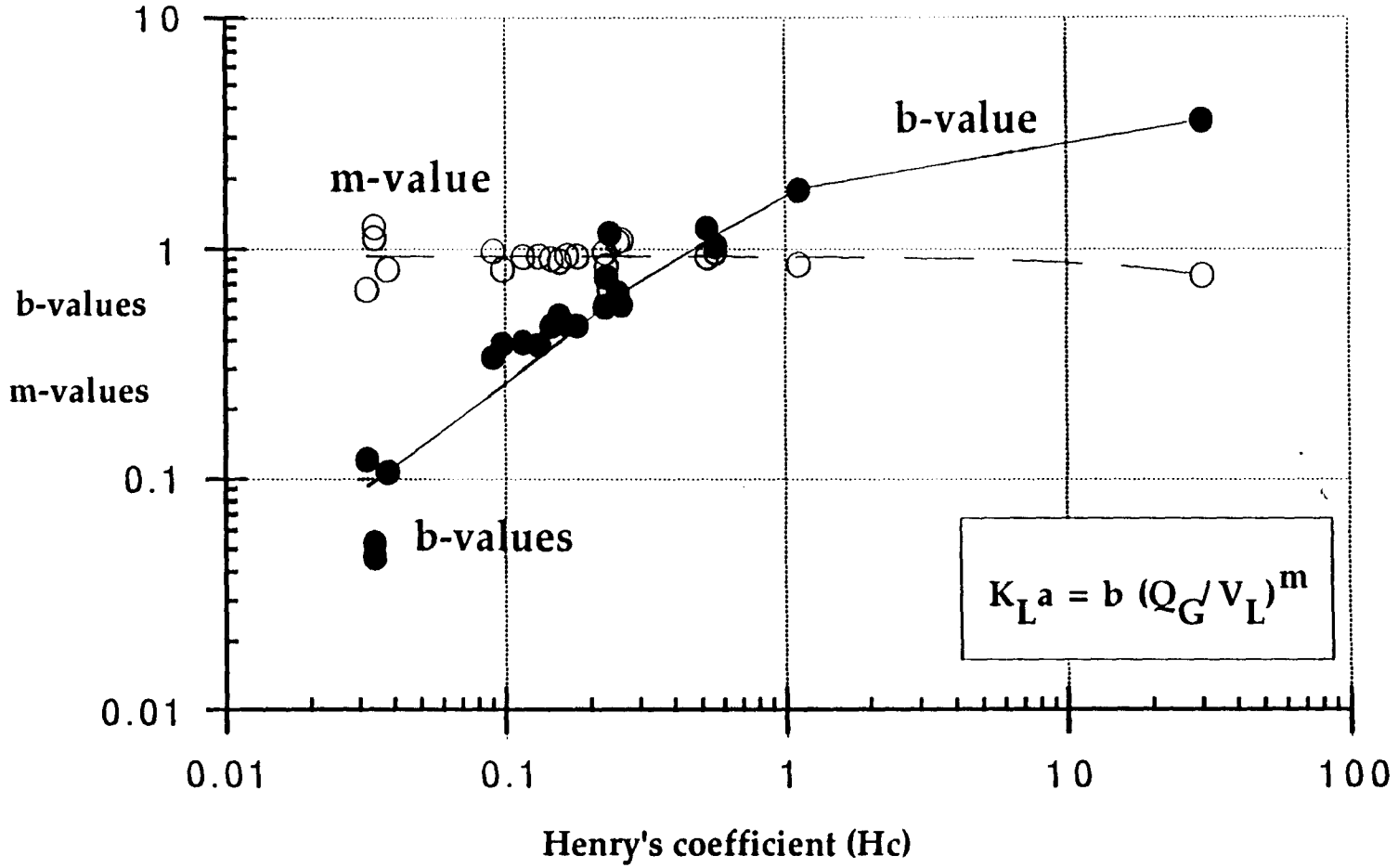

Figure 47. Summary of correlation parameters b and m for relating $K_L a = b\ (Q/V)^m$ versus Henry's coefficient in bubble column

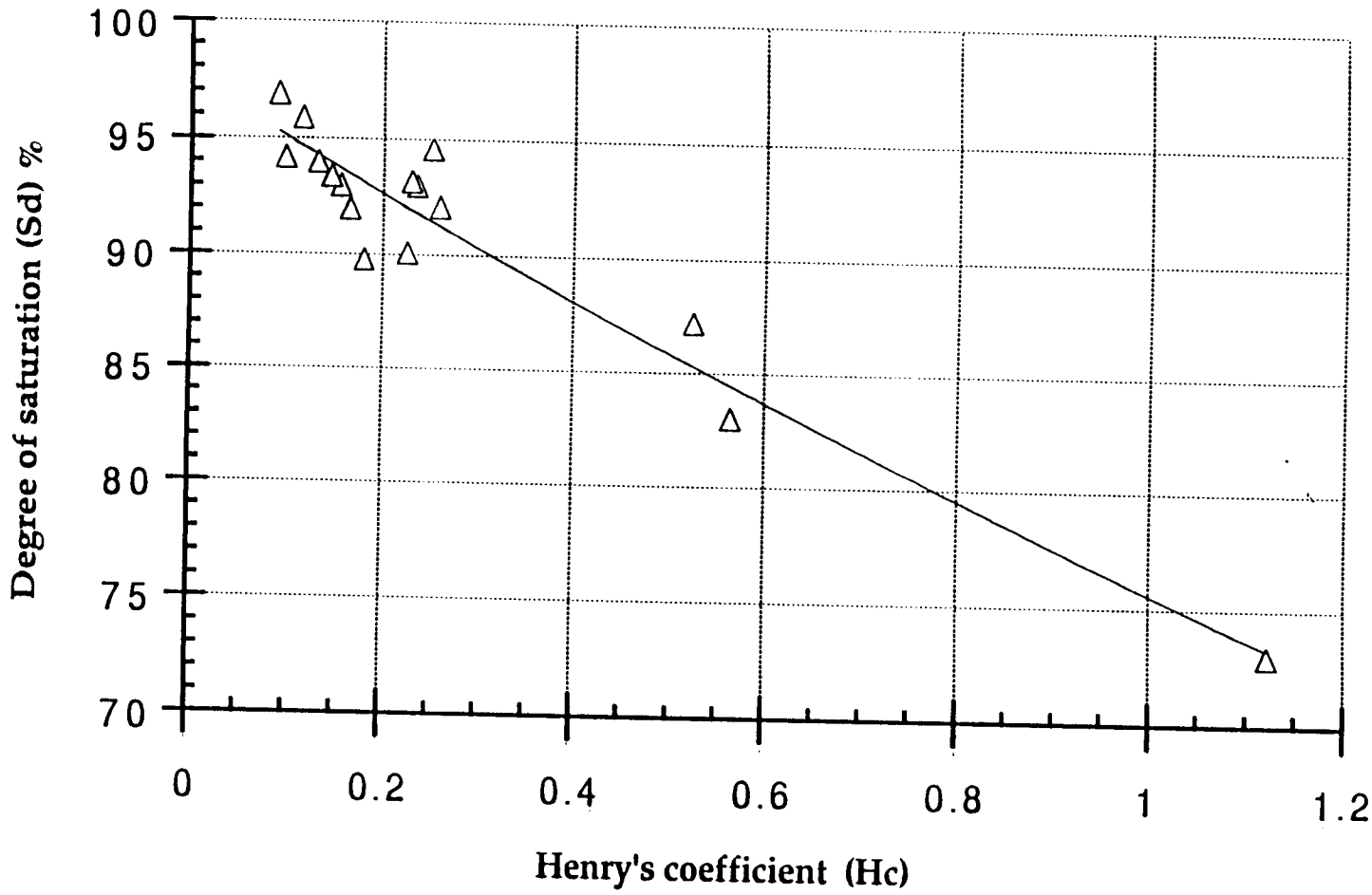

Figure 48. Mean value of degree of saturation (Sd) for twenty VOCs versus Hc in bubble column

of Sd is very high for low volatility compounds, such as EDB (8.9%), bromoform (11.8%), 1,1,2,2-TCA (22.4%), and naphthalene (16%). The accuracy of Sd depends on the slope of a log-linear regression of concentration ratio versus time which is obtained from the change of concentration with elapsed time. The reason for these high values for low volatility compounds can be explained by Figure 49. Figure 49 shows change of concentration versus time performed in the test number of BC12 with air flow rates of 1.75 scfh. Highly volatile compounds, such as CCl_4 and 111 TCA, were stripped completely within 150 min., whereas only 10% of naphthalene was removed in 150 min. Due to very low initial concentrations (usually less than 2 mg/L) and very short sampling intervals, the experimental precision for low volatility VOCs is less than that of high volatility VOCs.

4.3.3 Estimating the Ratio of $k_G a/k_L a$

The procedure used to estimate the ratio of $\frac{k_G a}{k_L a}$ was described in the surface aeration results section. A summary of the ratios of $\frac{k_G a}{k_L a}$ over the range of specific air flow rate in bubble column is listed in Table 17 and plotted in Figure 50. The ratios of $\frac{k_G a}{k_L a}$ were relatively constant between 2.2 to 4.6 for experiments performed with specific air flow rates from 2.47 to 7.19 (1/hr). The ratios in the bubble column were much smaller than those in surface aeration experiments. This implies that the gas-phase resistance in the bubble column is extremely important and must be considered.

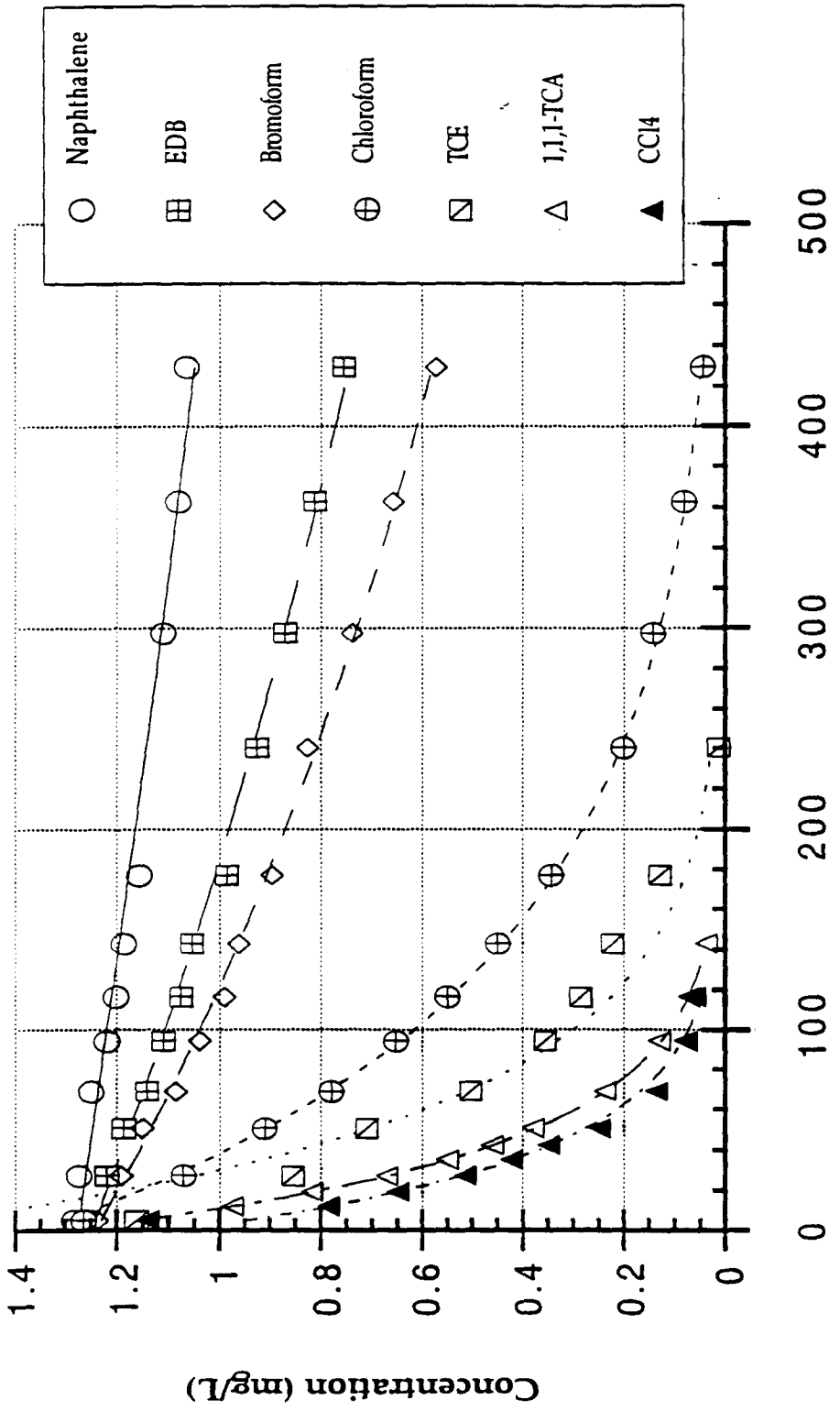

Figure 49. Typical plot of concentration versus time in bubble column (BC12, air flow rate = 1.75 scfh)

Table 17. Summary of gas-phase and liquid-phase mass transfer coefficients and its ratio in bubble column

	specific air flow rate	oxygen transfer coefficients	gas transfer coefficients	gas/liquid mass transfer ratio
Abbreviation	Q/V	KLa -O2	kGa	kGa/kLa
run\unit	(1/hr)	(1/hr)	(m/hr)	(-)
BC9	7.19	15.43	40.00	2.59
BC15	6.16	14.50	36.63	2.53
BC11	6.27	14.70	34.49	2.35
BC3	5.68	14.72	47.60	3.23
BC4	5.28	12.62	45.45	3.60
BC5	5.28	11.82	36.90	3.12
BC6	5.18	15.38	34.20	2.22
BC10	4.68	11.09	29.40	2.65
BC14	4.21	11.20	25.20	2.25
BC7	3.35	9.55	25.50	2.67
BC1	3.23	7.34	21.23	2.89
BC16	2.75	7.80	35.97	4.61
BC12	2.47	7.11	16.23	2.28

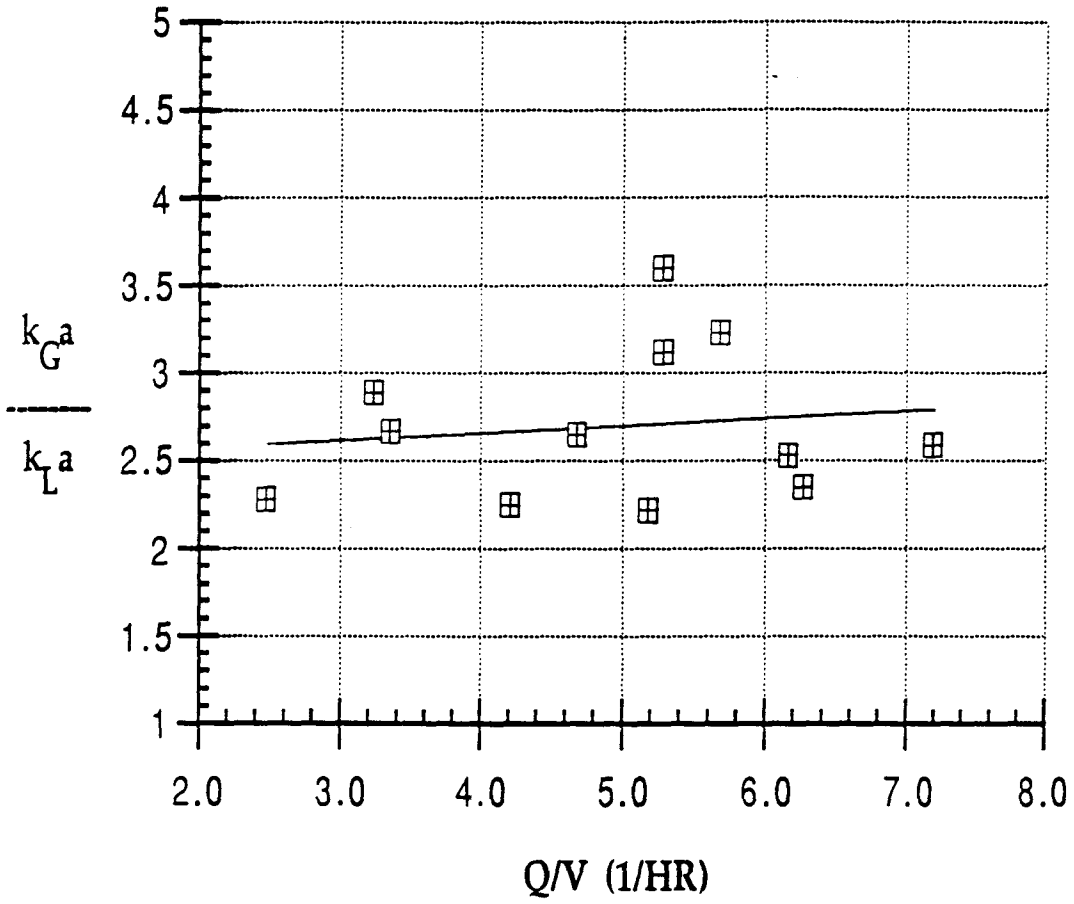

Figure 50. Correlation between ratios of gas-phase to liquid-phase mass transfer coefficient to specfic air flow rate

4.3.3.1 The Effect of Superficial Velocity on $k_G a$

The surface aeration experiments performed with consistent windspeeds of 1.8 to 2.4 (m/s) resulted in a relatively constant value of gas transfer coefficient ($k_G a$) of 126. However, the air phase hydrodynamic conditions in the bubble column varied with the air flow rate which created the different superficial velocity (v_s = air flow rate/column cross section area). The superficial velocities created in this study ranged from 0.044 to 0.128 (cm/sec), which produced $k_G a$'s ranging from 16 to 48. Accordingly, the $k_G a$-values are proportional to $v_s^{0.993}$. (Figure 51). The correlation denotes that $k_G a$ increases with increasing v_s. Figure 52 shows that $k_G a$ is proportional to $k_L a$, thus, there is a relative constant of ratio of $\frac{k_G a}{k_L a}$.

4.3.4 Results of Modification of Ψ-value: Ψ_m-value

The ratios of $\frac{k_G a}{k_L a}$ were used to estimate the fraction of liquid to overall mass transfer resistance for different specific air flow rates using equation (13). Thus, the Ψ-value incorporating the fraction of liquid resistance was used to determine the stripping rate of VOCs.

A summary of Ψ and Ψ_m-values for ten experiments are listed in Table 18. Figure 53 shows a comparison of Ψ and Ψ_m-values for ten experiments. The value of Ψ seems almost constant for twenty VOCs with different Hc's, whereas, Ψ_m-values decrease with decreasing Hc. Since $\Psi_m = \Psi \frac{R_L}{R_T}$, the difference between Ψ and Ψ_m can be illustrated by a comparison of the significance of $\frac{R_L}{R_T}$ (Table 19). The $\frac{R_L}{R_T}$ of

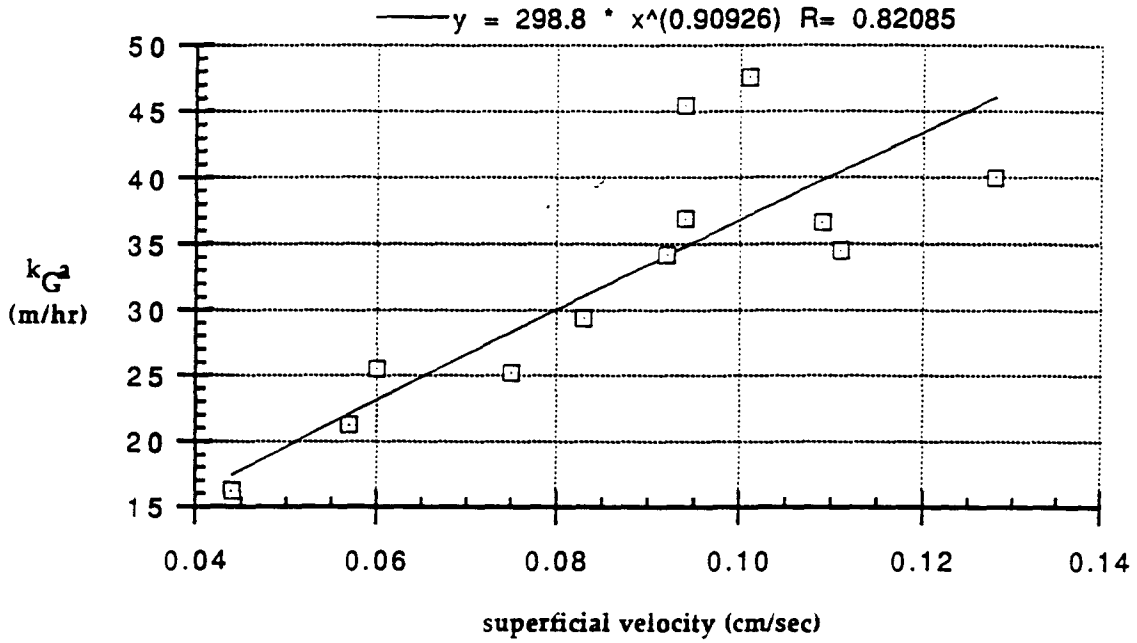

Figure 51. Correlation between gas-phase transfer coefficient and superficial velocity

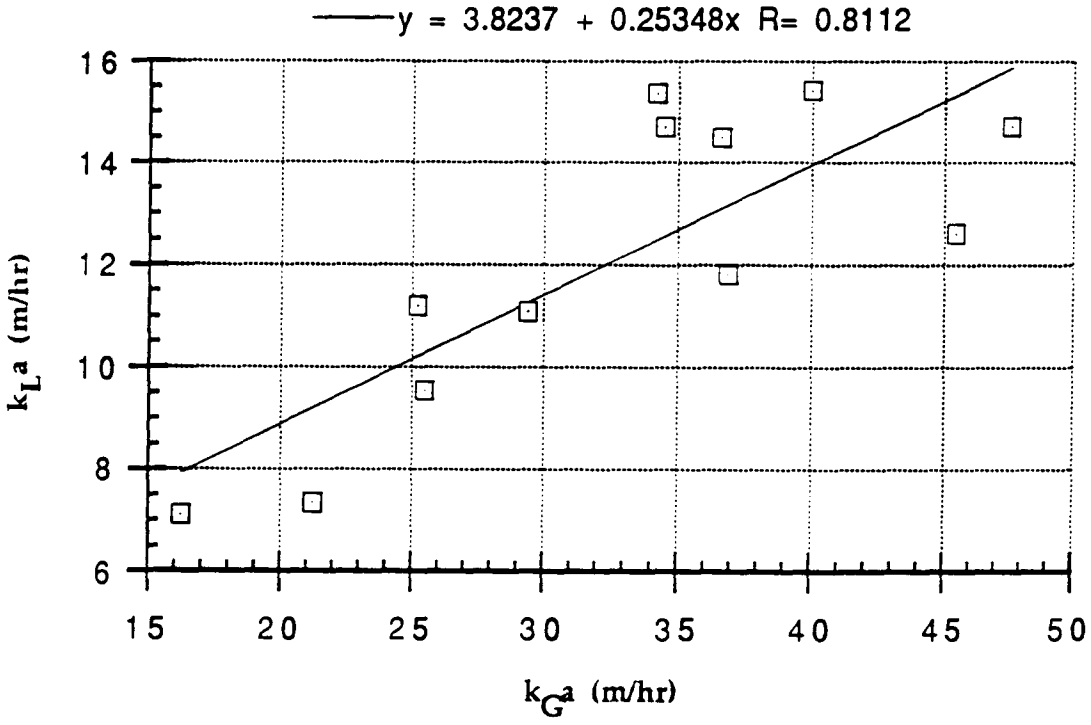

Figure 52. Plot of liquid-phase mass transfer coefficient versus gas-phase mass transfer coefficient

Table 18. Summary of Psi and Psi m-values in bubble column

Compounds	Hc	DL	Ψ	Ψ	Ψ-M	Ψ-M	Ψ-M	Ψ-M	Ψ-M	Ψ-M	Ψ-M	Ψ-M	Ψ-M	Ψ-M
run =>	(-)	T &C			BC9	BC15	BC3	BC4	BC5	BC6	BC10	BC14	BC7	BC12
Ratio =>					2.28	3.07	5.00	3.07	4.11	3.14	2.41	2.06	3.90	2.38
n =>		Y = 2.26	1.00	0.50	0.50	0.50	0.50	0.50	0.50	0.50	0.50	0.50	0.50	0.50
O2	30.04	1.971												
111TCA	0.525	0.844	0.43	0.65	0.36	0.40	0.47	0.40	0.45	0.41	0.37	0.34	0.44	0.36
PCE	0.565	0.834	0.42	0.65	0.37	0.41	0.48	0.41	0.45	0.42	0.38	0.35	0.45	0.37
CT	1.122	0.862	0.44	0.66	0.48	0.51	0.56	0.51	0.54	0.52	0.48	0.46	0.54	0.48
TCE	0.252	0.899	0.46	0.68	0.25	0.29	0.38	0.29	0.34	0.30	0.26	0.23	0.33	0.25
EBZ	0.260	0.708	0.36	0.60	0.22	0.27	0.34	0.27	0.31	0.27	0.23	0.21	0.30	0.23
12DCE	0.166	0.977	0.50	0.70	0.19	0.24	0.32	0.24	0.29	0.24	0.20	0.18	0.28	0.20
MXY	0.236	0.706	0.36	0.60	0.21	0.25	0.32	0.25	0.29	0.25	0.22	0.20	0.29	0.22
OXY	0.181	0.706	0.36	0.60	0.17	0.21	0.28	0.21	0.26	0.22	0.18	0.16	0.25	0.18
TLN	0.230	0.787	0.40	0.63	0.22	0.26	0.34	0.26	0.31	0.26	0.23	0.20	0.30	0.22
BZ	0.226	0.892	0.45	0.67	0.23	0.28	0.36	0.28	0.32	0.28	0.24	0.21	0.32	0.24
CLF	0.160	0.938	0.48	0.69	0.18	0.23	0.31	0.23	0.27	0.23	0.19	0.17	0.27	0.19
CBZ	0.146	0.8	0.41	0.64	0.16	0.20	0.27	0.20	0.24	0.20	0.17	0.15	0.23	0.16
13DCB	0.124	0.727	0.37	0.61	0.13	0.17	0.23	0.17	0.21	0.17	0.14	0.12	0.20	0.14
12DCB	0.087	0.725	0.37	0.61	0.10	0.13	0.18	0.13	0.16	0.13	0.11	0.09	0.15	0.10
14DCB	0.011	0.71	0.36	0.60	0.01	0.02	0.03	0.02	0.03	0.02	0.02	0.01	0.02	0.02
BBZ	0.099	0.775	0.39	0.63	0.12	0.15	0.21	0.15	0.18	0.15	0.12	0.11	0.17	0.12
BF	0.041	0.865	0.44	0.66	0.06	0.07	0.11	0.07	0.10	0.08	0.06	0.05	0.09	0.06
EDB	0.041	0.908	0.46	0.68	0.06	0.08	0.12	0.08	0.10	0.08	0.06	0.05	0.09	0.06
1122TCA	0.042	0.763	0.39	0.62	0.05	0.07	0.11	0.07	0.09	0.07	0.06	0.05	0.09	0.06
NAPH	0.038	0.668	0.34	0.58	0.05	0.06	0.09	0.06	0.08	0.06	0.05	0.04	0.08	0.05

Notes: Hc = Henry's constant, DL = liquid diffusivity [x 10^5 cm/sec]; T & C = Tyn and Calus correlation;
ratio = gas-film and to liquid-film mass transfer coefficient

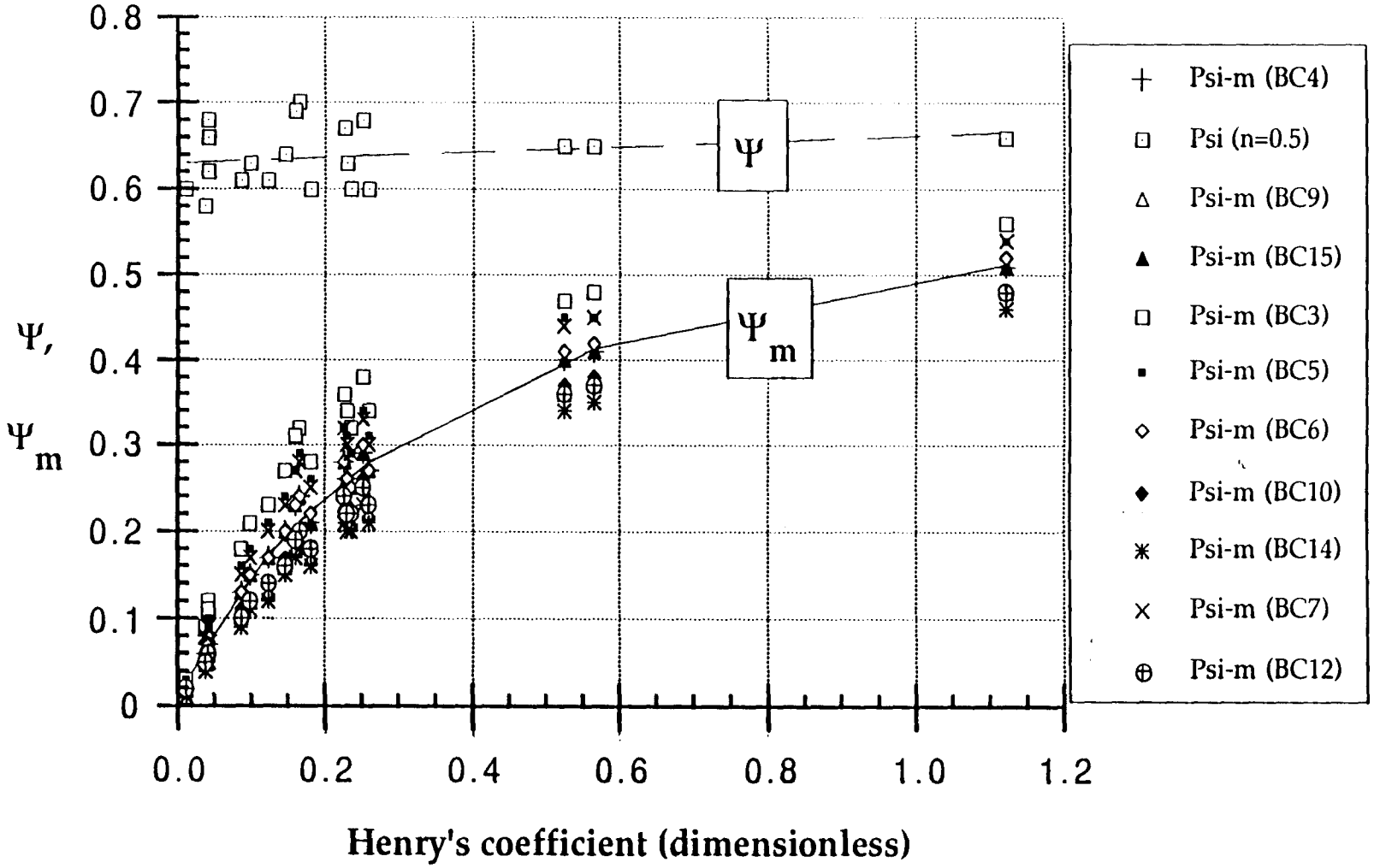

Figure 53. Comparison of Ψ and Ψ_m values for different air flow rates in bubble column

Table 19. Summary of fraction of liquid-film resistance to total resistance for twenty VOCs in bubble column

Run	Hc	BC9	BC15	BC3	BC4	BC5	BC6	BC10	BC14	BC7	BC12
Ratio		2.28	3.07	5.00	3.07	4.11	3.14	2.41	2.06	3.90	2.38
Compounds	n =>	0.50	0.50	0.50	0.50	0.50	0.50	0.50	0.50	0.50	0.50
O2	30.040	0.99	0.99	0.99	0.99	0.99	0.99	0.99	0.98	0.99	0.99
111TCA	0.525	0.54	0.62	0.72	0.62	0.68	0.62	0.56	0.52	0.67	0.56
PCE	0.565	0.56	0.63	0.74	0.63	0.70	0.64	0.58	0.54	0.69	0.57
CT	1.122	0.72	0.78	0.85	0.78	0.82	0.78	0.73	0.70	0.81	0.73
TCE	0.252	0.36	0.44	0.56	0.44	0.51	0.44	0.38	0.34	0.50	0.37
EBZ	0.260	0.37	0.44	0.57	0.44	0.52	0.45	0.39	0.35	0.50	0.38
12DCE	0.166	0.27	0.34	0.45	0.34	0.41	0.34	0.29	0.25	0.39	0.28
MXY	0.236	0.35	0.42	0.54	0.42	0.49	0.43	0.36	0.33	0.48	0.36
OXY	0.181	0.29	0.36	0.48	0.36	0.43	0.36	0.30	0.27	0.41	0.30
TLN	0.230	0.34	0.41	0.53	0.41	0.49	0.42	0.36	0.32	0.47	0.35
BZ	0.226	0.34	0.41	0.53	0.41	0.48	0.42	0.35	0.32	0.47	0.35
CLF	0.160	0.27	0.33	0.44	0.33	0.40	0.33	0.28	0.25	0.38	0.28
CBZ	0.146	0.25	0.31	0.42	0.31	0.38	0.31	0.26	0.23	0.36	0.26
13DCB	0.124	0.22	0.28	0.38	0.28	0.34	0.28	0.23	0.20	0.33	0.23
12DCB	0.087	0.17	0.21	0.30	0.21	0.26	0.21	0.17	0.15	0.25	0.17
14DCB	0.110	0.20	0.25	0.35	0.25	0.31	0.26	0.21	0.18	0.30	0.21
BBZ	0.099	0.18	0.23	0.33	0.23	0.29	0.24	0.19	0.17	0.28	0.19
BF	0.041	0.09	0.11	0.17	0.11	0.14	0.11	0.09	0.08	0.14	0.09
EDB	0.041	0.09	0.11	0.17	0.11	0.14	0.11	0.09	0.08	0.14	0.09
1122TCA	0.042	0.09	0.11	0.17	0.11	0.15	0.12	0.09	0.08	0.14	0.09
NAPH	0.038	0.08	0.10	0.16	0.10	0.14	0.11	0.08	0.07	0.13	0.08

ratio = gas-film and to liquid-film mass transfer coefficient

twenty VOCs versus Hc are plotted in Figure 54. $\frac{R_L}{R_T}$ decreases with decreasing Hc which is the same as the trend in Ψ_m. The gas-phase resistance has very little effect on highly volatile compounds, such as oxygen and CCl_4. However, the gas-phase resistance has a significant effect on the compounds with Hc below 0.6 in this study. The results show that Ψ is only valid when liquid-phase resistance is the predominant mass transfer mechanism.

A comparison of measured and predicted K_La of twenty VOCs for specific air flow rates from 1.75 to 5.10 scfh is shown in Tables 20a and 20b. Figure 55 and Appendix H show predicted versus measured K_La at each specific air flow rate. Good correlations were observed. Regression line slopes are from 0.9 to 1.08 which are all pretty close to 1.0. All the intercepts are exceptionally high with a range from 0.13 to 0.56, given by an overestimation of K_La_{O2} or underestimation of K_La_{VOC} due to the saturation phenomenon of VOCs in the bubbles.

The discrepancy between measured and predicted values of K_La of sixteen compounds (excluding EDB, bromoform, 1,1,2,2-TCA, and naphthalene) were large (from 13% to 34.2%). The major explanation for large variance is due to the high value of the intercepts. Other errors may arise form the experimental method used for measuring K_La_{O2} and K_La_{VOC}, and errors in estimates for liquid diffusivity, which were discussed in the surface aeration section (Section 4.2.5).

4.3.5 Estimating Stripping Rate by Dimensionless Parameters

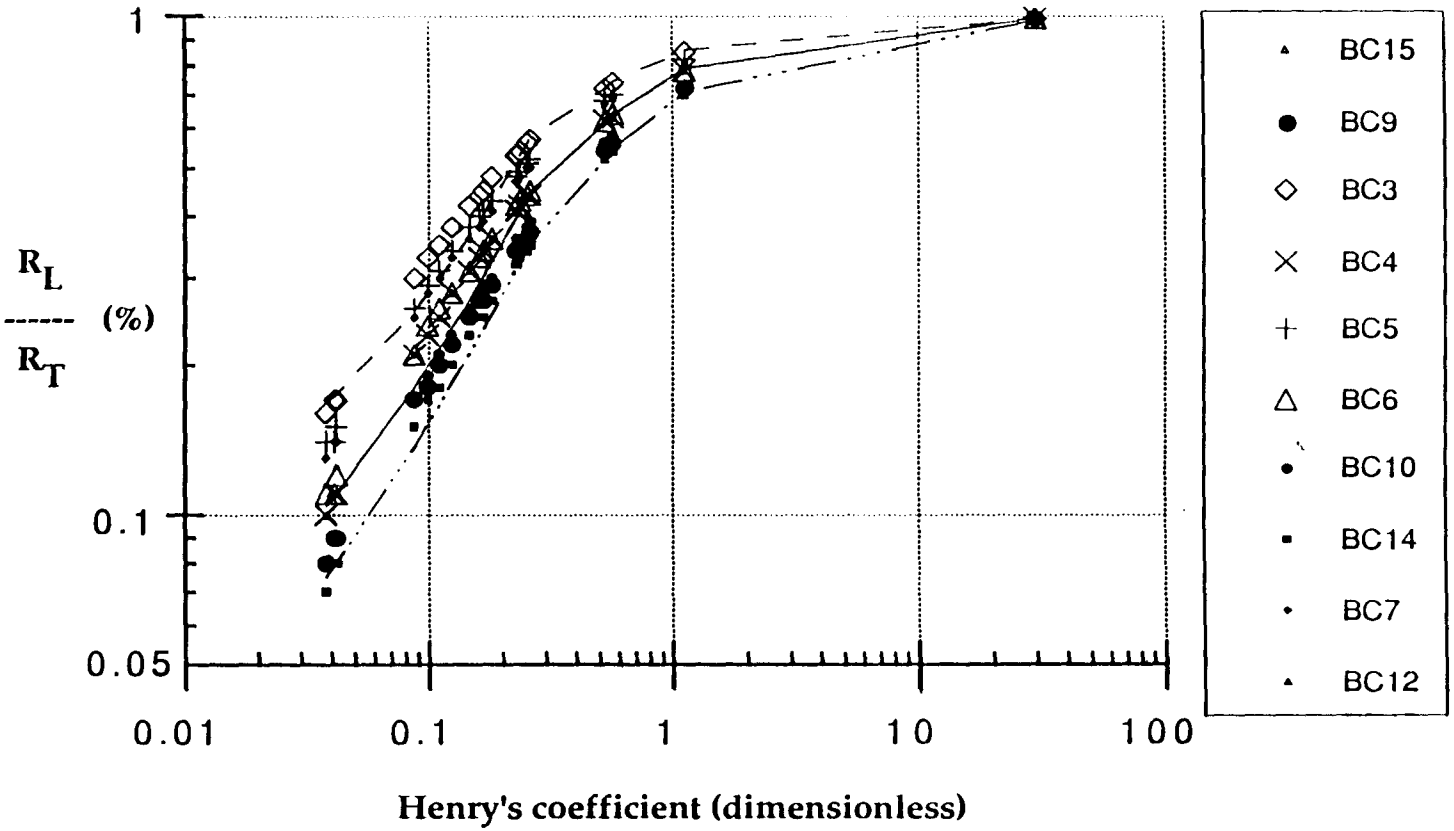

Figure 54. Dependence of fraction of liquid-phase resistance to overall resistance on Henry's coefficient in bubbel column

Table 20a. Estimated and measured mass transfer coefficient in bubble column

Run	BC9			BC15			BC3			BC4			BC5		
Ratio	2.28			3.07			5			3.07			4.11		
n=>	0.5			0.5			0.5			0.5			0.5		
Compounds	M-KLa	P-KLa	ARE#	M-KLa	P-KLa	ARE#	M-KLa	P-KLa	ARE#	M-KLa	P-KLa	ARE#	M-KLa	P-KLa	ARE#
O2	15.43	19		14.5	15.5		14.7	12		12.62	12.62		11.82	10.500	
111TCA	7.17	6.774	5.5	5.41	6.259	15.7	6.08	5.366	11.7	6.68	5.140	23.1	5.48	4.695	14.3
PCE	7.97	6.958	12.7	5.91	6.395	8.2	5.22	5.456	4.5	5.57	5.250	5.7	5.19	4.774	8.0
CT	10.01	9.034	9.8	8.73	7.944	9.0	8.25	6.522	21.0	7.05	6.501	7.8	6.59	5.706	13.4
TCE	6.03	4.682	22.3	4.21	4.566	8.5	3.98	4.123	3.6	4.61	3.765	18.3	3.90	3.608	7.5
EBZ	5.18	4.238	18.2	4.14	4.124	0.4	3.91	3.715	5.0	3.80	3.400	10.5	3.44	3.251	5.5
12DCE	2.95	3.673	24.5	2.62	3.684	40.6	2.56	3.426	33.8	2.00	3.044	52.2	1.92	2.998	56.2
MXY	4.77	3.978	16.6	4.09	3.897	4.7	2.45	3.536	44.3	3.71	3.215	13.3	3.28	3.094	5.7
OXY	2.98	3.322	11.5	2.46	3.314	34.7	3.18	3.064	3.7	2.16	2.737	26.7	2.01	2.681	33.4
TLN	4.20	4.130	1.7	3.57	4.054	13.5	7.04	3.685	47.7	3.45	3.344	3.1	3.06	3.224	5.4
BZ	3.56	4.347	22.1	2.70	4.271	58.2	2.56	3.887	51.9	2.88	3.524	22.4	3.00	3.402	13.4
CLF	2.67	3.503	31.2	2.50	3.522	40.9	2.46	3.284	33.5	2.21	2.911	31.7	2.49	2.874	15.4
CBZ	2.80	3.023	8.0	2.44	3.056	25.3	2.70	2.867	6.2	2.27	2.527	11.3	2.13	2.509	17.8
13DCB	1.89	2.543	34.6	1.51	2.596	71.9	1.82	2.460	35.2	1.86	2.148	15.5	1.73	2.153	24.4
12DCB	2.56	1.907	25.5	1.95	1.982	1.6	2.81	1.917	31.8	1.85	1.642	11.2	1.85	1.677	9.3
14DCB	2.18	2.287	4.9	2.09	2.348	12.4	2.10	2.242	6.8	1.57	1.945	23.9	1.91	1.962	2.7
BBZ	2.47	2.194	11.2	2.24	2.265	1.1	2.51	2.176	13.3	1.80	1.877	4.4	1.79	1.904	6.4
BF	0.54	1.076		0.36	1.148		0.88	1.146			0.954			1.003	
EDB	0.61	1.102		0.33	1.176		0.40	1.175		0.42	0.977		0.96	1.028	
1122TCA	0.56	1.033		0.24	1.101			1.099			0.915		0.60	0.962	
NAPH	0.54	0.882		0.29	0.943		0.29	0.944			0.783		0.66	0.826	
mean error			16.3			21.7			22.1			17.6			14.9

M-KLa = Measured KLa; P-KLa = Predicated KLa; ARE = Absolute Relative Error (%)

Table 20b. Estimated and measured mass transfer coefficient in bubble column

Run	BC6			BC10			BC14			BC7			BC12		
kGa/kLa	3.14			2.41			2.06			3.9			2.38		
n	0.5			0.5			0.5			0.5			0.5		
Compounds	M-KLa	P-KLa	ARE#	M-KLa	P-KLa	ARE#	M-KLa	P-KLa	ARE#	M-KLa	P-KLa	ARE#	M-KLa	P-KLa	ARE#
O2	13.38	11.5		11.09	11.09		11.2	12.5		9.55	9.55		7.11	8	
111TCA	5.38	4.684	12.9	4.19	4.053	3.3	4.70	4.250	9.6	4.12	4.199	1.9	3.55	2.908	18.1
PCE	5.02	4.784	4.7	4.20	4.159	1.0	4.31	4.373	1.5	2.96	4.273	44.4	2.81	2.984	6.2
CT	7.56	5.924	21.6	6.14	5.354	12.8	6.97	5.770	17.2	4.84	5.141	6.2	4.10	3.849	6.1
TCE	3.91	3.431	12.3	3.42	2.830	17.3	2.47	2.885	16.8	2.63	3.197	21.6	1.90	2.026	6.6
EBZ	3.50	3.098	11.5	3.05	2.560	16.1	2.80	2.613	6.7	2.16	2.882	33.4	1.87	1.833	2.0
12DCE	2.10	2.774	32.1	1.92	2.231	16.2	1.91	2.243	17.4	1.95	2.642	35.5	0.95	1.595	67.9
MXY	3.26	2.929	10.1	2.58	2.406	6.7	3.29	2.447	25.6	2.40	2.739	14.1	2.26	1.722	23.8
OXY	2.08	2.494	19.9	1.64	2.016	22.9	1.74	2.032	16.8	1.45	2.365	63.1	1.17	1.442	23.2
TLN	2.97	3.047	2.6	2.44	2.499	2.4	2.02	2.539	25.7	1.88	2.853	51.8	2.79	1.788	35.9
BZ	4.84	3.211	33.7	2.42	2.631	8.7	2.01	2.671	32.9	2.05	3.010	46.8	1.21	1.882	55.6
CLF	2.43	2.653	9.2	1.70	2.129	25.2	1.89	2.138	13.1	1.81	2.531	39.9	1.39	1.522	9.5
CBZ	2.01	2.303	14.6	1.83	1.839	0.5	1.47	1.841	25.3	1.53	2.207	44.3	1.08	1.314	21.7
13DCB	1.86	1.957	5.2	1.11	1.550	39.6	0.91	1.545	69.7	1.33	1.891	42.1	0.83	1.107	33.4
12DCB	1.75	1.497	14.5	1.51	1.166	22.8	1.56	1.152	26.1	1.27	1.467	15.5	0.89	0.832	6.5
14DCB	1.87	1.772	5.2	1.25	1.395	11.6	1.24	1.386	11.8	1.20	1.721	43.4	0.95	0.996	4.9
BBZ	1.69	1.710	1.2	1.33	1.340	0.7	1.58	1.328	16.0	1.17	1.668	42.6	0.92	0.957	4.0
BF	0.98	0.869		0.32	0.661		0.24	0.645			0.872		0.17	0.471	
EDB		0.890		0.50	0.677		0.36	0.661			0.894		0.17	0.483	
1122TCA	0.73	0.834		0.40	0.634		0.15	0.619			0.836		0.15	0.452	
NAPH		0.714		0.55	0.542		0.18	0.528		0.24	0.718		0.14	0.386	
mean error			13.2			13.0			20.8			34.2			20.3

M-KLa = Measured KLa; P-KLa = Predicated KLa; ARE = Absolute Relative Error (%)

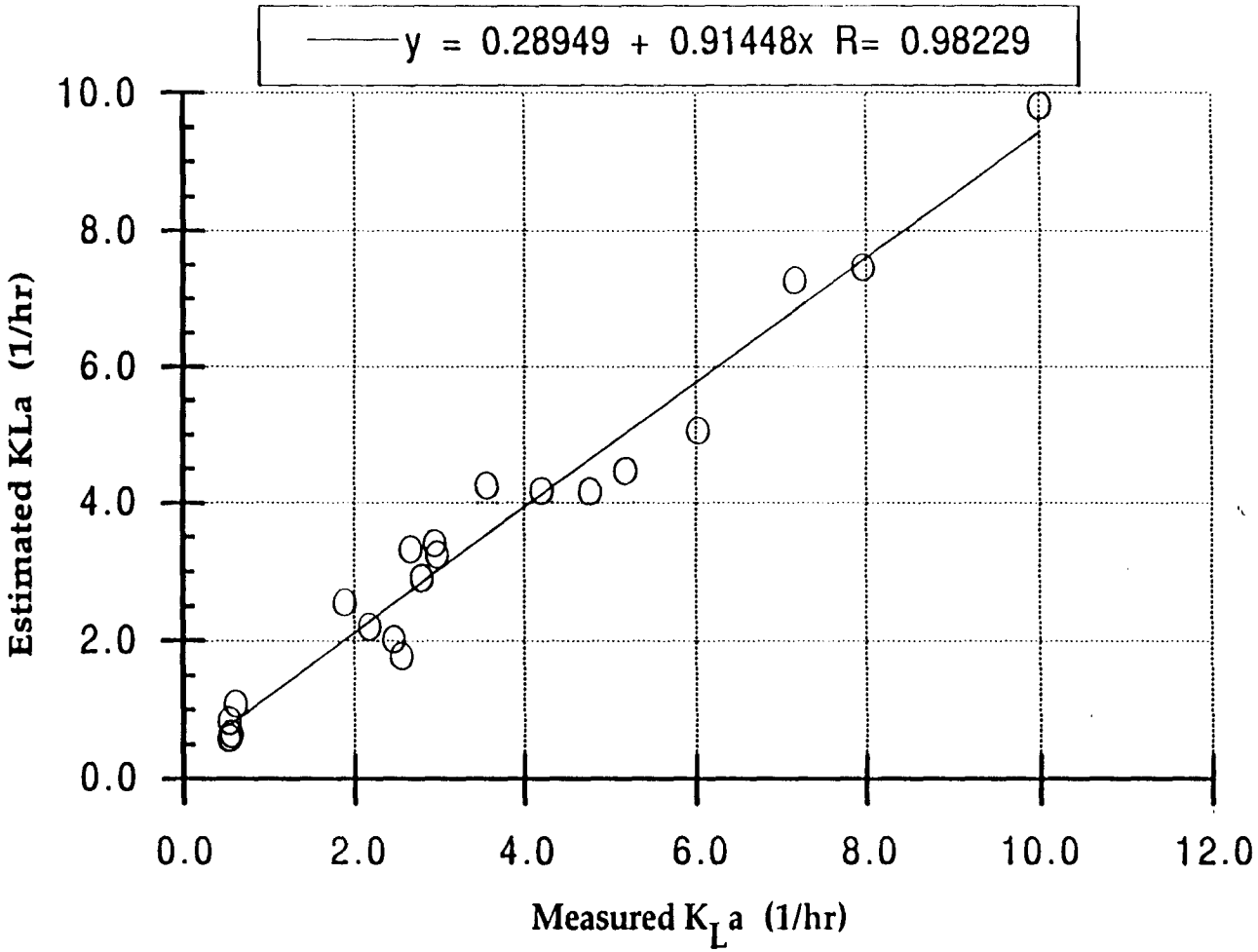

Figure 55. Comparison between estimated and measured mass transfer coefficient in bubble column (BC9, specific air flow rate = 7.19 1/hr)

Blackburn et al. (1984) have incorporated Henry's law coefficients and the air flow-to-liquid volume ratios to directly estimate the stripping rate in a 6 ft high, 6 in. diameter bubble column. They used the dimensionless Henry's law coefficient and experimental determined stripping rate parameters to correlate the dimensionless relationship. Unfortunately, they used slope as $K_L a$. In such a situation, their correlation is:

$$\text{Slope } \frac{V_L}{Q_G} = b\,(Hc)^m \tag{104}$$

where

V_L = liquid volume in the reactor [L],

Q_G = air flow rate [L/hr], and

b and m = power function constant.

If we compare equation (104) with equation (38), the b-value in equation (104) corresponds to Sd in equation (38) and m = 1. Put in another way, the slope of [Slope $\frac{V_L}{Q_G}$ versus Hc] is the degree of saturation (Sd). Table 21 summarizes a dimensionless parameter [Slope $\frac{V}{Q}$] for twenty VOCs in 14 experiments. The correlation of [Slope $\frac{V}{Q}$] to Hc for 14 sets of experiments for VOCs with Hc < 0.30 is shown in Figure 56 along with plots of linear and nonlinear (power) functions. These equations are as follows:

Linear correlation:

Table 21. Summary of a dimensionless parameter: Slope V /Q in bubble column

Run	Hc	BC9	BC15	BC11	BC3	BC4	BC5	BC6	BC10	BC14	BC7	BC1	BC16	BC12	BC8	Max	Mean	stdev	% CV
Q/V(1/hr)		7.19	6.16	6.27	5.68	5.28	5.28	5.18	4.68	4.21	3.35	3.23	2.75	2.47	1.62				
O2	30.02	2.15	2.35	2.34	2.59	2.39	2.24	2.58	2.37	2.66	2.85	2.27	2.84	2.88	3.30	3.30	2.56	0.32	12.5
111TCA	0.53	0.45	0.43	0.49	0.46	0.48	0.45	0.45	0.43	0.46	0.47	0.43	0.45	0.49	0.47	0.49	0.46	0.02	4.8
PCE	0.57	0.49	0.46	0.53	0.45	0.48	0.47	0.46	0.45	0.47	0.45	0.41	0.47	0.49	0.49	0.53	0.47	0.03	5.6
CT	1.12	0.80	0.80	0.82	0.81	0.78	0.75	0.82	0.77	0.87	0.81	0.73	0.86	0.87	0.89	0.89	0.81	0.05	5.7
TCE	0.25	0.24	0.24	0.24	0.24	0.24	0.25	0.25	0.24	0.23	0.24	0.22	0.23	0.24	0.24	0.25	0.24	0.01	3.6
EBZ	0.26	0.24	0.24	0.26	0.24	0.24	0.24	0.24	0.24	0.24	0.24	0.21	0.24	0.25	0.24	0.26	0.24	0.01	4.2
12DCE	0.17	0.15	0.15	0.16	0.15	0.15	0.15	0.15	0.15	0.16	0.16	0.14	0.15	0.15	0.16	0.16	0.15	0.00	3.2
MXY	0.24	0.22	0.22	0.22	0.20	0.22	0.22	0.22	0.21	0.23	0.22	0.19	0.22	0.23	0.23	0.23	0.22	0.01	5.3
OXY	0.18	0.16	0.16	0.16	0.17	0.16	0.16	0.16	0.15	0.16	0.16	0.15	0.17	0.17	0.17	0.17	0.16	0.01	4.1
TLN	0.23	0.21	0.21	0.21	0.23	0.22	0.21	0.21	0.21	0.20	0.21	0.21	0.21	0.23	0.22	0.23	0.21	0.01	3.6
BZ	0.23	0.20	0.19	0.20	0.20	0.21	0.21	0.22	0.20	0.20	0.21	0.20	0.20	0.20	0.21	0.22	0.20	0.01	3.5
CLF	0.16	0.14	0.15	0.15	0.15	0.15	0.15	0.15	0.14	0.15	0.15	0.14	0.15	0.16	0.15	0.16	0.15	0.00	3.0
CBZ	0.15	0.14	0.14	0.13	0.14	0.14	0.14	0.14	0.14	0.13	0.14	0.13	0.13	0.14	0.14	0.14	0.14	0.00	2.6
BBZ	0.10	0.09	0.09	0.09	0.10	0.10	0.10	0.10	0.09	0.09	0.10	0.09	0.10	0.10	0.10	0.10	0.09	0.00	4.0
13DCB	0.12	0.12	0.11	0.12	0.12	0.12	0.12	0.12	0.11	0.12	0.12	0.11	0.12	0.12	0.12	0.12	0.12	0.00	2.8
12DCB	0.09	0.08	0.09	0.09	0.09	0.08	0.09	0.09	0.08	0.08	0.09	0.07	0.09	0.09	0.09	0.09	0.08	0.00	4.2
14DCB	0.11	0.10	0.10	0.10	0.11	0.10	0.10	0.10	0.10	0.10	0.10	0.10	0.11	0.10	0.11	0.11	0.10	0.00	2.2
BF	0.04	0.03	0.03	0.04	0.04	0.04	0.05	0.04	0.03	0.03	0.05	0.05	0.03	0.03	0.03	0.05	0.04	0.01	19.3
EDB	0.04	0.04	0.03	0.03	0.03	0.04	0.04	0.04	0.04	0.04	0.05	0.04	0.04	0.03	0.04	0.05	0.04	0.00	10.6
1122TCA	0.04	0.04	0.03	0.03	0.05	0.05	0.04	0.04	0.04	0.02	0.05	0.04	0.02	0.03	0.04	0.05	0.04	0.01	25.3
NAPH	0.04	0.03	0.03	0.03	0.03	0.04	0.04	0.04	0.04	0.03	0.03	0.04	0.02	0.03	0.03	0.04	0.03	0.01	18.5

Notes: MAX = maximum; stdev = standard deviation; % CV = percentage of coefficient of variation

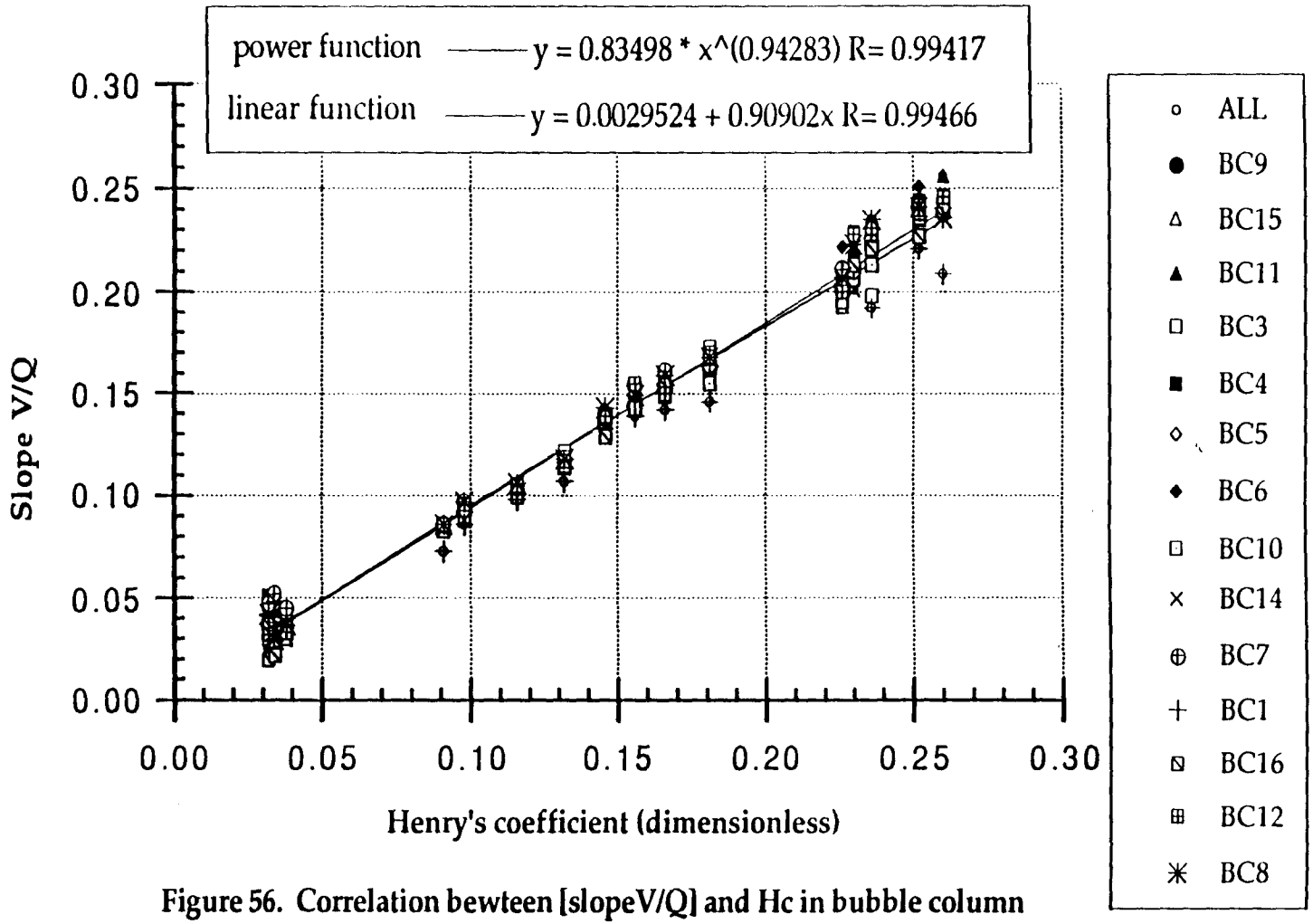

Figure 56. Correlation bewteen [slopeV/Q] and Hc in bubble column for compounds with Hc < 0.3

$$\text{Slope } \frac{V_L}{Q_G} = 0.003 + 0.91 \text{ (Hc)} \tag{105}$$

Nonlinear correlation:

$$\text{Slope } \frac{V_L}{Q_G} = 0.83 \text{ (Hc)}^{0.94} \tag{106}$$

The intercept of 0.003 in equation (105) and the m-value of 0.94 in equation (106) may be caused by the systematic or experimental error. The slopes of linear and non-linear regressions are 0.91 and 0.83 which correspond to 91% and 83% of saturation of VOCs in bubbles. Blackburn's results for pure water, b = 1.0 and m = 0.9 with 11 data points yields a correlation coefficient, r^2, of 0.991. It should be noted that Blackburn et al. (1984) selected toluene (Hc = 0.23), 1,3 dichlorobenzene (Hc = 0.11), methylethyl ketone (Hc = 9.4×10^{-4}), and phenol (Hc = 1.37×10^{-5}) for fitting the model. The volatility of these compounds are very low. For a 6 ft long bubble column, most of these low volatility compounds should nearly approach saturation. Then, we can assume Sd ≈ 1.0 which fits Blackburn's result of b-value of 1.0. If we correlate equation (104) with higher volatility compounds, we obtain an Sd of 60% and 74% for linear and power function, respectively (Figure 57). The method developed by Blackburn et al. (1984) offers a simpler approach for estimating stripping rates. As a matter of fact, they did not estimate stripping rate, but the slope of the negative log-linear regression of concentration ratio versus time. However, the b-value of the power function is not a constant; it depends on Sd of the VOCs. The determination of Sd depends on the volatility of VOCs, which is related to Hc.

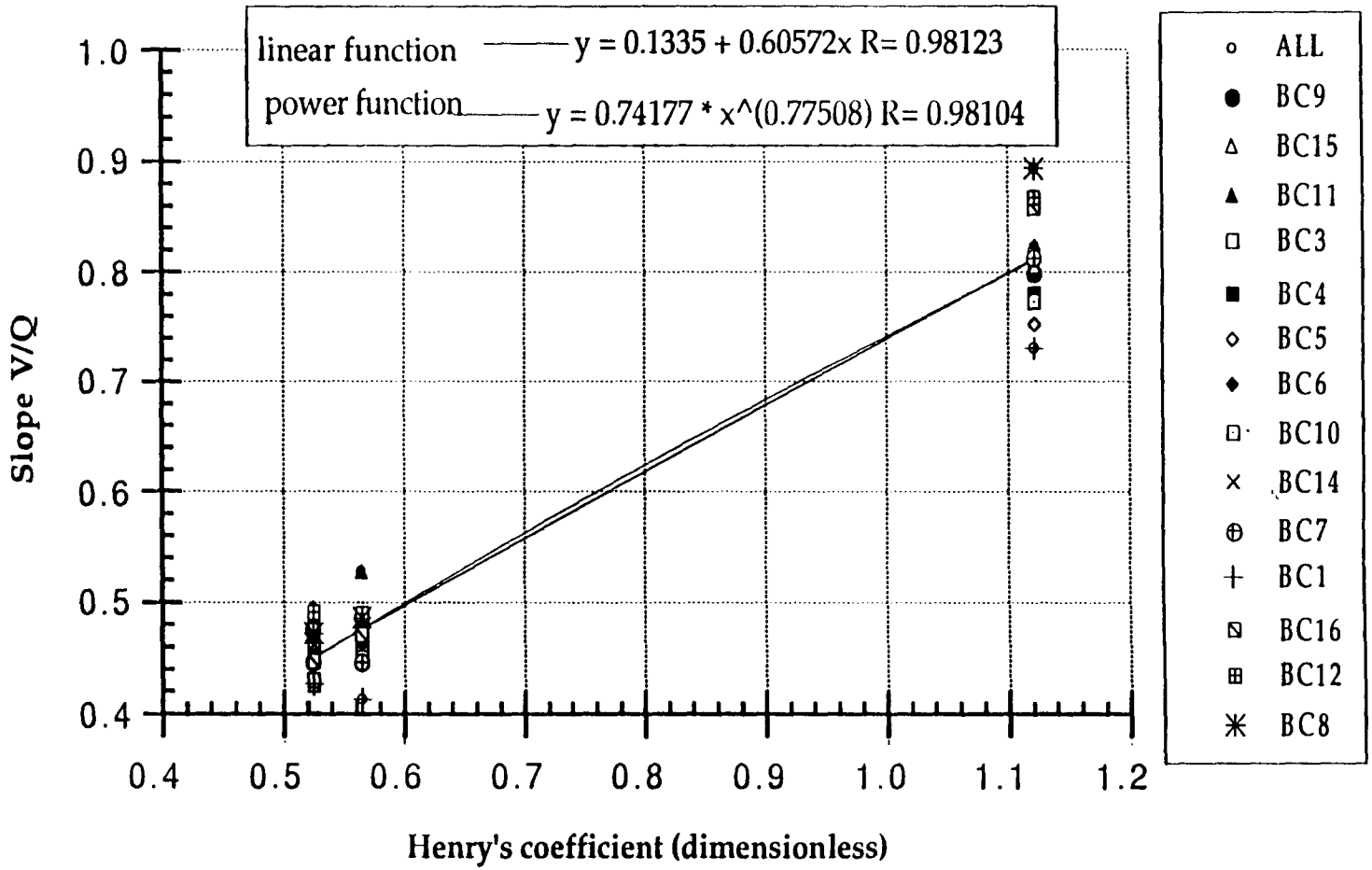

Figure 57. Correlation of [slopeV/Q] versus Hc for highly volatile compounds (Hc >0.5)

If we substitute equation (37) into equation (42), two dimensionless parameters [$K_L a \frac{V_L}{Q_G}$] and Hc can be related to form an equation as follows:

$$K_L a \frac{V_L}{Q_G} = -\ln(1 - Sd)Hc \tag{107}$$

where

$K_L a$	=	mass-transfer coefficient [1/hr],
Hc	=	Henry's coefficient [dimensionless],
V_L	=	liquid volume in the reactor [L],
Q_G	=	air flow rate [L/hr],
b and m	=	power function constant, and
-ln (1-Sd)	=	saturation parameter [dimensionless]

Comparing equation (107) with the power function of form $Y = b X^m$, the b-value is [-ln (1-Sd)] and m = 1.0. Roberts et al. (1983) have defined [-ln (1-Sd)] as a saturation parameter. The data from 14 experiments in this study (Table 22) is shown in Figure 58 along with plots of linear and power functions for relating $K_L a \frac{V}{Q}$ and Hc. The correlation of linear and power function with Hc < 0.27 for [-ln(1-Sd)] are 2.47 and 2.87 which corresponds to 91.6% and 94.3% degree of saturation for 14 runs of experiments. A comparison of methods determination of Sd between equations (104) and (107) is listed in Table 23.

According to the result of the linear function, the Sd-value obtained by equation (104) agreed well with equation (107). The difference is only 0.6%. For power function, the Sd-values obtained with equations (104) and (107) have high deviation

Table 22. Summary of a dimensionless parameter: KLa V /Q in bubble column

Run	Hc	BC9	BC15	BC11	BC3	BC4	BC5	BC6	BC10	BC14	BC7	BC1	BC16	BC12	BC8	Max	Mean	stdev	% CV
Q/V (1/hr)		7.19	6.16	6.27	5.68	5.28	5.28	5.18	4.68	4.21	3.35	3.23	2.75	2.47	1.62				
O2	30.02	2.23	2.45	2.44	2.71	2.49	2.32	2.70	2.47	2.78	2.99	2.37	2.98	3.03	3.50	3.50	2.68	0.35	13.2
111TCA	0.525	1.00	0.88	1.50	1.07	1.27	1.04	1.04	0.90	1.12	1.23	0.88	1.00	1.44	1.20	1.50	1.11	0.19	17.5
PCE	0.565	1.11	0.96	1.54	0.92	1.06	0.98	0.97	0.90	1.02	0.88	0.74	1.01	1.14	1.11	1.54	1.02	0.18	17.9
CT	1.122	1.39	1.42	1.48	1.45	1.33	1.25	1.46	1.31	1.65	1.44	1.18	1.62	1.66	1.79	1.79	1.46	0.17	11.7
TCE	0.252	0.84	0.68	0.80	0.70	0.87	–	1.33	0.73	0.59	0.78	0.53	0.59	0.77	0.80	1.33	0.77	0.20	25.8
EBZ	0.260	0.72	0.67	1.08	0.69	0.72	0.65	0.67	0.65	0.66	0.65	0.42	0.65	0.76	0.62	1.08	0.69	0.14	20.0
12DCE	0.166	0.41	0.42	0.50	0.45	0.38	0.36	0.41	0.41	0.45	0.58	0.32	0.44	0.38	0.52	0.58	0.43	0.07	15.7
MXY	0.236	0.66	0.66	0.70	0.43	0.70	0.62	0.63	0.55	0.78	0.71	0.40	0.64	0.92	1.20	1.20	0.69	0.20	28.7
OXY	0.181	0.41	0.40	0.42	0.56	0.41	0.38	0.40	0.35	0.41	0.43	0.30	0.51	0.48	0.47	0.56	0.42	0.07	15.4
TI.N	0.230	0.58	0.58	0.59	–	0.65	0.58	0.57	0.52	0.48	0.56	0.62	0.60	1.13	0.82	1.13	0.64	0.17	26.4
BZ	0.226	0.49	0.44	0.48	0.45	0.54	0.57	0.93	0.52	0.48	0.61	0.53	0.51	0.49	0.56	0.93	0.54	0.12	22.4
CLF	0.160	0.37	0.41	0.40	0.43	0.42	0.47	0.47	0.36	0.45	0.54	0.32	0.48	0.57	0.43	0.57	0.44	0.07	15.1
CBZ	0.146	0.39	0.40	0.38	0.48	0.43	0.40	0.39	0.39	0.35	0.46	0.35	0.31	0.44	0.55	0.55	0.41	0.06	14.5
BBZ	0.099	0.26	0.24	0.25	0.32	0.35	0.33	0.36	0.24	0.22	0.40	0.20	0.35	0.34	0.38	0.40	0.30	0.07	21.7
13DCB	0.124	0.36	0.32	0.34	0.49	0.35	0.35	0.34	0.32	0.37	0.38	0.25	0.41	0.36	0.39	0.49	0.36	0.05	15.1
12DCB	0.087	0.30	0.34	0.37	0.37	0.30	0.36	0.36	0.27	0.29	0.36	0.16	0.41	0.39	0.37	0.41	0.33	0.07	19.6
14DCB	0.108	0.34	0.36	0.36	0.44	0.34	0.34	0.33	0.28	0.38	0.35	0.25	0.39	0.37	0.44	0.44	0.36	0.05	14.3
BF	0.041	0.07	0.06	0.10	0.14	–		0.16	0.07	0.06	–	–	0.05	0.07	0.05	0.16	0.07	0.05	68.5
EDB	0.041	0.09	0.05	0.07	0.07	0.08	0.20	–	0.11	0.09	–	0.14	0.08	0.07	0.10	0.20	0.09	0.05	52.9
1122TCA	0.042	0.08	0.04	0.06	–	–	0.12	0.15	0.09	0.03	–	0.14	0.03	0.06	–	0.15	0.07	0.05	65.9
NAPH	0.038	0.08	0.05	0.09	0.05	–	0.13	–	0.12	0.04	0.07	–	0.03	0.06	0.09	0.13	0.07	0.03	44.5

Note: max = maximum value; stdev = standard deviation; % CV = coefficient of variation = stdev/mean

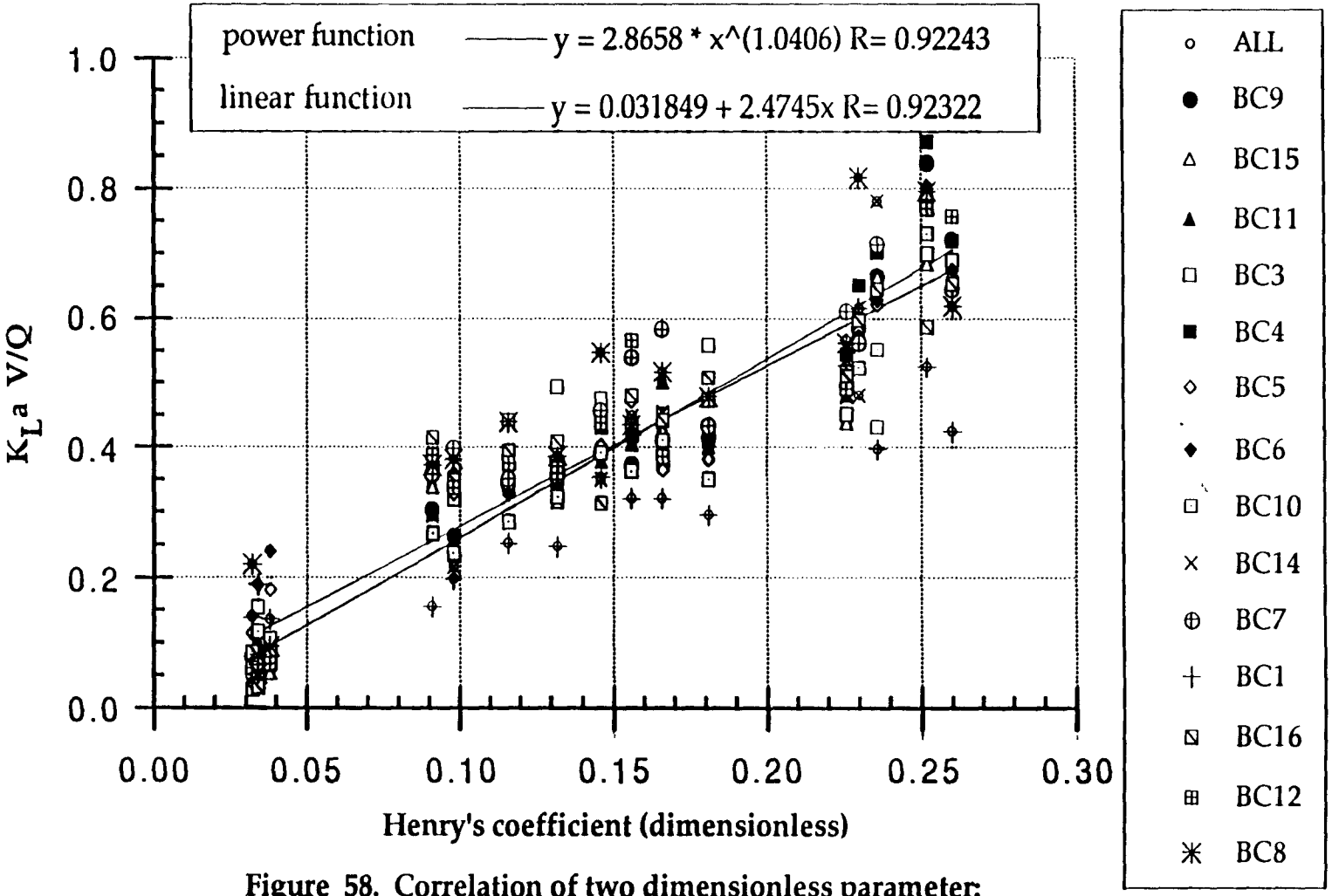

Figure 58. Correlation of two dimensionless parameter: K_La V/Q versus Hc for 14 experiments with Hc < 0.30

of 11.3%. The linear function has taken out the intercept of correlation which may come from experimental error; however, the power function includes the experimental error which generates higher discrepancy.

Table 23. Comparison of equations (104) and (107) for determinination of Sd

	Linear	Power	Diff. (%)	Equation
Sd (%)	91.6	94.3	2.7	107
Sd (%)	91.0	83.0	8.0	104
Diff. (%)	0.6	11.3	–	–

Note: Sd = Degree of saturation

Diff. = Difference

The method developed in this work has been confirmed by analysis of dimensionless parameters. The dimensionless parameter analysis incorporates the Henry's coefficient and the air flow-to-liquid volume ratio to directly yield the stripping rate constant. Equation (107) estimates the stripping rate constant from Henry's coefficient of VOCs following the form of $K_L a \frac{V}{Q} = b\ Hc^m$. The values of the stripping rate constant ($K_L a$) predicted from this methodology agree reasonably well with dimensionless analysis. This proves the validity of the developed methodology.

4.3.6 The Effect of Temperature on $K_L a$

4.3.6.1 Effect of Change of Water Temperature on $K_L a$

Because the diffusion coefficient and the viscosity vary with temperature, changes in water temperature may influence the $K_L a$-value. Since the oxygen concentration C_L^* is temperature dependent, it is essential to keep the reactor at constant temperature during the test. For short tests (30 min), fluctuations were less than 0.1 °C; whereas, for long runs (4 hrs), the temperature varied ± 0.3 °C. As stated in the surface aeration section, the temperature variation may cause slight, perhaps undetectable scatter in the results.

4.3.6.2 Effect of Change of Air Bubble Temperature on $K_L A$

It is necessary to evaluate the effect of air bubble temperature on oxygen transfer coefficient ($K_L a$) and saturation concentration (Cs*). Initially the temperature was held constant (20°C) and the values of $K_L a$ and Cs* were determined for various air flow rates (1.15 to 5.10 scfh). Thereafter, the air flow rate was held constant at 3.75 scfh in order to examine the effect of air bubble temperature on $K_L a$ and Cs*.

A summary of the $K_L a$'s and Cs*'s for experiments performed at temperatures of 15.0, 20.0, and 24.4 °C are listed in Table 24 and plotted in Figure 59. The mean values of $K_L a$ at 15.0 °C and 22.4 °C are 12.44 (1/hr) and 12.71 (1/hr) which are not

significantly different from the average values of 12.38 (1/hr) obtained at 20 °C. Such small differences of K_La between 15 °C and 24.4 °C are not significant compared to experimental errors at 20 °C. It is concluded that the effect of air temperature change of ± 5 °C on K_La and Cs* was not significant.

Table 24. Effect of air bubble temperature on oxygen transfer coefficient and saturation oxygen concentration

Test No	Air Temp.	Cs*	KLa
AT8	20.0 C	9.10	12.16
AT9	20.0 C	9.07	12.31
AT10	20.0 C	9.04	12.97
BC4	20.0 C	8.97	12.62
BC5	20.0 C	9.01	11.83
Mean		9.04	12.38
Stdev		0.05	0.44
% CV		0.54	3.54
AT14	15.0 C	8.97	12.65
AT15	15.0 C	9.03	12.17
AT16	15.0 C	8.99	12.50
Mean		8.99	12.44
Stdev		0.03	0.24
% CV		0.33	1.96
AT11	24.4 C	9.06	12.76
AT12	24.4 C	9.07	12.57
AT13	24.4 C	9.02	12.82
Mean		9.05	12.71
Stdev		0.03	0.13
% CV		0.32	1.03

Air Temp. = Air Bubble Temperature

Stdev = Standard Deviation

% CV = Coefficient Variation (%)

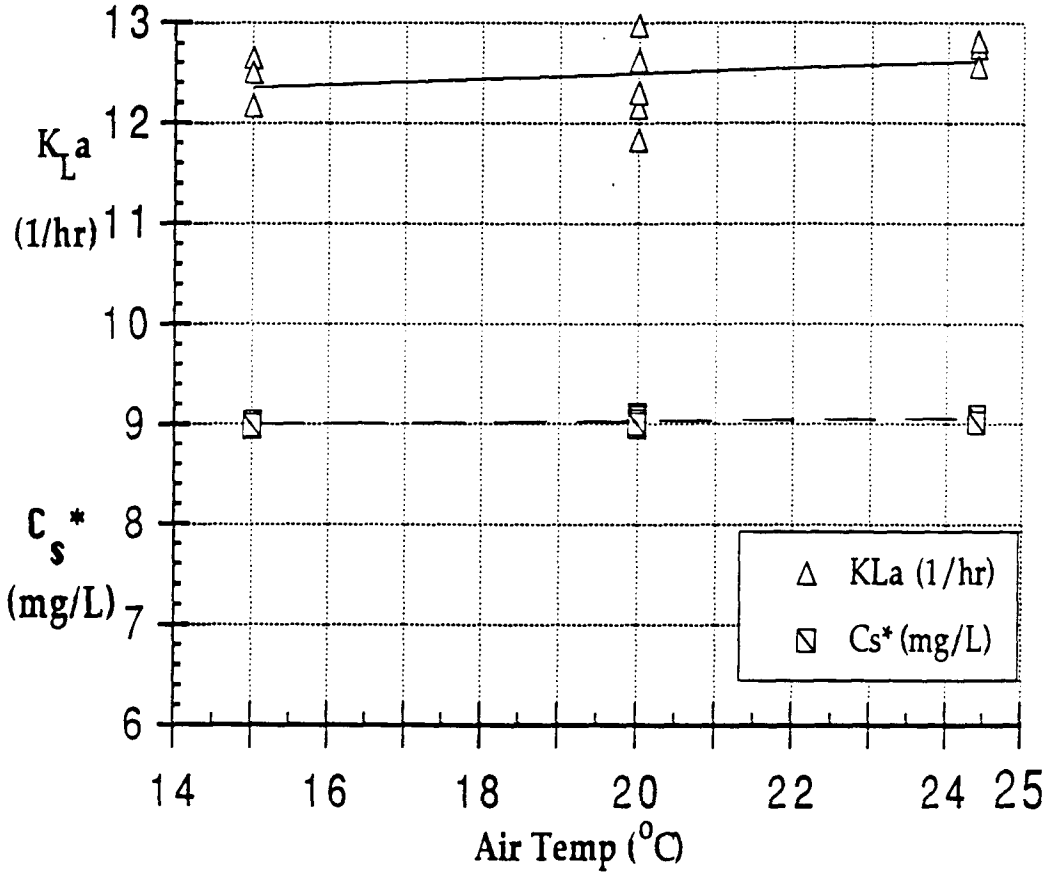

Figure 59. Effect of air bubble temperature on the oxygen transfer coefficient ($K_L a$, 1/hr) and oxygen saturation concentration (C_s^*, mg/L)

5. ENGINEERING SIGNIFICANCE

The objective of this section is to show the application of the novel methodology - Ψ_m concept by means of an example from surface (SA) and bubble column (BC) aeration in the activated sludge process of a wastewater treatment plant. The stripping rates of twenty VOCs for both SA and BC were compared for a range of specific power input between 15 and 80 watt/m^3.

Ψ_m is defined in equation (60) and is repeated here as follows:

$$\Psi_m = \left[\frac{D_{LVOC}}{D_{LO2}}\right]^n \frac{R_L}{R_T} = \Psi \frac{R_L}{R_T} \tag{60}$$

Equation (60) indicates that Ψ_m depends not only on the diffusivity, but also on the fraction of liquid resistance to total resistance. The concept of Ψ_m-value can be used to determine the stripping rates of volatile and semi-volatile compounds, if the oxygen transfer coefficient and hydrodynamic conditions are known for a specific aeration basin. These calculations assume that adsorption and biodegradation are not significant.

5.1 Estimating Stripping Rates in Surface Aeration

Surface aeration systems are rated in terms of their oxygen transfer rate expressed as kilograms of oxygen per kilowatt-hour under standard conditions. Standard conditions exist when the temperature is 20°C, 760 mm Hg, the dissolved oxygen is 0.0 mg/L, and the test liquid is tap water. Testing and rating are normally done under nonsteady-state conditions using fresh water, deaerated with sodium sulfite. Commercial size surface aerators now available range in efficiency from 1.2 to 2.4

[Kg O_2/Kw-h] (Metcalf and Eddy, 1979). According to equation (15), the oxygen transfer coefficient can be calculated from:

$$K_L a = \frac{Nc}{Cs^*} \frac{P}{V} \tag{108}$$

where

Nc = oxygen transfer rate [kg O_2/Kw-h],

P = brake power of aerator [Kw],

V = volume of basin [m^3], and

Cs* = oxygen saturation concentration [kg O_2/m^3] for 20°C, 760 mm Hg,

= 9.17×10^{-3} [kg O_2/m^3].

Therefore, the relationship between the $K_L a$ and the specific power input is in the following range:

$$(K_L a)_{O_2} = \frac{1.2}{9.17 \times 10^{-3}} \frac{1}{1000} \left[\frac{P}{V}\right] = 0.13 \left[\frac{P}{V}\right] \tag{109}$$

$$(K_L a)_{O_2} = \frac{2.4}{9.17 \times 10^{-3}} \frac{1}{1000} \left[\frac{P}{V}\right] = 0.26 \left[\frac{P}{V}\right] \tag{110}$$

where the units of $(K_L a)_{O_2}$ and $(\frac{P}{V})$ are [hr^{-1}] and [watt/m^3], respectively.

Roberts et al. (1983), conducted lab experiments using a batch laboratory apparatus with a liquid volume of 0.0073 m^3 over the specific power range $10 < \frac{P}{V} <$ 200 watt/m^3, found the following relationship:

$$(K_L a)_{O_2} = 0.09 \left[\frac{P}{V}\right] \tag{111}$$

where the units of $(K_La)_{O_2}$ and $(\frac{P}{V})$ are [hr^{-1}] and [watt/m^3], respectively.

In order to compare our results with laboratory-scale bubble column, equation (111) of laboratory-scale surface aeration relationship was used to estimate K_La of oxygen. Table 25 shows the results of Ψ_m-value of twenty VOCs in surface aeration. The K_La of oxygen incorporating Ψ_m was used to estimate K_La of VOCs. The K_La of oxygen and twenty VOCs are shown in Table 26. In order to estimate the fraction of liquid resistance, the k_Ga-value of 128 obtained in Section 4.2.4 and K_La of oxygen interpreted from specific power input (equation 111) were used to estimate the ratio of $\frac{k_Ga}{K_La}$.

5.2 Estimating Stripping Rates in Bubble Column

The program, developed by ASCE for nonlinear estimation of oxygen transfer parameters, was used to estimate standard oxygen transfer efficiency (SOTE) of experimental air flow in this study. Table 27 shows the results of P/V, SOTE corresponding to experimental air flow rate. The oxygen-transfer efficiencies were between 10.5% and 6.9% for air flow rates from 1.15 to 5.10 scfh. Figure 60 shows that SOTE decreases with increasing air flow rate. The higher air flow produces bigger air bubbles which results in smaller specific surface area. According to Metcalf and Eddy (1979), the oxygen-transfer efficiency of medium-bubble is between 6% and 15%. Therefore, medium-bubble size refers to the experimental air flow rate used in this study. Reported oxygen transfer efficiency of bubble diffused aeration systems range from 0.6 - 1.2 [kg O_2/Kw-h] for medium-bubble (Metcalf and Eddy, 1979, pp. 497). The value of 1.0 [kg O_2/Kw-h] was selected to correlate

Table 25. Psi-m value of twenty VOCs in surface aeration (Calculation)

Compounds		O2	CT	PCE	111TCA	TCE	EBZ	MXY	TLN	BZ	OXY	12DCE	CLF	CBZ	BBZ	13DCB	14DCB	12DCB	EDB	BF	1122TCA	NAPH
	Hc =>	30.0	1.12	0.57	0.525	0.25	0.26	0.24	0.23	0.23	0.18	0.166	0.16	0.15	0.1	0.124	0.108	0.087	0.041	0.041	0.042	0.038
P/V	DL =>	1.97	0.86	0.83	0.844	0.9	0.71	0.71	0.79	0.89	0.71	0.977	0.94	0.8	0.78	0.727	0.71	0.725	0.908	0.865	0.763	0.668
(w/m3)	Ψ =>	0.5	0.66	0.65	0.65	0.68	0.60	0.60	0.63	0.67	0.60	0.70	0.69	0.64	0.63	0.61	0.60	0.61	0.68	0.66	0.62	0.58
	Ratio																					
15	102.8	1.24	0.66	0.64	0.64	0.65	0.58	0.57	0.61	0.64	0.57	0.67	0.65	0.60	0.57	0.56	0.55	0.55	0.55	0.53	0.51	0.46
20	77.8	1.65	0.65	0.64	0.64	0.64	0.57	0.57	0.60	0.64	0.56	0.65	0.64	0.59	0.55	0.55	0.54	0.53	0.52	0.50	0.48	0.44
25	62.7	2.04	0.65	0.63	0.64	0.64	0.56	0.56	0.59	0.63	0.55	0.64	0.63	0.57	0.54	0.54	0.52	0.51	0.49	0.48	0.45	0.41
30	52.5	2.44	0.65	0.63	0.63	0.63	0.56	0.55	0.58	0.62	0.54	0.63	0.62	0.56	0.53	0.53	0.51	0.50	0.46	0.45	0.43	0.39
35	45.2	2.83	0.65	0.63	0.63	0.62	0.55	0.55	0.58	0.61	0.53	0.62	0.61	0.55	0.51	0.52	0.50	0.48	0.44	0.43	0.41	0.37
40	39.7	3.22	0.65	0.62	0.62	0.61	0.55	0.54	0.57	0.61	0.53	0.61	0.60	0.54	0.50	0.50	0.49	0.47	0.42	0.41	0.39	0.35
45	35.4	3.61	0.65	0.62	0.62	0.61	0.54	0.53	0.56	0.60	0.52	0.60	0.59	0.53	0.49	0.49	0.48	0.46	0.40	0.39	0.37	0.34
50	32.0	4.00	0.64	0.62	0.62	0.60	0.54	0.53	0.56	0.59	0.51	0.59	0.58	0.52	0.48	0.49	0.47	0.45	0.39	0.37	0.36	0.32
55	29.2	4.39	0.64	0.61	0.61	0.59	0.53	0.52	0.55	0.58	0.50	0.58	0.57	0.52	0.47	0.48	0.46	0.44	0.37	0.36	0.34	0.31
60	26.8	4.78	0.64	0.61	0.61	0.59	0.52	0.52	0.54	0.58	0.50	0.57	0.56	0.51	0.46	0.47	0.45	0.42	0.36	0.34	0.33	0.30
65	24.8	5.16	0.64,	0.61	0.61	0.58	0.52	0.51	0.54	0.57	0.49	0.57	0.55	0.50	0.45	0.46	0.44	0.41	0.34	0.33	0.32	0.28
70	23.1	5.55	0.64	0.60	0.60	0.58	0.51	0.51	0.53	0.56	0.48	0.56	0.54	0.49	0.44	0.45	0.43	0.40	0.33	0.32	0.31	0.27
75	21.6	5.93	0.64	0.60	0.60	0.57	0.51	0.50	0.53	0.56	0.48	0.55	0.53	0.48	0.43	0.44	0.42	0.40	0.32	0.31	0.30	0.26
80	20.3	6.31	0.63	0.60	0.60	0.56	0.50	0.50	0.52	0.55	0.47	0.54	0.53	0.48	0.42	0.43	0.41	0.39	0.31	0.30	0.29	0.25

Table 26. Mass transfer coefficient of oxygen and twenty VOCs in surface aeration (Calculation based on Table 25)

w/m3	Ratio	O2	CT	PCE	111TCA	TCE	EBZ	MXY	TLN	BZ	OXY	12DCE	CLF	CBZ	BBZ	13DCB	14DCB	12DCB	EDB	BF	1122TCA	NAPH
15	102.8	1.24	0.82	0.80	0.80	0.81	0.72	0.72	0.75	0.80	0.71	0.83	0.81	0.74	0.71	0.70	0.69	0.68	0.68	0.66	0.63	0.58
20	77.8	1.65	1.08	1.05	1.05	1.06	0.94	0.93	0.98	1.05	0.92	1.08	1.05	0.96	0.91	0.91	0.88	0.87	0.85	0.83	0.78	0.72
25	62.7	2.04	1.33	1.29	1.30	1.30	1.15	1.15	1.21	1.28	1.12	1.31	1.28	1.17	1.10	1.10	1.07	1.05	1.00	0.97	0.92	0.84
30	52.5	2.44	1.59	1.53	1.54	1.53	1.36	1.35	1.42	1.51	1.32	1.54	1.50	1.37	1.28	1.28	1.24	1.21	1.13	1.10	1.05	0.95
35	45.2	2.83	1.84	1.77	1.78	1.76	1.56	1.55	1.63	1.73	1.51	1.76	1.72	1.57	1.45	1.46	1.41	1.37	1.25	1.21	1.16	1.05
40	39.7	3.22	2.08	2.01	2.01	1.98	1.76	1.74	1.84	1.95	1.69	1.97	1.92	1.75	1.61	1.63	1.57	1.52	1.36	1.32	1.26	1.13
45	35.4	3.61	2.33	2.24	2.24	2.19	1.95	1.93	2.03	2.16	1.87	2.17	2.12	1.93	1.76	1.79	1.72	1.65	1.46	1.41	1.35	1.21
50	32.0	4.00	2.57	2.47	2.47	2.40	2.14	2.11	2.23	2.36	2.04	2.37	2.31	2.10	1.91	1.94	1.86	1.79	1.54	1.50	1.43	1.28
55	29.2	4.39	2.82	2.69	2.70	2.61	2.32	2.29	2.41	2.56	2.21	2.56	2.49	2.26	2.04	2.09	2.00	1.91	1.63	1.57	1.51	1.35
60	26.8	4.78	3.06	2.91	2.92	2.81	2.50	2.47	2.60	2.76	2.37	2.75	2.67	2.42	2.18	2.23	2.13	2.03	1.70	1.65	1.58	1.41
65	24.8	5.16	3.29	3.13	3.14	3.00	2.68	2.64	2.77	2.95	2.53	2.92	2.84	2.58	2.30	2.37	2.26	2.14	1.77	1.71	1.64	1.47
70	23.1	5.55	3.53	3.35	3.35	3.20	2.85	2.80	2.95	3.13	2.68	3.10	3.01	2.72	2.42	2.50	2.38	2.25	1.83	1.78	1.70	1.52
75	21.6	5.93	3.77	3.57	3.57	3.38	3.02	2.97	3.12	3.31	2.83	3.26	3.17	2.87	2.53	2.62	2.49	2.35	1.89	1.83	1.76	1.56
80	20.3	6.31	4.00	3.78	3.78	3.57	3.18	3.13	3.28	3.49	2.97	3.43	3.33	3.01	2.64	2.74	2.60	2.44	1.95	1.89	1.81	1.61

Table 27. Oxygen transfer performance in bubble column

Test No.	Flow rate (scfh)	KLa-O2 (1/hr)	SOTR (lb/hr)	SOTE (%)	Power (watt)	P/V* (watt/m3)
BC9	5.10	15.43	0.0061	6.92	2.77	137.9
BC15	4.37	14.50	0.0054	7.12	2.46	122.2
BC11	4.45	14.70	0.0055	7.25	2.50	124.2
BC3	4.03	14.72	0.0061	8.71	2.77	137.9
BC4	3.75	12.62	0.0050	7.65	2.27	113.1
BC5	3.75	11.82	0.0047	7.28	2.14	106.3
BC6	3.68	13.38	0.0050	7.93	2.27	113.1
BC10	3.32	11.09	0.0044	7.67	2.00	99.5
BC14	2.99	11.20	0.0040	8.13	1.82	90.5
BC7	2.38	9.55	0.0038	9.56	1.73	85.9
BC1	2.29	7.34	0.0035	8.79	1.59	79.1
BC16	1.95	7.80	0.0032	9.71	1.46	72.5
BC12	1.75	7.11	0.0028	9.36	1.27	63.3
BC8	1.15	5.35	0.0021	10.47	0.95	47.5

* Assuming SAE = 1.0 kg O2/Kw-h

SOTR = Standard Oxygen Transfer Rate

SOTE = Standard Oxygen Transfer Efficiency

Liquid volume = 20.1 Liters

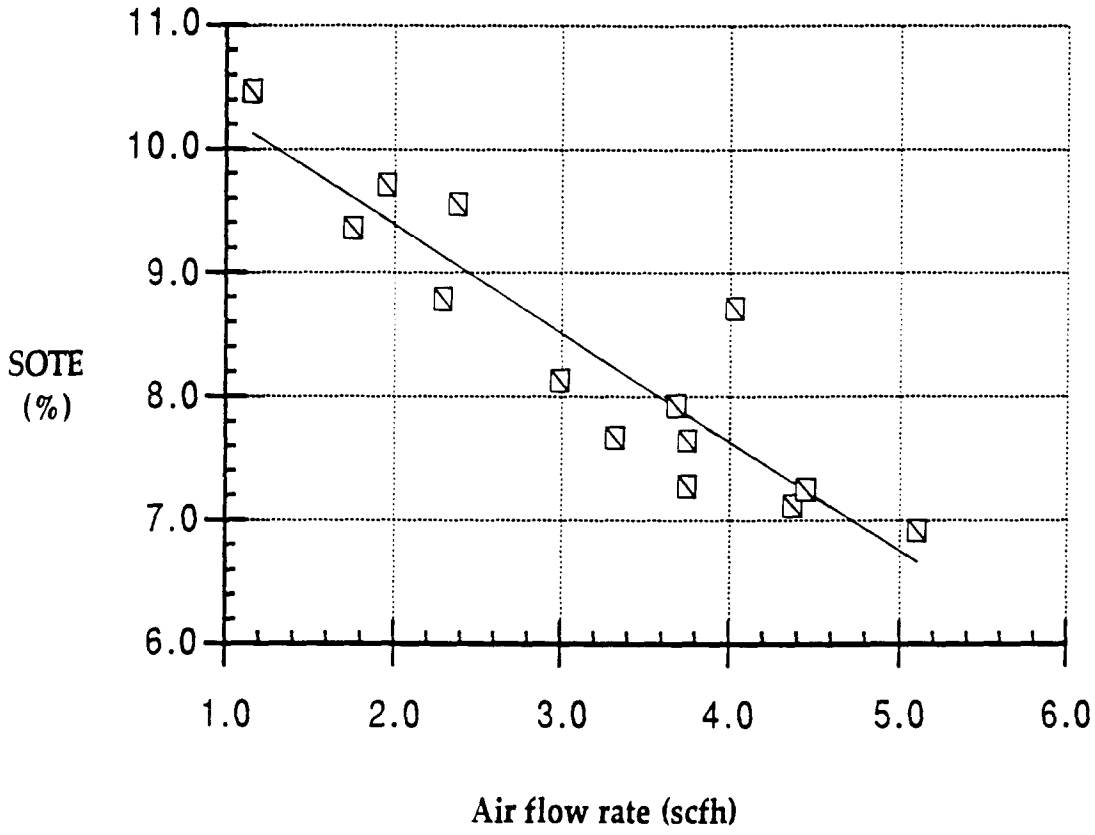

Figure 60. Standard oxygen transfer efficiency (SOTE) versus air flow rate in bubble column

$(K_La)_{O_2}$ to $(\frac{P}{V})$. The correlation between $(K_La)_{O_2}$ and $(\frac{P}{V})$ is shown in Figure 61 and given by:

$$(K_La)_{O_2} = 0.0915\left[\frac{P}{V}\right]^{1.0441} \tag{112}$$

Equation (112) was used to estimate the K_La of oxygen in the bubble column. Table 28 shows the results of Ψ_m-value of twenty VOCs. As was done for surface aeration, the K_La of oxygen incorporating Ψ_m was used to estimate K_La of VOCs. The results of K_La of oxygen and VOCs are shown in Table 29. As was stated in the results in the bubble column section, k_Ga is proportional to superficial velocity (v_s). The correlation between k_Ga and v_s plotted in Figure 62 was used to determine the ratio of $\frac{k_Ga}{K_La}$ in order to estimate the fraction of liquid resistance.

5.3 A Comparison of Stripping Rate Between Surface Aeration and Bubble Column

Typical selected stripping rates for ten VOCs from surface aeration (SA) and bubble column (BC) are plotted in Figure 63 and Appendix K. The calculated results indicate that the rate of oxygen transfer of BC is better than that of SA; whereas, the stripping rates of VOCs from SA are higher than that from BC, except for the most volatile compound studied, CCl_4. The volatility of CCl_4 is high enough in the given hydrodynamic condition. Consequently, the gas-resistance is not very significant to limit the stripping rate of CCl_4 in the bubble column. However, the stripping rate of CCl_4 during SA is still higher than that from BC for a given oxygen transfer rate. According to Figure 63 and Appendix K, it is apparent that stripping rates for VOCs

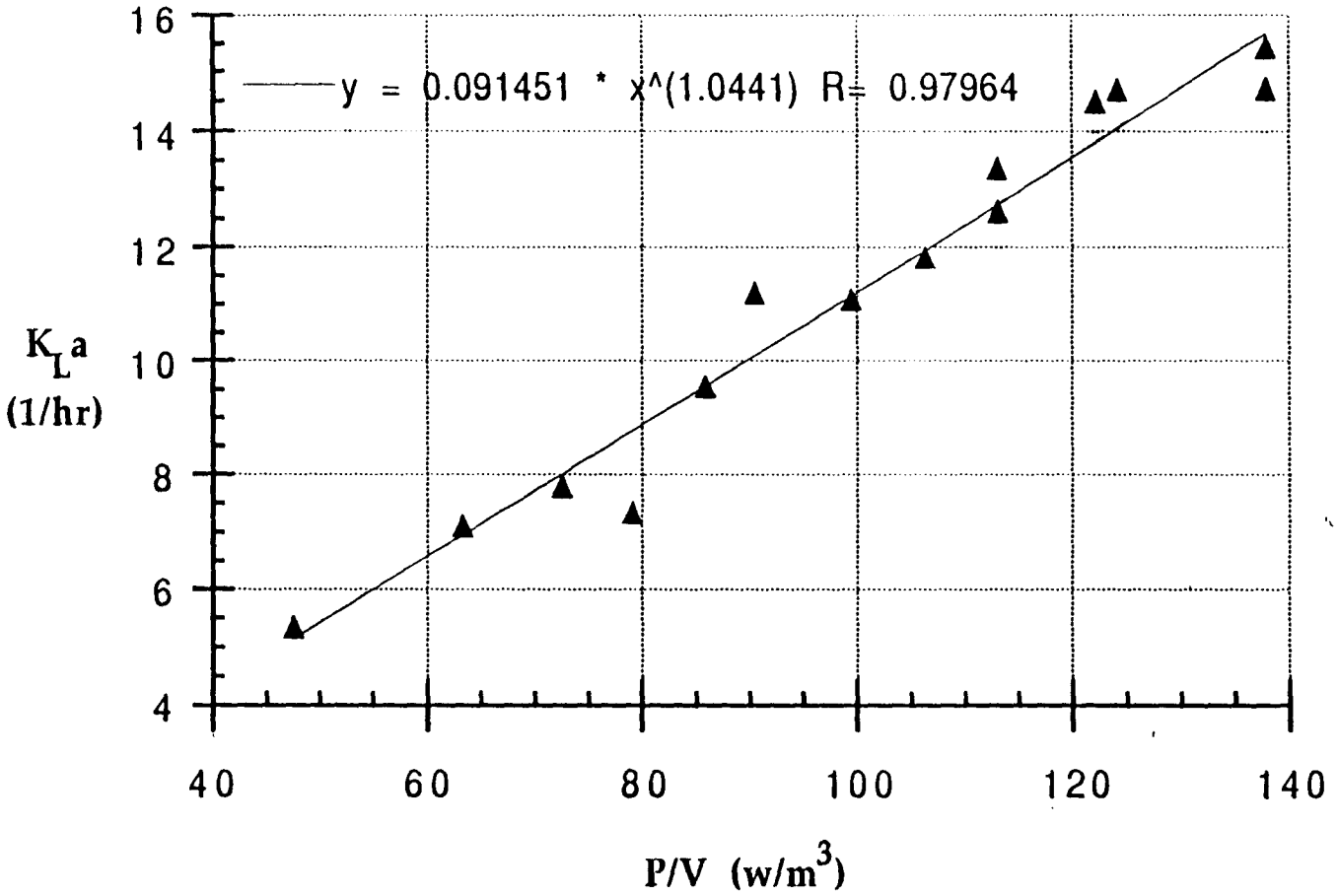

Figure 61. Correlation of oxygen transfer coefficient to specific power input in bubble column

Table 28. Psi-m value of twenty VOCs in bubble column (calculation)

Compounds		O2	CT	PCE	111TCA	TCE	EBZ	MXY	TLN	BZ	OXY	12DCE	CLF	CBZ	BBZ	13DCB	14DCB	12DCB	EDB	BF	1122TCA	NAPH
	Hc =>	30.02	1.122	0.565	0.525	0.252	0.26	0.236	0.23	0.226	0.181	0.166	0.16	0.146	0.099	0.124	0.108	0.087	0.041	0.041	0.042	0.038
P/V	DL =>	1.971	0.862	0.834	0.844	0.899	0.708	0.706	0.787	0.892	0.706	0.977	0.938	0.8	0.775	0.727	0.71	0.725	0.908	0.865	0.763	0.668
(w/m3)	Ψ =>	0.5	0.66	0.65	0.65	0.68	0.60	0.60	0.63	0.67	0.60	0.70	0.69	0.64	0.63	0.61	0.60	0.61	0.68	0.66	0.62	0.58
	Ratio																					
15	1.7	1.55	0.44	0.32	0.31	0.21	0.19	0.17	0.18	0.19	0.14	0.16	0.15	0.13	0.09	0.11	0.09	0.08	0.05	0.04	0.04	0.04
20	1.9	2.09	0.45	0.33	0.32	0.21	0.19	0.18	0.19	0.20	0.15	0.17	0.16	0.14	0.10	0.11	0.10	0.08	0.05	0.05	0.05	0.04
25	1.9	2.63	0.45	0.34	0.33	0.22	0.20	0.19	0.20	0.21	0.16	0.17	0.16	0.14	0.10	0.12	0.10	0.09	0.05	0.05	0.05	0.04
30	2.0	3.19	0.46	0.35	0.34	0.23	0.21	0.19	0.20	0.21	0.16	0.18	0.17	0.15	0.10	0.12	0.11	0.09	0.05	0.05	0.05	0.04
35	2.1	3.74	0.46	0.35	0.34	0.23	0.21	0.20	0.21	0.22	0.17	0.18	0.17	0.15	0.11	0.13	0.11	0.09	0.05	0.05	0.05	0.04
40	2.2	4.30	0.47	0.36	0.35	0.24	0.22	0.20	0.21	0.22	0.17	0.19	0.18	0.15	0.11	0.13	0.11	0.10	0.06	0.05	0.05	0.04
45	2.2	4.87	0.47	0.36	0.35	0.24	0.22	0.21	0.21	0.23	0.17	0.19	0.18	0.16	0.11	0.13	0.12	0.10	0.06	0.05	0.05	0.05
50	2.3	5.43	0.48	0.37	0.36	0.25	0.22	0.21	0.22	0.23	0.18	0.19	0.18	0.16	0.12	0.13	0.12	0.10	0.06	0.06	0.05	0.05
55	2.3	6.00	0.48	0.37	0.36	0.25	0.23	0.21	0.22	0.23	0.18	0.20	0.19	0.16	0.12	0.14	0.12	0.10	0.06	0.06	0.06	0.05
60	2.4	6.57	0.48	0.37	0.36	0.25	0.23	0.22	0.22	0.24	0.18	0.20	0.19	0.16	0.12	0.14	0.12	0.10	0.06	0.06	0.06	0.05
65	2.4	7.15	0.48	0.38	0.37	0.26	0.23	0.22	0.23	0.24	0.18	0.20	0.19	0.17	0.12	0.14	0.12	0.11	0.06	0.06	0.06	0.05
70	2.5	7.72	0.49	0.38	0.37	0.26	0.23	0.22	0.23	0.24	0.18	0.20	0.20	0.17	0.12	0.14	0.13	0.11	0.06	0.06	0.06	0.05
75	2.5	8.30	0.49	0.38	0.37	0.26	0.24	0.22	0.23	0.24	0.19	0.21	0.20	0.17	0.12	0.14	0.13	0.11	0.06	0.06	0.06	0.05
80	2.5	8.88	0.49	0.38	0.37	0.26	0.24	0.22	0.23	0.25	0.19	0.21	0.20	0.17	0.13	0.15	0.13	0.11	0.06	0.06	0.06	0.05

Table 29. Mass transfer coefficient of oxygen and twenty VOCs in bubble column (calculation)

(w/m3)	Ratio	O2	CT	PCE	111TCA	TCE	EBZ	MXY	TLN	BZ	OXY	12DCE	CLF	CBZ	BBZ	13DCB	14DCB	12DCB	EDB	BF	1122TCA	NAPH
15	1.7	1.55	0.68	0.50	0.48	0.32	0.29	0.27	0.28	0.29	0.22	0.24	0.23	0.20	0.14	0.17	0.15	0.12	0.07	0.07	0.07	0.06
20	1.9	2.09	0.93	0.69	0.67	0.45	0.41	0.38	0.39	0.41	0.31	0.35	0.33	0.28	0.20	0.24	0.21	0.18	0.10	0.10	0.09	0.08
25	1.9	2.63	1.20	0.90	0.87	0.59	0.53	0.50	0.52	0.54	0.41	0.45	0.43	0.37	0.27	0.31	0.27	0.23	0.13	0.13	0.12	0.11
30	2.0	3.19	1.47	1.11	1.08	0.73	0.66	0.62	0.64	0.67	0.51	0.57	0.54	0.46	0.33	0.39	0.34	0.29	0.17	0.16	0.16	0.13
35	2.1	3.74	1.74	1.32	1.29	0.88	0.79	0.74	0.77	0.81	0.62	0.68	0.65	0.56	0.40	0.47	0.42	0.35	0.20	0.19	0.19	0.16
40	2.2	4.30	2.02	1.54	1.50	1.03	0.93	0.87	0.91	0.95	0.73	0.80	0.77	0.66	0.48	0.55	0.49	0.41	0.24	0.23	0.22	0.19
45	2.2	4.87	2.30	1.76	1.72	1.18	1.07	1.00	1.04	1.10	0.84	0.93	0.88	0.76	0.55	0.64	0.57	0.48	0.28	0.27	0.26	0.22
50	2.3	5.43	2.58	1.99	1.94	1.34	1.21	1.14	1.18	1.24	0.95	1.05	1.00	0.87	0.63	0.73	0.65	0.55	0.32	0.30	0.30	0.25
55	2.3	6.00	2.87	2.22	2.16	1.50	1.36	1.28	1.32	1.39	1.07	1.18	1.13	0.97	0.71	0.82	0.73	0.61	0.36	0.34	0.33	0.29
60	2.4	6.57	3.16	2.45	2.39	1.66	1.51	1.42	1.47	1.55	1.18	1.31	1.25	1.08	0.79	0.91	0.81	0.68	0.40	0.38	0.37	0.32
65	2.4	7.15	3.46	2.69	2.62	1.83	1.66	1.56	1.62	1.70	1.30	1.44	1.38	1.19	0.87	1.00	0.89	0.75	0.44	0.42	0.41	0.35
70	2.5	7.72	3.75	2.92	2.85	2.00	1.81	1.70	1.77	1.86	1.43	1.58	1.51	1.30	0.95	1.10	0.97	0.83	0.48	0.46	0.45	0.39
75	2.5	8.30	4.05	3.16	3.08	2.17	1.96	1.85	1.92	2.02	1.55	1.72	1.64	1.42	1.03	1.19	1.06	0.90	0.53	0.51	0.49	0.42
80	2.5	8.88	4.35	3.40	3.32	2.34	2.12	1.99	2.07	2.18	1.67	1.85	1.77	1.53	1.12	1.29	1.15	0.98	0.57	0.55	0.54	0.46

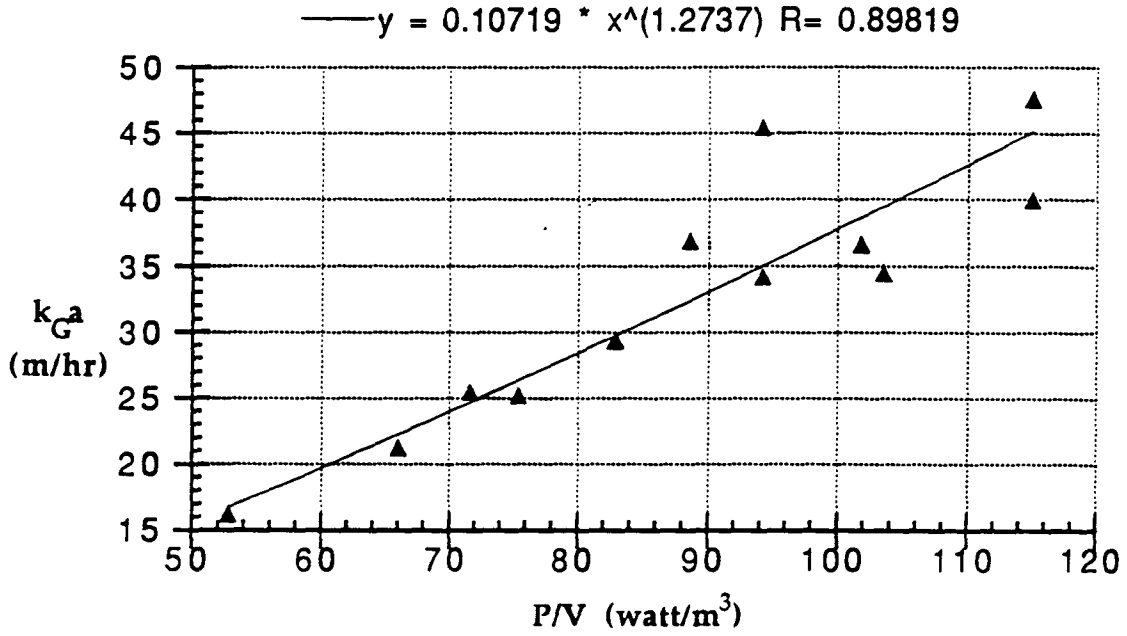

Figure 62. Correlation between $k_G a$ and specific power input (P/V) in bubble column

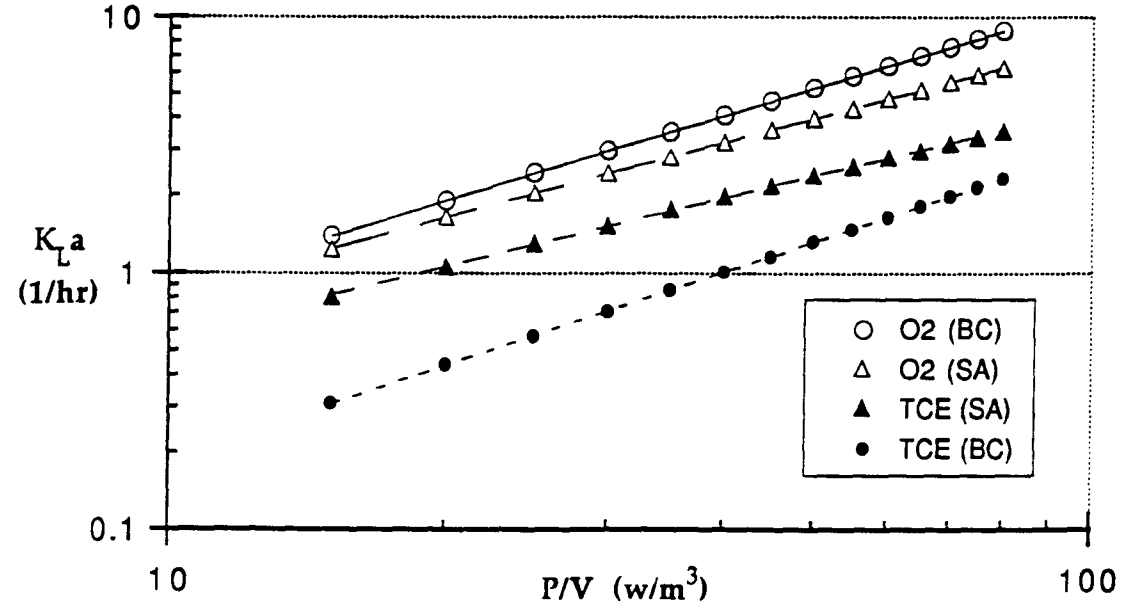

Figure 63. Comparison of mass transfer coefficient of oxygen and TCE in surface aeration (SA) and bubble column (BC)

are greater with SA than with BC. These results can be attributed to the higher gas-resistance which occurs in the bubble column.

For a given aeration tank, the rate of oxygen transfer can be determined by its performance via SOTE. Thereafter, the rate of oxygen transfer can be used to predict the stripping rates of VOCs by means of the novel concept of Ψ_m. The example given in this section is based upon laboratory experiments. The model needs to be verified with field measurements at a full-scale treatment plant.

6. CONCLUSIONS

6.1 Henry's Coefficient

Four techniques were compared for determining dimensionless Henry's coefficient (Hc), and the Equilibrium Partitioning in Closed Systems (EPICS) method with analysis of the aqueous phase was selected for its superior precision, simplicity, and the capacity to handle large numbers of samples in a reasonably short time. Prior to performing EPICS tests, the time required to approach equilibrium was determined. Results showed that complete equilibrium for twenty volatile organic compounds (VOCs) was achieved within about 30 min. on a shaker table at 2500 RPM.

A sensitivity analysis of EPICS volume ratio to the change of Hc for three Hc-values (1.2, 0.2, and 0.01) was performed to determine the volume ratios to minimize errors (Figure 64). For Hc of 1.2, a volume ratio of 5 was required to produce a coefficient of variation (CV) less than 5%; whereas, a volume ratio of 50 was essential for Hc of 0.04. A volume ratio of 10 was satisfactory for Hc of 0.2. For low volatility compounds, greater precision in the EPICS procedure can be attained as the volume ratio is increased. Experiments were carried out with the volume ratio of 10, since the largest serum bottle available had a volume of 120 ± 0.5 ml and the analytical balance had a capacity of 160 g with precision of 0.0001 g. The results show that the precision of the EPICS procedure decreases as Hc decreases, except for CCl_4. The high CVs of CCl_4 are due to its lower GC response which produces higher deviations.

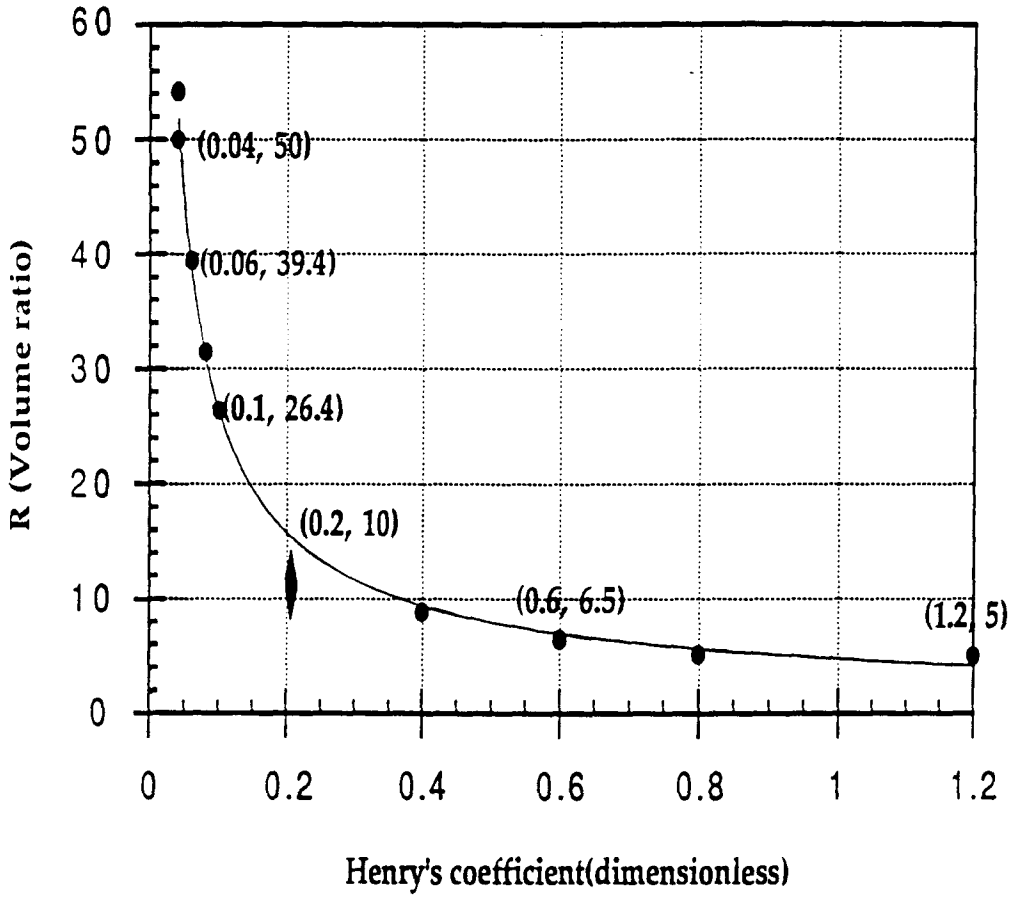

Figure 64. Correlation of volume ratio within EPICS bottles pair to Henry's coefficient based upon less than 7.5 % of ($\Delta H/H$) caused by a 5% error of liquid-phase concentration ratio ($\Delta R/R$, R = Cw1/Cw2)

The previously reported and new estimates Hc data for twenty VOCs are summarized in Table 3 and plotted in Figure 65. The consistency of the data from this study for most of the compounds is noted. Mackay and Shiu (1981) compiled values from a number of sources and found wide variations. In particular, the Hc-values of low volatility compounds are rarely reported in the literature and published values have wide variations. In this study, the higher Hc-values for low volatility compounds were used to better fit the mass-transfer model of the bubble column.

6.2 Surface Aeration

In bench-scale surface aeration, the mass-transfer coefficient for oxygen and twenty VOCs were simultaneously measured. Using these measurement, the $\frac{k_G a}{k_L a}$ ratios were determined by nonlinear regression. Thereafter, the $\frac{k_G a}{k_L a}$ ratios were used to estimate the fraction of liquid phase resistance to total resistance ($\frac{R_L}{R_T}$). The Ψ_m-values were used to predict the stripping rates for twenty VOCs over a range of hydrodynamic conditions in order to verify the novel concept. Finally, the relationship between stripping rates of VOCs and specific power input were determined as a protocol for scale-up application. The following conclusions are made:

1. The hydrodynamic condition during surface aeration was expressed in terms of specific power input ($\frac{P}{V}$) and velocity gradient (G). At the unbroken water surface, the mass transfer coefficient ($K_L a$) of oxygen was proportional to $(\frac{P}{V})^{0.45}$ and $G^{0.91}$, respectively. The $K_L a$ of twenty VOCs was proportional

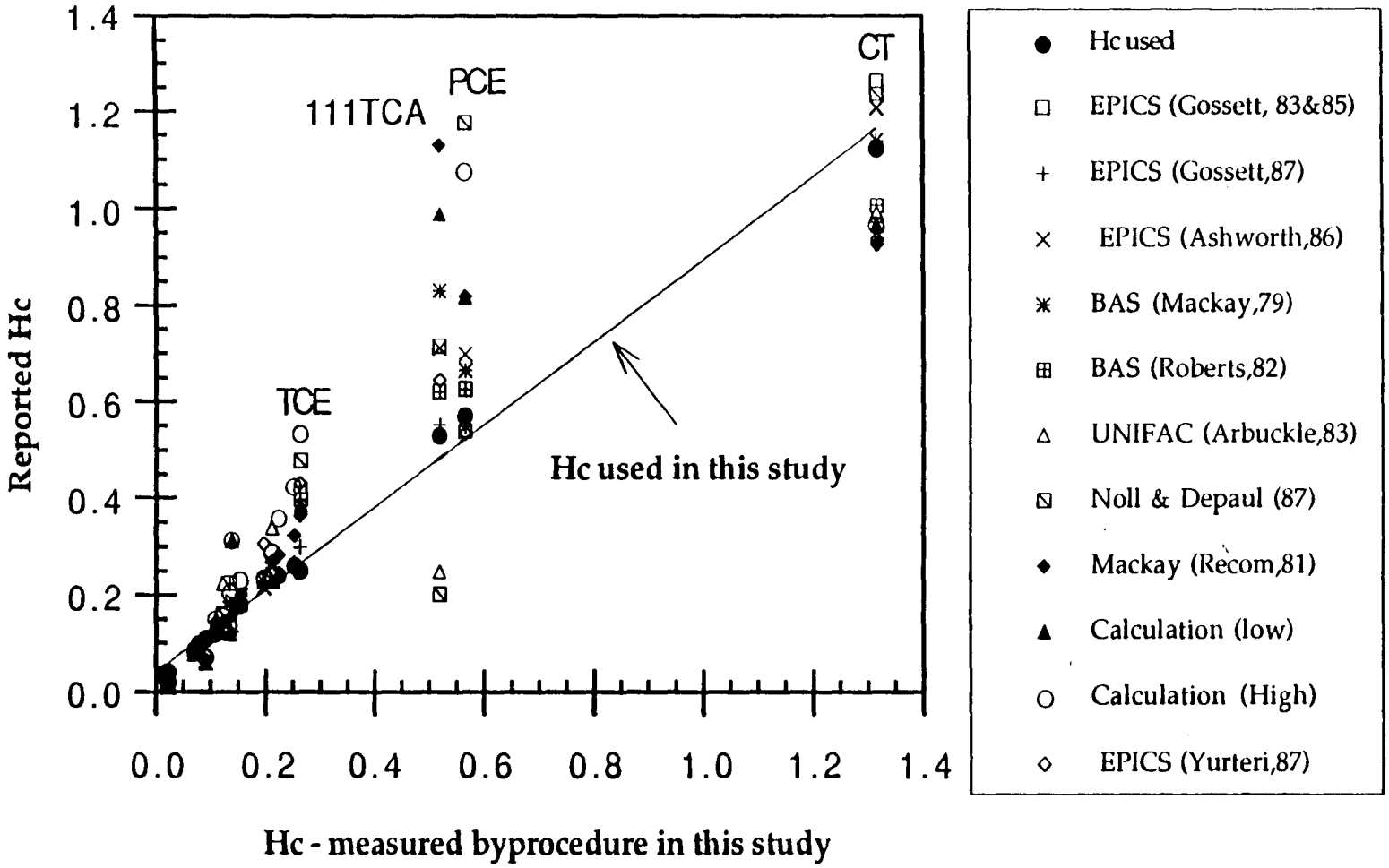

Figure 65. Comparison between reported and present Henry's constant for twenty VOCs

to $(\frac{P}{V})^n$, with n ranging from 0.26 to 0.43. The n-value of oxygen and twenty VOCs were very close to the reported range of 0.20 and 0.40 by Kozinski and King (1966).

2. For a given $\frac{P}{V}$, $\frac{R_L}{R_T}$ decreases with increasing Hc. The gas-phase resistance has a very significant effect for compounds with Hc < 0.2 under the hydrodynamic conditions used in this work (Figure 66). $\frac{R_L}{R_T}$ significantly decreases with increasing $\frac{P}{V}$

3. Ψ_m-value, estimated from $\frac{R_L}{R_T}$ and the liquid diffusivity of VOCs, was used to predict the stripping rates for twenty VOCs over a range of hydrodynamic conditions using the K_La of oxygen. Good correlations between estimated and measured values of K_La of twenty VOCs were observed (Figure 67), which proves the validity of Ψ_m concept.

4. It is necessary to have sufficient air flow in the headspace for removal of VOCs from the liquid phase, especially for low volatility compounds. The results obtained from one series of experiments suggest that covering aeration tanks may reduce the volatilization rate of VOCs.

6.3 Bubble-Column

The developed methodology, transfer parameter [-ln(1-Ds)/Sd], was used to estimate the mass-transfer coefficient of twenty VOCs (Sd represents degree of satura-

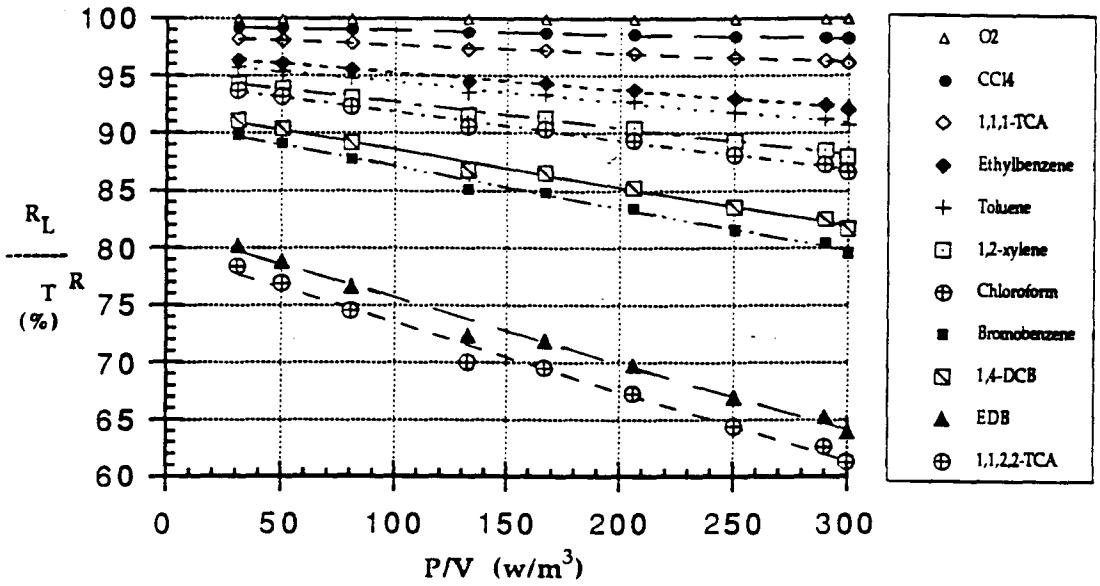

Figure 66. Effect of specific power input on liquid-film resistance in surface aeration

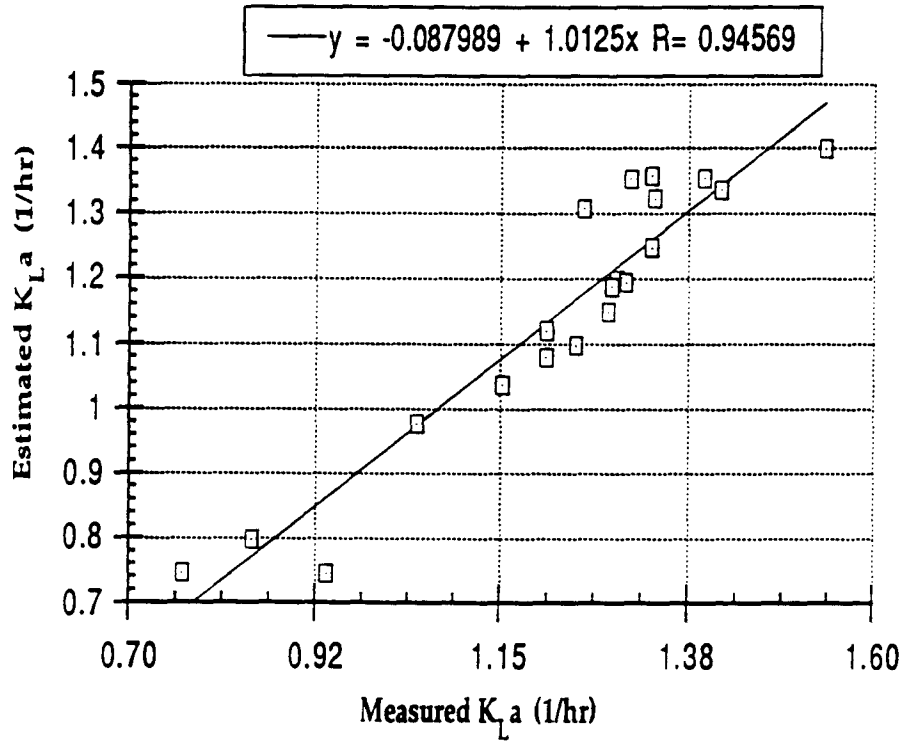

Figure 67. Comparison between estimated and measured mass transfer coefficients in surface aeration (400rpm)

tion of bubbles). As was done in surface aeration, the parameters $\frac{k_G a}{k_L a}$, $\frac{R_L}{R_T}$, Ψ_m and prediction of the stripping rates of twenty VOCs were estimated. The conclusions, based on the results of the bubble-column experiments, are as follows:

1. The flow behavior of the bubble column, such as the air holdup ratio (ε), specific interfacial area (a), wall effects, bubble diameters, and K_L-values were studied in order to quantify the hydrodynamic conditions. The dependence of interfacial area (a) and K_L-values on AFR were correlated. The increase in the rate of mass transfer was mainly dependent on an increase in the interfacial area (a) and was only secondarily dependent on increased K_L-values (Figure 68).

2. The $K_L a$'s of twenty VOCs at different air flow rates were correlated to produce a simple power function of the form, $Y = b\ X^m$. The m-values of the power function were all very close to 1.0 over a range of Hc from 0.04 to 30.2, which indicates that the relationship between $K_L a$ and $\frac{Q_G}{V_L}$ is linear (Figure 69). The increase of b-value for twenty VOCs implies that higher Henry's coefficient corresponds to higher mass-transfer coefficients.

3. Gas-phase resistance becomes increasingly significant as Hc decreases for a given specific air flow rate. Figure 70 shows that Sd increases with decreasing Hc.

4. The value of Ψ is approximately constant for twenty VOCs with different Hc's and various specific power inputs; whereas, Ψ_m-values decrease with decreas-

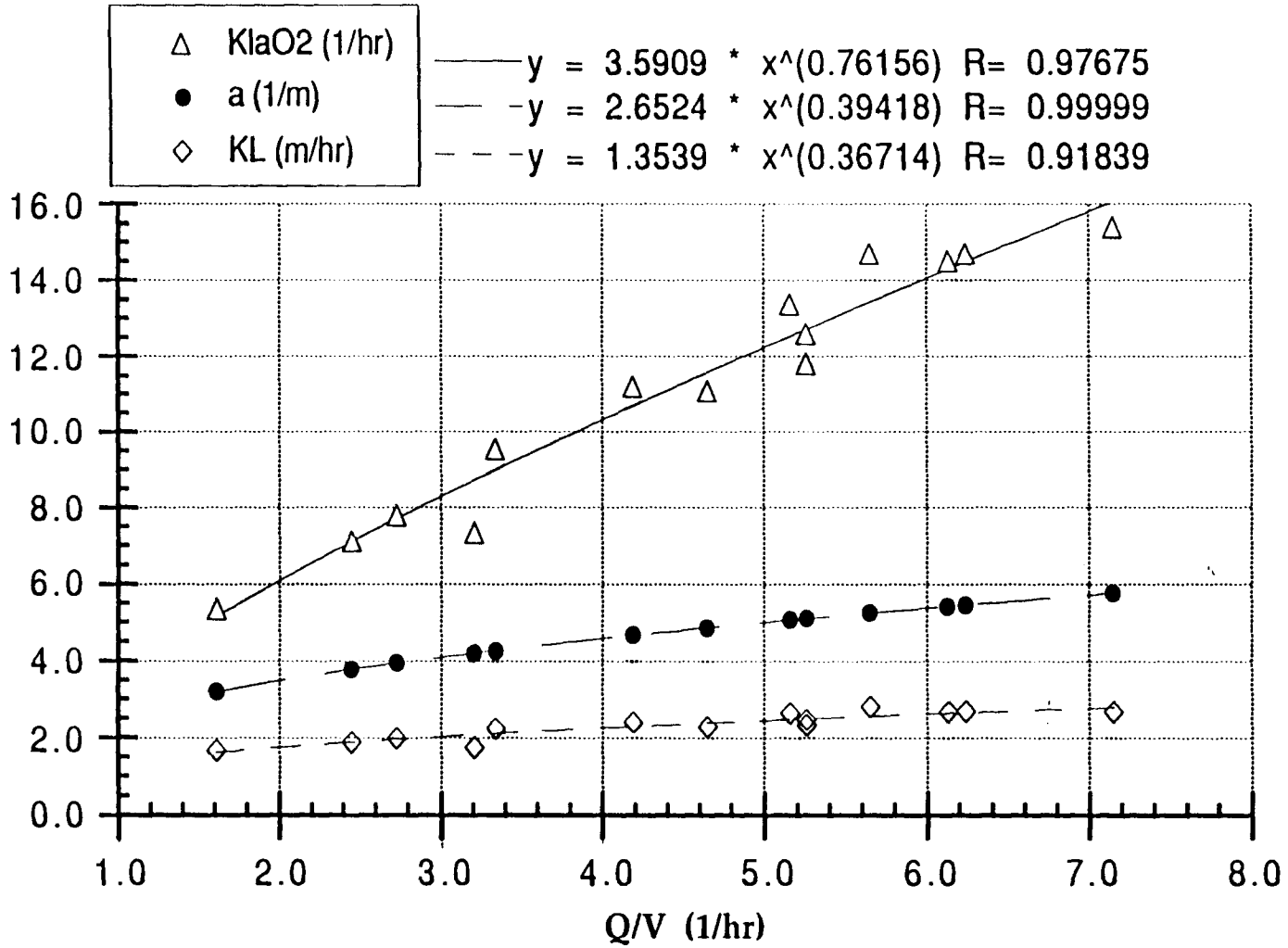

Figure 68. Correlation of oxygen transfer coefficient, interfacial area, and mass-transfer coefficient to specific air flow rates in buuble column

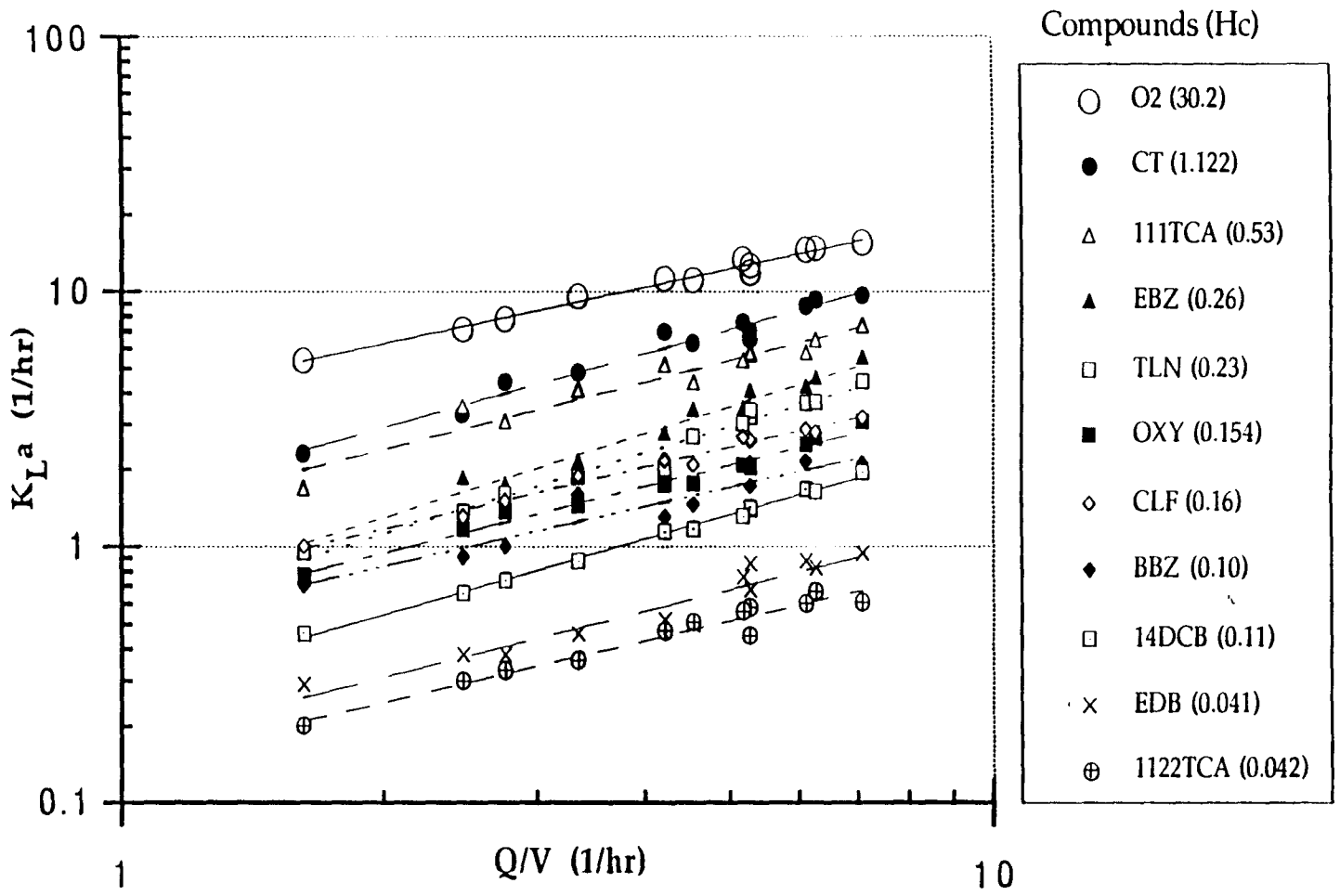

Figure 69. Mass transfer coefficients as a function of specific air flow rate and Henry's coefficient in bubble column

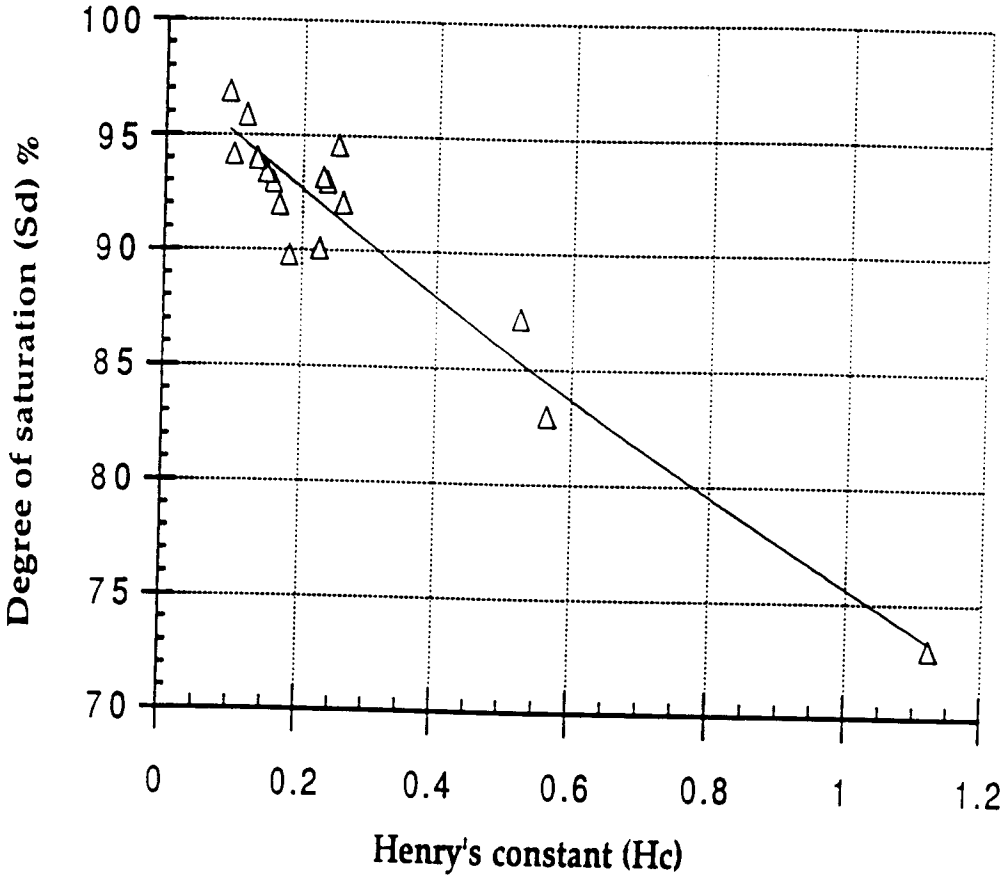

Figure 70. Mean value of degree of saturation (Sd) for twenty VOCs versus Hc in bubble column

ing Hc (the same trend as for $\frac{R_L}{R_T}$ (Figure 71). The results show that using Ψ is only valid when liquid-phase resistance is the predominant mass transfer resistance. Good correlations between estimated and measured values of K_La of twenty VOCs were observed when using the Ψ_m parameters (Figure 72).

5. The developed methodology, use of transfer parameter to predict stripping rate of VOCs, has been confirmed by analysis of dimensionless parameters. Use of dimensionless parameters to predict the stripping rate of VOCs incorporates the Hc and the air flow-to-liquid volume ratio and has the form: $K_La\frac{V_L}{Q_G} = b\ Hc^m$. However, the value of b is not a constant, and depends on Sd of the VOCs in the bubble column. The data from Table 22 is shown in Figure 73 along with plots of linear and power functions. The correlation of linear and power function with Hc < 0.27 for b = - ln (1-Sd) are 2.47 and 2.87 which corresponds to 91.6% and 94.3% degree of saturation for 14 runs of experiments.

6.4 Estimating the Ratio of k_Ga/k_La in Surface Aeration and Bubble Column

Figures 74 and 75 show that k_Ga and $\frac{k_Ga}{k_La}$ ratios in surface aeration and bubble column, respectively. The ratio of $\frac{k_Ga}{k_La}$ should rely on the hydrodynamic conditions of windspeed in the air phase and mixing condition in the water, phase, instead of being a fixed value as suggested by previous studies. The surface aeration experiments performed with constant windspeeds of 1.8 to 2.4 (m/s) resulted in a relatively constant gas transfer coefficient (k_Ga) of 128. However, the air phase hydrodynamic

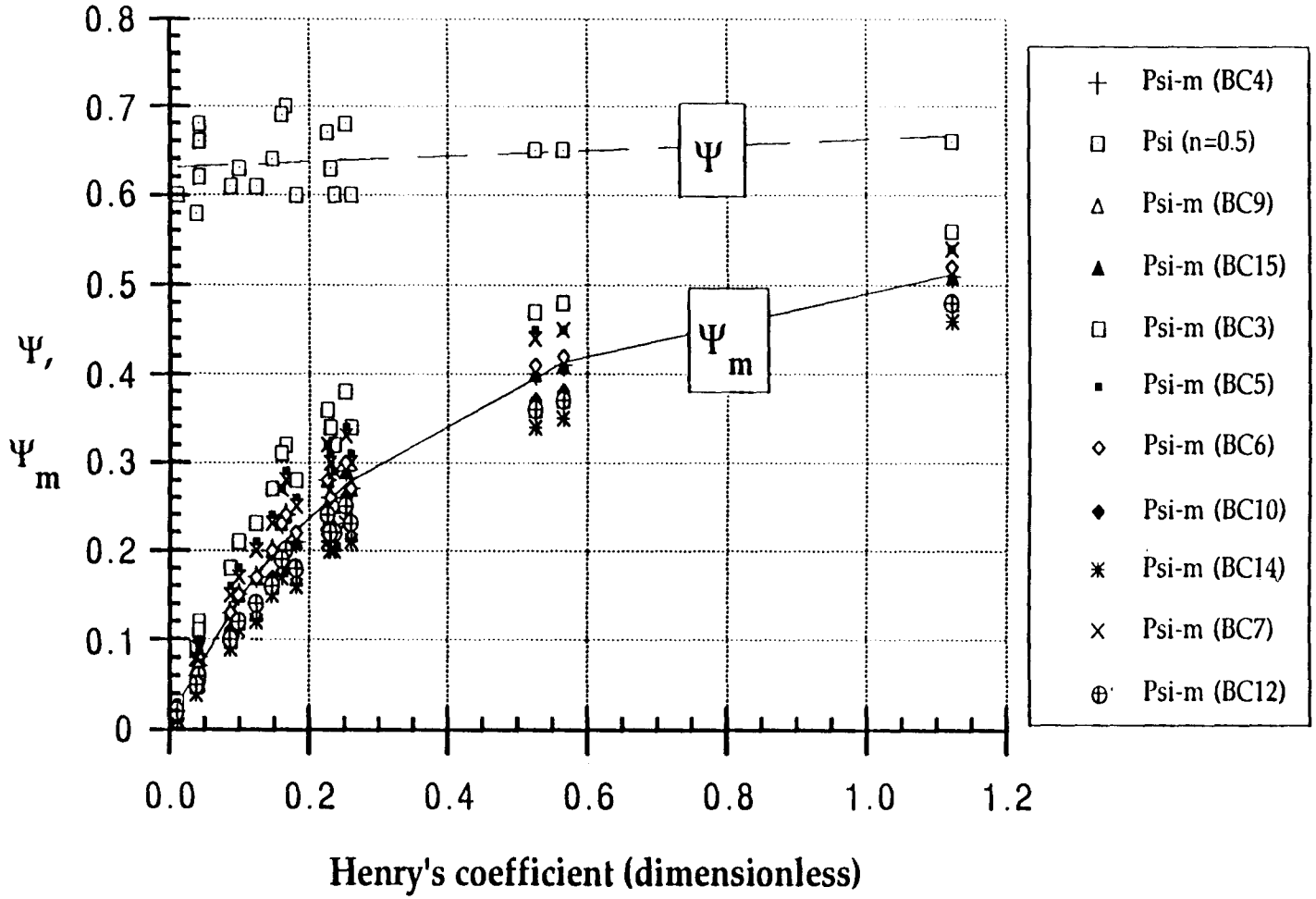

Figure 71. Comparison of Ψ and Ψ_m values for different air flow rates in bubble column

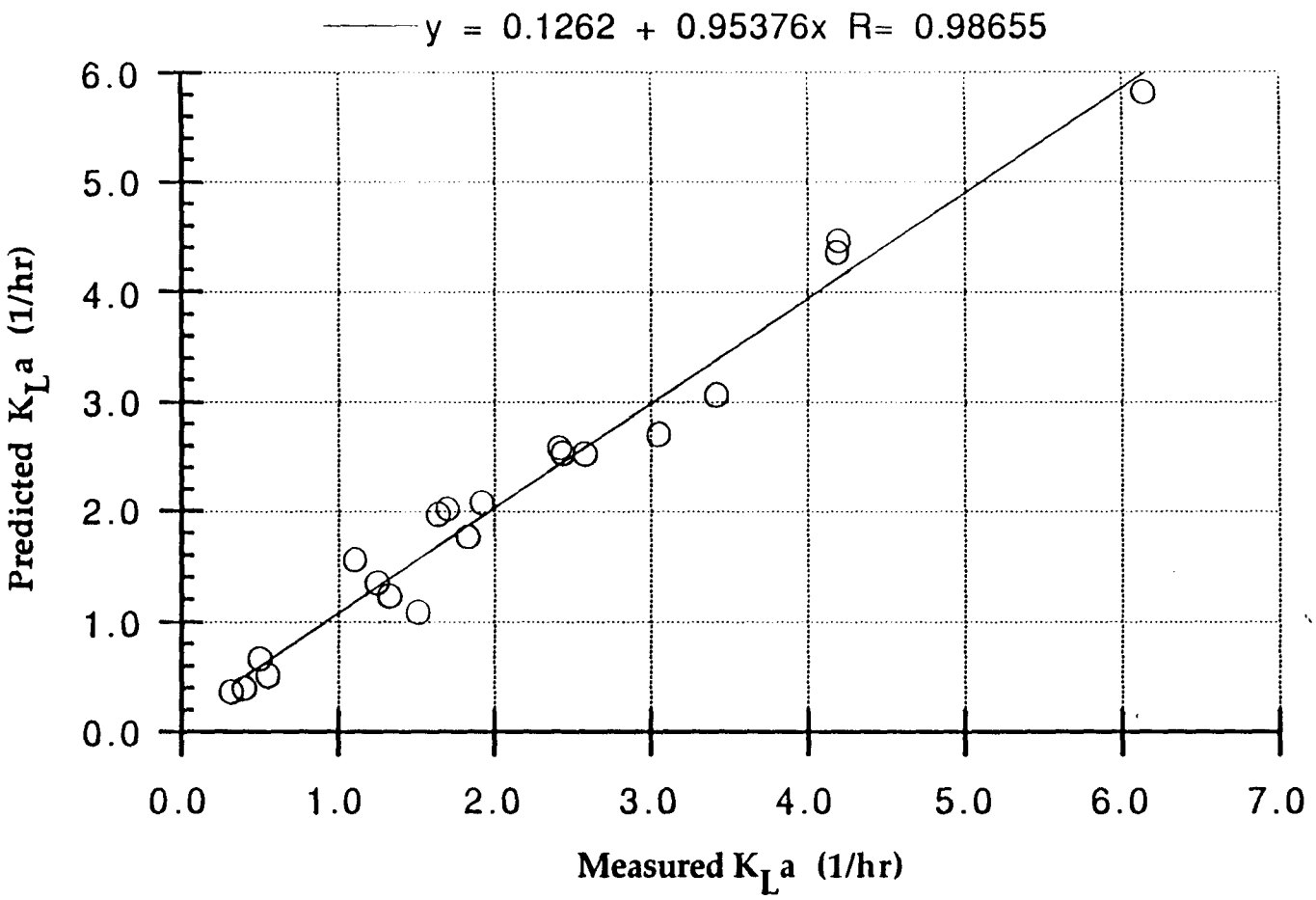

Figure 72. Comparison between predicted and measured mass transfer coefficients in bubble column (BC10, specific air flow rate = 4.68 1/hr)

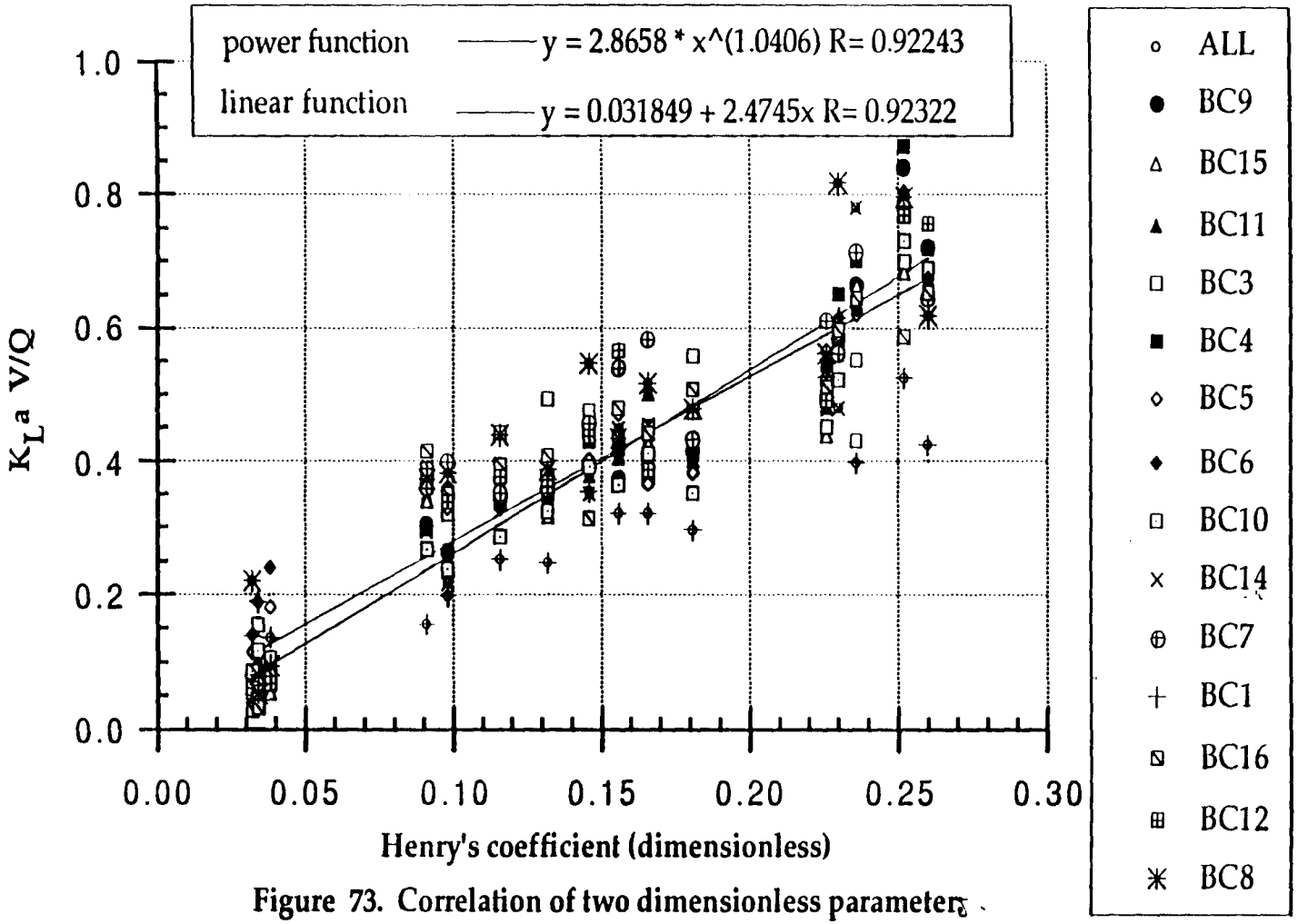

Figure 73. Correlation of two dimensionless parameters $K_L a$ V/Q versus Hc for 14 experiments with Hc < 0.30

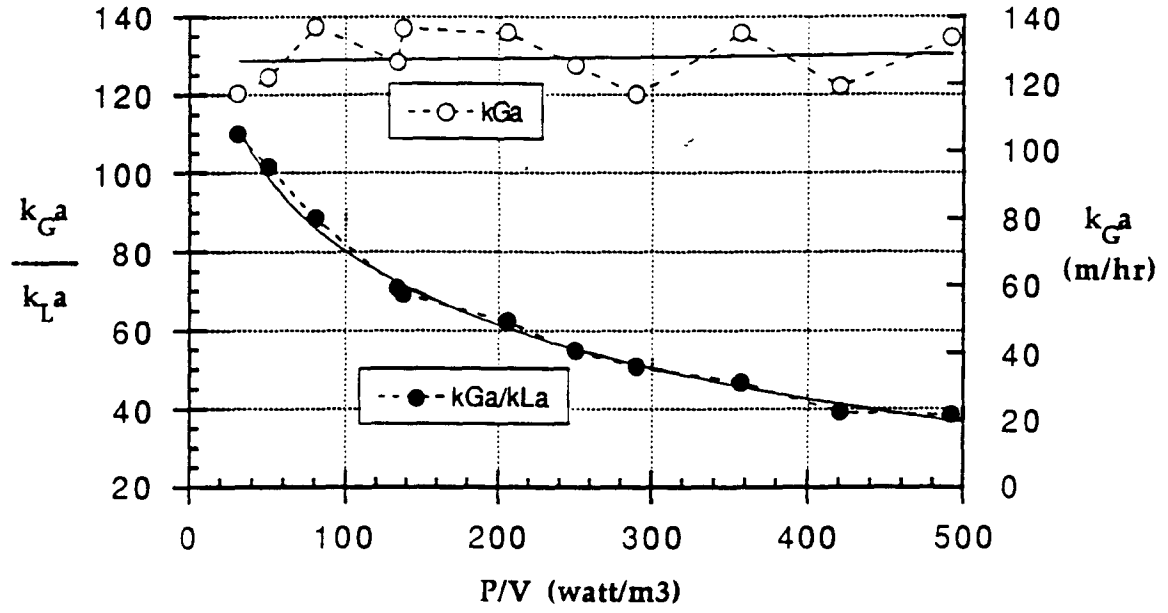

Figure 74. Correlation of $k_G a$ and $k_G a$ / $K_L a$ to specific power input in surface aeration

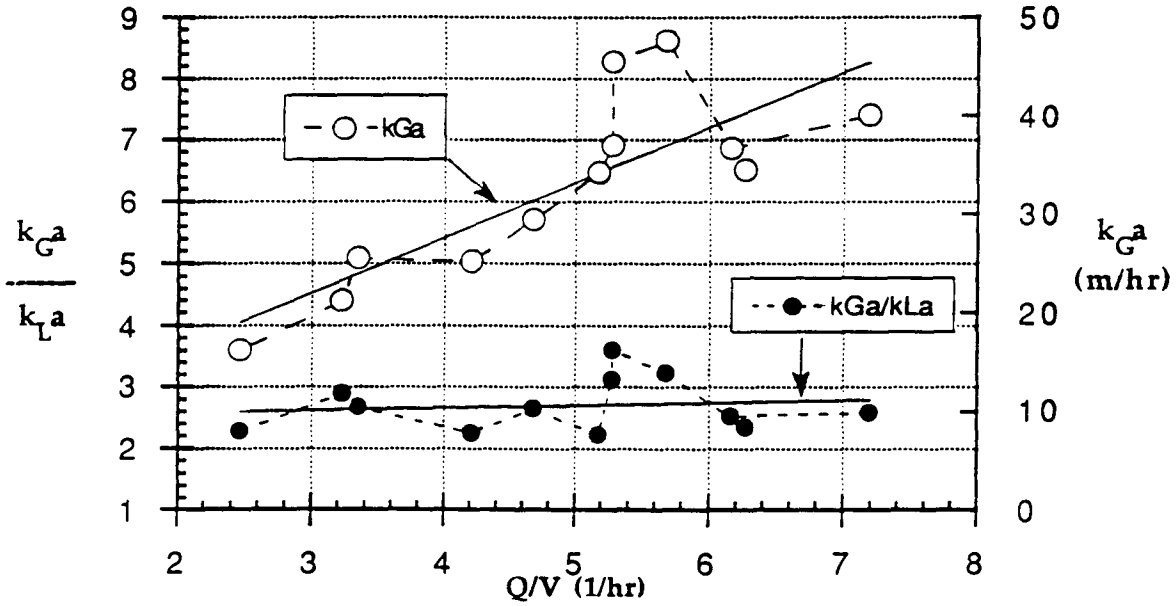

Figure 75. Correlation of k_G and $k_G a/k_L a$ to specific air flow rate in bubble column

condition in the bubble column varied with the air flow rate which resulted in different superficial velocities (v_s). The $k_G a$'s were between 16 and 48 which resulted from the change of v_s-values from 0.044 to 0.128 (cm/sec).

Accordingly, the $k_G a$-value is approximately proportional to the v_s in the bubble column. Since $k_G a$ is proportional to $k_L a$ in the bubble column, there is a relatively constant ratio of $\frac{k_G a}{k_L a}$. However, the ratio of $\frac{k_G a}{k_L a}$ decreases with increasing specific power input or Reynolds number due to the nearly constant $K_G a$-value. The correlation between the ratio of $\frac{k_G a}{k_L a}$ and the Reynolds number for surface aeration is very close to that of Roberts (1984), because both experiments were performed with the same windspeed of 1.8 - 2.4 (m/s). The ratios of $\frac{k_G a}{k_L a}$ in the bubble column (2.2-4.6) were much smaller than those in the surface aeration experiments (38-110). This implies that the gas-phase resistance in the bubble column is much more important than it is in the surface aeration.

6.5 Engineering Significance

The Ψ_m concept can be used to estimate volatilization of low volatility compounds. Simple extrapolation of Ψ may greatly overestimate VOC stripping. The results show that using aeration systems which have low values of $k_G a$, as compared to $k_L a$ (i.e. fine bubble diffusers) minimize VOC losses.

REFERENCES

1. Akita, K., and F. Yoshida (1974), "Bubble Size, Interfacial Area and Liquid-phase Mass Transfer Coefficient in Bubble Columns," *Ind. Eng. Chem. Process Des. Dev.* 13(1), pp. 84-91.

2. APHA-AWWA-WPCF, (1985), *Standard Methods for the Examination of Water and Wastewater*, 16th Edition, American Public Health Association, Washington, D. C., 1268 pp.

3. Arbuckle, W. B., (1983), " Estimating Activity Coefficients for Use in Calculating Environmental Parameters," *Environmental Science and Technology,* Vol. 17, 537.

4. ASCE Oxygen Transfer Standards Committee (1984), "A Standard for the Measurement of Oxygen Transfer in Clean Water," ISBN 0-87262-430-7, New York.

5. Atlas, E., Ronald Foster, and C. S. Giam (1982), "Air-sea Exchange of High Molecular Weight Organic Pollutants: Laboratory Studies," *Environmental Science and Technology,* Vol. 16, No. 5. 283.

6. Baillod, C.R., W.L. Paulson, J.J. McKeown, and H.J. Campbell,Jr. (1986), "Accuracy and Precision of Plant Scale and Shop Clean Water Oxygen Transfer Tests," *J. Water Poll. Cont. Fed.,* Vol. 58, No.4, 290-299.

7. Baillod, C.R., J. C. Crittenden, J.R. Mihelcic, T.N. Rogers, and L. Grady, (1990), "Transport and Fate of Toxics in Wastewater Treatment Facilities," WPCF Research Foundation Project 90-1, *J. Water Poll. Cont. Fed.,*

8. Barnhart, E.L. (1969), "Transfer of Oxygen in Aqueous Solutions," *J. San. Eng. Div., ASCE,* 95(SA3), pp. 645-661.

9. Blackburn, J.W., W.L. Troxler, K.N. Truong, R.P. Zink, S.C. Meckstroth, J.R. Florence, A. Groen, G.S. Sayler, R.W Beck, R.A. Minear, A. Breen, and O. Yagi (1985), "Organic Chemical Fate Prediction in Activated Sludge Processes," EPA-600/2-85/102 US EPA, Cincinnati, Ohio.

10. Boyle, W.C., P.M. Berthouex, and T.C. Rooney (1974), "Pitfalls in Parameter Estimation for Oxygen Transfer Data," *J. San. Eng. Div., ASCE,* 100(EE2), 391-408.

11. Boyle, W.C., E. Wong, and E.M. Aieta, R.A. Frank, J.J. Vasconcelos, and A.A. Dille (1989), "Air Emission Studies for Aeration Basins at the Los Angeles Glendale Water Reclamation Plant," James M. Montgomery, Pasadena, CA.

12. Brown, L.C. and C.R. Baillod (1982), "Modeling and Interpreting Oxygen

Transfer Data," *J. Env. Eng. Div., ASCE,* Vol.108, No.4, 607-628.

13. Calderbank, P.H., and M.B. Moo-Young (1961), "The Continuous Phase Heat and Mass Transfer Properties of Dispersions," *Chem. Eng. Sci.,* 16:39-54.

14. Chang, D.P.Y., E.D. Schroeder, and R.L. Corsi (1987), "Emissions of Volatile and Potentially Toxic Organic Compounds from Sewage Treatment Plants and Collection Systems," Submitted to California Air Resources Board.

15. Chapman, C.M., L.G. Gilbaro, and A.W. Nienow (1982), "A Dynamic Response Technique for the Estimation of Gas-liquid Mass Transfer Coefficients in a Stirred Vessel," *Chemical Engineering Science,* Vol. 37, No. 6, 891-896.

16. Clift, R., J.R. Grace, and M.E. Weber (1978), *Bubbles, Drops and Particles,* Academic Press, New York, 380 pp.

17. Coppock, P.D., and G.T. Meiklejohn (1951), "The Behavior of Gas Bubbles in Relation to Mass Transfer," *Trans. Instn. Chem. Engrs.,* 29:78-86.

18. Danckwerts, P.V. (1951), "Significance of Liquid-film Coefficients in Gas Absorption," *Ind. Eng. Chem.,* 43, pp.1460-1467.

19. Dilling, W.L. (1977), "Interphase Transport Process. II. Evaporation Rates of Chloromethanes, Ethanes, Ethylenes, Propanes, and Propylenes from Dilute Aqueous Solutions. Comparisons with theoretical predictions," *Environmental Science and Technology,* 11(4), 405-409.

20. Eckenfelder W.W. (1959), "Absorption of Oxygen from Air Bubbles in Water," *J. Sanit. Eng. Div., ASCE,* Vol. 85, No. SA4, pp. 89-98.

21. Eckenfelder W.W. and Ford D.L. (1967), " Engineering Aspects of Surface Aeration Design," Proc. 22nd Purdue Industrial Waste Conference, pp. 279-291.

22. Eckenfelder, W.W. and D.L. Ford (1968), "New Concepts in Oxygen Transfer and Aeration," Advances in Water Quality Improvements, Ed. by Gloyna, E.F. and W.W. Eckenfelder, University of Texas Press, 215-236.

23. Fair, J.R., A.J. Lambright, and J.W. Anderson (1962), "Heat Transfer and Gas Holdup in a Sparged Contactor," *Ind. Eng. Chem. Process Des. Dev.,* pp. 33-36.

24. Garner, F.H., and D. Hammerton (1954), "Circulation Inside Gas Bubbles," *Chem. Eng. Sci.,* 3(1), 1-11.

25. Goodgame, T.H., and T.K. Sherwood, (1954), "The Additivity of Resistances Between Phases, *"Chem. Eng. Sci.,* 3(2):37-42.

26. Grace, J.R., T. Wairegi, and T.H. Nguyen, (1976), " Shapes and Velocities of Single Drops and Bubbles Moving Freely through Immiscible Liquids," *Trans. Instn. Chem. Engrs.*, 54:167-173.

27. Gossett, James M. (1987), "Measurement of Henry's Law Constants for C1 and C2 Chlorinated Hydrocarbons," *Environmental Science and Technology*, Vol. 21, No.2, 202.

28. Habermann, W.L., and R.K. Morton (1956), "An Experimental Study of Bubbles Moving in Liquids," *Trans. ASCE*, pp. 227-250.

29. Hammerton, D. and F.H. Garner (1954), "Gas Absorption from Single Bubbles," *Trans. Instn. Chem. Engrs.*, 32:S18-S24.

30. Higbie, R. (1935), "The Rate of Absorption of a Pure Gas into a Still Liquid During Short Periods of Exposure," *Trans. AIChE*, Vol.31, 365-388.

31. Holland, F.A., and F.S. Chapman (1966), *Liquid Mixing and Processing in Stirred Tanks*, Reinhold Publishing Corporation, New York, NY.

32. Hwang, H.J. (1983), "Comprehensive Studies of Oxygen Transfer under Nonideal Conditions," A dissertation, University of California, Los Angeles.

33. Jackson, M.L. and G.W. Hoech, (1977), "A Comparison of Nine Aeration Devices in a 43-foot Deep Tank," A report to the Northwest Pulp and Paper Association.

34. Jackson, M.L. and C-C. Shen, (1978), "Aeration and Mixing in Deep Tank Fermentation Systems," *AIChE J.*, Vol. 24, No. 1, pp. 63-71.

35. Kavanaugh, M.C., and R.R. Trussell (1980), "Design of Aerator Towers to Strip Volatile Contaminants from Drinking Water, *"J. Amer. Water Works Assoc.*, Vol. 71, No.12, pp. 684-692.

36. Kincannon, D.F., A. Weinert, R. Padorr, and E.L. Stover (1983), "Predicting Treatability of Multiple Organic Priority Pollutant Wastewaters from Single-pollutant Treatability Studies," Proceedings 37th Industrial Waste Conf., May 1982, Purdue University, J. Bell, Ed., Ann Arbor Science, Ann Arbor, Michigan, 640-650.

37. Kincannon, D.F. and E.L. Stover (1983), "Determination of Activated Sludge Bio Kinetic Constants for Chemical and Plastic Industrial Wastewater," EPA-600/2-83-073A, US EPA, Cincinnati, Ohio.

38. King, H.R., (1955), "Mechanics of Oxygen Absorption in Spiral Flow Aeration Tanks: I. Derivation of Formulas," *Ser. Ind. Wastes*, Vol. 27, No. 8, pp. 894-908.

39. King, H.R., (1955), "Mechanics of Oxygen Absorption in Spiral Flow Aeration

Tanks: II. Experimental Works," *Ser. Ind. Wastes*, Vol. 27, No. 9, pp. 1007-1026.

40. Kishinevsky M.Kh. and Serebryansky V.T. (1956), "The Mechanism of Mass Transfer at the Gas-liquid Interface with Vigorous Stirring," *J. Appl. Chem.*, USSR, 29, 27.

41. Lalezary, S., M. Pirbazari, M.J. McGuire, S.W. Krasner, (1984), "Air Stripping of Taste and Odor Compounds from Water," *J. Am. Water Works Assoc.*, Vol. 76, 83.

42. Lewis, W.K. and W.G. Whitman (1924), "Principles of Gas Absorption," *Ind. Eng. Chem.*, 16, pp. 1215-1220.

43. Libra, J.A. (1991), "Volatilization of Organic Compounds in an Aerated Stirred Tank Reactor," A Dissertation, University of California, Los Angeles.

44. Lincoff, A.H. and J.M. Gossett (1984), "The Determination of Henry's Constant For Volatile Organics by Equilibrium Partitioning in Closed Systems," in *Gas Transfer at Water Surfaces*, W. Brutsaert and G.H. Jirka (eds.), D. Reidel Publishing Co., 17-25.

45. Liss, P.S., and P.G. Slater (1974), "Flux of Gases Across the Air-sea Interface," *Nature*, 247, pp. 181-184.

46. Lugg, G. A. (1968), "Diffusion Coefficients of Some Organic and Other Vapors in Air," *Anal. Chem.*, Vol. 40, No. 7, pp. 1072-1077.

47. Mackay, D., and A. W. Wolkoff, (1971), "Rate of Evaporation of Low-solubility Contaminants from Water Bodies to Atmosphere," *Environmental Science and Technology*, Vol. 7, No.7, pp. 611-614.

48. Mackay, D. and P.J. Leinonen, (1975), "Rate of Evaporation of Low-solubility Contaminants from Water Bodies to Atmosphere," *Environmental Science and Technology*, Vol. 9, No. 13, pp. 1179.

49. Mackay, D., W.Y. Shiu, and R.P. Sutherland (1979), "Determination of Air-water Henry's Law Constants for Hydrophobic Pollutants," *Environmental Science and Technology*, Vol. 13, No. 3,pp. 333-337.

50. Mackay, D. and W.Y. Shiu. (1981), "A Critical Review of Henry's Law Constants for Chemicals of Environmental Interest," *J. Phys. Chem. Ref. Data*, Vol. 10, No. 4, pp. 1175 - 1199.

51. Mackay D., and A.T.K. Yeun, (1983), " Mass Transfer Coefficient Correlations for Volatilization of Organic Solutes from Water," *Environmental Science and Technology*, Vol. 17, No.4.

52. Masutani, G.K. (1988), "Dynamic Surface Tension Effects on Oxygen

Transfer in Activated Sludge," A dissertation, University of California, Los Angeles.

53. Matter-Mueller, C., W.Gujer, and W. Giger (1981), "Transfer of Volatile Substances from Water to the Atmosphere," *Water Research,* Vol.15, 1271.

54. Metcalf and Eddy, Inc (1979), *Wastewater Engineering: Treatment, Disposal, Reuse,* 2nd Edition, McGraw-Hill Book Co., New York, N.Y., 920 pp.

55. Motarjemi, M., G.J. Jameson, (1978), "Mass Transfer from Small Bubbles - the Optimum Bubble Size for Aeration," *Chemical Engineering Science,* 33, pp.1415-1423.

56. Mueller, J.S. and H.D. Stensel (1990), "Biologically Enhanced Oxygen Transfer in the Activated Sludge Process," *J. Water Pollut. Cont. Fed.,* Vol.62, No.2, 193-203.

57. Mumford, R.L. and J.L. Schnoor, "Air Stripping of Volatile Organics in Water," Proceedings AWWA 1982 Annual Conference, Miami Beach, FL, 1982.

58. Munz, C. and P.V. Roberts (1984), "The Ratio of Gas Phase to Liquid Phase Mass Transfer Coefficients in Gas-liquid Contacting Processes," in Gas Transfer at Water Surfaces, W. Brutsaert and G.H. Jirka (eds.), D. Reidel Publishing Co., 35-45.

59. Munz, C., and P.V. Roberts, (1986), "Effects of Solute Concentration and Cosolvents on the Aqueous Activity Coefficient of Halogenated Hydrocarbons," *Environmental Science and Technology,* Vol. 20, 830.

60. Munz, C., and P.V. Roberts, (1987), "Air-Water Phase Equilibria of Volatile Organic Solutes," *Journal AWWA,* Vol. 79, 62.

61. Namkung, E. and Bruce E. Rittman, (1987), "Estimating VOC Missions from Publicly Owned Treatment Works," *J. Water Poll. Cont. Fed.,* Vol 59, No. 7, pp. 670.

62. Nicholson, B.C. (1984), "Henry's Law Constants for the Trichlomethanes: Effect of Water Composition and Temperature," *Environmental Science and Technology,* Vol. 18, 518.

63. Othmer, D.F., and M.S. Thakar (1953), "Correlating Diffusion Coefficients in Liquid," *Ind. Eng. Chem.,* Vol. 45, pp. 589-593.

64. Paulson, W.C., (1979), "Review of Test Procedures, In: Proceedings: Workshop Towards and Oxygen Transfer Standard," W.C. Boyle (Ed.), EPA-600/9-78-021, Municipal Environmental Research Laboratory, U.S. Environmental Protection Agency, Cincinnati, OH, 41-49.

65. Philichi, T.L. and M.K. Stenstrom (1989), "The Effects of Dissolved oxygen Probe Lag on Oxygen Transfer Parameter Estimation," *J. Water Pollut. Cont. Fed.*, Vol 61, No.1, 83-86.

66. Platford, R.F. (1977), "Thermodynamics of Miscible Liquid Mixtures of Carbon Tetrachloride, n-Octanol and Water at 20oC," *J. Chem. Soc., Faraday Trans. 1, Vol. 73, 267.*

67. Rathbun, R.E., W.S. Doyle, D.J. Shultz, and D.Y. Tai (1978), "Laboratory Studies of Gas Tracers for Reaeration," *J. Env. Eng. Div., ASCE,* Vol. 104, No.2, 215-229.

68. Rathbun, R.E. and D.Y. Tai (1982), "Volatilization of Organic Compounds from Streams," *J. Env. Eng. Div., ASCE,* Vol. 105, EE5, 953.

69. Rathbun, R.E., and Y. Tai Doreen (1986), "Gas-film Coefficients for the Volatilization of Ethylene Dibromide from Water," *Environmental Science and Technology,* Vol. 20, No. 9, pp. 949-952.

70. Redmon, D., W.C. Boyle, and L. Ewing (1983), "Oxygen Transfer Efficiency Measurements in Mixed Liquor using Off-gas Techniques," *J. Wat. Pollut. Cont. Fed.,* Vol. 55, No.11, 1338-1347.

71. Reid, R.C., J.M. Prausnitz, and T.K. Sherwood (1987), *The Properties of Gases and Liquids,* 4th Ed., McGraw-Hill Book. Co. New York, 688 pp.

72. Roberts, P.V., C. Munz, P. Daendliker, and C. Matter-Mueller (1982), "Volatilization of Organic Pollutants in Wastewater Treatment-Model Studies," EPA-600/S2-84-047, USEPA, Cincinnati, Ohio.

73. Roberts, P.V., and P.G. Daendliker (1983), "Mass Transfer of Volatile Organic Contaminants from Aqueous Solution to the Atmosphere During Surface Aeration," *Environmental Science Technology,* Vol. 17, No., 8, 1983, pp. 484-489.

74. Roberts, P.V., C. Munz, and P. Daendliker (1984a), "Modeling Volatile Organic Solute Removal by Surface and Bubble Aeration," *J. Wat. Pollut. Cont. Fed.,* Vol. 56, 157-163.

75. Roberts, P.V. (1984b), "Dependence of Oxygen Transfer Rate on Energy Dissipation during Surface Aeration and In Stream Flow," In *Gas Transfer at Water Surfaces,* D. Reidel Publishing Co., pp. 347-355.

76. Rushton, J.H., E.W. Costich, and H.J. Everett (1950), "Power Characteristics of Mixing Impellers," *Chem. Eng. Progress,* 46.

77. SAS User's Guide, (1982), *Statistical Analysis System,* SAS Institute Inc., Raleigh, North Carolina.

78. Schmidtke, N.W., H. Imre (1977), "Scale-up Methodology for Surface Aerated Reactors," *Prog. Wat. Tech.*, Vol. 9, pp. 477-493.

79. Sherwood, T.K., P.L. Pigford, and C.R. Wilke (1975), *Mass Transfer*, McGraw-Hill Book Company, New York, 677 pp.

80. Skelland, A.H.P. (1974), *Diffusional Mass Transfer*, John Wiley & Sons, New York, 510 pp.

81. Shinji Nagata (1975) *Mixing Principles and Applications*, John Wiley & Sons, New York.

82. Smith, J.H., D.C. Bomberger, and D.L. Haynes (1980), "Prediction of the Volatilization Rates of High-volatility Chemicals from Natural Water Bodies," *Environmental Science Technology*, Vol. 14, No., 11, pp. 1332-1337.

83. Smith, J.H., D.C. Bomberger, and D.L. Haynes (1981), "Volatilization Rates of Intermediate and Low Volatility Chemicals from Water," *Chemosphere*, Vol. 10, No.3, 281-289.

84. Smith, J.H., D. Mackay, and C.W.K. Ng (1983), "Volatilization of Pesticides from Water," *Residue Reviews*, Springer-Verlag, New York, Inc., Vol. 85, 73-88.

85. Stenstrom, M.K. and R.G. Gilbert (1981), "Review Paper: Effects of Alpha, Beta, and Theta Factor upon the Design, Specification and Operation of Aeration Systems," *Water Research*, Vol. 15, 643-654.

86. Stenstrom, M.K. (1988), "Nonlinear Regression Program for K_La Evaluation," Civil Engineering Department, UCLA.

87. Stenstrom, M.K. (1990), "Upgrading Existing Activated Sludge Treatment Plants With Fine Pore Aeration Systems," *Wat. Sci. Tech.*, Vol. 22, No.7/8, 245-251.

88. Tamir, A. and J. Merchuk, "Effect of Diffusivity on Gas-side Mass Transfer Coefficient," *Chem. Eng. Sci.*, Vol. 33, No. 9, pp. 1371-1374 (1978).

89. Tamir, A. and J. Merchuk, "Effect of Diffusivity on Gas-side Mass Transfer Coefficient," *Chem. Eng. Sci.*, Vol. 34, No. 8, pp. 1077 (1979).

90. Truong, K.N., and J.W. Blackburn (1984), "The Stripping of Organic Chemicals in Biological Treatment Processes," *Environ. Prog.*, Vol. 3, No. 3, 143-152.

91. Uhl, V.W., and J.a.V. Essen (1987), *Scale-up of Fluid Mixing Equipment*, Scale-up and Mixing, New York, American Institute of Chemical Engineers, 267 pp.

92. US Environmental Protection Agency (1982), "Fate of Priority Pollutants in Publicly Owned Treatment Works, "Vol. 1, EPA-440/1-82/303, US EPA, Office of Water Regulations and Standards, Washington, D.C.

93. Verschueren, K. (1977), *Handbook of Environmental Data on Organic Chemicals,* Van Nostrand Reinhold Co., New York, 699 pp.

94. Viessman, W., Jr., J.W. Knapp, G.L. Lewis, T.E. Harbaugh (1977), *Introduction to Hydrology,* Harper & Row, Publishers, 704 pp.

95. Vincent, V. (1986), "Review of Evaporation of Solutes from Water," California Air Resources Board , 23 pp.

96. Wilke, C.R., and P.C. Chang, (1955), "Correlation of Diffusion Coefficients in Dilute Solutions," *AIChE. J.,* Vol. 1, pp. 264-270.

97. Wilke, C.R., and C.Y. Lee (1955), "Estimation of Diffusion Coefficients for Gases and Vapors," *Ind. Eng. Chem.,* Vol. 47, No. 6, pp. 1253-1257.

98. Yadav, G.D. and M.M. Sharma (1979), "Effect of Diffusivity on True Gas-side Mass Transfer Coefficient in a Model Stirred Contactor with a Plane Liquid Interface," *Chemical Engineering Science,* 34, 1423.

99. Yurteri, C., David F. Ryan, John J. Callow, Mirat D. Gurol (1987), " The Effect of Chemical Composition of Water on Henry's Law Constant," *J. Water Poll. Cont. Fed.,* Vol. 59, No. 11, pp. 950-956.

Appendix A

Derivation of Ψ_M for VOCs

Appendix A: Derivation of Ψ_M for VOCs:

The general mathematical expression for the Two-Resistance model is as follows:

$$K_{LVOC} = \frac{1}{\frac{1}{k_{LVOC}} + \frac{1}{Hc\, k_{GVOC}}} \qquad \text{(A-1)}$$

where

K_{LVOC} = Overall liquid–film mass transfer coefficient [time $^{-1}$]

k_{LVOC}, k_{GVOC} = local liquid–film and gas -film mass transfer coefficients, respectively [time $^{-1}$]

Hc = Henry's law constant [dimensionless]

The fraction of liquid-film resistance to total resistance was previously derived as equation (13), repeated here:

$$\frac{R_L}{R_T} = \frac{R_L}{R_L+R_G} = \frac{1}{1+\frac{R_G}{R_L}} = \frac{1}{1+\frac{1}{\frac{k_G}{Hc\, k_L}}} \qquad \text{(A-2)}$$

Multiplication of both sides of equation (A-1) by $\frac{1}{k_{LVOC}}$ gives:

$$\frac{K_{LVOC}}{k_{LVOC}} = \frac{1}{1+\frac{k_{LVOC}}{Hc\, k_{GVOC}}} = \frac{R_L}{R_T} \qquad \text{(A-3)}$$

Previously studies was defined the proportional relationship of **local** VOCs and oxygen mass transfer coefficients as Ψ:

$$\Psi = \frac{k_{LVOC}}{k_{LO2}} = \left(\frac{D_{LVOC}}{D_{LO2}}\right)^n \qquad \text{(A-4)}$$

where

Ψ = local mass-transfer coefficient proportionality [dimensionless]

D_{LVOC}, D_{LO2} = liquid diffusivilities for VOC and O_2 [L^2/time]

The proportional relationship of **overall** VOCs and oxygen mass transfer coefficients can be expressed as Ψ_M:

$$\Psi_M = \frac{K_{LVOC}}{K_{LO2}} \qquad \text{(A-5)}$$

Because $k_{LO_2} \approx K_{LO_2}$, then

$$\Psi_M = \frac{K_{LVOC}}{k_{LO2}} \qquad \text{(A-6)}$$

Multiplying the numerator and denominator into equation (A-6) by k_{LVOC} gives

$$\Psi_M = \frac{k_{LVOC}}{k_{LO_2}} \frac{K_{LVOC}}{k_{LVOC}} \qquad \text{(A-7)}$$

Substituting equation (A-3) and (A-4) into equation (A-7) results in:

$$\Psi_M = \left(\frac{D_{LVOC}}{D_{LO2}}\right)^n \frac{R_L}{R_T} = \Psi \frac{R_L}{R_T} \qquad \text{(A-8)}$$

Appendix B

SAS NLIN Procedure and Typical Output

Appendix B

```
1          SAS(R) LOG    OS SAS 5.18              MVS/XA JOB IGPCCHU1 STEP GO

NOTE: COPYRIGHT (C) 1984,1988 SAS INSTITUTE INC., CARY, N.C.  27512, U.S.A.
NOTE: THE JOB IGPCCHU1 HAS BEEN RUN UNDER RELEASE 5.18 OF SAS AT THE UNIVERSITY OF
      CALIFORNIA, LOS ANGELES (01274003).
NOTE: SAS OPTIONS SPECIFIED ARE:
      SORT=25

1           DATA A B;
2           INFILE R375AREA;
3           INPUT DL DG HC KL;
4           ID = 1;
5           IF _N_=1 THEN OUTPUT A; ELSE OUTPUT B;


NOTE: INFILE R375AREA IS:
      DSNAME=IGPCCHU.R375AREA,
      UNIT=DISK,VOL=SER=DATA80,DISP=SHR,
      DCB=(BLKSIZE=6160,LRECL=80,RECFM=FB)

NOTE: 21 LINES WERE READ FROM INFILE R375AREA.
NOTE: DATA SET WORK.A HAS 1 OBSERVATIONS AND 5 VARIABLES. 1066 OBS/TRK.
NOTE: DATA SET WORK.B HAS 20 OBSERVATIONS AND 5 VARIABLES. 1066 OBS/TRK.
NOTE: THE DATA STATEMENT USED 0.04 SECONDS AND 808K.

6           DATA A; SET A; RENAME DL=DLREF DG=DGREF HC=HCREF KL=KLREF;

NOTE: DATA SET WORK.A HAS 1 OBSERVATIONS AND 5 VARIABLES. 1066 OBS/TRK.
N   ': THE DATA STATEMENT USED 0.02 SECONDS AND 748K.

7           DATA C; MERGE B A; BY ID;
8           DLIR = DL/DLREF; DGIR = DG/DGREF;

NOTE: DATA SET WORK.C HAS 20 OBSERVATIONS AND 11 VARIABLES. 510 OBS/TRK.
NOTE: THE DATA STATEMENT USED 0.02 SECONDS AND 796K.

9           DATA D; SET C; X=1/KL; Y=1/DLIR; Z=1/DGIR; W=1/HC;

NOTE: DATA SET WORK.D HAS 20 OBSERVATIONS AND 15 VARIABLES. 378 OBS/TRK.
NOTE: THE DATA STATEMENT USED 0.02 SECONDS AND 748K.

10          PROC NLIN BEST=50 PLOT;
11                    PARMS A = 0.42 TO 0.48 BY 0.01,
12                          B = 0.0075 TO 0.0085 BY 0.0001,
13                          MN = 0.4 TO 0.9 BY 0.05;
14                   MODEL X = A*Y**MN + B*W*Z**MN;
15                     DER.A = Y**MN;
16                     DER.B = W*Z**MN;
17                     DER.MN = LOG(MN)*(A*Y**MN + B*W*Z**MN);
18                     OUTPUT OUT=S5A R=YR PARMS=A B MN;
NOTE: THE DATA SET WORK.S5A HAS 20 OBSERVATIONS AND 19 VARIABLES. 300 OBS/TRK.
NOTE: THE PROCEDURE NLIN USED 4.58 SECONDS AND 1148K AND PRINTED PAGES 1 TO 3.

19          DATA S5A6; SET S5A;
20          IA = 1/A;  IB = 1/B;
23          RUN;

NOTE: SAS INSTITUTE INC.
      SAS CIRCLE
      PO BOX 8000
      CARY, N.C. 27512-8000
```

Appendix B

SAS

NON-LINEAR LEAST SQUARES GRID SEARCH DEPENDENT VARIABLE X

A	B	MN	RESIDUAL SS
0.48	0.0082	0.50	0.0682104269587
0.48	0.0083	0.50	0.0682665102272
0.48	0.0081	0.50	0.0684097291080
0.48	0.0084	0.50	0.0685779789136
0.48	0.0080	0.50	0.0688644166751
0.48	0.0085	0.50	0.0691448330177
0.48	0.0079	0.50	0.0695744896600
0.48	0.0078	0.50	0.0705399480627
0.48	0.0077	0.50	0.0717607918832
0.46	0.0077	0.55	0.0726557054701
0.46	0.0078	0.55	0.0726783347238
0.46	0.0076	0.55	0.0729167454650
0.46	0.0079	0.55	0.0729846332260
0.47	0.0085	0.50	0.0730692010522
0.47	0.0075	0.55	0.0732272569719
0.48	0.0076	0.50	0.0732370211215
0.46	0.0075	0.55	0.0734614547085
0.46	0.0080	0.55	0.0735746009769
0.47	0.0084	0.50	0.0736756366625
0.47	0.0076	0.55	0.0739757465450
0.46	0.0081	0.55	0.0744482379763
0.47	0.0083	0.50	0.0745374576906
0.48	0.0075	0.50	0.0749686357777
0.47	0.0077	0.55	0.0750079053667
0.46	0.0082	0.55	0.0756055442243
0.47	0.0082	0.50	0.0756546641365
0.47	0.0078	0.55	0.0763237334370
0.47	0.0081	0.50	0.0770272560002
0.46	0.0083	0.55	0.0770465197209
0.45	0.0082	0.55	0.0773220030379
0.45	0.0081	0.55	0.0774578956066
0.45	0.0083	0.55	0.0774697797179
0.45	0.0080	0.55	0.0778774574238
0.45	0.0084	0.55	0.0779012256465
0.47	0.0079	0.55	0.0779232307559
0.45	0.0079	0.55	0.0785806884895
0.45	0.0085	0.55	0.0786163408236
0.47	0.0080	0.50	0.0786552332817

SAS

NON-LINEAR LEAST SQUARES SUMMARY STATISTICS DEPENDENT VARIABLE X

SOURCE	DF	SUM OF SQUARES	MEAN SQUARE
REGRESSION	2	16.715459749	8.357729875
RESIDUAL	18	0.067580940	0.003754497
UNCORRECTED TOTAL	20	16.783040689	
(CORRECTED TOTAL)	19	0.496126484	

PARAMETER	ESTIMATE	ASYMPTOTIC STD. ERROR	ASYMPTOTIC 95 % CONFIDENCE INTERVAL LOWER	UPPER
A	0.4853987344	0.01329124083	0.45747505810	0.51332241068
B	0.0079800115	0.00081663273	0.00626434116	0.00969568187
MN	0.5000000000	0.00000000000	0.50000000000	0.50000000000

Appendix C

Calculations of Gas and Liquid Diffusivity

Table C-1. Liquid molar volumes at the normal boiling point

compounds	B.P.	M.W.	Vc	Vb [cm3/mole] T&C	Schroeder	Le Bas	Expt.# Values
O2		32.00	73.4	25.7	25.6	25.6	27.90
12DCE	47.50	96.94	225.5	82.8	84.0	86.0	
PCE	121.00	165.83	290.0	107.7	119.0	128.0	
CT	76.50	153.80	276.0	103.0	105.0	113.2	102.00
111TCA	74.10	133.41	283.0	105.8	108.5	114.5	
TCE	87.00	131.39	256.0	95.2	101.5	107.1	
BZ	80.00	78.11	259.0	96.4	84.0	111.0	
EBZ	136.00	106.20	374.0	141.6	126.0	155.4	
TLN	110.00	92.13	316.0	118.7	105.0	133.2	
MXY	139.00	106.16	376.0	142.4	126.0	155.4	
OXY	144.40	106.17	369.0	139.7	126.0	155.4	
CBZ	132.00	112.60	308.0	115.6	101.5	131.9	
CLF	61.70	119.40	239.0	88.6	87.0	92.3	
13DCB	173.00	147.00	359.0	135.7	119.0	152.8	
12DCB	179.00	147.00	360.0	136.1	119.0	152.8	
14DCB	174.00	147.00	372.0	140.9	119.0	152.8	
BBZ	156.00	157.02	324.0	121.9	108.5	134.3	
BF	149.50	252.80	272.0	101.5	108.5	99.5	
NAPH	217.90	128.20	410.0	156.0	126.0	177.6	
EDB	131.60	187.88	252.0	93.7	91.0	91.0	
1122TCA	146.20	167.90	332.0	125.0	140.0	135.4	

Notes: B. P. = boiling point (C); T + C = Tyn and Calus vorrelation;

Vc = critical point [cm3/mole], M.W. =molecular weight, [g/mole]

Expt.#=experimental

Table C-2. Infinite dilution diffusion coefficients in water
(Wilke-Change Method)

	DL x 100,000 [cm/s] at 20 C							
	Y = 2.60 Vb from				Y = 2.26 Vb from			
Compounds	T&C	Schroeder	Le Bas	Expt*	T&C	Schroeder	Le Bas	Expt*
O2	2.11	2.12	2.12	2.01	1.97	1.98	1.98	1.88
12DCE	1.05	1.04	1.02		0.98	0.97	0.96	
PCE	0.89	0.84	0.81		0.83	0.79	0.75	
CCl4	0.92	0.91	0.87	0.92	0.86	0.85	0.81	0.86
111TCA	0.90	0.89	0.86		0.84	0.83	0.80	
TCE	0.96	0.93	0.90		0.90	0.86	0.84	
BZ	0.96	1.04	0.88		0.89	0.97	0.82	
EBZ	0.76	0.81	0.72		0.71	0.76	0.67	
TLN	0.84	0.91	0.79		0.79	0.85	0.73	
MXY	0.76	0.81	0.72		0.71	0.76	0.67	
OXY	0.77	0.81	0.72		0.71	0.76	0.67	
CBZ	0.86	0.93	0.79		0.80	0.86	0.74	
CLF	1.01	1.02	0.98		0.94	0.95	0.92	
13DCB	0.78	0.84	0.73		0.73	0.79	0.68	
12DCB	0.78	0.84	0.73		0.73	0.79	0.68	
14DCB	0.76	0.84	0.73		0.71	0.79	0.68	
BBZ	0.83	0.89	0.78		0.77	0.83	0.73	
BF	0.93	0.89	0.94		0.87	0.83	0.88	
NAPH	0.72	0.81	0.66		0.67	0.76	0.62	
EDB	0.97	0.99	0.99		0.91	0.92	0.92	
1122TCA	0.82	0.76	0.78		0.76	0.71	0.73	

Note: Expt.* = experimental values

Table C-3. Infinite gas difusivities for twenty VOCs and oxygen

Compounds	DG x 100 [cm2/sec]		
	T&C	Vb from Schroeder	Le Bas
O2	21.315	21.344	21.344
12DCE	9.447	9.392	9.306
PCE	7.770	7.461	7.240
CCl4	8.158	8.095	7.852
111TCA	8.176	8.091	7.916
TCE	8.475	8.260	8.083
BZ	8.946	9.446	8.450
EBZ	7.151	7.509	6.877
TLN	7.923	8.330	7.555
MXY	7.123	7.497	6.866
OXY	7.162	7.476	6.847
CBZ	7.752	8.171	7.340
CLF	8.928	8.992	8.784
13DCB	6.941	7.329	6.603
12DCB	6.912	7.307	6.583
14DCB	6.830	7.325	6.600
BBZ	7.283	7.637	6.995
BF	7.650	7.445	7.710
NAPH	6.480	7.087	6.130
EDB	8.105	8.198	8.198
1122TCA	7.208	6.876	6.973

Appendix D

Correlation of mass transfer coefficient to specific power input in surface aeration

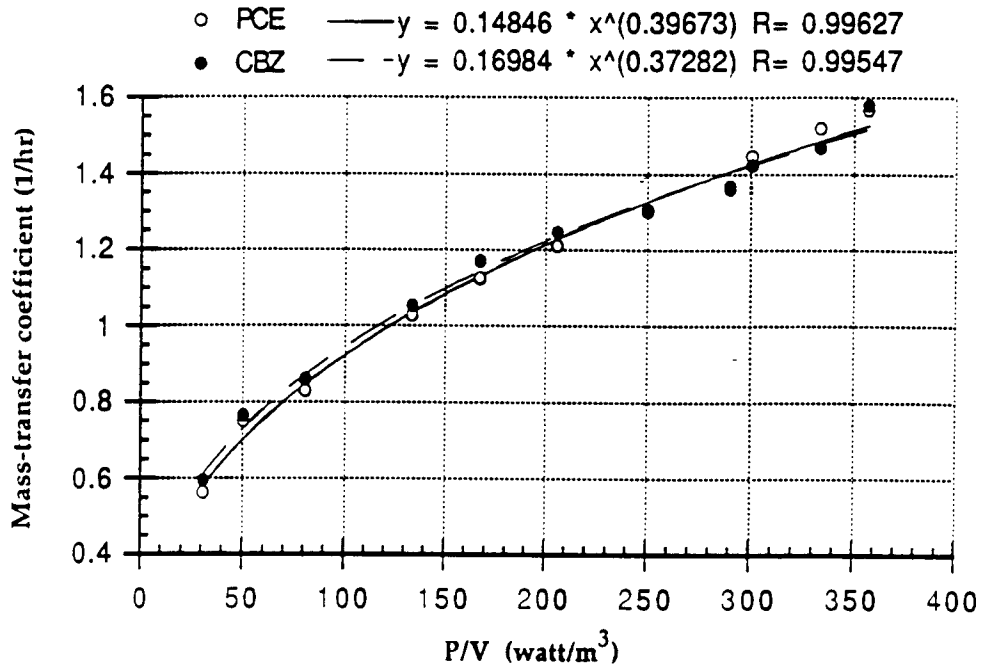

Figure D1. Correlation of mass transfer coefficient to specific power input (PCE,CBZ)

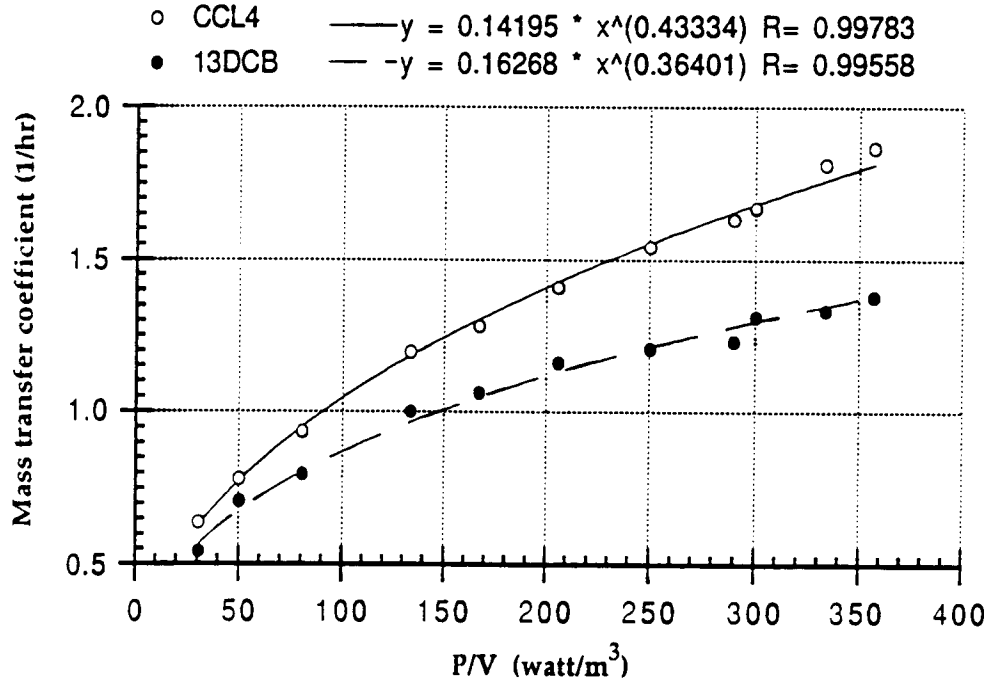

Figure D2. Correlation of mass transfer coefficient to specific power input (CT, 13DCB)

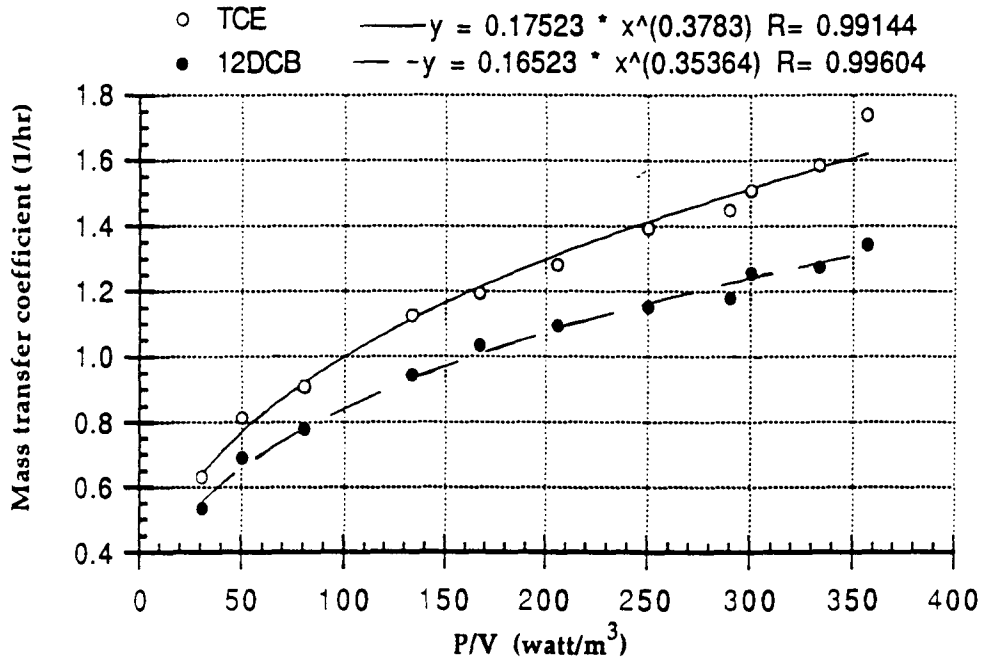

Figure D3. Correlation of mass transfer coefficient to specific power input (TCE,12DCB)

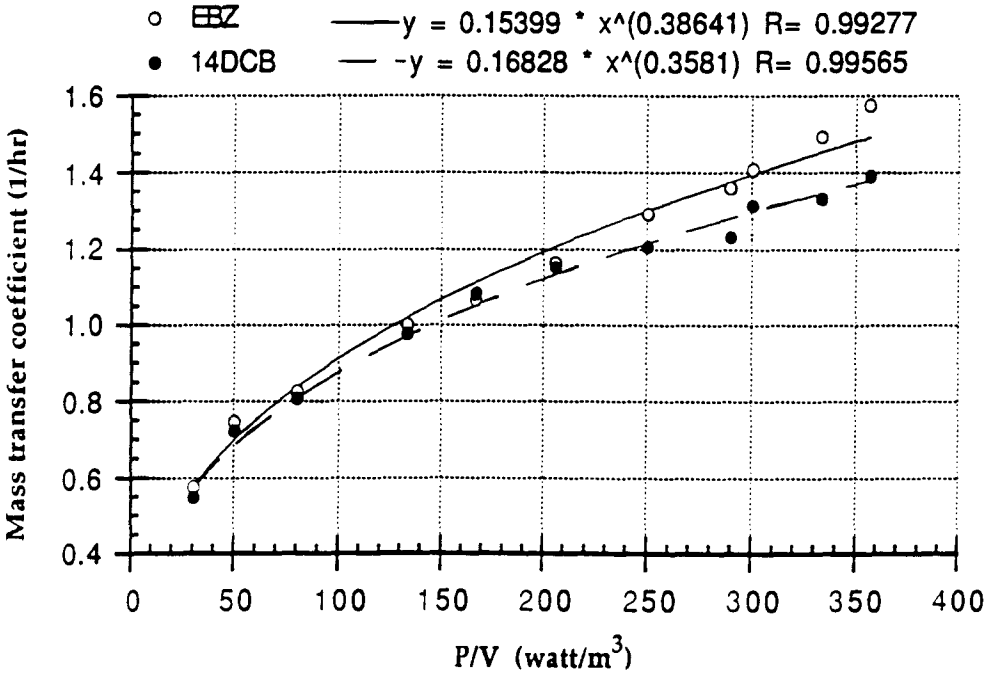

Figure D4. Correlation of mass transfer coeffiicient to specific power input (EBZ, 14DCB)

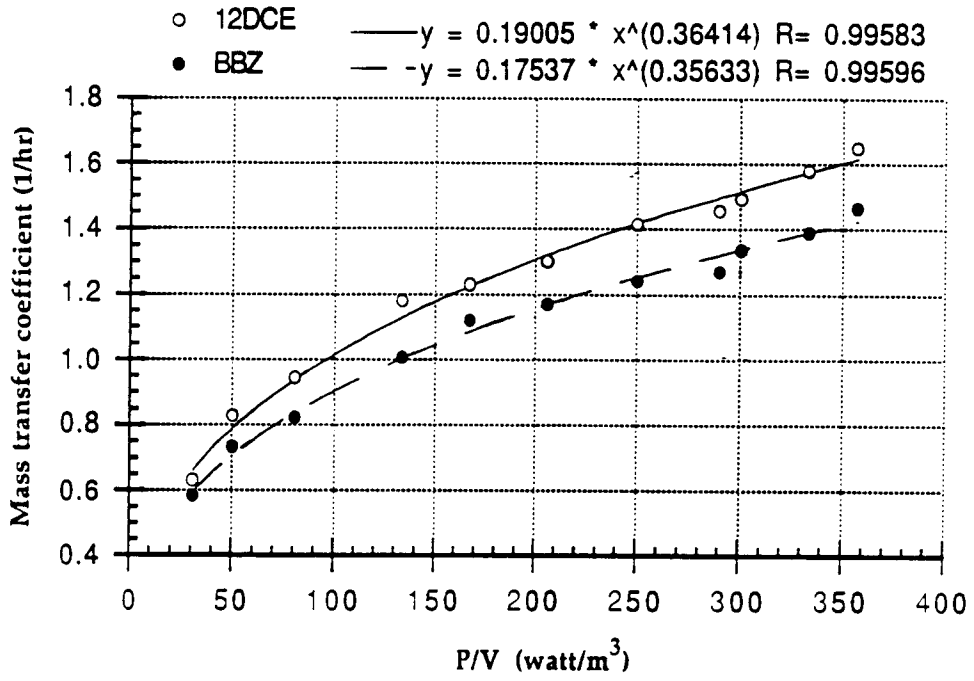

Figure D5. Correlation of mass transfer coefficient to specific power input (12DCE, BBZ)

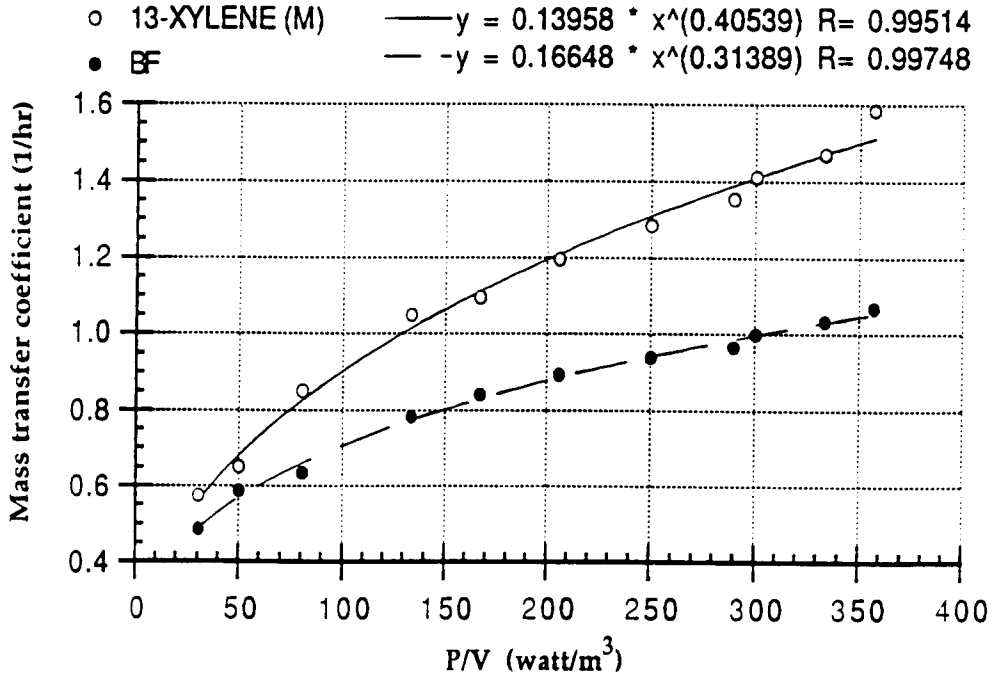

Figure D6. Correlation of mass transfer coefficient to specific power input (MXY, BF)

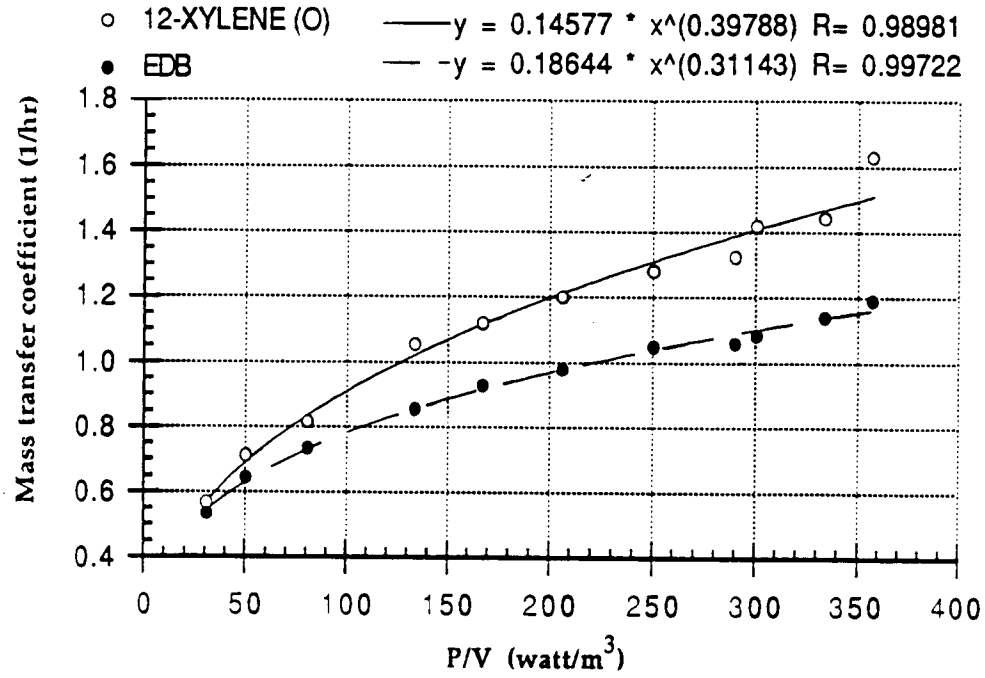

Figure D7. Correlation of mass transfer coefficient to specific power input (OXY, EDB)

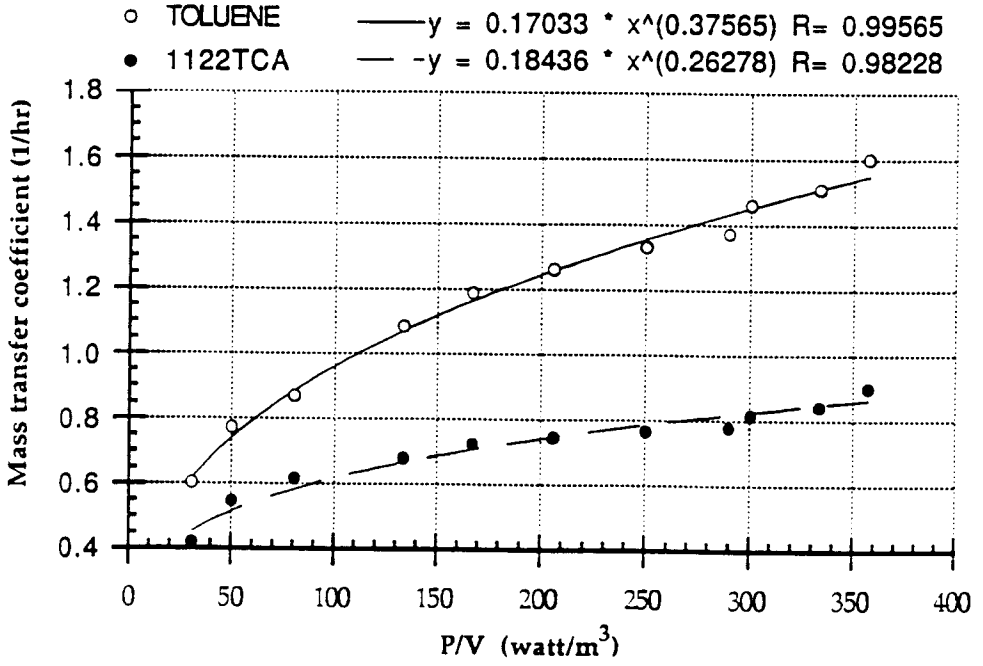

Figure D8. Correlation of mass transfer coefficient to specific power input (TLN, 1122TCA)

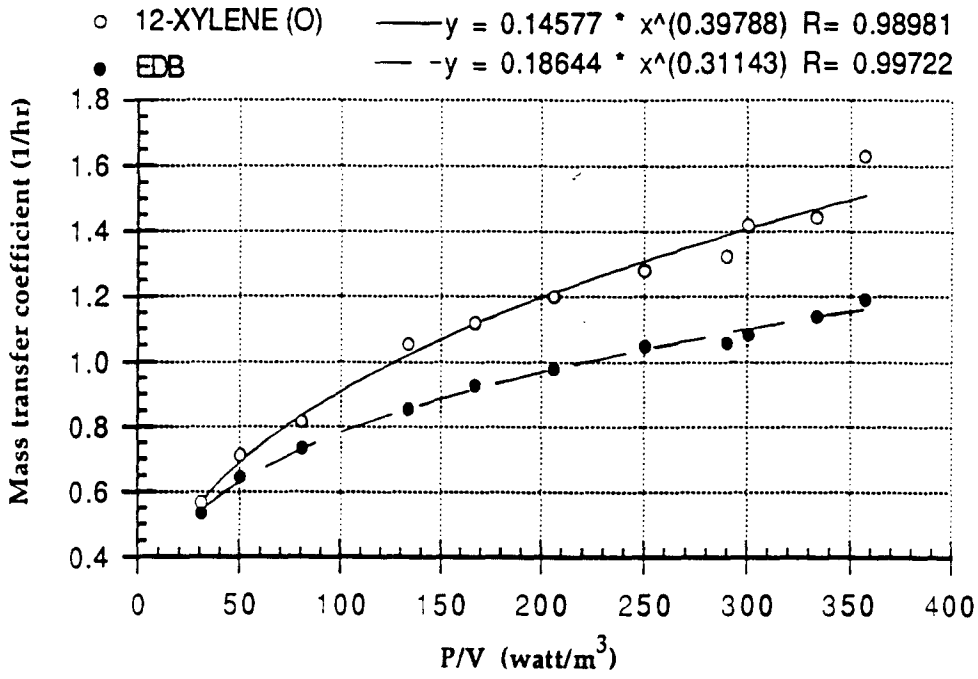

Figure D7. Correlation of mass transfer coefficient to specific power input (OXY, EDB)

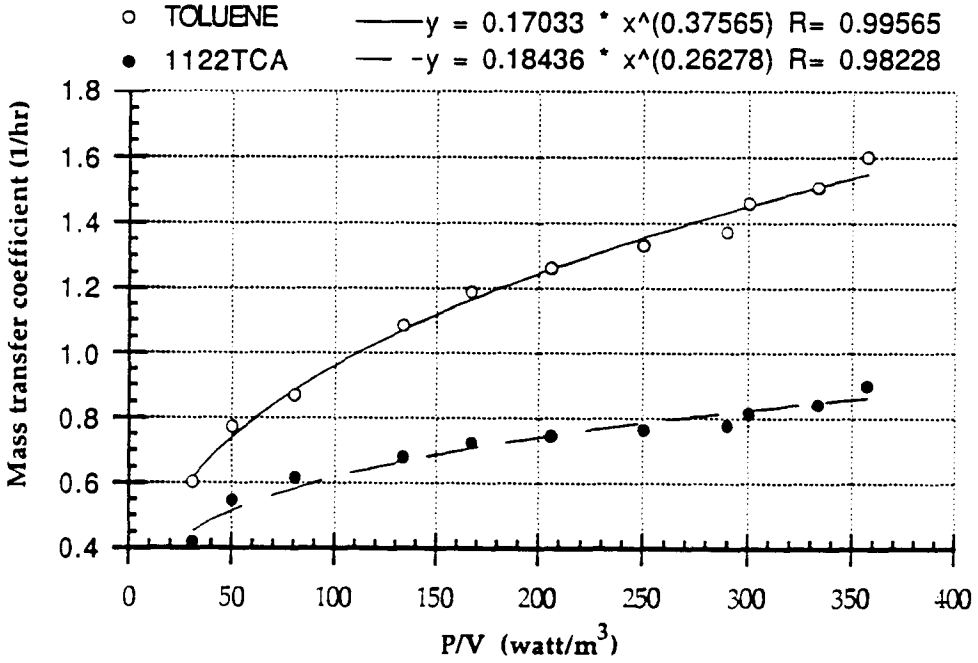

Figure D8. Correlation of mass transfer coefficient to specific power input (TLN, 1122TCA)

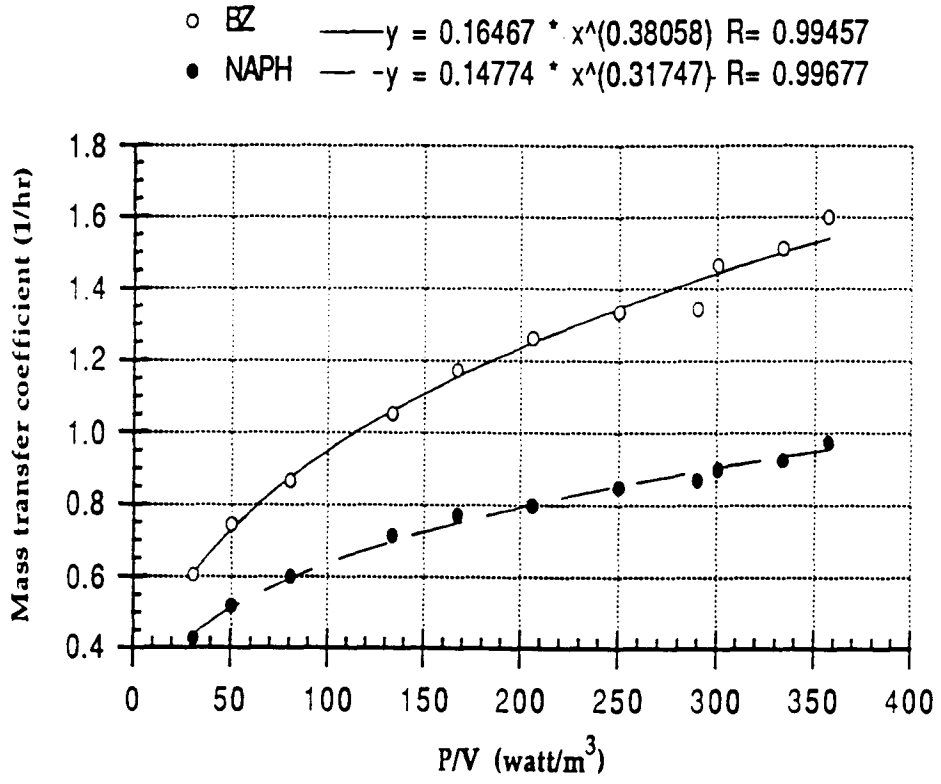

Figure D9. Correlation of mass transfer coefficient to specific power input (BZ, NAPH)

Appendix E

Correlation of mass transfer coefficient to velocity gradient in surface aeration

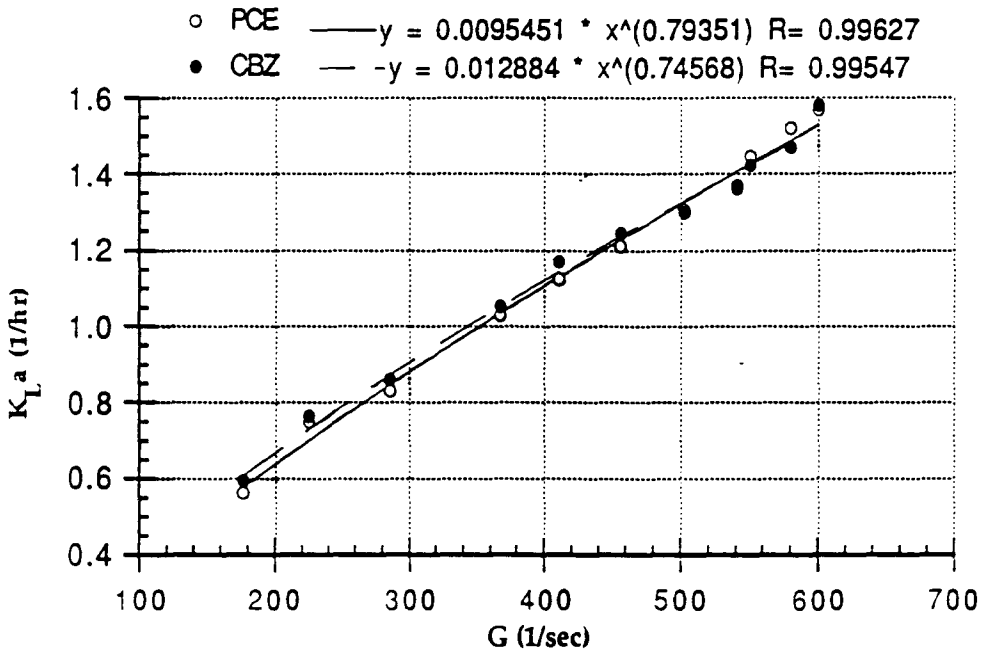

Figure E1. Correlation of mass transfer coefficient to specific power input in surface aeration (PCE, CBZ)

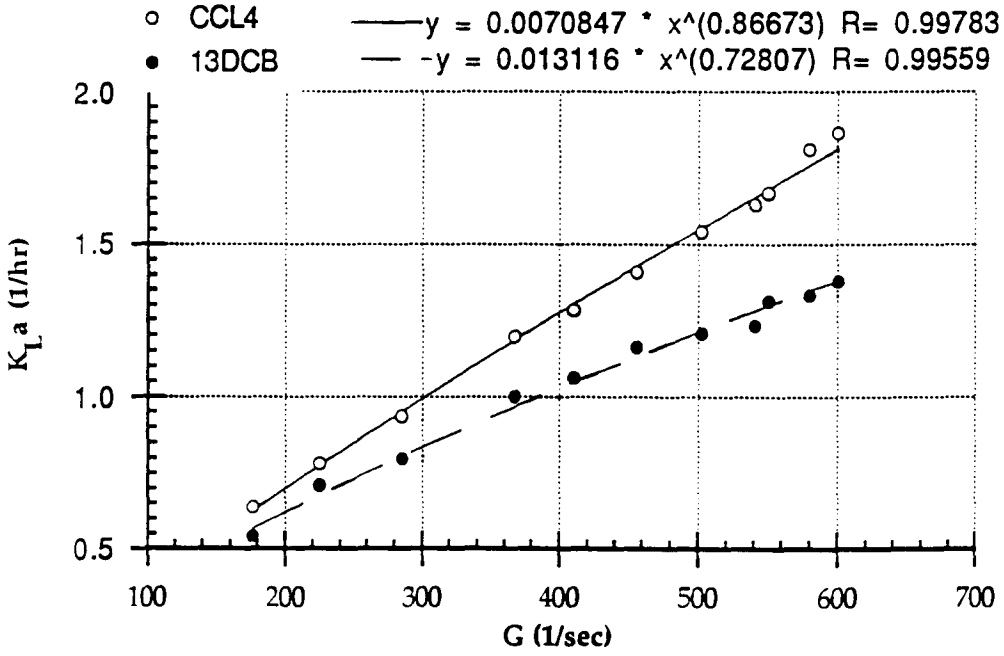

Figure E2. Correlation of mass transfer coefficient to velocity gradient in surface aeration (CT, 13DCB)

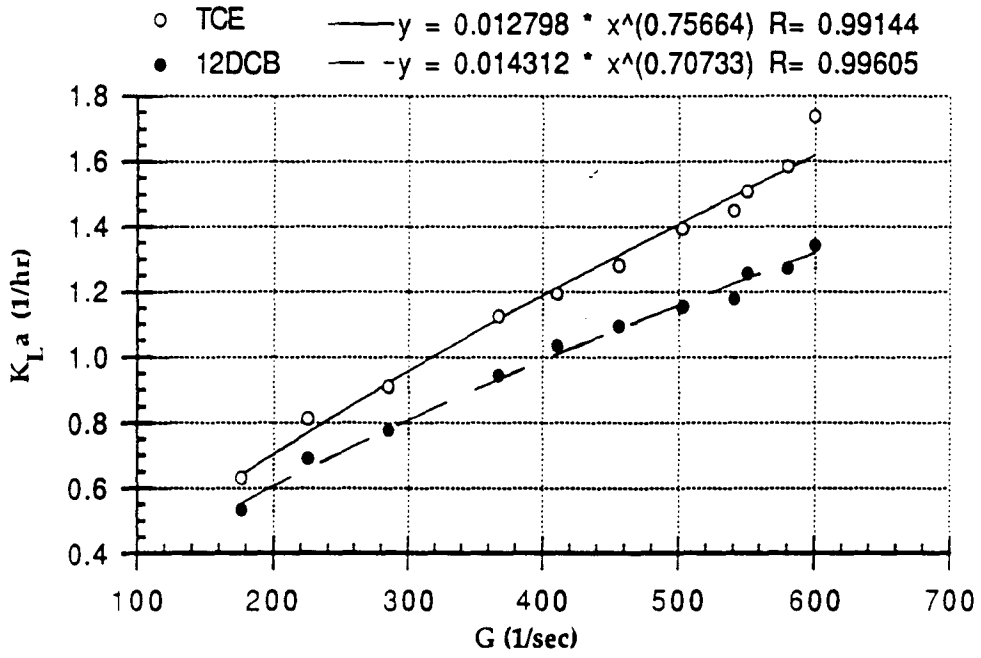

Figure E3. Correlation of mass transfer coefficient to velocity gradient in surface aeration (TCE, 12DCB)

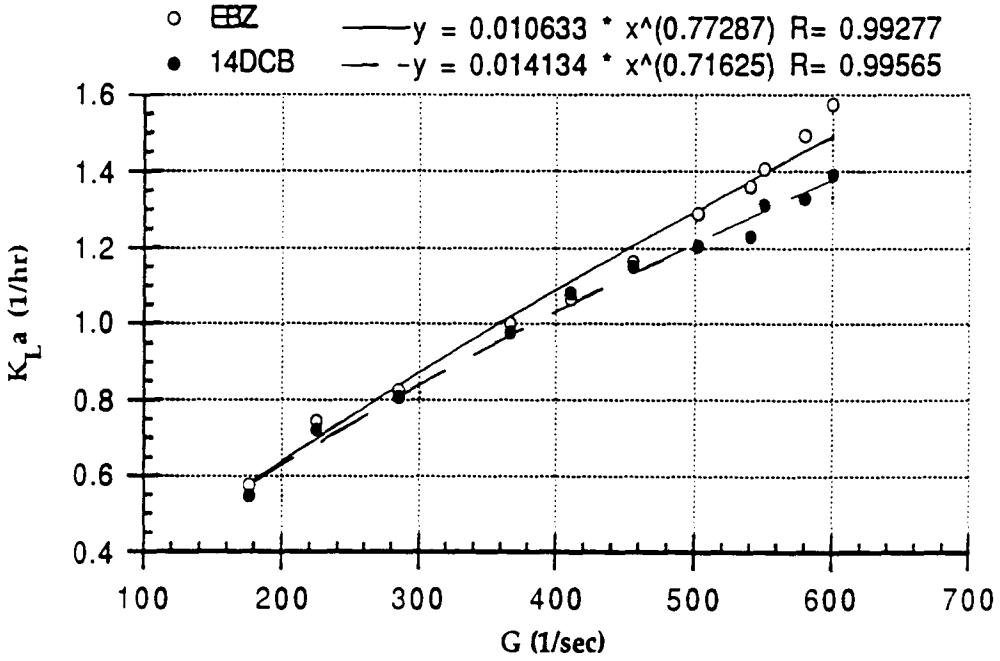

Figure E4. Correlation of mass transfer coefficient to velocity gradient in surface aeration (EBZ,13DCB)

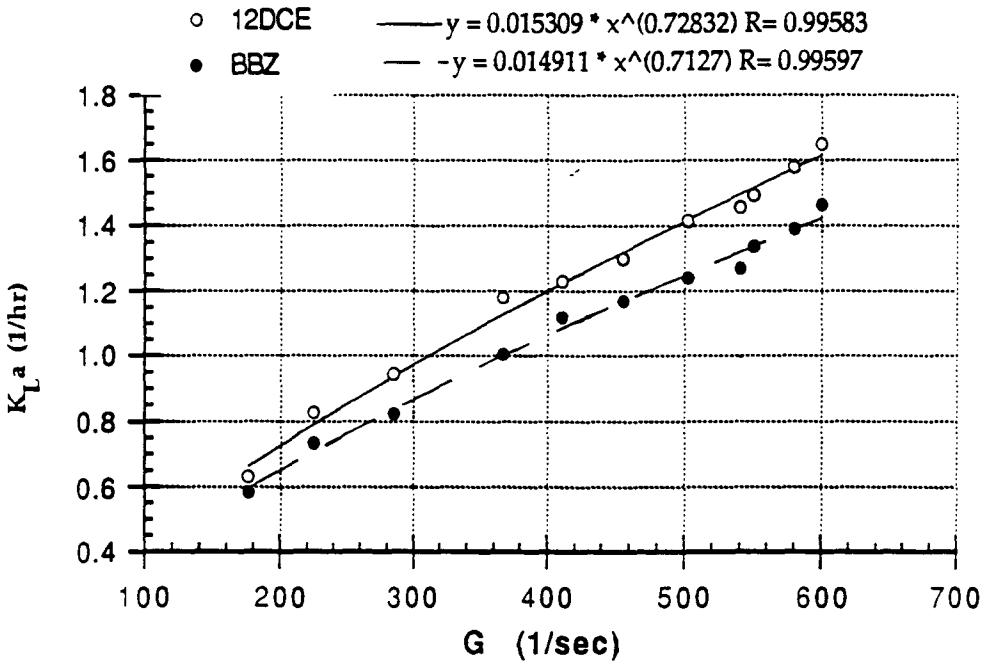

Figure E5. Correlation of mass transfer coefficient to velocity gradient in surface aeration (12DCE,BBZ)

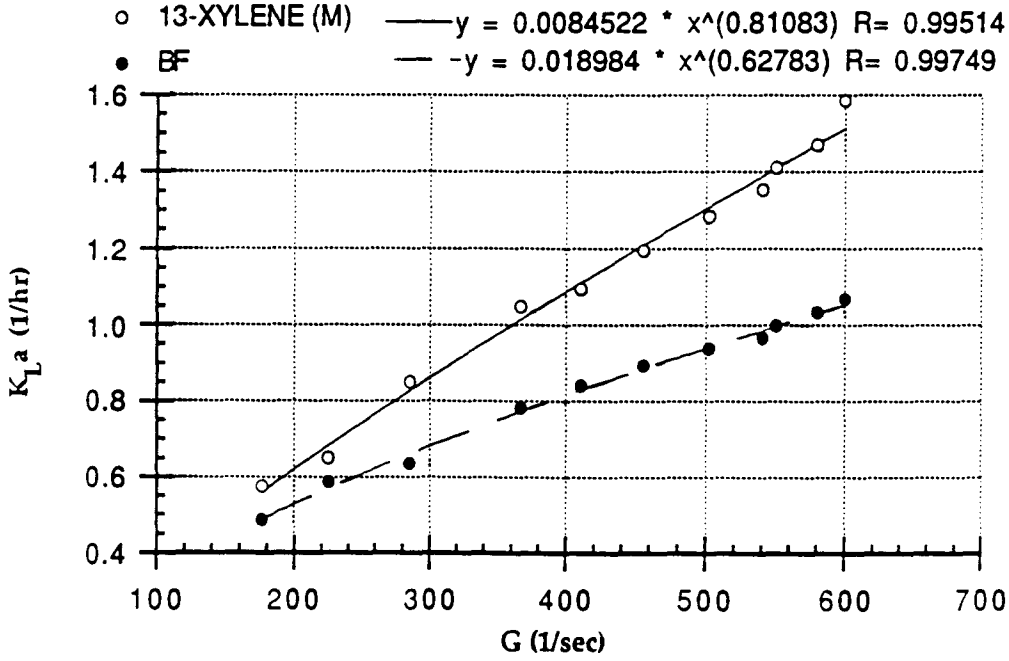

Figure E6. Correlation of mass transfer coefficient to velocity gradient in surface aeration (MXY,BF)

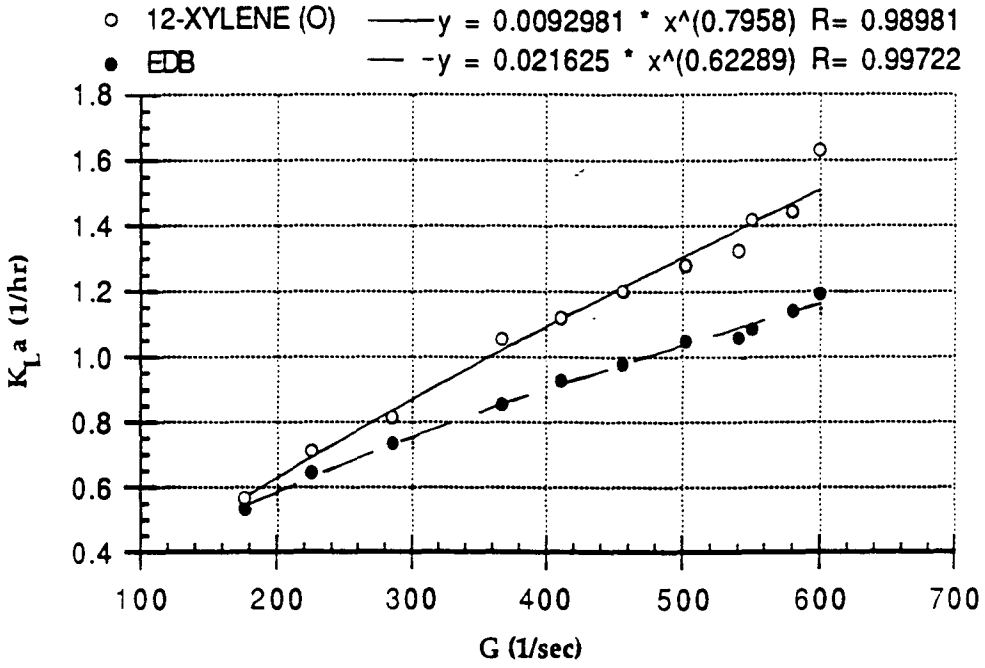

Figure E7. Correlation of mass transfer coefficient to velocity gradient in surface aeration (OXY,EDB)

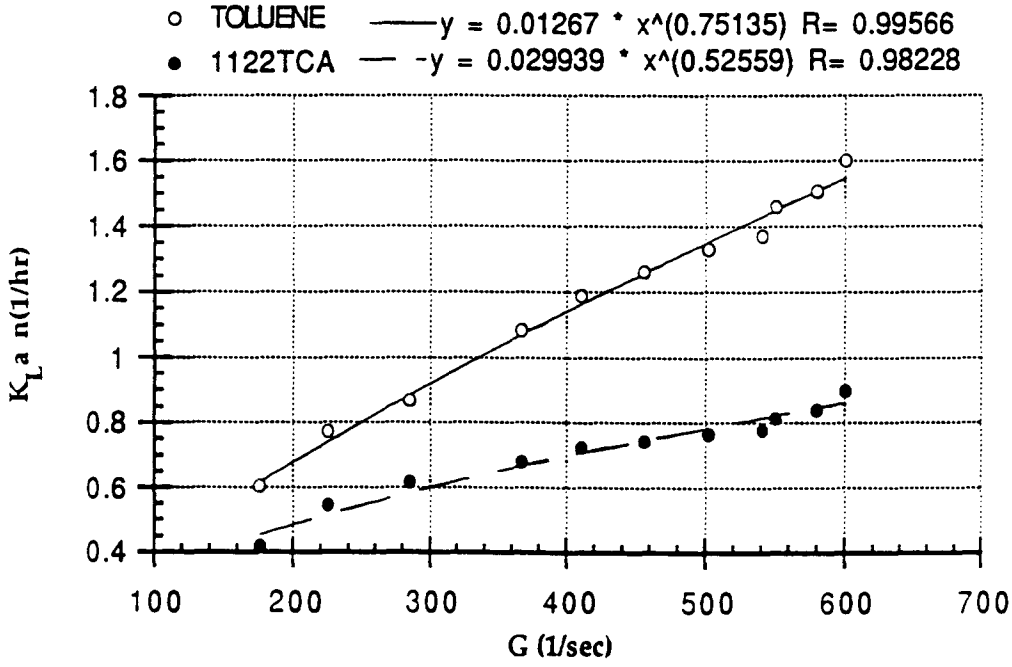

Figure E8. Correlation of mass transfer coefficient to velocity gradient in surface aeration (TLN,1122TCA)

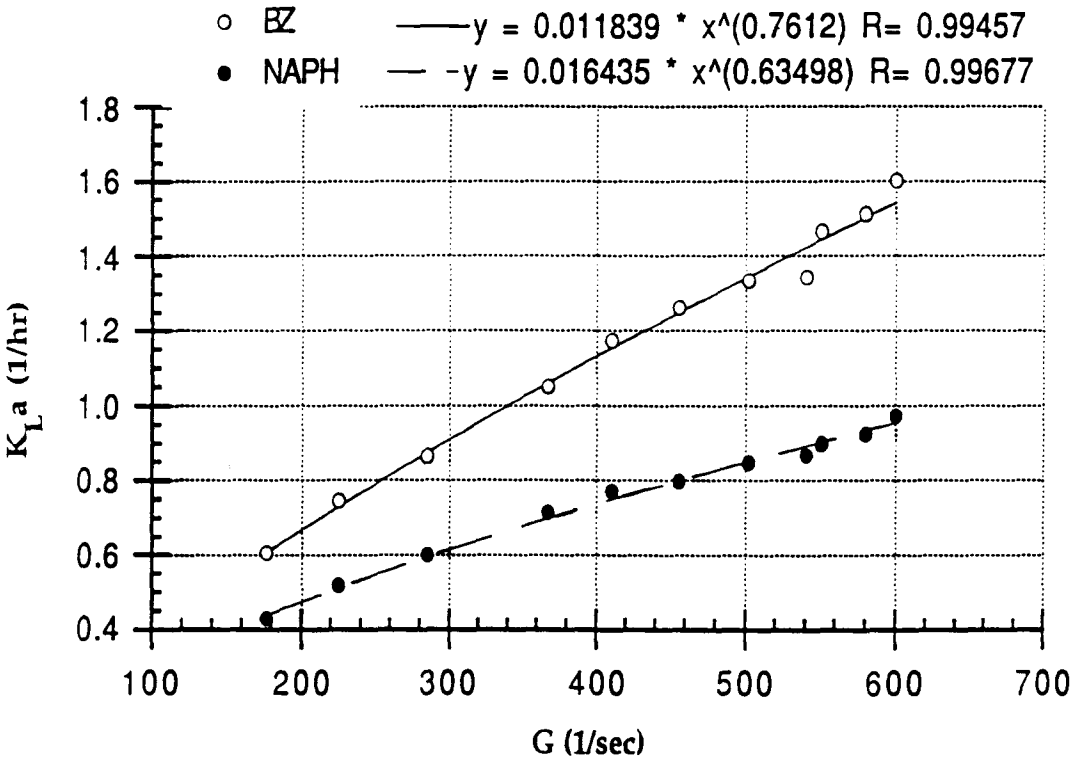

Figure E9. Correlation of mass transfer coefficient to velocity gradient in surface aeration (BZ,NAPH)

Appendix F

Comparison between estimated and measured mass transfer coefficient in surface aeration

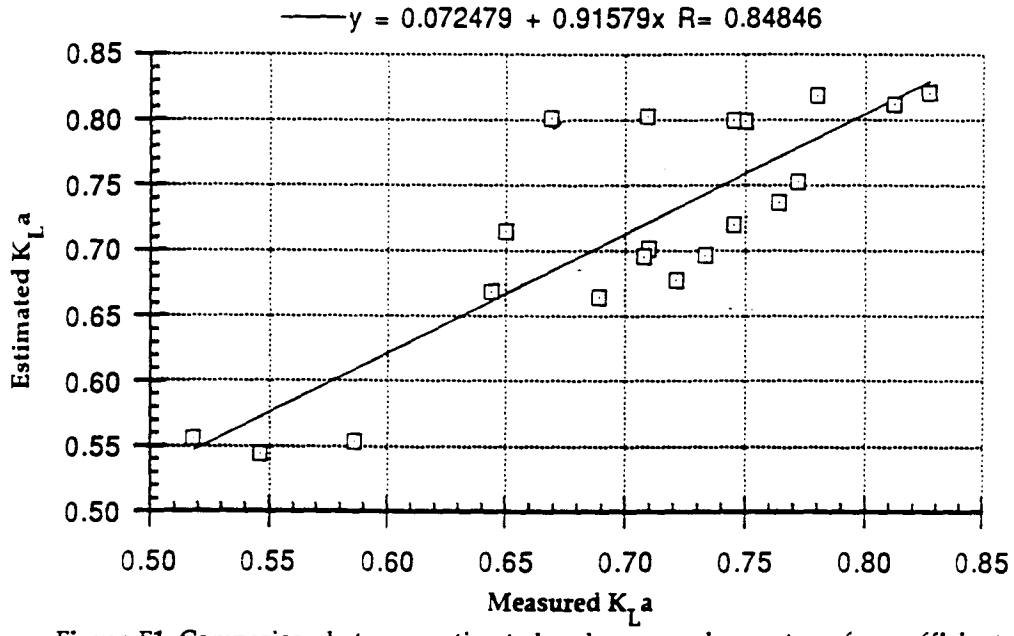

Figure F1. Comparison between estimated and measured mass transfer coefficient in surface aeration (235 rpm)

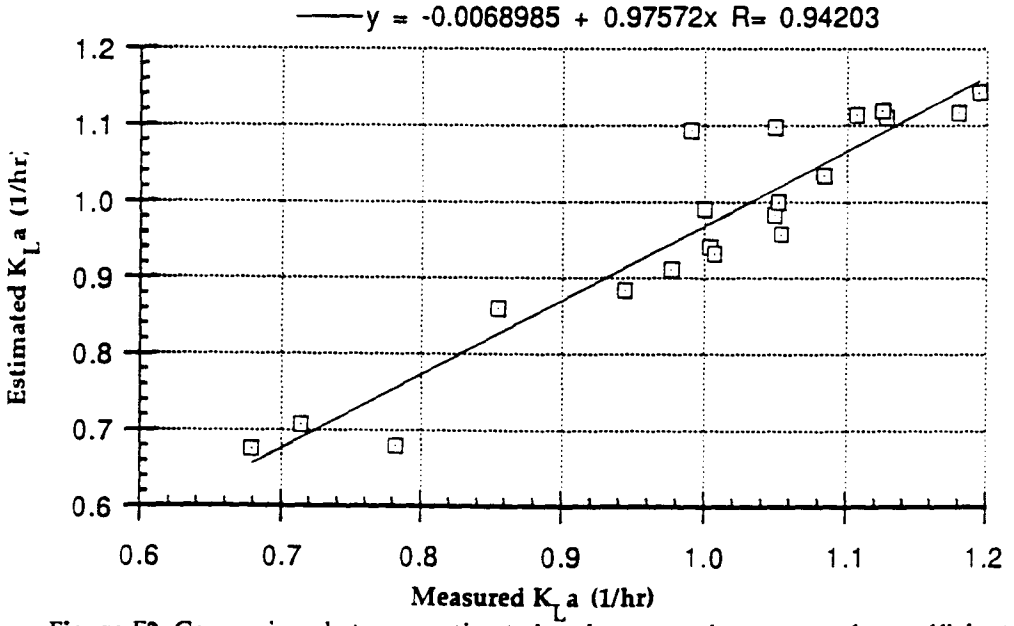

Figure F2. Comparison between estimated and measured mass transfer coefficients in surface aeration (325rpm)

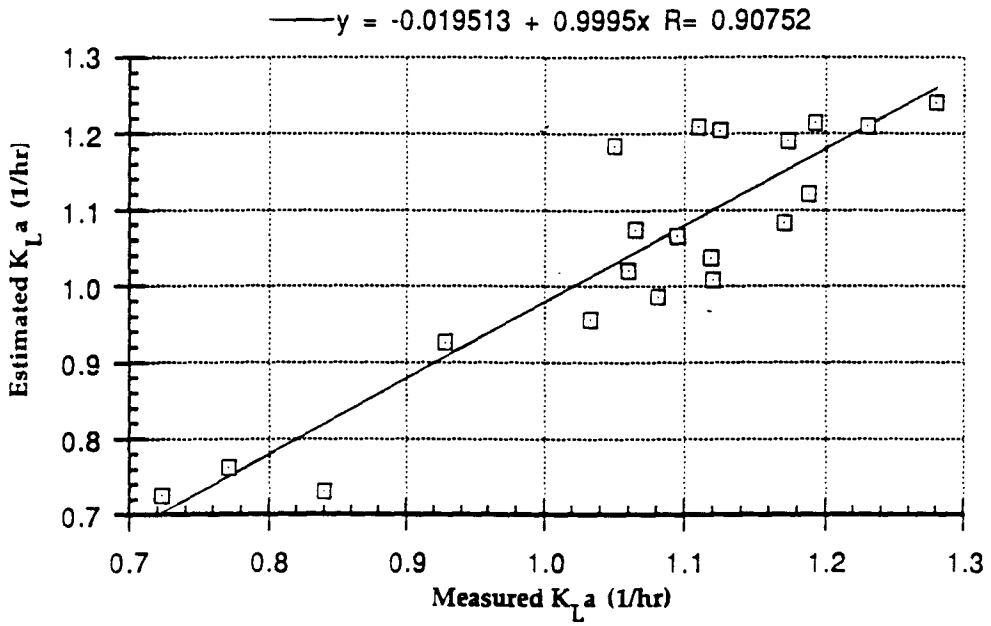

Figure F3. Comparison of estimated and measured mass transfer coefficients in surface aeration (350rpm)

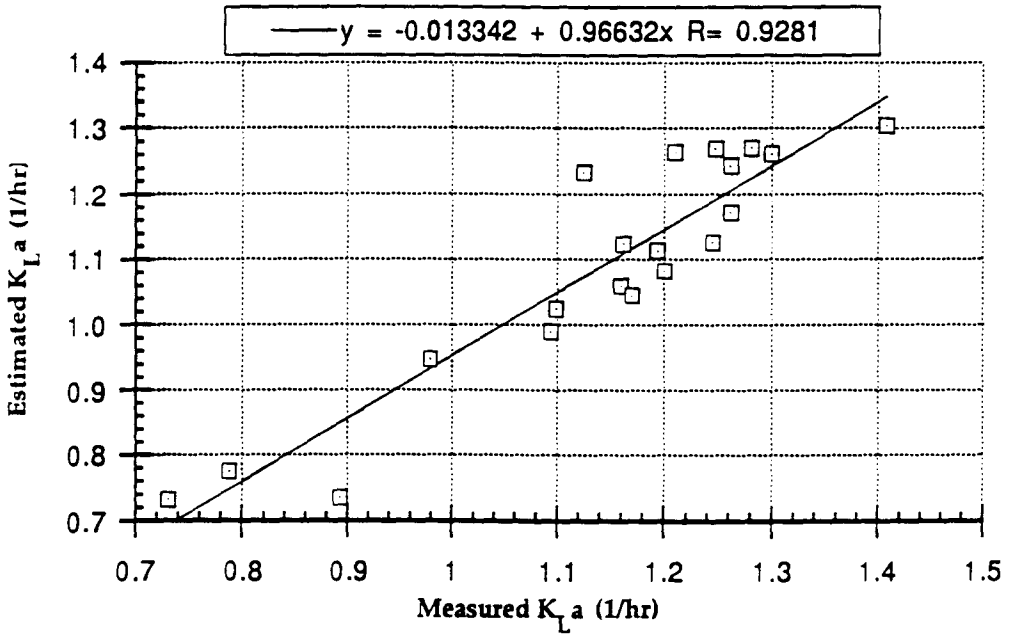

Figure F4. Comparison between estimated and measured mass transfer coefficients in surface aeration (375rpm)

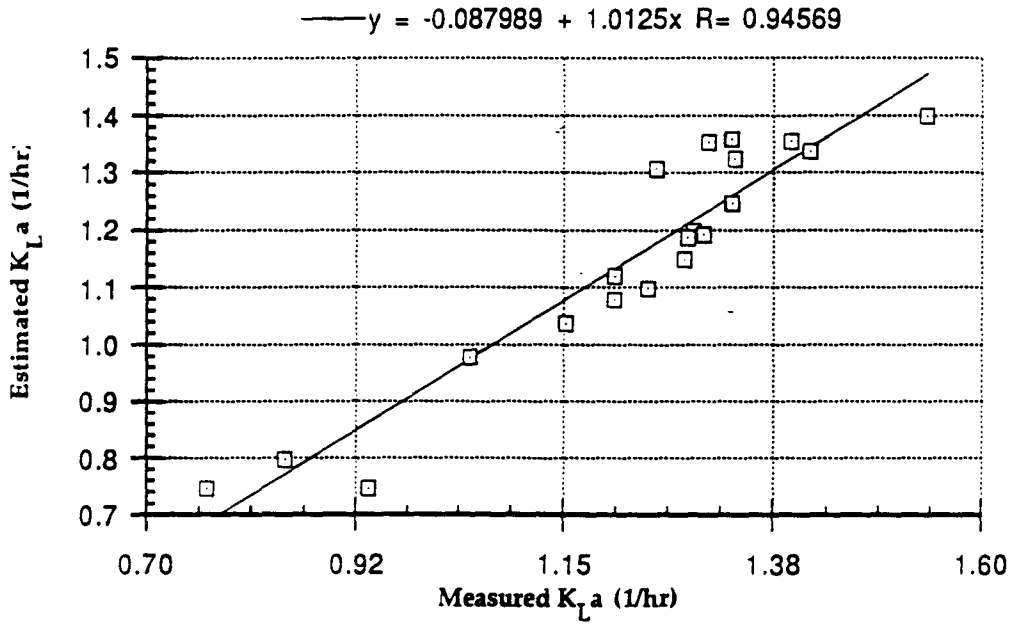

Figure F5. Comparison between estimated and measured mass transfer coefficients in surface aeration (400rpm)

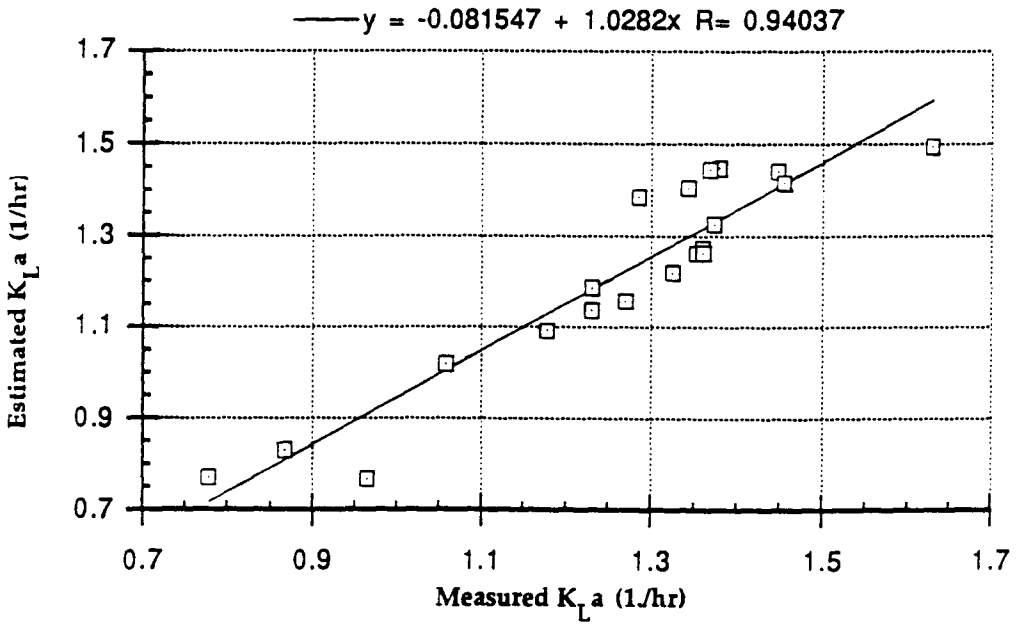

Figure F6. Comparison between estimated and measured mass transfer coefficients in surface aeration (420rpm)

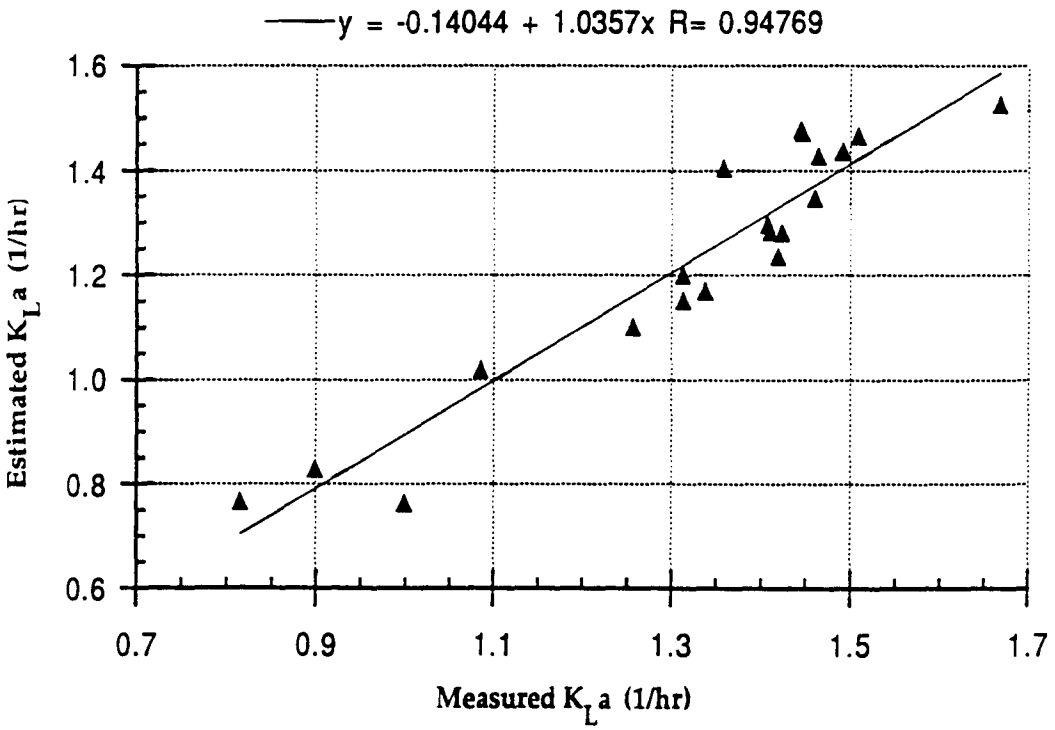

Figure F7. Comparison between estimated and measured mass transfer coefficients in surface aeration (425rpm)

Appendix G

Correlation of mass transfer coefficient to specific air flow rate in bubble column

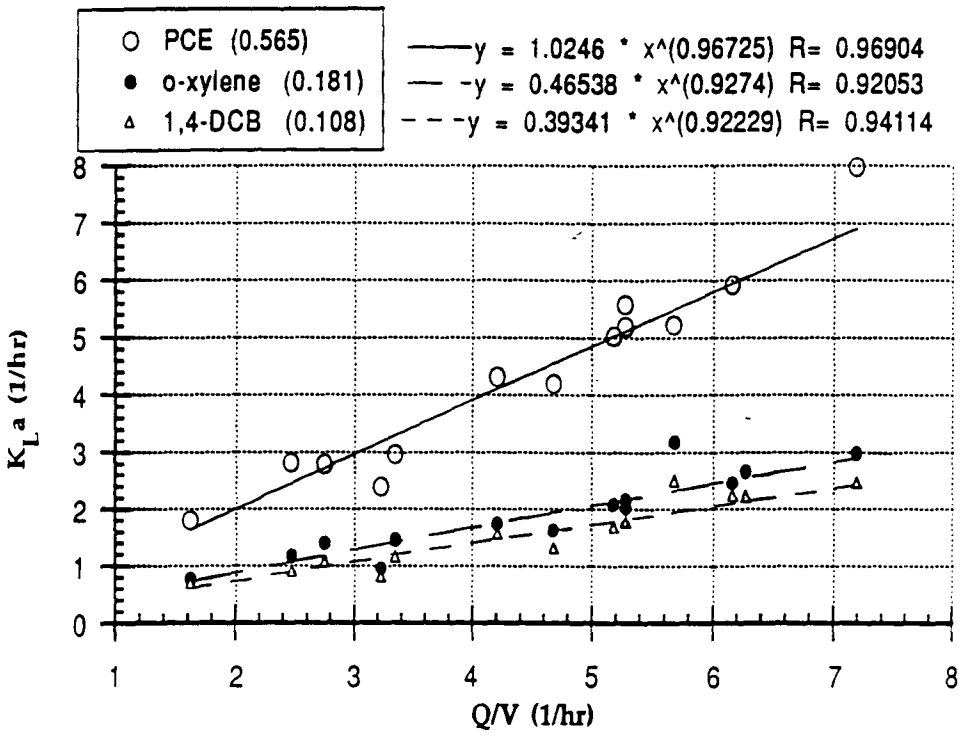

Figure G1. Correlation of mass transfer coefficient to specific air flow rate (PCE, OXY,14DCB)

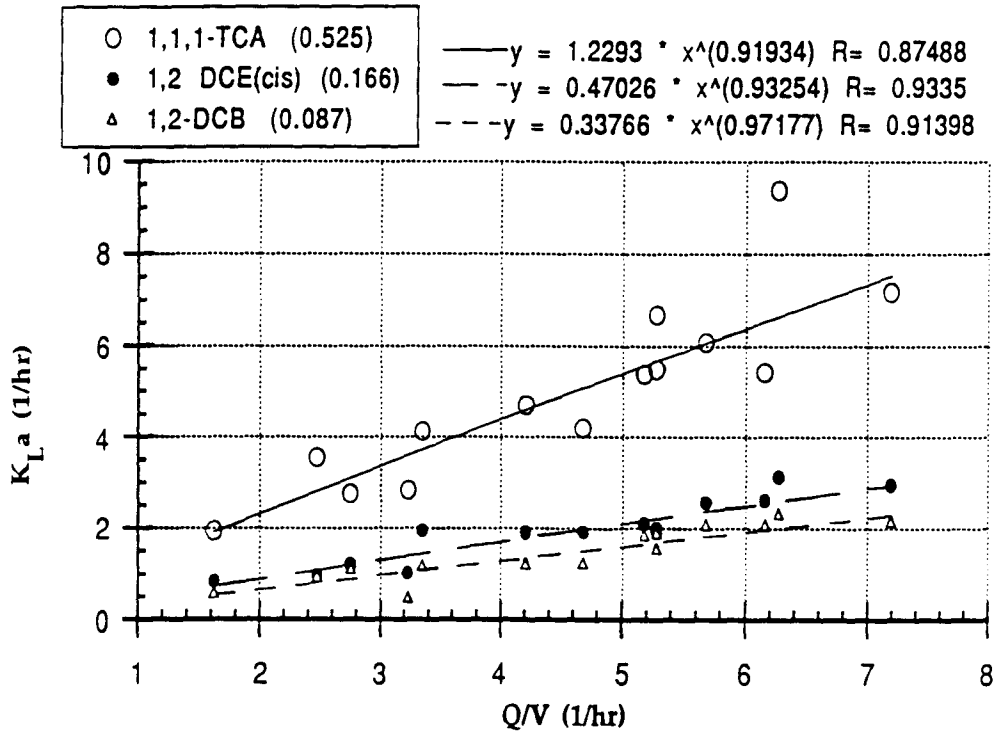

Figure G2. Correlation of mass transfer coefficient to specific air flow rate (111TCA,12DCE,12DCB)

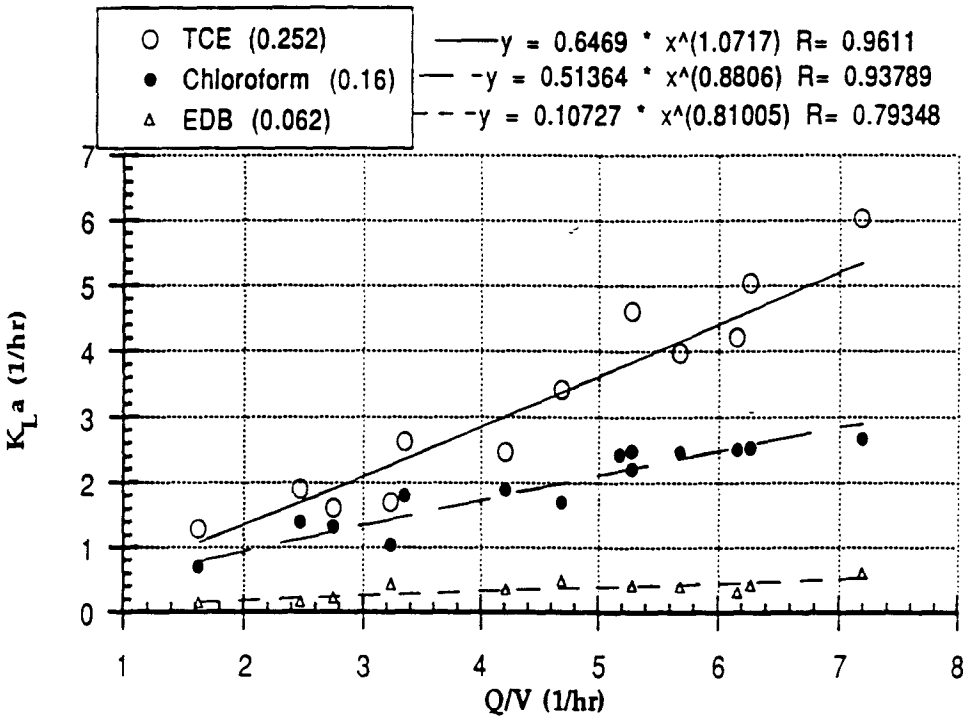

Figure G3. Correlation of mass transfer coefficient to specific air flow rate (TCE,CLF,EDB)

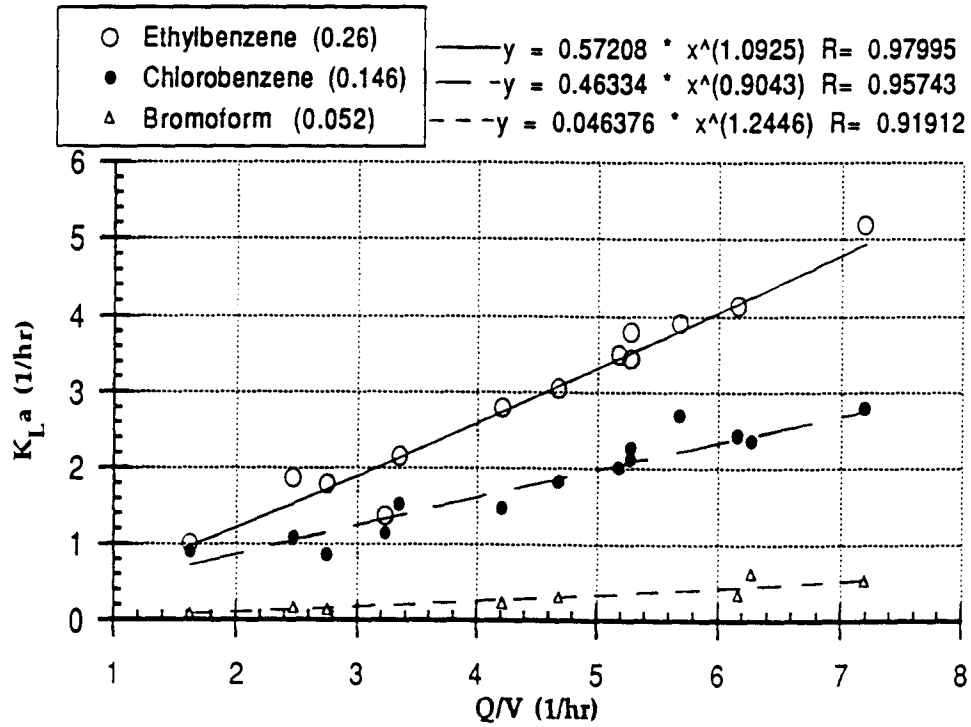

Figure G4. Correlation of mass transfer coefficient to specific air flow rate (EBZ,CBZ,BF)

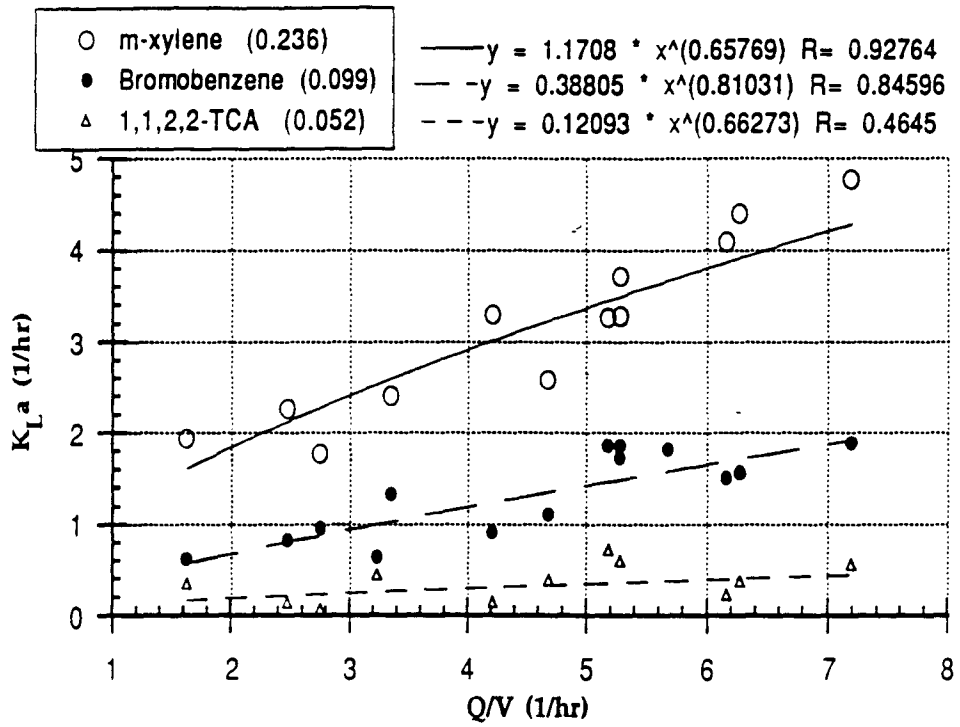

Figure G5. Correlation of mass transfer coefficient to specific air flow rate (MXY,BBZ,1122TCA)

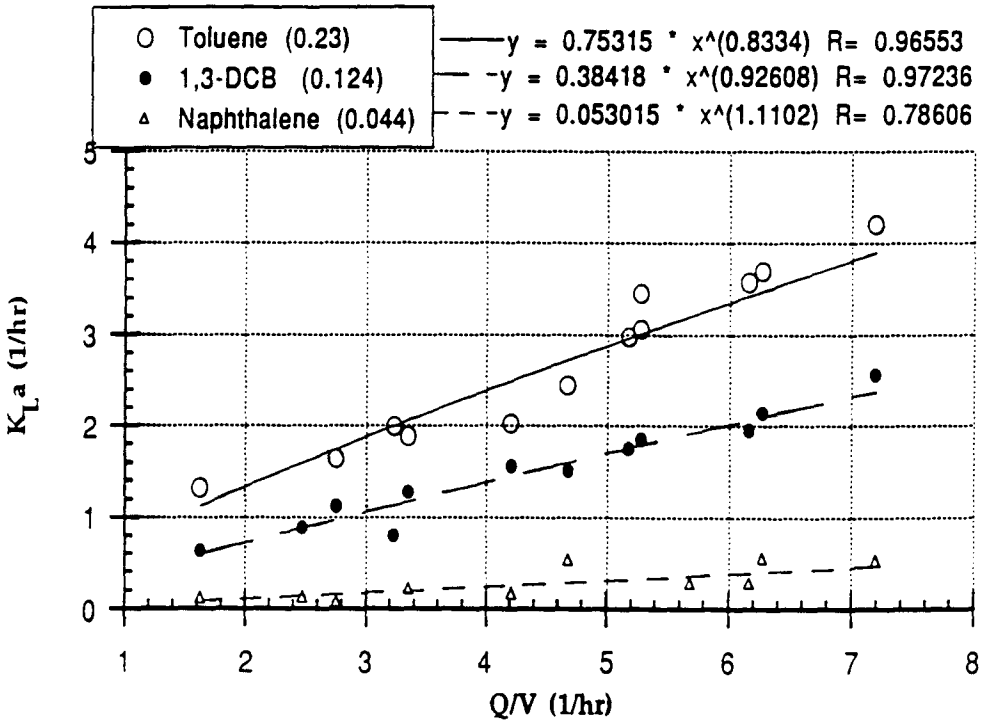

Figure G6. Correlation of mass transfer coefficient to specific air flow rate (TLN,13DCB,NAPH)

Appendix H

Comparison between estimated and measured mass transfer coefficients in bubble column

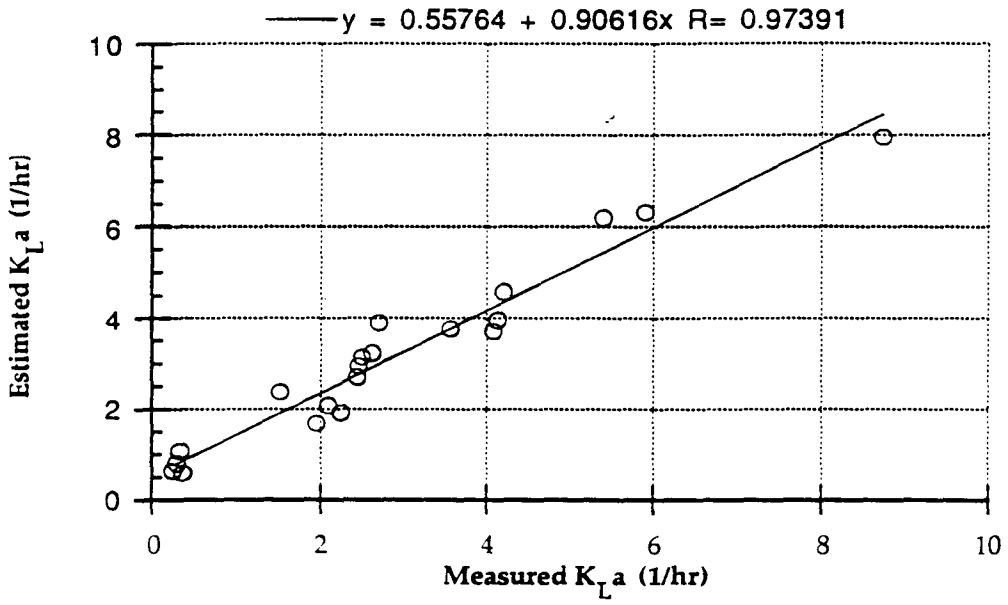

Figure H1. Comparison between estimated and measured mass transfer coefficient in bubble column (BC15, specific air flow rate = 6.16 1/hr)

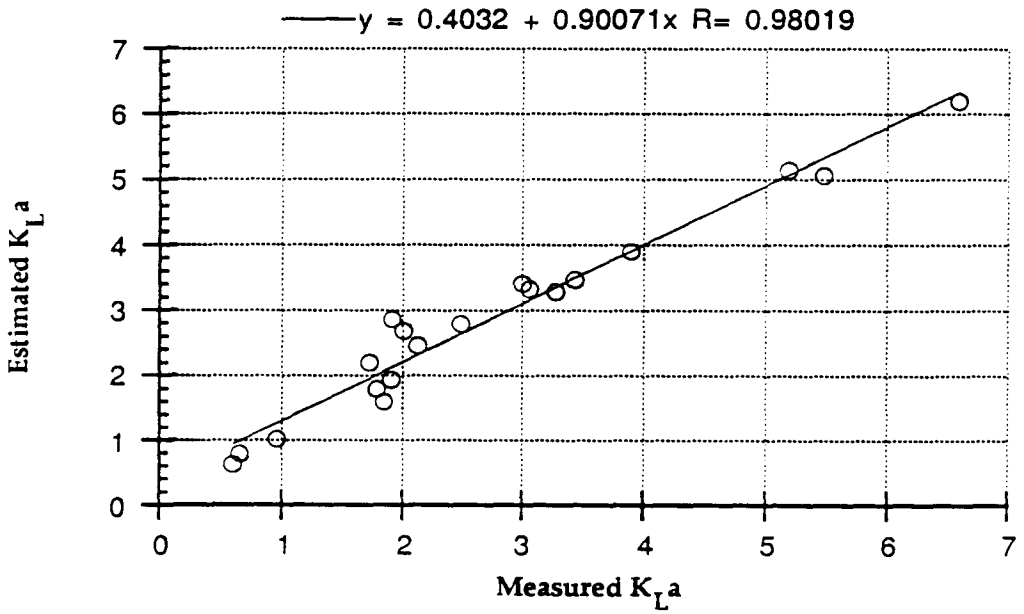

Figure H2. Comparison between estimated and measured mass transfer coefficient in bubble column (BC5, specific air flow rate = 5.28 1/hr)

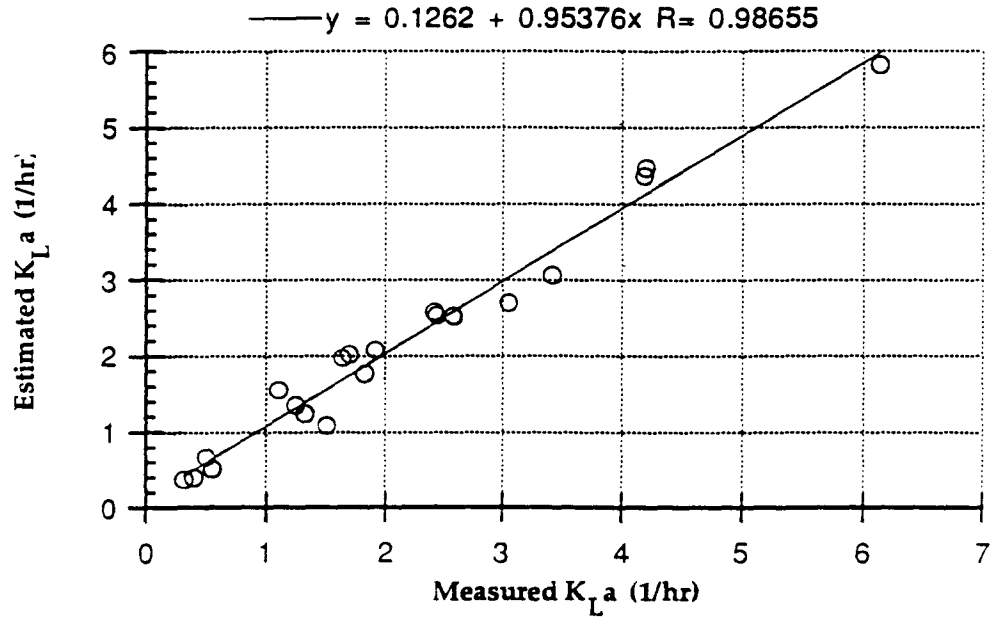

Figure H3. Comparison between estimated and measured mass transfer coefficients in bubble column (BC120, specific air flow rate = 4.68 1/hr)

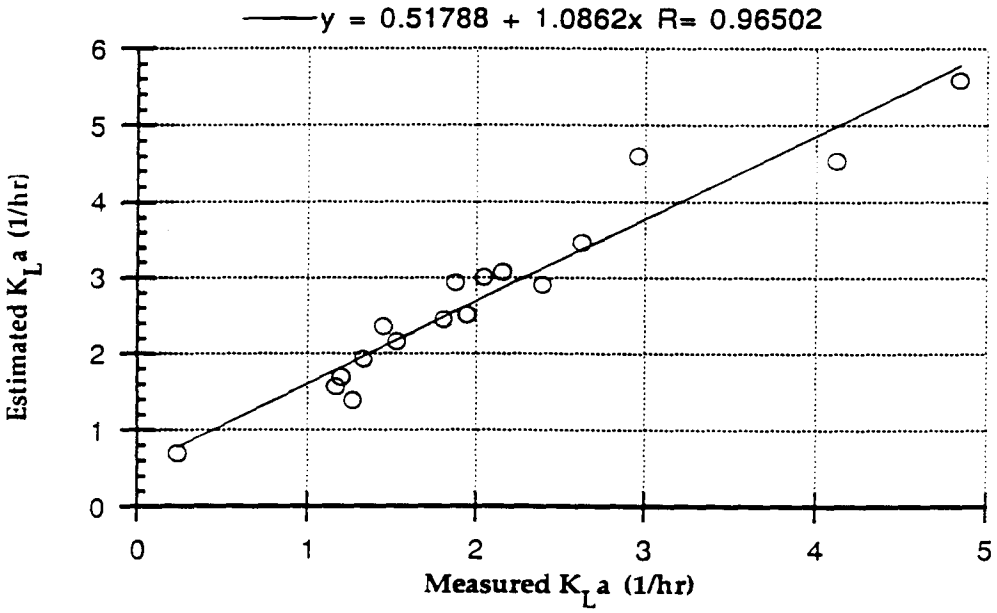

Figure H4. Comparison between estimated and measured mass transfer coefficients in bubble column (BC7, specific air flor rate = 3.55 1/hr)

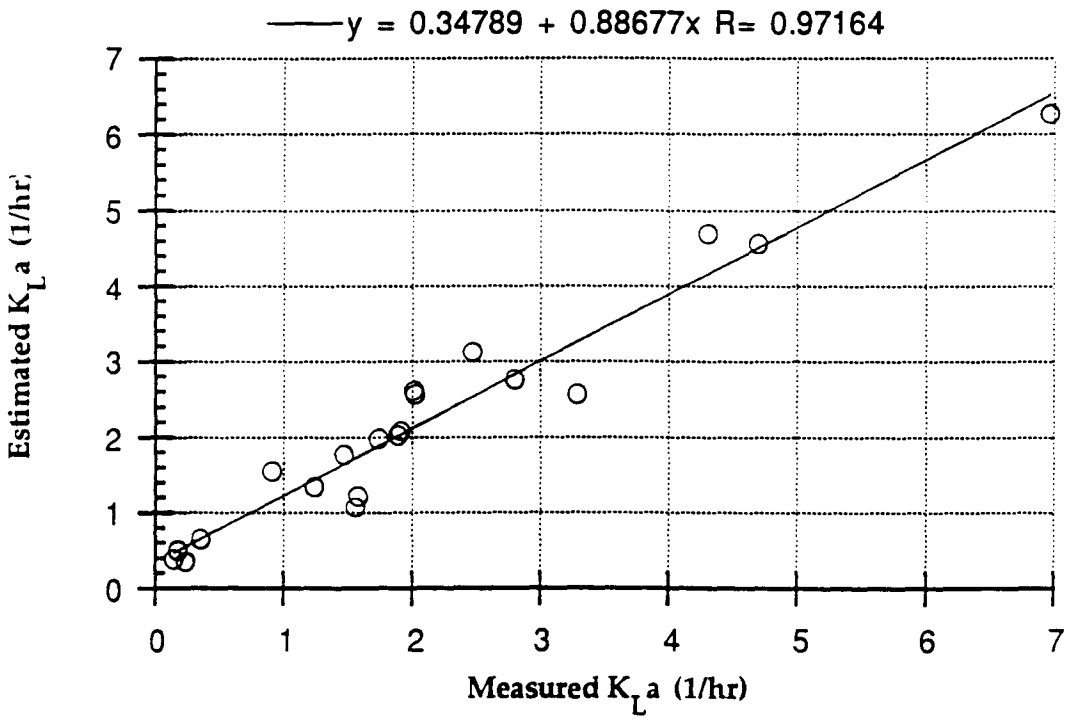

Figure H5. Comparison between estimated and measured mass transfer coefficients in bubble column (BC14, specific air flow rate = 4.21 1/hr)

Appendix K

Comparison of mass transfer coefficients of oxygen and volatile organic compounds in surface aeration and bubble column

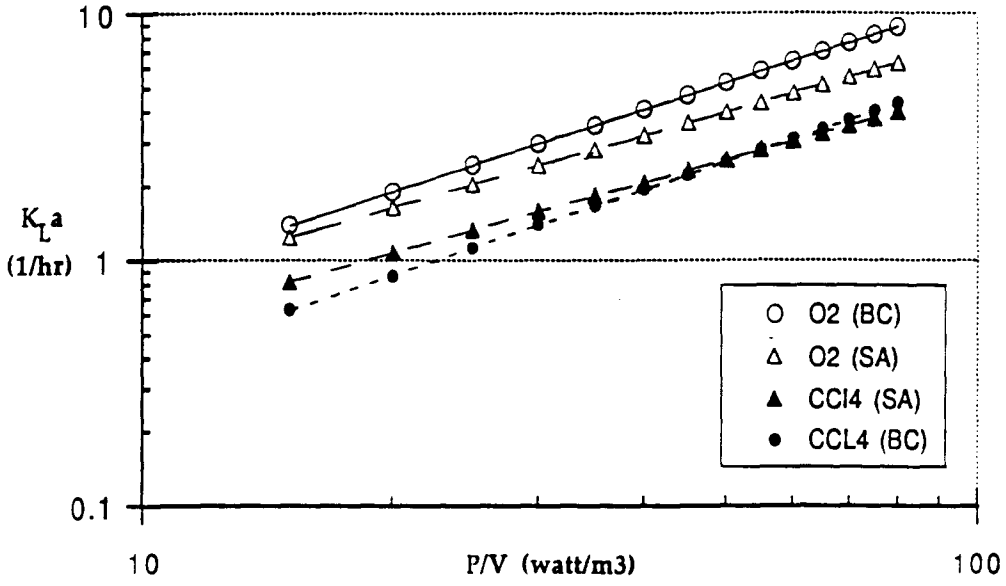

Figure K1. Comparison of mass transfer coefficients of oxygen and CCl_4 in surface aeration (SA) and bubble column (BC)

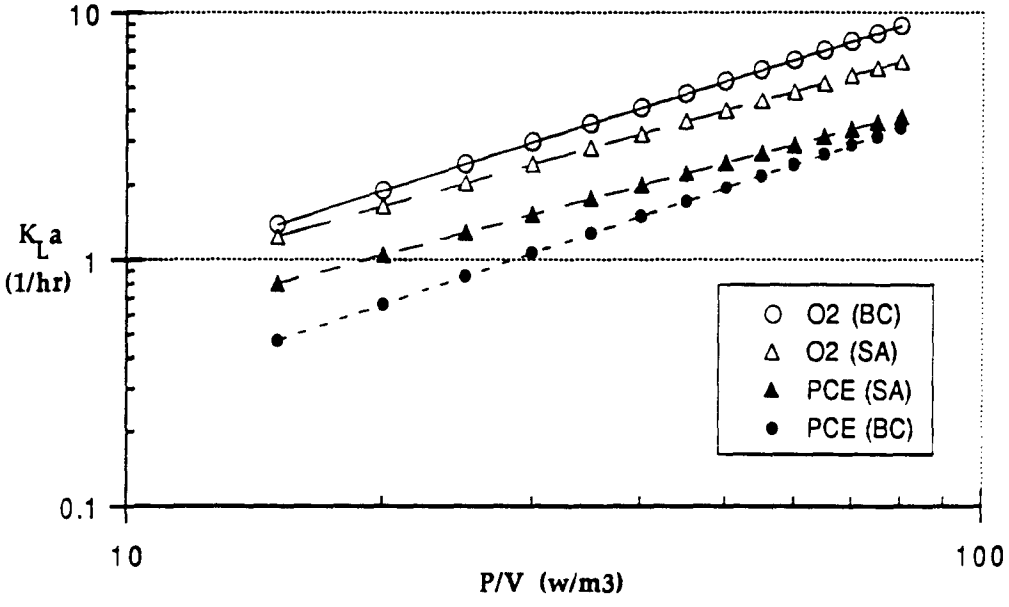

Figure K2. Comparison of mass transfer coefficients of oxygen and PCE in surface aeration (SA) and bubble column (BC)

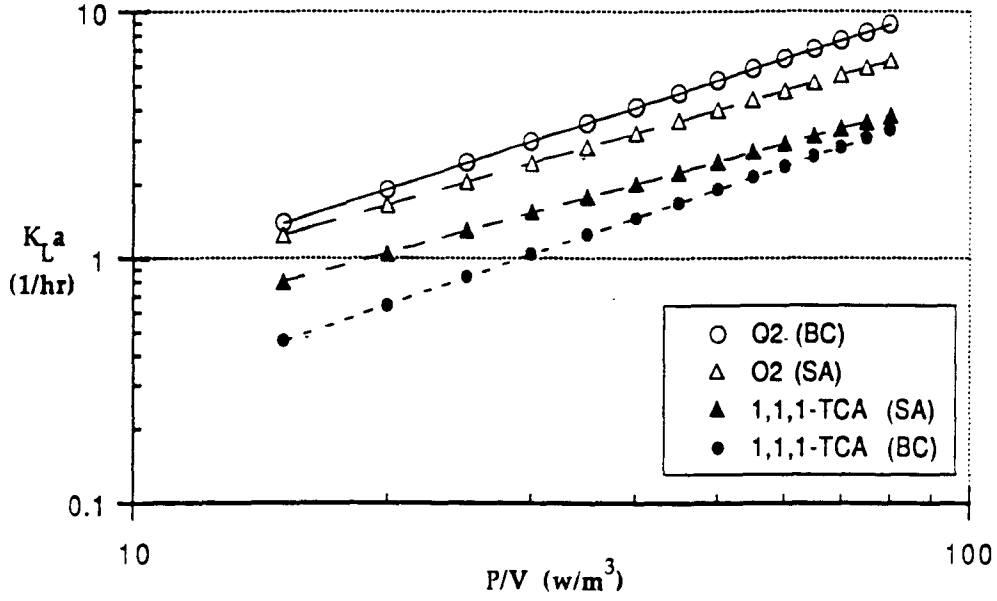

Figure K3 Comparison of mass transfer coefficients of oxygen and 111TCA in surface aeration (SA) and bubble column (BC)

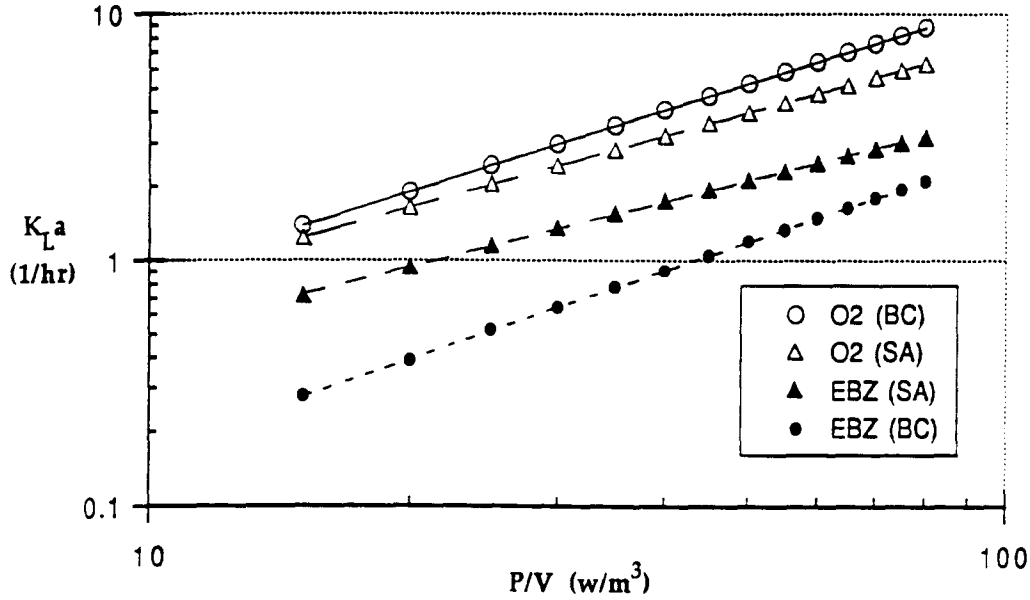

Figure K4. Comparison between mass transfer coefficients of oxygen and EBZ in surface aeration (SA) and bubble column (BC)

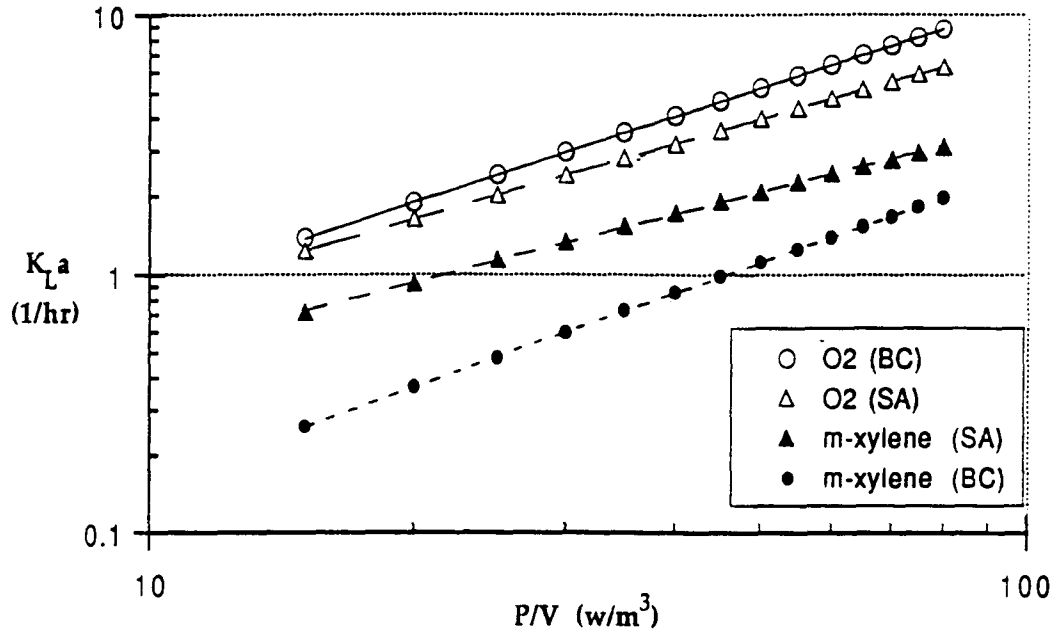

Figure K5. Compariosn between mass transfer coefficients of oxygen and MXY in surface aeration (SA) and bubble column (BC)

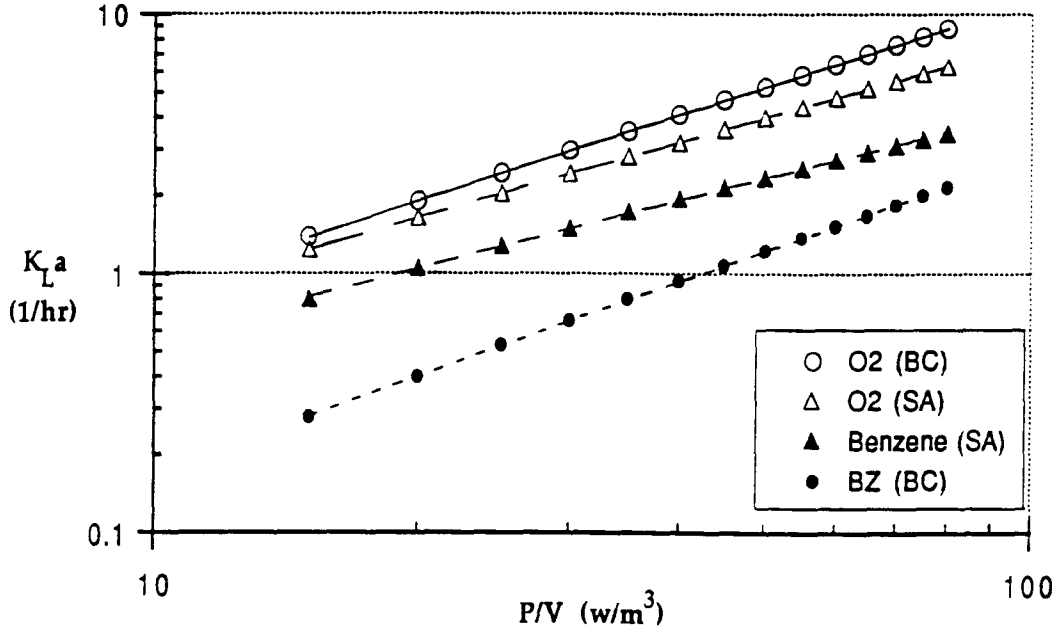

Figure K6. Comparison between mass transfer coefficients of oxygen and Benzene in surface aeration (SA) and bubble column (BC).

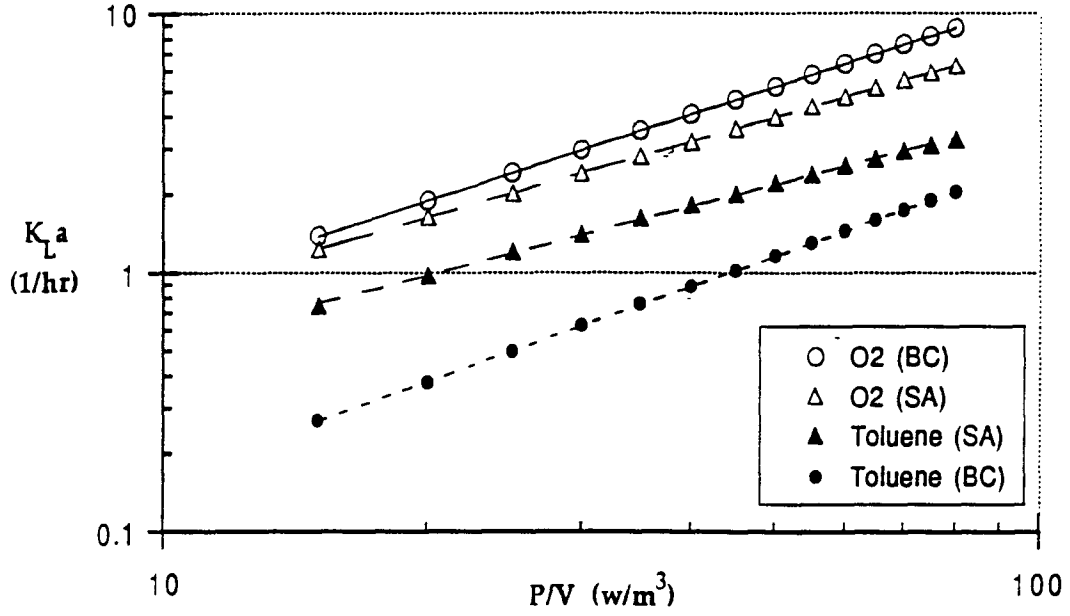

Figure K7. Comparison between mass transfer coefficient of oxygen and toluene in surface aeration (SA) and bubble column (BC)

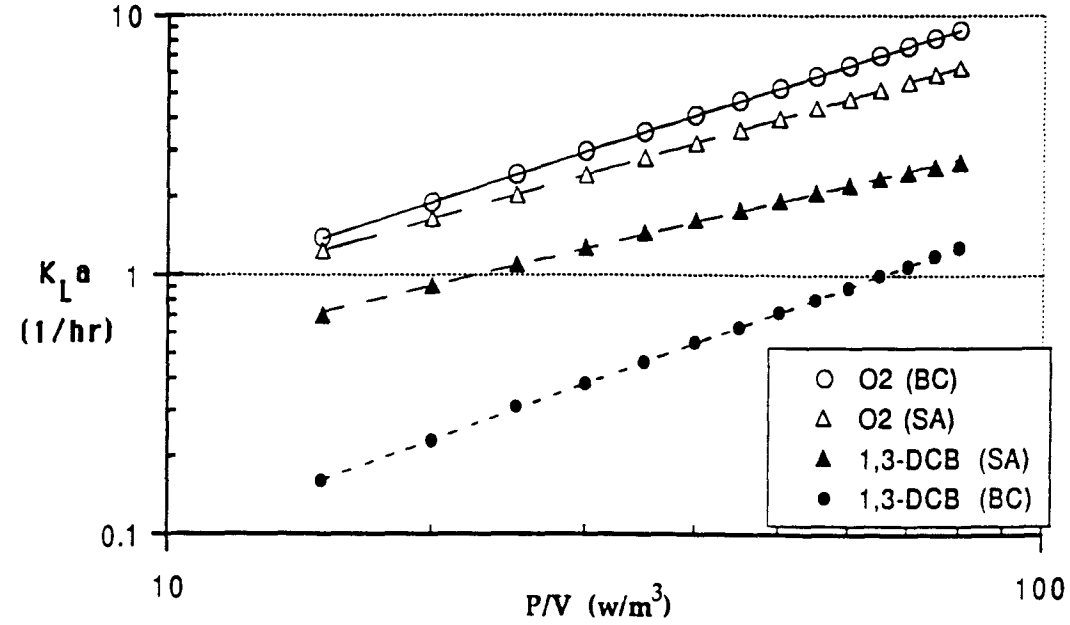

Figure K8. Comparison between mass transfer coefficient of oxygen and 13DCB in surface aeration (SA) and bubble column (BC)

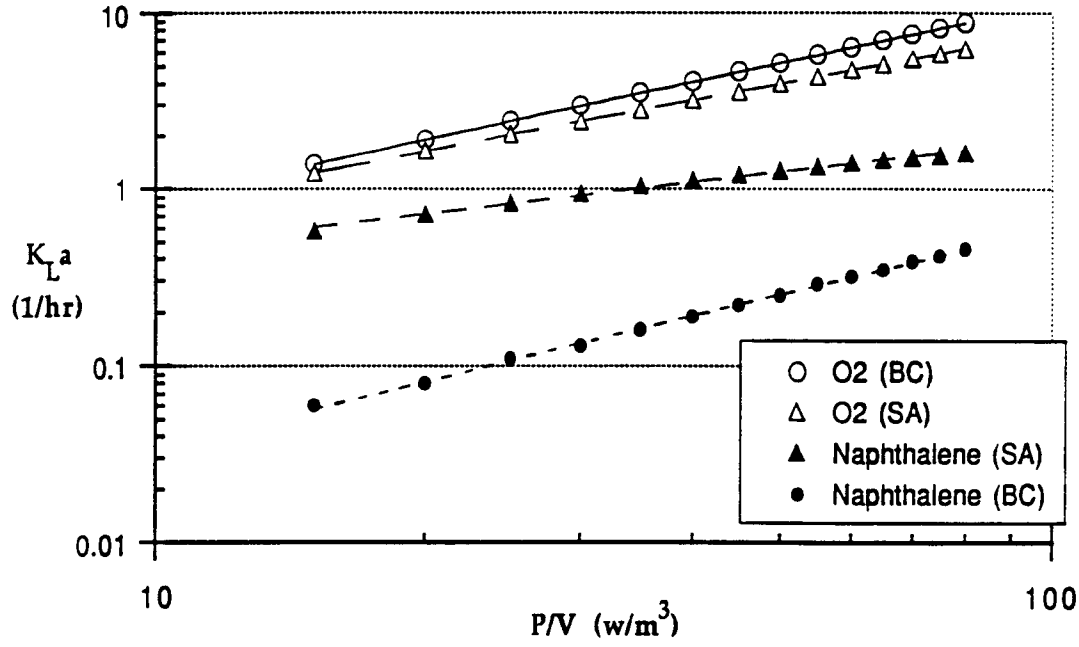

Figure K9. Comparison between mass transfer coefficient of oxygen and naphthalene in surface aeration (SA) and bubble column (BC)